UNIVERSITY OF SOUTHAMPTON

FACULTY OF ENGINEERING AND PHYSICAL SCIENCES

School of Chemistry

Unravelling the Effects of Hypoxia on Purine Biosynthesis in Cancer

by

Cyrielle DOIGNEAUX

Thesis for the degree of Doctor of Philosophy

March 2020

UNIVERSITY OF SOUTHAMPTON

ABSTRACT

FACULTY OF ENGINEERING AND PHYSICAL SCIENCES

Chemistry

Thesis for the degree of Doctor of Philosophy

UNRAVELLING THE EFFECTS OF HYPOXIA ON PURINE BIOSYNTHESIS IN CANCER

Cyrielle Doigneaux

The purinosome is a dynamic metabolic complex composed of the six enzymes of the *de novo* purine biosynthesis that assembles in response to elevated purine demand. Its formation translates in an increase to the rate of the pathway in order to maintain the purine pool. This complex was first described to form in an artificially induced purine-depleted environment but later studies demonstrated its ability to form in pathological contexts, thus making the purinosome a promising therapeutic target to control purine synthesis.

In various cancers, solid tumours often display hypoxic regions where oxygen deprivation induces a cellular response aiming at maintaining cell growth and proliferation, and contributes to the tumours resistance to treatments. In hypoxic cells, the heterodimeric transcription factor Hypoxia-Inducible Factor 1 (HIF-1) is responsible for the regulation of many target genes that ensure the response and adaptation of cancer cells to hypoxia. One of the most important adaptation mechanisms regulated by HIF is the metabolic reprogramming which supports the malignant phenotype of hypoxic tumours. As such, improving the current understanding of the metabolic adaptation to hypoxia is of high interest in order to further develop new therapeutic strategies to target hypoxic cancer cells.

This work describes and investigates the formation of the purinosome complex in hypoxic cancer cells. Multiple cellular and biochemical approaches were used in order to characterise and understand the formation of the complex in low oxygen environments. The purinosome formation was found to be linked to HIF and to be modulated by various metabolic stimuli, thus indicating a link between the formation of the complex and its function. In contrast to its previously reported function in purine-depleted conditions, the hypoxic purinosome did not correlate with increased *de novo* synthesis of purines.

This study lays the foundation for further investigations aiming at understanding the exact function of the purinosome in hypoxic cancer cells and raises the possibility that inhibiting purinosome formation in hypoxia might be of high therapeutic interest to specifically target hypoxic cancer cells.

Table of Contents

Table of Tables

Table of Figures

Academic Thesis: Declaration of Authorship

I, CYRIELLE DOIGNEAUX

declare that this thesis and the work presented in it are my own and has been generated by me as the result of my own original research.

Unravelling the Effects of Hypoxia on Purine Biosynthesis in Cancer

I confirm that:

1. This work was done wholly or mainly while in candidature for a research degree at this University;
2. Where any part of this thesis has previously been submitted for a degree or any other qualification at this University or any other institution, this has been clearly stated;
3. Where I have consulted the published work of others, this is always clearly attributed;
4. Where I have quoted from the work of others, the source is always given. With the exception of such quotations, this thesis is entirely my own work;
5. I have acknowledged all main sources of help;
6. Where the thesis is based on work done by myself jointly with others, I have made clear exactly what was done by others and what I have contributed myself;
7. None of this work has been published before submission

Signed: .....

Date: .....

Acknowledgements

Firstly, I would like to thank Prof. Ali Tavassoli for giving me the opportunity to carry out this research and for all his help, advice and support throughout my PhD. I would also like to thank our collaborators at Penn State University, Prof. Stephen Benkovic and Dr Anthony Pedley for their support and help during this project.

I would like to thank the Tavassoli group, past and present members, for their help and support during these last few years. Special thank you goes to Katherine Lennard for her warm welcome and all her help when first I joined the lab; to Andy Foster, for his help, advice, support in this project and for being a great friend over these last few years.

A huge thank you to my family for everything. Thank you to my little sister Estelle, for always supporting and encouraging me. A massive thank you to my parents for everything they have done for me since forever, thank you for helping me get to where I am today and for supporting me over the years in everything I undertook, especially this PhD.

Finally, I would like to thank my partner, Florian, for being an amazing source of motivation and inspiration every day and for his continuous love and support throughout the years. Thank you for always believing in me.

Definitions and Abbreviations

2-DG	2-deoxyglucose
3-PG	3-phosphoglycerate
5,10-mTHF	5,10-methylenetetrahydrofolate
6-AN	6-aminonicotinamide
10-f-THF	10-formyltetrahydrofolate
ADSL	Adenylosuccinate lyase
ADSS	Adenylosuccinate synthetase
ADP	Adenosine diphosphate
AICAR	5-aminoimidazole-4-carboxamide ribonucleotide
AIR	5-aminoimidazole ribonucleotide
ALDO	Aldolase
AMP	Adenosine monophosphate
APRT	Adenine phosphoribosyltransferase
Arnt	Aryl hydrocarbon receptor nuclear translocator
ATIC	5-aminoimidazole-4-carboxamide ribonucleotide formyltransferase / IMP cyclohydrolase
ATP	Adenosine triphosphate
bHLH	Basic helix-loop-helix
BME	β-mercaptoethanol
CAIR	5-phosphoribosyl-4-carboxy-5-aminoimidazole
CBP	cAMP response element-binding protein (CREB)-binding protein
DAPI	4',6-diamidino-2-phenylindole

DFX	Deferoxamine
DHA	Dihydroxyacetone phosphate
DMEM	Dulbecco's modified Eagle's medium
DMSO	Dimethyl sulfoxide
DNA	Deoxyribonucleic acid
DPBS	Dulbecco's phosphate buffer saline
dTMP	Deoxythymidine monophosphate
DTT	Dithiothreitol
EDTA	Ethylenediaminetetraacetic acid
ENO	Enolase
ETC	Electron transport chain
FAD	Flavin adenine dinucleotide
FAICAR	5-Formaminoimidazole-4-carboxamide ribotide
FBS	Foetal bovine serum
FGAR	5'-Phosphoribosyl-N-formylglycinamide
FGAM	5'-Phophoribosylformylglycinamidine
FGAMS	Phosphoribosylformylglycinamidine synthase
FIH	Factor inhibiting HIF
fMet	Formylmethionine
G3BP	Ras GTPase-activating protein-binding protein
G6P	Glucose-6-phosphate
G6PD	Glucose-6-phosphate dehydrogenase
GAPDH	Glyceraldehyde-3-phosphate dehydrogenase
GAR	Glycinamide ribonucleotide

GART	Glycinamide ribonucleotide formyltransferase
GDP	Guanosine diphosphate
GFP	Green fluorescent protein
GLUT	Glucose transporter
GMP	Guanosine monophosphate
GMPS	GMP synthase
GPI	Glucose phosphate isomerase
GTP	Guanosine triphosphate
HIF	Hypoxia-inducible factor
HK	Hexokinase
HSP	Heat shock protein
HPRT	Hypoxanthine/guanine phosphoribosyltransferase
HRE	Hypoxia response element
HRP	Horseradish peroxidase
IMP	Inosine monophosphate
IMPDH	Inosine monophosphate dehydrogenase
KO	Knockout
LB	Lysogeny broth
LDHA	Lactate dehydrogenase A
MEM	Modified Eagle’s medium
MS	Mass spectrometry
NAD	Nicotinamide adenine dinucleotide
NADP	Nicotinamide adenine dinucleotide phosphate
MTHFD	Methylenetetrahydrofolate dehydrogenase

mTOR	Mammalian target of rapamycin
OCM	One-carbon metabolism
ODDD	Oxygen-dependent degradation domain
OFP	Orange Fluorescence Protein
PAGE	Polyacrylamide gel electrophoresis
PAICS	Phosphoribosylaminoimidazole carboxylase and phosphoribosylaminoimidazole succinocarboxamide synthetase
PAS	Per / Arnt/ Sim
PBS	Phosphate buffer saline
PCR	Polymerase chain reaction
PDH	Pyruvate dehydrogenase
PDK1	Pyruvate dehydrogenase kinase 1
PFKL	Phosphofructokinase liver
PFKP	Phosphofructokinase platelet
PGAM	Phosphoglycerate mutase
PGD	6-phosphogluconate dehydrogenase
PGK	Phosphoglycerate kinase
PHD	Prolyl hydroxylase domain
PHGDH	Phosphoglycerate dehydrogenase
PLA	Proximity ligation assay
PPAT	Aminophosphoribosyltransferase
PPi	Inorganic pyrophosphate
PPP	Pentose phosphate pathway
PRA	Phosphoribosylamine

PRPP	Phosphoribosyl pyrophosphate
PRPS1	PRPP synthetase
qPCR	Quantitative polymerase chain reaction
RIPA	Radioimmunoprecipitation assay
RNA	Ribonucleic acid
ROI	Region of interest
ROS	Reactive oxygen species
RPMI	Roswell park memorial institute
RT	Room temperature
SAICAR	Phosphoribosylaminoimidazolesuccinocarboxamide
SDS	Sodium dodecyl sulphate
SHMT	Serine hydroxymethyltransferase
shRNA	Short hairpin ribonucleic acid
siRNA	Small interfering ribonucleic acid
SOC	Super optimal broth with catabolite expression
SRRF	Super-resolution radial fluctuations
SSP	Serine synthesis pathway
TAD	Transactivation domain
TAE	Tris-acetate-EDTA
TALDO	Transaldolase
TCA	Tricarboxylic Acid
TKT	Tranketolase
TOM20	Translocase of outer mitochondrial mitochondrial membrane 20
THF	Tetrahydrofolate

TPI	Triose phosphate isomerase
VEGF	Vascular endothelial growth factor
VHL	Von Hippel Lindau
WT	Wild type
XMP	Xanthosine monophosphate

Chapter 1 Introduction

1.1 Hypoxia and Hypoxia-Inducible Factors

Maintaining oxygen homeostasis in cells and tissues is essential in the survival of mammalian species. At normal atmospheric pressure, the oxygen levels in the air remain constant at 21% oxygen, and this is referred to as normoxia (**Figure 1**). Although normoxia is commonly used as the physiological oxygen level in *in vitro* biological experiments, it is to mention that the "normal" oxygen levels in a given tissue are much lower than the normoxic levels and are referred to as physioxia. These tissue specific oxygen levels vary depending on the tissue observed, with the highest physioxic levels observed being in the lung alveoli (14.5% oxygen). When the oxygen homeostasis is disturbed, normal tissues can be exposed to low oxygen levels known as hypoxia (<2% oxygen).[1, 2] Hypoxia occurs at different stages of life such as during embryonic development or intense exercise, but it is also frequently encountered in various pathologies such as stroke, cardiac arrest and cancer.[3-5]

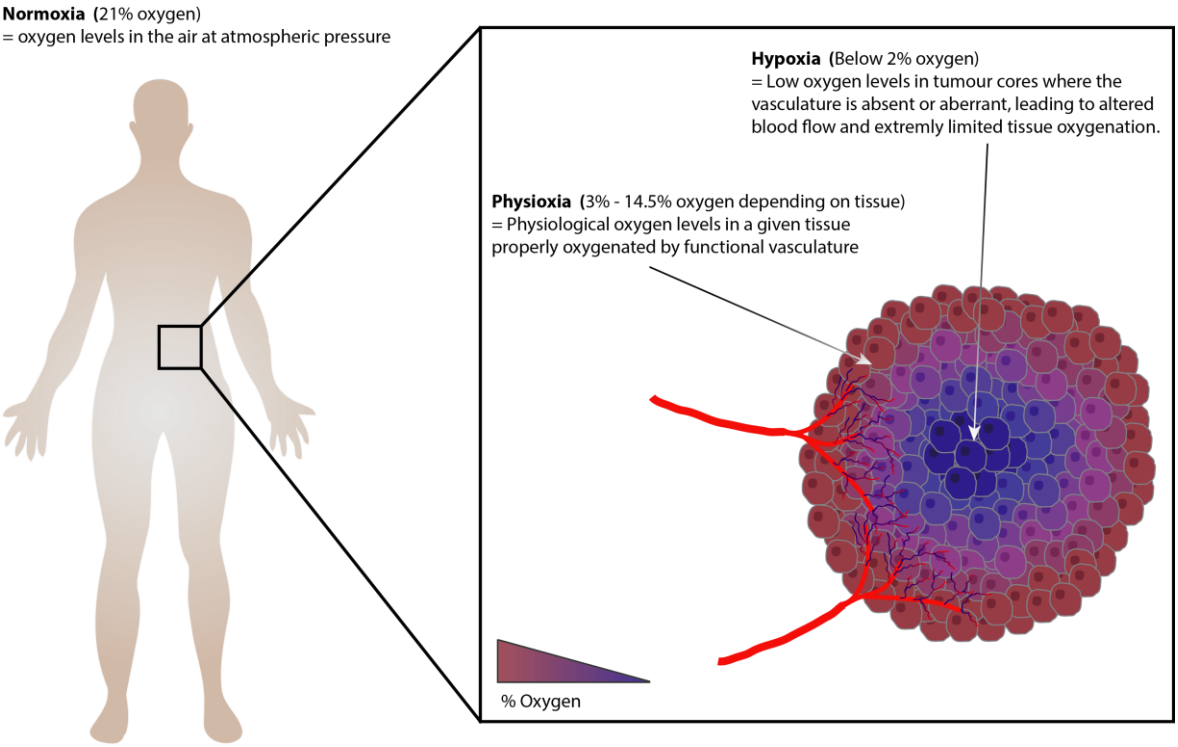

Figure 1. Biological meaning and representation of normoxia, physioxia and hypoxia.

Hypoxia is commonly found in tumour cores where cell survival and proliferation are enhanced and uncontrolled. As the tumour tissue expands, the distance between the local vasculature and the tumour cells increases, thus limiting the oxygen diffusion and enhancing the hypoxic microenvironment. In the same way, tumour hypoxia induces the formation of new aberrant

blood vessels that display chaotic blood flows and leakages, leading to limited blood supply and oxygen delivery.[6-8] Human tumours containing hypoxic regions often display enhanced malignant progression, aggressiveness and increased metastasis abilities resulting in resistance to therapy and poor prognosis.[9-13]

The above-mentioned characteristics of tumour hypoxia are the result of the activation of the cellular response to low oxygen environments. Although an unbalanced oxygen homeostasis can be toxic to the cells, hypoxic tumour cells can activate signalling and metabolic pathways enabling their survival, proliferation and ensure the restoration of blood supply.[14, 15] The transcription factor hypoxia-inducible factor-1 (HIF-1) has been found to be the most important regulator of the cellular hypoxia response as it transcriptionally regulates many genes, with the majority of these being involved in tumorigenic processes.[16] The mechanisms underlying the hypoxia response, including the functions of HIF, have been widely studied over the last twenty years in order to understand how cells adapt to these low oxygen levels, but many more mechanisms remain to be uncovered.

1.1.1 HIF-1 structure

HIF-1 is a heterodimeric transcription factor composed of two subunits, 1α and 1β, with 1β also referred to as the aryl hydrocarbon receptor nuclear translocator (Arnt). Although both subunits are constantly being expressed, the 1α subunit is also continuously degraded in presence of oxygen and is only stabilised in low oxygen conditions. In these conditions, 1α is subsequently translocated into the nucleus where it dimerises with the nuclear 1β subunit, thus enabling the formation of the active heterodimer.

Both subunits display similar structural characteristics and belong to the basic helix-loop-helix/Per-Arnt-Sim (bHLH/PAS) family of transcription factors. The protein members of the bHLH/PAS family all contain an N-terminal region comprised of a bHLH domain followed by a PAS domain, itself comprised of two regions, PAS A and PAS B.[17] The main differences between the α and β subunits are found in the C-terminal region of the proteins. Although both subunits contain at least one transactivation domain (TAD), 1α also displays an oxygen-dependent-degradation-domain (ODDD) essential in its regulation, whose functions will be discussed in more depth in section 1.1.2 (**Figure 2**).

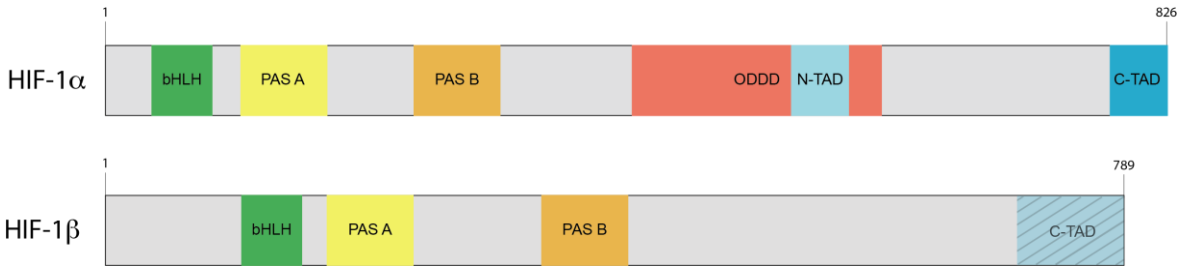

Figure 2. Domain structure of HIF-1α and HIF-1β. bHLH: basic helix-loop-helix; PAS: Per/Arnt/SIM; ODDD: oxygen-dependent-degradation-domain; TAD: transactivation domain.

The bHLH and PAS domains are responsible for the heterodimerisation and DNA binding of the HIF complex to DNA. [20] The PAS domains, which are found in many diverse species, are known to work as a protein-protein interaction motif.[18] In the case of the HIF complex, they contribute to the heterodimerisation of the complex and a truncation of either PAS domain renders the formation of the complex less efficient.[19, 20] Each bHLH domain from 1α and 1β form an α-helix and upon dimerisation of the complex, the two helices constitute the direct interface between the protein complex and the major groove of the DNA helix (**Figure 3**). The DNA binding site of HIF is a consensus DNA sequence, (A/G)CGTG, present within the Hypoxia-Response-Element (HRE).

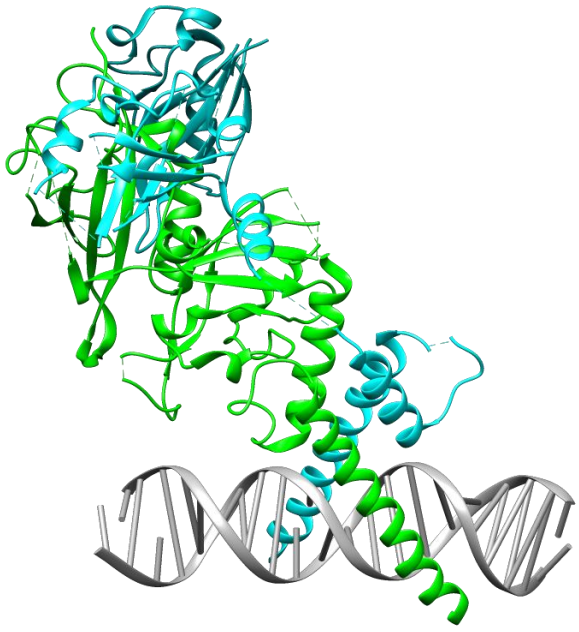

Figure 3. Crystal structure of HIF-1 bound to the HRE DNA motif. 1α is represented in green. 1β is represented in cyan. The DNA helix is represented in grey. PDB 4ZPR.[21]

Following dimerisation and DNA binding, the complex requires the recruitment of coactivators to ensure the formation of the active transcription factor. This recruitment process involves the

transactivation domains (TADs) found in the C-terminal region of the proteins, although the C-TAD present in the 1β isoform is not used in the hypoxia-induced gene expression.[22, 23] The 1α subunit contains two distinct transactivation domains: the N-terminal transactivation domain (N-TAD) and the oxygen-regulated C-terminal transactivation domain (C-TAD).[24]

Although a few transcriptional coactivators of the HIF complex have been reported, p300/CREB binding protein (CBP) is the only one known to directly bind to HIF.[25, 26] Both the N-TAD and C-TAD are involved in the transactivation of HIF and were found to bind different domains within p300/CBP. [27, 28] The main role of this coactivator is to link HIF to the basal transcription machinery and other potential coactivators but can also act to relax the chromatin prior the transcription process through its histone acyltransferase activity.[29]

The binding of the HIF heterodimer to the DNA regulatory region of the target genes and its subsequent transactivation enables the overexpression of many genes involved in the hypoxic response. However, the complex remains constantly regulated by tight oxygen-dependent and independent mechanisms.

1.1.2 Regulation of HIF-1

The main role of the HIF transcription factor is to rapidly and efficiently induce a cellular response to low oxygen environments by acting as an oxygen sensor and transcriptional effector.

As previously mentioned, the HIF heterodimer is composed of two subunits, 1α and 1β, which are constitutively expressed. However, HIF's role as an oxygen sensor only relies upon the α subunit as 1β is unaffected by oxygen levels. The alpha subunit is regulated on a post-translational level by various oxygen-dependent mechanisms that enable the inactivation or degradation of the protein. Although the protein is constantly being expressed, the presence of oxygen induces its degradation within 5 minutes.[30] The continuous production of HIF-1α, even in presence of oxygen, enables a rapid hypoxic response when oxygen levels drop.

To prevent HIF's activity in normoxia, two main mechanisms act upon post-translational modifications of the protein on three specific residues: Pro402 and Pro564, found within the N-TAD in the ODDD, and Asn803 located within the C-TAD (**Figure 4a**). These three residues are hydroxylated so as to induce HIF-1α degradation or inactivation.

The main oxygen-dependent regulation of 1α relies on its degradation (**Figure 4b**). In normoxia, the Pro402 and Pro564 residues are recognised by a prolyl-hydroxylase domain-containing protein (PHD) that utilises oxygen, iron and α-ketoglutarate as substrates to hydroxylate the two prolines.[31, 32] Three different isoforms of PHD (PHD1, PHD2 and PHD3) have been reported, but

PHD2 was found the most important isoform involved in HIF-1α degradation with little or no effect from the two other isoforms on HIF-1α's degradation.[31, 33] Hydroxylation of these two residues induces their subsequent recognition by the Von Hippel-Lindau tumour suppressor protein (VHL).[34-36] VHL is a component of an E3-ligase complex also composed of an Elongin B/C (Elo B/C) that links VHL to a Cullin-2 protein (Cul2).[37] The latter is itself bound to a Ring-box protein (Rbx1) which binds a ubiquitin-carrying E2 enzyme. E2 acts as a ubiquitin conjugating enzyme and is responsible for the downstream ubiquitination of the target protein, in this case, HIF-1α. The polyubiquitin tail of HIF-1α acts as a recognition tag for addressing the protein to the proteasome where it is subsequently degraded.

In addition to the VHL-dependent degradation of HIF in normoxia, a second level of oxygen-dependent control of HIF is ensured by Factor-Inhibiting HIF (FIH) (**Figure 4c**). FIH is a hydroxylase that utilises the same substrates as the PHDs to hydroxylate the Asn803 residue in normoxic conditions.[38, 39] In contrast with the PHD-mediated prolyl-hydroxylation, the asparaginyl-hydroxylation of Asn803 does not induce the degradation of HIF but rather its inactivation. Located within the C-TAD domain, Asn803, once hydroxylated, prevents the binding of the CBP/p300 coactivators to the C-TAD, thus inhibiting the transactivation of HIF.[39]

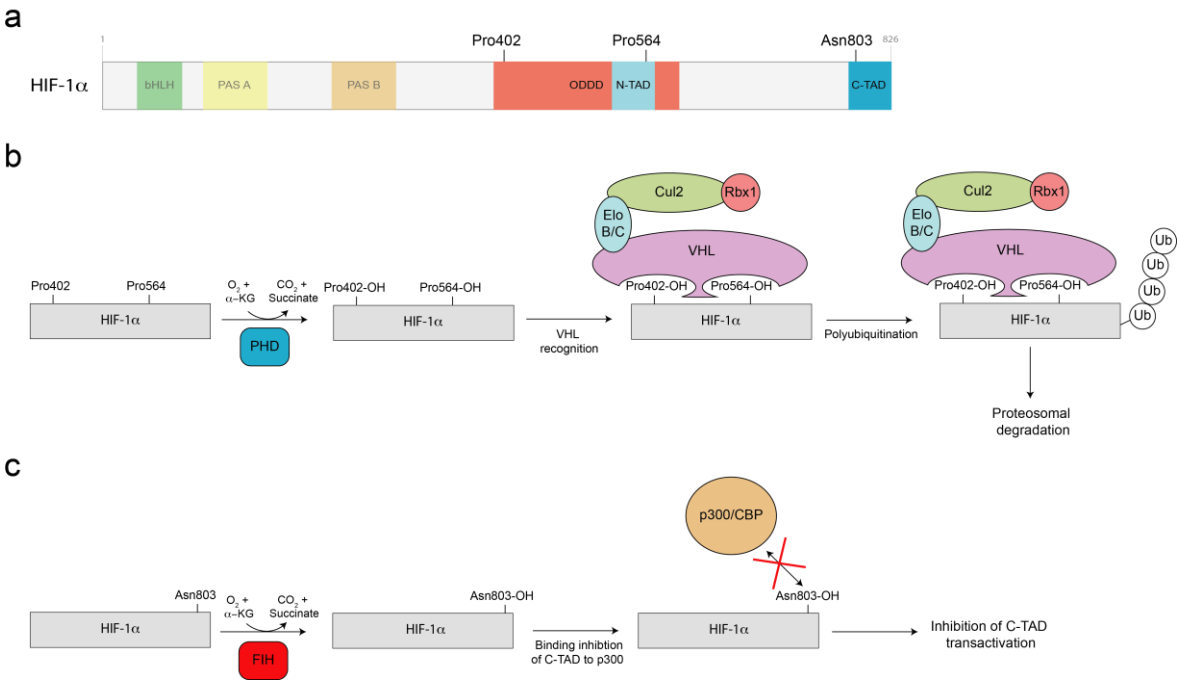

Figure 4. **Oxygen-dependent regulation of HIF by hydroxylases. (a)** Structure of HIF-1α displaying the location of the three residues hydroxylated in normoxia. **(b)** PHD-mediated hydroxylation of Pro402 and Pro564 and subsequent VHL recognition. **(c)** Hydroxylation of Asn803 by FIH inducing an inhibition of transactivation. Cul2: Cullin-2; Elo B/C: Elongin B and C; FIH: Factor-Inhibiting HIF; PHD: Prolyl hydroxylase domain containing protein; Rbx1: Ring-box 1 ; VHL: Von Hippel-Lindau.

The PHD-mediated hydroxylation of Pro402 and Pro564, as well as the FIH-mediated hydroxylation of Asn803, entirely rely on the availability of oxygen which is used as substrate for the two hydroxylases. Although the presence of oxygen enables the hydroxylation of the above-mentioned residues and the downstream inactivation and degradation of HIF-1α, FIH displays a greater affinity for molecular oxygen than the PHDs.[40] On a mechanistic aspect, this means that as the oxygen levels decrease, the inhibition of the PHDs will occur before the inhibition of FIH. At intermediate oxygen levels, whilst the PHDs are inhibited and HIF-1α subsequently stabilised, the molecular oxygen levels are still sufficient for FIH to function thus leading to a partial hydroxylation of HIF on Asn803 only. In these conditions, HIF-1α can accumulate within the cells but the C-TAD transactivation cannot occur, leading to a transcriptional activation of genes specific to the N-TAD.[41] In severe hypoxia, FIH is eventually inhibited enabling a full activation of transcription.

As described, the oxygen-dependent regulation of HIF occurs by post-translational modification of the protein enabling its stabilisation and transactivation in hypoxic conditions. However, HIF is also regulated by many other pathways that are oxygen-independent. In particular, HIF-1α protein levels and transcriptional activity can be regulated by many external factors such as cytokines or growth factors, which can activate downstream signalling pathways such as PI3K/Akt/mTOR and MAPK.[42-44] In addition to acting directly upon HIF-1α synthesis or transcriptional activation, mechanisms involving oxygen-independent degradation of HIF-1α have been described. The receptor of activated protein kinase 1 (RACK1) can bind 1α and subsequently recruit an E3 ligase complex to ubiquitinate HIF and tag it for proteosomal degradation independently of VHL.[45] Similarly, Hsp70 is able to bind 1α and recruit the ubiquitin ligase carboxyl terminus of Hsc70-interacting protein (CHIP), thus inducing HIF ubiquitination and its subsequent degradation.[46] Another E3 ubiquitin ligase, known as the hypoxia-associated factor (HAF), has been reported to promote the ubiquitination and consequent degradation of HIF-1α independently of VHL and oxygen levels.[47]

The tight regulation of HIF-1α ensures a proper and rapid cellular response to decreased oxygen levels. HIF-1 is responsible for the activation of a large number of genes but the hypoxia response and associated HIF regulation is more complex. Two more isoforms of the HIF-α subunit, namely HIF-2α and HIF-3α, co-exist with HIF-1α in order to contribute to the regulation of the hypoxia response.

1.1.3 HIF isoforms and their differential roles

1.1.3.1 HIF-2α and HIF-3α

In 1992, Semenza *et al*., reported for the first time the transcriptional activation of the gene encoding for erythropoietin (EPO) in response to hypoxia.[48] This finding enabled the discovery of the HIF-1 transcription factor, which in their study was composed of HIF-1α and HIF-1β. The 1α isoform was thus the first α subunit of the HIF transcription factor to be described but following this, it has been shown that there are three genes encoding for three distinct isoforms of the HIF-α subunit: HIF-1α, HIF-2α and HIF-3α. In addition to being the first isoform described, 1α is also ubiquitously expressed whereas HIF-2α and HIF-3α were shown to be tissue specific.[49, 50]

HIF-2α and HIF-3α, like their 1α counterpart, belong to the bHLH-PAS family. The three proteins thus display a high degree of homology between conserved bHLH and PAS domains which leads to common functions, such as their ability to dimerise with 1β. Indeed, 1α and 2α display 67% and 84% of homology between their PAS domains and bHLH domains, respectively.[49] In comparison, HIF-3α displays 57% and 74% of homology between its PAS domains and bHLH domains compared to HIF-1α.[51]

It should be noted that HIF-3α, in addition to having less homology with 1α than the 2α isoform, possesses characteristics that distinguish it from 1α and 2α. First, the 3α mRNA can splice so as to lead to a number of different isoforms which all lack the C-TAD domain.[50] This specific feature indicates that, in contrast with 1α and 2α, the 3α isoform can presumably act not as a transcription factor once bound to 1β due to a lack of transactivation. In addition, HIF-3α mRNA levels were found to be upregulated in hypoxia in a HIF-1 dependent-manner whereas no effect of HIF-2 were observed.[52] In addition to binding to 1β, different variants of 3α can also interact with HIF-1α and HIF-2α thus potentially competing with 1β and subsequently inhibiting HIF-induced gene expression.[53]

As previously mentioned, HIF-2α, also known as endothelial PAS protein 1 (EPAS1), displays a high degree of homology with HIF-1α. In addition to the high homology between their PAS and bHLH domains, HIF-2α also contains a C-TAD as well as an N-TAD located within the ODDD, both similar to the ones previously described for HIF-1α (see **section 1.1.1**, **Figure 2**). The presence of these three domains implies that HIF-2α is regulated in an oxygen-dependent manner in the same manner as HIF-1α. Indeed, the two proline residues within the ODDD as well as the asparagine residue in the C-TAD found in 1α are conserved in 2α. The three residues are located within the same domains but are found at slightly different positions than in their 1α counterparts. The HIF-2α Pro405, Pro531 and Asn851 residues are subjected to the same oxygen-mediated

hydroxylation mechanisms than in the 1α isoform, leading to HIF-2α degradation in the presence of oxygen and stabilisation in hypoxia.[35, 54]

Crystal structures of the 2α/1β and 1α/1β heterodimers bound to their HRE showed that the high homology between the primary sequences of 1α and 2α is reflected in their tertiary structures, as the two transcription factor complexes in their active conformation are indistinguishable from one another.[21]

The presence of the transactivation domains within the 2α isoform indicates that, like for 1α, upon dimerisation to 1β and subsequent DNA binding, the 2α/1β complex forms a fully active transcription factor referred to as HIF-2. Although structurally very similar, HIF-1 and HIF-2 have both common and unique target genes, conferring them distinct functions throughout the hypoxia response process.[55]

1.1.3.2 HIF-1α and HIF-2α: implication in cancer and target genes

High levels of HIF-α have been observed in a wide range of human cancer cells, and in many cases were found to correlate with poor prognosis.[56-58] However, it should be noted that HIF-1α has also been reported to correlate with a positive outcome in some cell subtypes such as renal clear carcinoma cells (RCC).[59] In addition, in some cancer cell types only one of the two α isoforms correlates with poor outcome despite both isoforms being present, suggesting the existence of differential roles between the two proteins.[60, 61] This differential response between 1α and 2α can partly be explain by the fact that, despite targeting common genes, each isoform also regulates unique target genes.

HIF targets are comprised of many proteins involved in diverse cellular functions such cellular metabolic adaptation, pH regulation, angiogenesis, cell proliferation, invasion and erythropoiesis. Modifications of these diverse cellular processes enable the creation of a favourable environment for tumour progression, aggressiveness and metastasis ability (**Figure 5**).

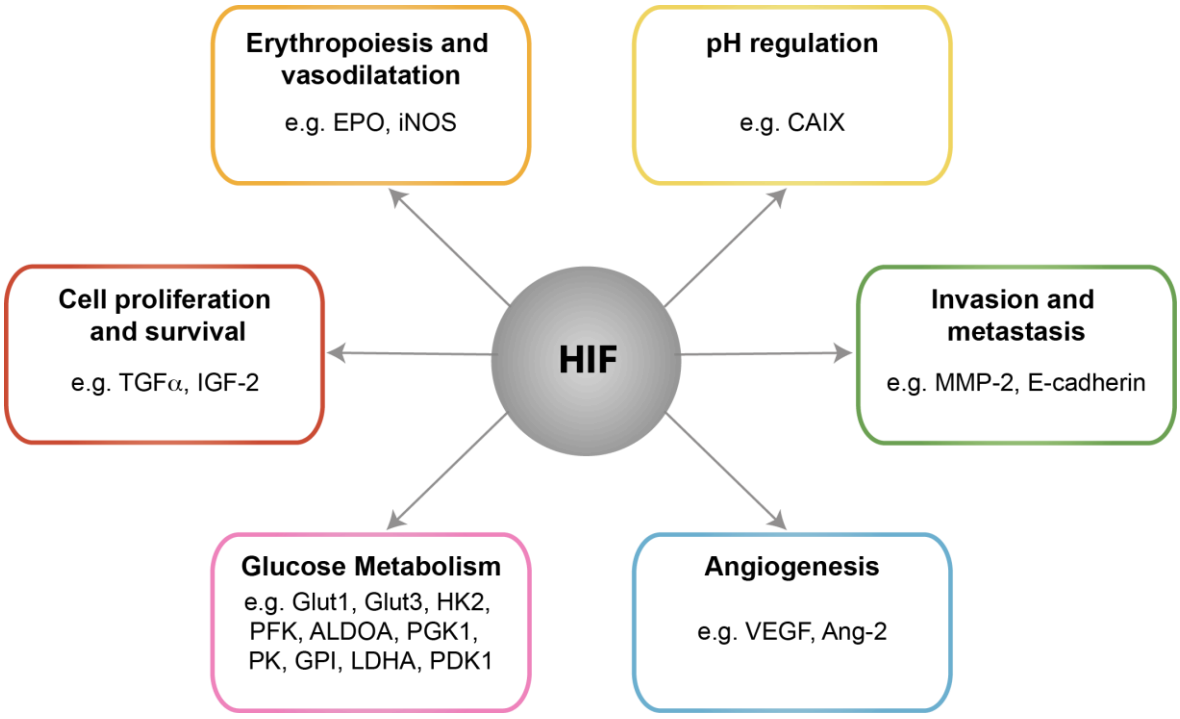

Figure 5. **Target genes of HIF and downstream functions.** In order to enable an efficient adaptation to low oxygen environments, HIF regulates the gene expression of a wide variety of targets involved in many different cellular functions such as pH regulation, invasion, metastasis, angiogenesis, glucose metabolism, cell proliferation and survival as well as erythropoiesis and vasodilatation.

Healthy mammalian tissues require proper oxygenation to function, and the low oxygen tension found in tissues experiencing hypoxia leads to the upregulation of genes involved in angiogenesis, erythropoiesis and vasodilation in order to restore the oxygen homeostasis.

The first step into tissue reoxygenation is the formation of new vasculature. New blood vessels ensure not only oxygen but also nutrient delivery, indispensable for the formation and development required for the early stage of malignant tumour progression. Tumour hypoxia induces the upregulation of many genes in order to activate angiogenesis. As an example of such, the vascular endothelial growth factor (VEGF), whose upregulation is induced by both HIF-1 and HIF-2 depending on cell types, enables the formation of new blood vessels.[62, 63] This process happens by binding of VEGF to its receptor (VEGFR) which induces the subsequent activation of downstream signalling pathways. VEGFR was found to be upregulated in hypoxia in a HIF-dependent manner, with different isoforms of the receptor being expressed in different cancer cell types.[64, 65] Due to its role in angiogenesis, VEGF also plays a major role during embryo development as well as organogenesis throughout the adult life.[66]

In addition to VEGF, many other pro-angiogenic factors such as fibroblast growth factor (FGF), platelet-derived growth factor (PDGF) and angiopoietin-1/2 (Ang-1/2) are upregulated in hypoxia to ensure the formation of the new vasculature.[67, 68]

To support the restoration of oxygen delivery, HIF also upregulates genes involved in the formation of new red blood cells, known as erythropoiesis. One of the most important proteins involved in erythropoiesis is erythropoietin (EPO). The *epo* gene has been known to be induced in hypoxia for many years, which sustained the existence of oxygen-dependent gene regulation. Work based on the *epo* gene locus enabled the discovery of HIF-1, although further studies then demonstrated that the *epo* gene is solely modulated by HIF-2.[48, 69, 70] In order to efficiently deliver oxygen via the newly made vasculature and the increased number of blood cells available, HIF mediates the increase in expression of inducible nitric oxide synthase (iNOS), an enzyme responsible, among other functions, for the vasodilatation of the blood vessels.[71]

The process of tumour development implies the ability of cancer cells to survive and to keep proliferating. To ensure these functions, HIF upregulates the expression of various proteins such as transformant growth factor-α (TGF-α), insulin-like growth factor 2 (IGF2) and IGF-binding proteins.[72, 73]

One of the features of tumour hypoxia, in addition to aggressive cell growth, is enhanced invasiveness and metastasis ability. In some types of aggressive and invasive cancers such as malignant gliomas and breast cancers (among others), HIF plays a role in facilitating tumour cell detachment and downstream invasion by downregulating genes encoding for adhesion molecules such as E-cadherin (E-cad), and upregulating the expression of the matrix metalloproteinase-2 (MMP-2).[74-77] Decreased expression of E-cadherin enables cell detachment and is partly responsible for the so-called epithelial-to-mesenchymal transition (EMT), known as a key step towards tumour invasion. In addition, MMP-2 is an enzyme responsible for the degradation of the extracellular matrix. It is considered as a pro-angiogenic factor and its HIF-induced upregulation contributes to the relaxation of the tumour tissue.[78] Altogether, these proteins contribute to the hypoxia-mediated decrease in cell adhesion and induce the detachment and spreading of the tumour, thus conferring invasiveness properties to cancer cells.

The metabolism of healthy mammalian tissues relies upon the availability of oxygen in order to carry out most of the cellular processes, especially the synthesis of the energy molecule, ATP. Because of this dependence, mammalian systems are extremely sensitive to changes in their surrounding oxygen tension and an exposure to low oxygen environments requires an adaptation of the cellular metabolism.[79]

Hypoxic cancer cells are known to switch their metabolism from cellular respiration to an oxygen-independent aerobic glycolysis in order to ensure the synthesis of ATP. To carry out this switch, the glucose metabolism is upregulated in hypoxia with the majority of the genes involved in this process being under the regulation of HIF-1 only (**Figure 6**). The uptake of glucose is increased via the enhanced expression of glucose transporters such as GLUT1 and GLUT3 with *glut1* being one of the rare metabolism-related gene mediated by both HIF-1 and HIF-2.[63, 80-84] In order to efficiently process the uptaken molecules of glucose, most of the glycolysis enzymes are also upregulated (e.g hexokinase 1 and 2 (HK1 and HK2), phosphofructokinase (PFK), phosphoglycerate kinase 1 (PGK1), etc.), thus leading to an increased production of pyruvate, the latter being subsequently converted into lactate via the HIF-1-upregulated lactate dehydrogenase (LDHA).[63, 83, 85, 86] To further ensure the conversion of pyruvate into lactate, HIF-1 activates a second regulatory mechanism by inducing the expression of pyruvate dehydrogenase kinase 1 (PDK1).[83] PDK1 can inhibit pyruvate dehydrogenase (PDH), thus preventing the conversion of pyruvate into acetyl-coA which subsequently inhibits the tricarboxylic acid (TCA) cycle.[87] Lactate can then be exported from the cells by its transporter, monocarboxylate transporter 4 (MCT4), which is itself upregulated by HIF-1.[88] MCT4 ensures the proton-coupled transport of lactate and thus contributes to the intracellular deacidification and subsequent extracellular decrease in pH.[89] In the same way, HIF-1 induces the expression of the metalloenzyme carbonic anhydrase IX (CAIX) which enables the conversion of carbon dioxide and water into HCO_3^- and H^+ in order to maintain an alkaline intracellular pH and extracellular acidic pH.[90] Acidic extracellular pH is a common hallmark of cancer, especially in solid tumours and the maintenance of an alkaline intracellular pH is known to facilitate tumorigenicity and cell proliferation.[91, 92]

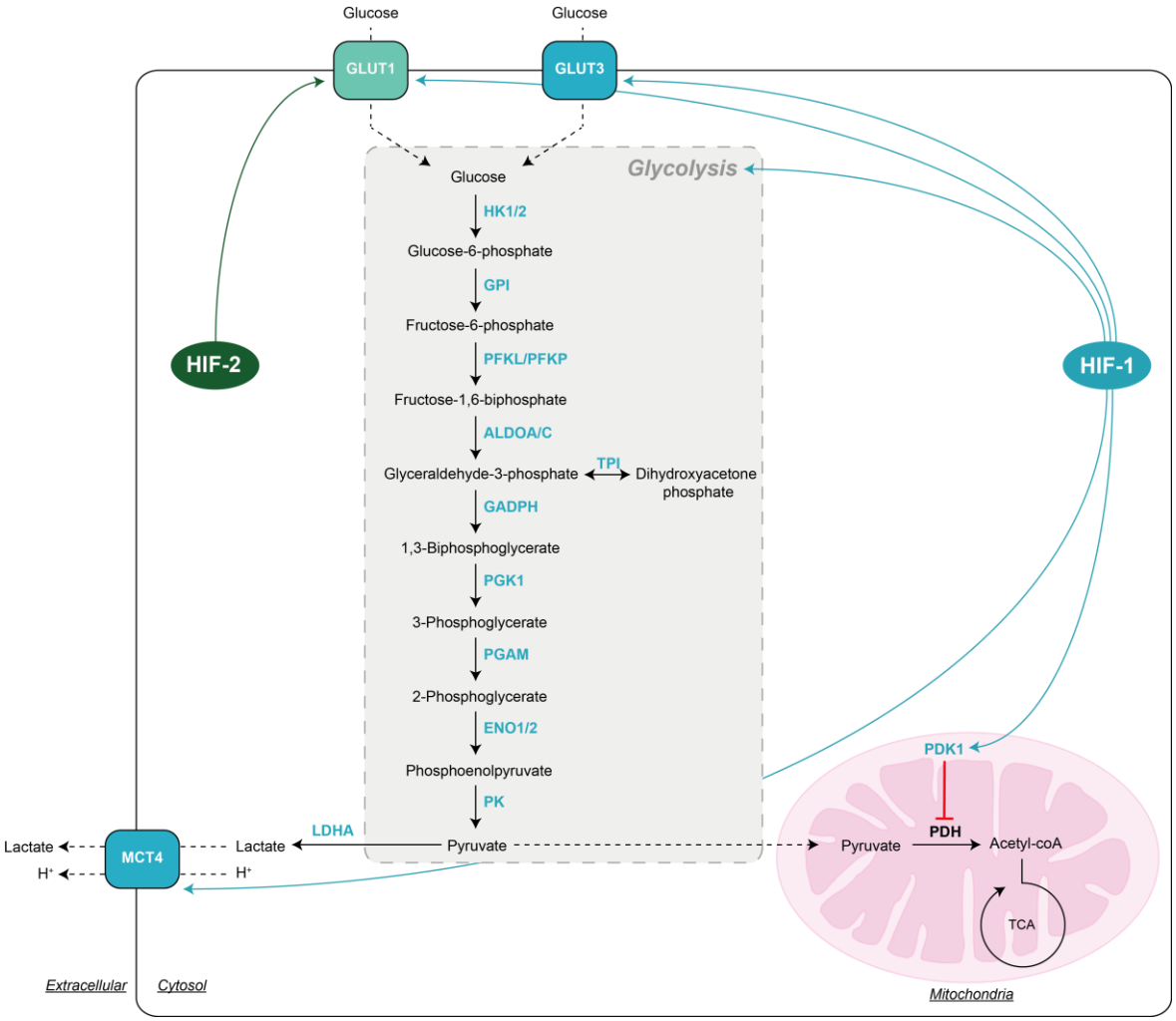

Figure 6. **Regulation of the glucose metabolism by HIF.** Blue proteins are upregulated by HIF-1. GLUT1 is upregulated by both HIF-1 and HIF-2. Glycolysis pathway is carried out in the cytosol and is represented in the dashed light grey box. All the glycolytic enzymes displayed are upregulated by HIF-1.[63, 83, 85, 86, 93-96] HIF-1 affects the mitochondrial metabolism by upregulating PDK1 which downstream inhibits PDH. This prevents the conversion of pyruvate into acetyl-coA and its subsequent entrance in the TCA cycle, thus leading to a slow down/arrest of the TCA cycle. Instead, accumulated pyruvate is rewired towards conversion into lactate via upregulation of LDHA. HIF maintains the intracellular pH by increasing the export of lactate via the upregulation of MCT4.

The upregulation of glucose metabolism by HIF-1 symbolises the differential roles between 1α and 2α. However, glucose metabolism is only one of many metabolic pathways impacted by hypoxia. Many cross-talks exist between metabolic pathways which makes the metabolic cell adaptation to low oxygen environments much more complex.

1.1.4 Adaptation of cell metabolism to hypoxia

Healthy human cells require oxygen to produce their energy molecule, ATP (**Figure 7a**). In physiological conditions, glucose is imported from the extracellular environment and converted into pyruvate via glycolysis (as previously described in **section 1.1.3.2** and **Figure 6**). The conversion of one molecule of glucose during the glycolysis process enables the formation of 2 molecules of ATP. Pyruvate is subsequently transported into the mitochondria where it gets converted into acetyl-coA, the first substrate of the TCA cycle. The TCA cycle is comprised of 8 reactions and constitutes the second step of cellular respiration after glycolysis. Its main role is to produce the reduced cofactors NADH and $FADH_2$ which can then be used as electron donors in the mitochondrial electron transport chain (ETC), the third and last step of cellular respiration. The conversion of one molecule of glucose by the glycolysis / TCA pathway yields 2 molecules of $FADH_2$ and 10 of NADH. Electrons from these reduced cofactors are transferred to O_2 in the ETC which leads to the formation of the oxidised forms of the factors and protons. The latter are pumped across the inner mitochondrial membrane creating a proton-motive force enabling the synthesis of ATP by ATP synthase. The overall energy production of this process is 36 ATP molecules (2 from glycolysis, 2 from TCA and 32 from ETC) per molecule of glucose.

In hypoxia, the reduced O_2 availability leads to a slowdown of the ETC due to the lack of a terminal electron acceptor, thus inducing an important decrease in the mitochondrial ATP production (**Figure 7b**). Due to this limited ETC rate, NADH levels increase leading to a reduction in the rate of the NADH-producing TCA reactions. Overall, hypoxia induces an almost complete shutdown of the mitochondrial cellular respiration, and the ATP production in these conditions mostly relies upon the glycolytic production. In these conditions, the previously described HIF-induced upregulation of the glycolysis pathway enables the maintenance of a favourable glycolytic rate and ensures a sufficient glycolytic ATP production to support cell growth.

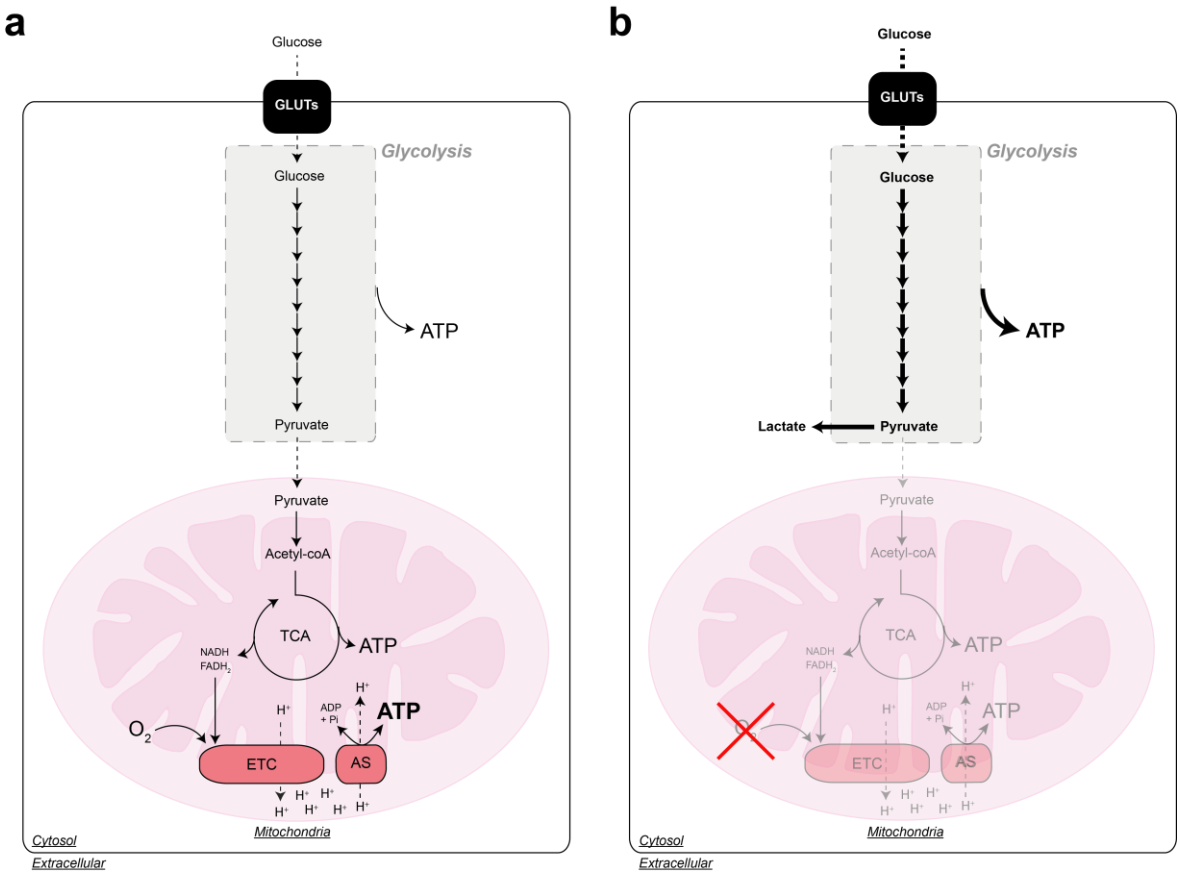

Figure 7. Switch from oxidative phosphorylation to aerobic glycolysis in hypoxia.
(a) Mammalian cells exposed to normal oxygen environments metabolise glucose via the glycolysis pathway. The final product, pyruvate, is transported into the mitochondria and ensures the functioning of the TCA and ETC. In the ETC, electrons are transferred to the terminal acceptor O_2 which enables the synthesis of ATP by ATP synthase (AS). **(b)** In hypoxia, the lack of O_2 prevents the activity of the ETC which induces a slowdown / arrest of the TCA cycle. Pyruvate is converted into lactate and the synthesis of ATP mostly relies on enhanced glycolytic ATP production.

Glycolysis produces intermediate molecules that are used as substrates by branched metabolic pathways. Thus, maintaining glucose metabolism is crucial, not only to enable ATP production, but also to ensure the synthesis of biosynthetic building blocks such as ribose-phosphates and one-carbon units required in amino acid and nucleotide synthesis. As the glycolytic rate increases in hypoxia, the levels of glycolytic intermediates build up and the branched pathways metabolising these substrates are upregulated in order to efficiently process them (**Figure 8**).

As an example of such, glycolysis is directly branched to the pentose phosphate pathway (PPP). The product of the first glycolytic step, glucose-6-phosphate (G6P), can either be processed by the next steps of glycolysis or be used as a substrate in the oxidative branch of the PPP. The oxidative

PPP is comprised of three irreversible enzymatic steps that enable the production of two molecules of NADPH as well as one molecule of ribulose-5-phosphate, which can subsequently be converted into ribose-5-phosphate, used in the synthesis of nucleotides. NADPH plays an essential role in scavenging reactive oxygen species (ROS) and thus enables cell survival under stress conditions.

The first substrate of the oxidative PPP, G6P, is converted into 6-phosphogluconolactone by the enzyme glucose-6-phosphate dehydrogenase (G6PD). This reaction simultaneously forms one of the two NADPH molecules produced during the oxidative PPP. As the first enzyme of the pathway, G6PD is considered as the "gatekeeper" of the PPP and its activity conditions the rate of the pathway. Contradictory data have been reported on the expression of G6PD in hypoxia. The enzyme was found to be upregulated in hypoxia in different cell types and to be downregulated in breast cancer cell lines, which might suggest that the reliance of hypoxic cancer cells on PPP is likely to be cell-type dependent.[97-99]

The last enzyme of the oxidative PPP, 6-phosphogluconate dehydrogenase (PGD), catalyses the conversion of 6-phosphogluconate into ribulose-5-phosphate and simultaneously forms the second NADPH molecule of the PPP. PGD was shown to be up-regulated by HIF-1 in hypoxia, suggesting an increased rate of the pathway in hypoxia.[100]

Furthermore, it is interesting to note that in some cells lines, HIF-1α was shown to increase the synthesis of ribose-5-phosphate via the non-oxidative branch of the PPP by upregulating the expression of the transketolase enzyme.[101] In addition, metabolomic analyses showed increased levels of PPP intermediates which strengthened the hypothesis of an hypoxia-induced increased flux through the PPP.[102]

Aside from its hypoxia-induced upregulation, the PPP is commonly enhanced in cancer cells and plays a major role in their metabolic adaptation.[103] Cancer cells are known to switch their glucose metabolism from cellular respiration (previously described) to aerobic glycolysis. Despite the presence of oxygen, cancer cells rewire their glucose metabolism into lactate production rather than mitochondrial oxidative phosphorylation so as to solely rely on glycolysis for energy production, in the same way as hypoxic cells. This phenomenon is known as the Warburg effect.[104, 105] Growing evidence suggests that, in the same way as glycolysis, higher flux through the PPP is observed in cancer cells. In fact, G6PD and PGD have both been reported to play a role in the proliferation of different cancer cell types and G6PD has been associated with poor patient outcome. [106, 107] It is unsurprising to observe an increased rate of the PPP in cancer cells as this pathway enables an increase in the NADPH and ribose phosphates production, which play a major role in preventing ROS-induced stress and sustaining nucleotide synthesis, respectively.

In addition to the PPP, the *de novo* synthesis of serine, also known as the serine synthesis pathway (SSP), is a biosynthetic pathway branched to glycolysis. Serine is an amino acid that plays a central role in the biosynthesis of many molecules as it acts as a precursor for the synthesis of the nonessential amino acids glycine and cysteine that are both involved in nucleotide synthesis, especially purines, as well as lipid and amino acid metabolisms.[108] The glycolytic intermediate 3-phosphoglycerate (3-PG) is converted into serine by a series of three enzymatic steps. The three enzymes catalysing these reactions, namely phosphoglycerate dehydrogenase (PHGDH), phosphoserine aminotransferase 1 (PSAT1) and phosphoserine phosphatase (PSPH) were reported to be upregulated in cancer cell lines experiencing hypoxia.[98] The enhanced hypoxic rate of the SSP leads to an increased availability of serine that can further be converted into glycine by serine hydroxymethyltransferases (SHMTs), which have a cytosolic isoform (SHMT1) and a mitochondrial isoform (SHMT2).[109, 110] Via its conversion into glycine by SHMT, serine supplies carbon to the one-carbon metabolism, and particularly to the folate cycle. During this reaction, serine donates one carbon to tetrahydrofolate (THF) to enable the production of 5,10 methylenetetrahydrofolate (5,10-mTHF), which can subsequently be used in thymidine synthesis or act as a precursor for 10-formyl tetrahydrofolate (10-f-THF), a co-factor required in *de novo* purine biosynthesis. As the rate of serine synthesis increases, SHMT2 levels were found to be upregulated in hypoxia in a HIF-1-dependent manner solely in cells expressing high levels of MYC, so as to efficiently catabolise the newly synthesised serine.[111] Cells displaying low expression levels of MYC did not show an upregulation of SHMT2 in hypoxia, however, overexpression of MYC in these cells restored SHMT2 upregulation in hypoxia, suggesting that the hypoxia-induced upregulation of SHMT2 is cell type dependent (i.e expression levels of MYC).[111] In addition, when upregulated in hypoxia, SHMT2 was shown to be required to maintain redox homeostasis in hypoxic cells, likely by maintaining high levels of NADPH. Indeed, the conversion of 5,10-mTHF into 10-f-THF by the methylenetetrahydrofolate dehydrogenase (MTHFD) enzyme enables the concomitant formation of NADPH. As SHMT2 modulates the entry of a carbon unit into the folate metabolism and thus regulates its rate, SHMT2 activity acts upon the redox homeostasis of the cells. Therefore, increased SHMT2 activity likely induces an enhanced production of ROS-scavenging NAPDH.

The reliance of cancer cells on serine synthesis has been widely defined over the years.[108, 112, 113] Metabolic flux through the SSP was found to be increased in tumour cells compared to their healthy counter-parts, especially in the case of the PHGDH enzyme.[114, 115] In addition, studies carried out on tumours showed a strong correlation between increased PHGDH activity and upregulation of SHMT2 activity, suggesting that SHMT and the SSP are critical for tumour development.[116]

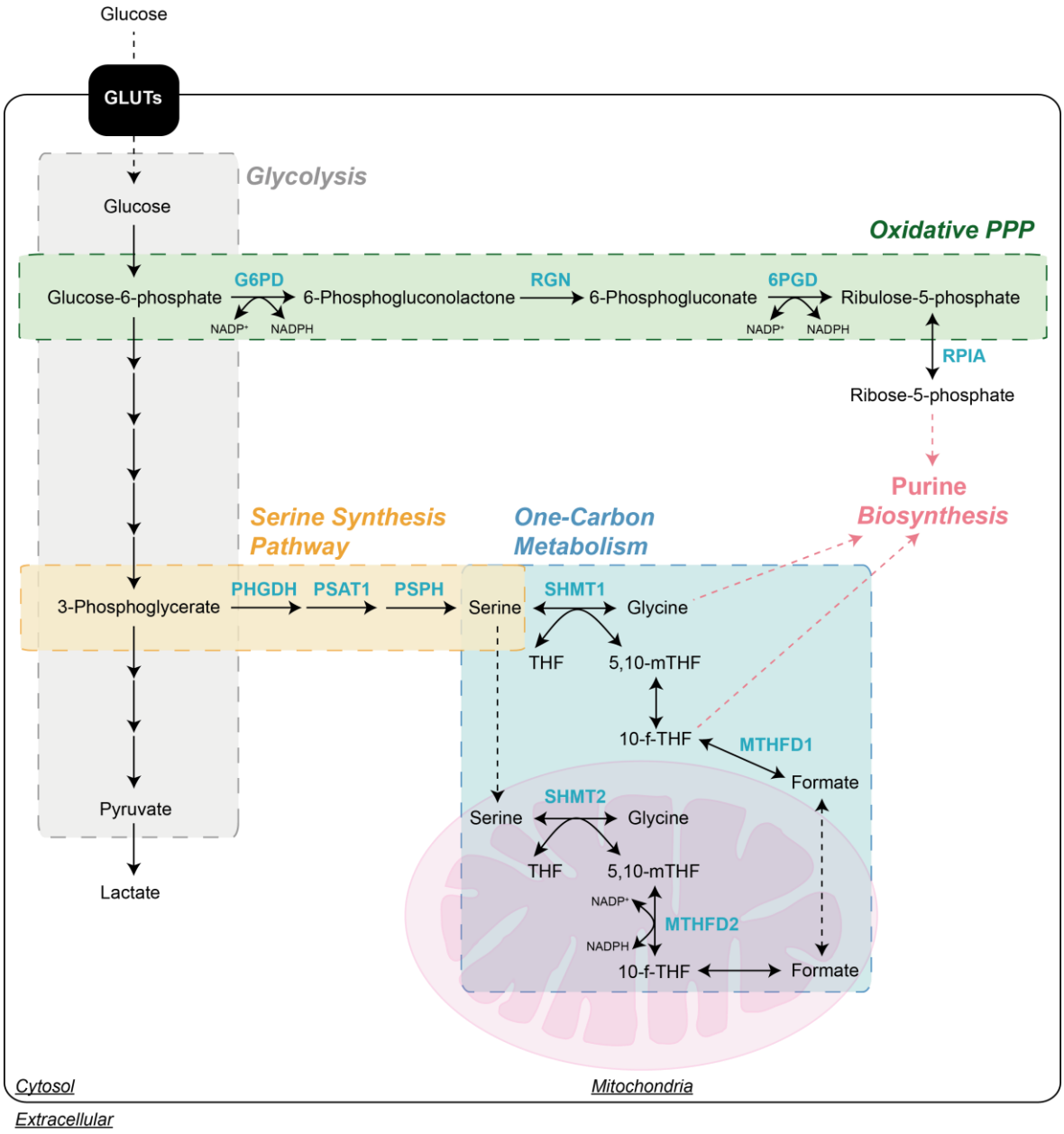

Figure 8. **Interconnections of metabolic pathways impacted by hypoxia.** Metabolic pathways are linked to one another, as some intermediates of one pathway are used as substrates for another. The main energy input of the cells is glucose, which is subsequently transformed in the glycolysis pathway (grey pathway). Different intermediates of the glycolysis pathway feed parallel metabolisms, such as glucose-6-phosphate which is used as substrate by the pentose phosphate pathway (PPP – green pathway) and 3-phosphoglycerate, which is a substrate of the *de novo* synthesis of serine (yellow pathway). Serine is subsequently used in the serine/glycine metabolism and downstream folate cycle that together constitute the one-carbon metabolism (blue pathway). One-carbon metabolism is carried out in both the cytoplasm and the mitochondria. All of these pathways provide substrates and cofactors for the synthesis of purines (red pathway).

In mild hypoxia (0.5%-2% oxygen), the cell metabolism is reprogrammed in order to prevent cell death and ensure the synthesis of molecules required for cell growth and proliferation. Both the PPP and SSP contribute to these processes by (i) enabling the synthesis of NADPH required for ROS-detoxification, preventing cell damage and downstream apoptosis (ii) ensuring the formation of biosynthetic building blocks required for the synthesis of vital macromolecules such as nucleotides.

Maintaining cell growth and proliferation implies that the cells keep synthesising DNA and RNA, essential to ensure a plethora of cellular functions, including the ability to carry out mitosis. Over the years, increased flux through the previously described pathways has been described in hypoxic cells and, due to their major input into nucleotide synthesis, the latter has been hypothesised to be upregulated following the increased availability of substrates and cofactors. However, very little is known about the effect of hypoxia on nucleotide synthesis. As cancer cells, and especially hypoxic cells, manage to maintain cell growth and proliferation, it is thought that their nucleotide synthesis is likely to adapt to these low oxygen environments.

Nucleotides are comprised of two distinct types of base, the pyrimidines and the purines. Both contain a ribose unit synthesised by the PPP, but the *de novo* synthesis of purines requires co-factors produced by the above-mentioned SSP and one-carbon metabolism. Due to the hypoxic reprogramming of the PPP, SSP and one-carbon metabolism, it is highly possible that the purine biosynthetic pathway is affected by low-oxygen environments.

1.2 The purines and their biosynthesis

1.2.1 Structures and roles of the purines

Purines are amongst the most abundant metabolic substrates in living organisms. They are involved in many vital cellular processes such as signalling, energy storage, synthesis of cofactors but more importantly, they are building blocks for the synthesis of nucleic acids. Out of the four common bases found in nucleic acids, two of them, adenine (A) and guanine (G), belong to the purine class of molecules. This way, purines constitute 50% of the DNA and RNA.

The term “purine” originally describes the purine ring, which constitutes the backbone of the purine bases, nucleosides and nucleotides. The purine ring is composed of six-membered and five-membered nitrogen-containing fused rings (**Figure 9**). Addition of different functional groups onto the purine ring leads to the formation of distinct bases. Indeed, addition of an amino group onto the C6 of the purine ring leads to the formation of adenine. Similarly, guanine is constituted

of a purine ring onto which an amino group and a carbonyl group have been added onto the C2 and C6 positions, respectively.

Adenine and guanine, also referred to as the purine bases (or nucleobases), are mainly used as precursors for the synthesis of purine nucleosides. The latter are formed by addition of a pentose unit onto the N9 of the nucleobase, resulting in the formation of adenosine and guanosine. The pentose unit found in nucleosides is a ribose-5-phosphate, product of the pentose phosphate pathway (see **section 1.1.4**).

Purine nucleosides serve as precursors for the synthesis of purine nucleotides. One phosphate group is added onto the purine nucleoside enabling the formation of their nucleotide monophosphate counter-part, namely adenosine monophosphate, known as AMP and guanosine monophosphate, known as GMP.

Depending on the needs of the cells, an additional one or two phosphate groups can be added onto AMP and GMP, resulting in the formation of the di- and tri- phosphate nucleotides: ADP, ATP, GDP and GTP.

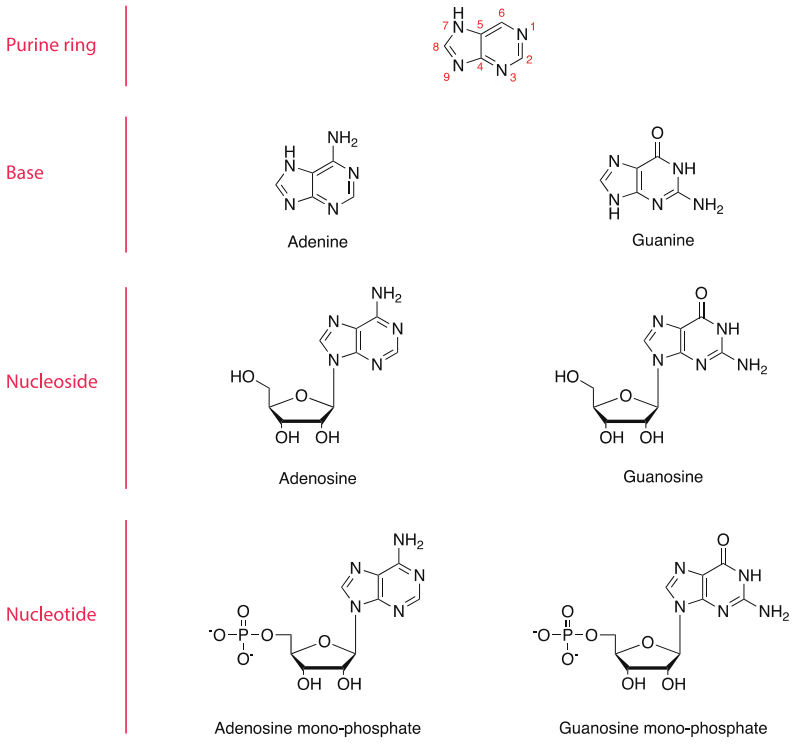

Figure 9. **Structure of purines.** The purine ring is composed of six-membered and five-membered nitrogen-containing fused rings. Each purine base displays different chemical functions added onto the purine ring. Addition of a ribose-5-phosphate onto the purine base enables the formation of the corresponding purine nucleoside.

Purine nucleotides can then be formed by adding a phosphate group onto the ribose unit of the nucleosides.

Purines perform a wide and diverse range of functions. As an example of such, GTP plays a key role in energy transfer as well as signal transduction via its binding to GTP-binding proteins, also referred to as G-proteins.[117] G-proteins, either heterotrimeric or monomeric, link the activation of a receptor by the binding of an extracellular signal to its downstream signalling effects. G-proteins in their inactive form are bound to GDP and upon receptor activation, GDP is exchanged for GTP. Binding of GTP induces the activation of the G-protein and subsequently activates the biochemical cascades aimed at modifying their ultimate target proteins. [116] This signalling process is terminated by the hydrolysis of the GTP molecule to GDP, which places the G-protein back in its inactive state.[118, 119]

The second purine triphosphate, ATP, is a vital metabolite as it constitutes the molecular unit of energy transfer in cells. Hydrolysis of ATP enables the generation of energy required for all cellular functions. In addition, ATP also plays an important role in signalling, both intracellular and extracellular.[120] Indeed, ATP is involved in intracellular signal transduction as its phosphate groups can be used by kinases in the reactions of phosphate transfer, which subsequently enable the activation of downstream enzymatic cascades.

ATP also acts as a major component of a specific type of extracellular signalling referred to as the purinergic signalling.[121] Mediated in part by ATP, the purinergic signalling is also modulated by ADP and adenosine. This specific form of signalling consists in the activation of purinergic receptors by the above-mentioned adenine-derived purines so as to regulate diverse cellular functions. The activation of these membrane-bound purinergic receptors by the binding of purines implies that purines are present in the extracellular environment. To modulate the extracellular availability of purines, the purinergic signalling is comprised of transporters, enzymes and purinergic receptors. There are different classes of purinergic receptors, each of them being specifically activated by certain nucleotides or nucleosides. As an example of such, the P1 purinergic receptor can only be activated by adenosine, whereas the P2Y receptor can be activated by both ADP and ATP (as well as UDP and UTP), all of them being nucleotides.[122] Thus, different adenine-based purines are required in the extracellular environment. To ensure this, nucleotide transporters allow the export of nucleotides and nucleosides from the cell.[123, 124] In addition, membrane-bound ectonucleotidases ensure the degradation of ATP into ADP, ADP into AMP and AMP into adenosine so as to enable the availability of all types of adenine-derived purines when required and the subsequent activation of their specific purinergic receptor.[125]

Purinergic signalling is commonly found under physiological conditions but over the years, it was found that purinergic signalling also plays a role in diverse pathological conditions, especially in cancer.[126, 127] In fact, ATP and adenosine are found in increased quantities in the tumour microenvironment (TME) and many malignant tumours were found to overexpress several purinergic receptors.[128-130] In addition, as the conversion of ATP into adenosine represents one of the basis of physiological purinergic signalling, it was found that the nucleotide-metabolising enzymes responsible for this conversion are also key components of the TME and happen to be activated by HIF-1α in hypoxic TME.[131, 132] The increased expression of these enzymes leads to increased extracellular adenosine levels which can subsequently activate the adenosine-mediated purinergic signalling, known to have an important immunosuppressive activity favouring the malignant context of tumour development.[133, 134]

Overall, increased extracellular purine availability coupled to the enhanced expression of key modulators of the purinergic signalling within the TME stimulate the purinergic signalling which subsequently favours immunosuppressive activity, stimulation of tumour growth as well as enhanced metastasis ability.[135-137] However, it is to note that, although the stimulation of purinergic signalling has been reported to mostly sustain the TME, some studies highlighted a decreased growth proliferation of tumour cells resulting from purinergic activation.[138-140]

As purinergic signalling represents a promising therapeutic target for cancer, diverse therapy strategies are currently being developed to inhibit this process in tumour cells, although the presence of purinergic receptors on normal cells limits the therapeutic potential and downstream effects of this approach.

As purines are involved in many cellular functions, they are also found as components of diverse molecules and cofactors such as the nicotinamide adenine dinucleotide (NAD), NAD phosphate (NADP) and flavin adenine dinucleotide (FAD). NAD is a small molecule composed of two nucleotide monophosphates. The two bases found in this dinucleotide are adenine and nicotinamide, and the two nucleotides are bound by their phosphate groups. NAD is one of the most important cofactors in the cell metabolism as it mediates redox reactions in various pathways such as glycolysis, TCA cycle, oxidative phosphorylation and serine biosynthesis. High levels of NAD in cells enables the enhanced rate of the enzymatic reactions that use NAD as a co-enzyme and thus sustains the rates of the pathways. In cancer cells, including hypoxic cancer cells, as metabolic pathways such as glycolysis and serine biosynthesis are affected, the replenishment of NAD maintains the rate of these pathways and thus sustains cell growth and proliferation. In the same way, NADP plays an important role in redox reactions, especially in the pentose phosphate pathway (as described in **section1.1.4**). Maintenance of NADP levels in cells enables a

proper functioning of the PPP with the resulting production of NADPH, required for major redox functions and prevention of cell death.

Purines, used in their nucleoside and nucleotide forms as well as components of cofactors, are thus involved in a plethora of cellular functions vital for cells. Aside from these cellular functions, the main role of purines is their function as building blocks for DNA and RNA. As the A and G bases compose 50% of the cellular nucleic acid pool of the cells, purines are thus vital cellular metabolites.

In regards to the major functions ensured by purines in cells, it is clear that their biosynthesis requires an excellent coordination and regulation to constantly ensure nucleotide production, DNA synthesis and subsequent cell growth, division and proliferation.

1.2.2 Biosynthesis of purines

In mammalian cells, levels of purine nucleotides are maintained by the coordination of two pathways: the salvage pathway and the *de novo* biosynthetic pathway (**Figure 10**).

Under physiological conditions, most of the purine pool is synthesised by the recycling of degraded purine bases via the salvage pathway (**Figure 10**, **red pathway**).[141-143] These purine bases, namely adenine, guanine and hypoxanthine, can result from DNA degradation or be imported from the extracellular environment. In the salvage pathway, the bases are converted into their corresponding nucleotide monophosphate via three parallel one-step enzymatic reactions that transfer a ribose unit from phosphoribosyl pyrophosphate (PRPP) onto the nucleobase. These three recycling enzymatic reactions are catalysed by two enzymes: adenosine phosphoribosyl transferase (APRT) that converts adenine into AMP, and hypoxanthine-guanine phosphoribosyl pyrophosphate (HGPRT, also called HPRT) that converts guanine and hypoxanthine into GMP and inosine monophosphate (IMP), respectively.

The salvage pathway enables the formation of nucleotides in a cost-effective way as the one-step enzymatic reactions do not require energy consumption. However, when cells require a high input of nucleotides for processes such as DNA amplification or high energy-consuming metabolisms, the *de novo* biosynthesis of purines is upregulated in order to meet the purine demand of the cells, maintain the nucleotide pool and enable the cell to carry out multiple metabolisms at the same time.[141, 143-145]

Originally characterised in avian liver enzymes 60 years ago, the *de novo* synthesis of purines is a series of 10 chemical steps catalysed by six enzymes, three of them being multifunctional (**Figure 10**, **blue pathway**).[146] The first reaction of the pathway is catalysed by phosphoribosyl

amidotransferase (PPAT) which ensures the conversion of PRPP into 5-phosphoribosylamine (PRA). PRA is then transformed into formylglycinamide ribonucleotide (FGAR) via two consecutive reactions catalysed by phosphoribosylglycinamide synthase (GARS) and phosphoribosylglycinamide formyltransferase (GAR Tfase), respectively. GARS and GAR Tfase constitute two domains of the trifunctional GART (also known as TrifGART). FGAR is subsequently converted in N-formylglycinamidine ribonucleotide (FGAM) by phosphoribosylglycinamidine synthase (FGAMS) during the fourth step of the pathway. The fifth step is catalysed by the third domain of GART, phosphoribosylaminoimidazole synthetase (AIRS), which enables the conversion of FGAM into aminoimidazole ribonucleotide (AIR). The next step of the pathway is catalysed by the bifunctional phosphoribosyl aminoimidazole carboxylase (CAIRS) / phosphoribosyl aminoimidazole succinocarboxamide synthetase (SAICARS) (PAICS). PAICS converts AIR into N-succinocarboxyamide-5-aminoimidazole ribonucleotide (SAICAR) in two concerted steps. SAICAR in then used as substrate by adenylosuccinate lyase (ADSL) which transforms it into aminoimidazole-4-carboxamide ribonucleotide (AICAR). This reaction constitutes the only reversible reaction of the pathway. Finally, the last two steps of the pathway are catalysed by a bifunctional enzyme, 5-aminoimidazole-4-carboxamide ribonucleotide formyltransferase (AICAR Tfase) / IMP cyclohydrolase (IMPCH), known as ATIC. These last two steps enable the conversion of AICAR into IMP, the final product of the *de novo* purine biosynthesis and main precursor of *de novo* synthesis of AMP and GMP.

The formation of AMP from IMP is a two-step process. The first reaction is catalysed by adenylosuccinate synthetase (ADSS) and ensures the conversion of IMP into adenylosuccinate (AMPS). The subsequent conversion of AMPS into AMP is catalysed by ADSL. In the same way, IMP is transformed into GMP by two consecutive reactions. The first transforms IMP into xanthosine monophosphate (XMP) and is catalysed by IMP dehydrogenase (IMPDH). GMP is then produced from XMP via the enzymatic activity of GMP synthase (GMPS).

Both *de novo* and salvage pathways use one molecule of PRPP as their first substrate to form one molecule of IMP. PRPP results from the conversion of ribose-5-phosphate, the final product of the PPP (**Figure 10**, **green pathway**), by PRPP synthetase 1 (PRPS1). To convert PRPP into IMP by the *de novo* biosynthetic route, the six enzymes of the pathway rely on many amino acids and cofactors, namely two molecules each of glutamine and 10-f-THF, one molecule each of aspartate, glycine and carbon dioxide, as well as five molecules of ATP. As previously described in **section 1.1.4** and **Figure 8**, most of these cofactors are provided by parallel metabolisms such as glycolysis, serine biosynthesis and one-carbon metabolism, indicating that *de novo* purine biosynthesis highly relies on the efficiency of its associated pathways to function.

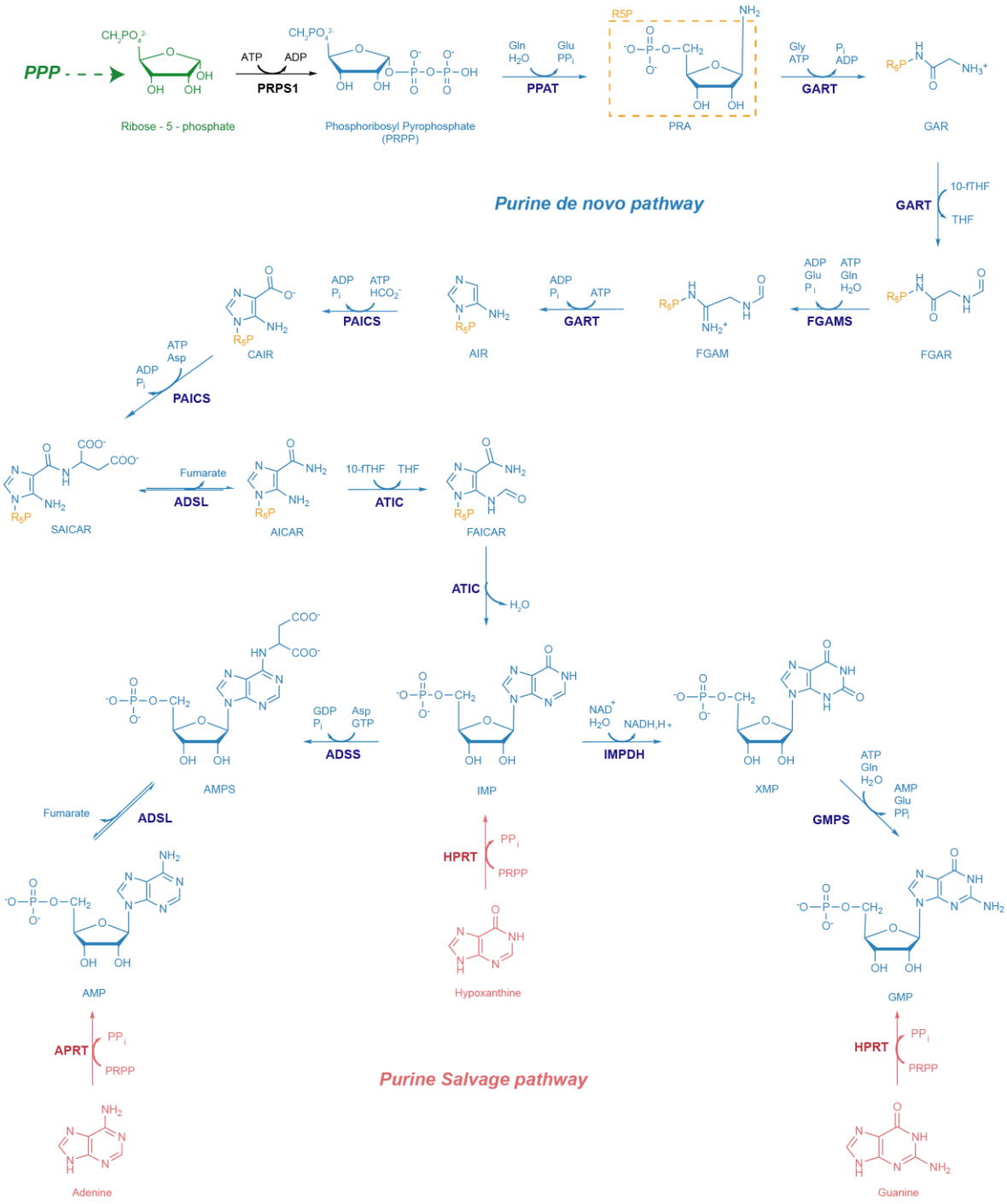

Figure 10. **Purine Biosynthesis Pathways.** The pool of purines in cells is maintained by the coordination of the salvage (red pathway) and the *de novo* pathways (blue pathway). In physiological conditions, purines are produced from the salvage pathway which consists in three parallel enzymatic reactions in which APRT converts adenine into AMP, and HPRT converts guanine and hypoxanthine into GMP and IMP, respectively. In conditions of high purine demand, the *de novo* pathway is activated to maintain the pool of purines. This pathway, comprised of by six enzymes, uses PRPP, the final product of the PPP (green pathway) as substrate and leads to one molecule of IMP as final product. IMP can then be further converted into AMP or GMP.

The purine metabolism has been demonstrated to be involved in many disorders such as gout, the Lesch-Nyhan syndrome and cancer. Although the Lesch-Nyhan syndrome has a genetic origin as it results from mutations within the gene encoding for HGPRT, the implication of purines in cancer relies on their metabolism and functions. As previously described in **section 1.2.1**, the purinergic signalling plays a key role in cancer development and progression.[126] In the same way, inosine has been shown to enhance the proliferation of melanoma cells.[147] In addition to purine metabolites, biosynthetic purine enzymes are also involved in cancer development. Studies carried out on lung cancer samples from patients showed that the enzymes of the *de novo* pathway, PAICS and PPAT, were amplified in a number of cancer tissues and were involved in tumour growth, cancer progression and invasion.[148] Furthermore, in this same study, the expression of both proteins was suggested as markers for disease outcome as they correlated with poor patient survival.

In addition to their implication in cancer via purinergic signalling, the role of purines as building blocks of DNA and RNA made them an ideal target to prevent nucleic acid synthesis and downstream cancer cell growth and proliferation. As such, one of the oldest class of molecules used in chemotherapy are the purine antimetabolites that act by either inhibiting the *de novo* synthesis of purines or by replacing naturally occurring purines in the nucleic acid strands.[149] There are currently more than 10 purine antimetabolites that are routinely used in cancer treatment. For example, 6-mercaptopurine acts by competing with hypoxanthine for HGPRT, thus inducing the formation of thio IMP (TIMP) instead of IMP and subsequently preventing the formation of AMP and GMP.[150] 6-mercaptopurine also inhibits PPAT, the first enzyme of the *de novo* purine biosynthesis, which thus alters the synthesis of purines and subsequent formation of nucleic acid strands.[151] Another class of molecules used to target *de novo* purine synthesis is the antifolates.[152] Antifolates constitute a class of antimetabolites that display similar structures to natural folate derivatives but act by blocking the enzymes involved in the synthesis of these folate derivatives. The first and most common example of an antifolate is methotrexate. Methotrexate was first used in the clinic in the early 1950s, and it is only in 2004 that the second antifolate was approved for cancer treatment.[153] Methotrexate is an inhibitor of the dihydrofolate reductase (DHFR) enzyme that converts dihydrofolate (DHF) into THF.[154] Inhibition of DHFR prevents the formation of 10-f-THF from THF, thus blocking the *de novo* synthesis of purines.

Because of all the above-mentioned physiological roles attributed to purines and their implication in various diseases, purine metabolites represent a cornerstone of the cellular metabolism. Over the last years, a renewed interest towards understanding the purine metabolism enabled the discovery of new levels of regulation and organisation within this metabolism thus providing a new insight into how cells regulate their purine need.

1.3 The purinosome complex

1.3.1 Introduction to the notion of metabolon and discovery of the purinosome

For many years, enzymes belonging to the same pathway have been hypothesised to cluster in order to facilitate the metabolic flux through the pathway. In 1985, Paul A. Srere introduced the notion of metabolon which refers to a "supramolecular complex of sequential metabolic enzymes and structural cellular elements".[155] His work on metabolons mainly focused on the TCA cycle and demonstrated that five sequential enzymes of the TCA cycle were clustering together at the inner mitochondrial membrane in order to efficiently produce α-ketoglutarate from fumarate.[156, 157] Following this discovery, more metabolons have been characterised in various pathways such as glycolysis and pyrimidine biosynthesis.[158-160] However, it should be noted that a metabolon does not always include all the enzymes of the concerned pathway. The formation of a metabolon prevents the diffusion or interaction of metabolic intermediates with other cellular components so as to ensure an efficient processing of these metabolites through the pathway.

In the *de novo* purine biosynthesis pathway, the instability of some intermediates as well as the non-sequential enzymatic activity of GART raised the hypothesis that the enzymes of the pathway could form a metabolon. Indeed, PRA, the product of the first reaction of the pathway, is unstable in solution and requires to be directly transferred to GART which was found to correlate with the clustering of PPAT and GART.[161, 162] In the same way, GART catalyses steps two, three and five of the pathway with FGAMS catalysing the fourth step, thus suggesting an interaction between these two enzymes.[163]

For many years, the existence of a metabolon within the *de novo* purine biosynthesis was hypothesised and assed by different copurification techniques that could not determine the existence of such a complex. It is only many years later, with the technical progress of fluorescence microscopy, that the existence of a metabolon within the *de novo* purine biosynthesis was proven.

In 2008, Benkovic *et al*., by studying the enzymes of the pathway tagged with fluorescent proteins using fluorescent microscopy, discovered the existence of a macro-complex comprised of the six enzymes of the *de novo* purine pathway that they named the purinosome (**Figure 11**).[164] In order to observe the formation of the complex, the authors maintained the cells in a media deprived of purines, referred to as purine-depleted media, which mechanically forced the cells to synthesise their own purines as they were not able to uptake them from the extracellular environment or to salvage extracellular nucleosides. The first observation of purinosome complexes was obtained by transfecting into HeLa cells two plasmid constructs encoding for GART and FGAMS, both fused to

a different fluorescent protein (GFP and OFP, respectively). Although the fluorescently tagged enzymes displayed an homogenous fluorescence throughout the cytoplasm when cells were placed in the presence of purines (**Figure 11a**), in purine-depleted media, both enzymes formed purinosomes and were found to colocalise within the complex (**Figure 11b**). The study was extended to the other four enzymes of the pathway which were all found to colocalise with FGAMS in purine-depleted conditions. In the same study, the authors demonstrated that this clustering was not an artefact of transfection or protein overexpression by showing the presence of the purinosome complexes in purine-depleted conditions via the immunostaining of GART.

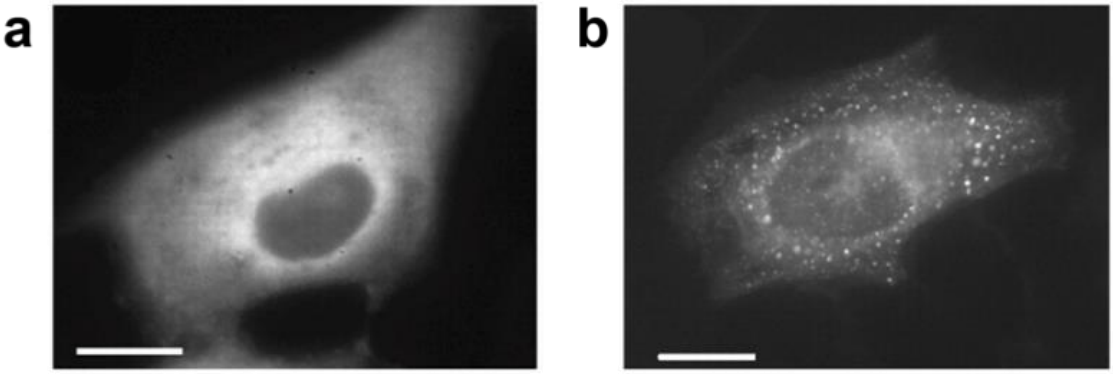

Figure 11. Purinosome formation in HeLa cells maintained in purine-depleted conditions. From An, S.; Kumar, R.; Sheets, E. D.; Benkovic, S. J., Reversible compartmentalisation of de novo purine biosynthetic complexes in living cells. Science 2008, 320 (5872), 103-106. Reprinted with permission from AAAS.[164] HeLa cells were transfected with a plasmid encoding for FGAMS-GFP. **(a)** HeLa cell in purine-rich media displayed an homogenously distributed fluorescence. **(b)** HeLa cell maintained in purine-depleted conditions formed purinosomes.

The existence of such a complex raised many more questions about the organisation of the complex itself and its regulation. Since then, many studies were carried out and provided a broad and deeper understanding of the structure of the complex, its physiological relevance as well as its interactions with other cellular components, including proteins and cellular compartments.

1.3.2 Physical characteristics of the complex

The purinosome was firstly described as a complex containing the six enzymes of the *de novo* purine biosynthesis but little was known about the actual organisation of the complex. Further studies determining the coefficient of diffusion of the individual proteins as well as proximity studies enabled the determination that the complex was formed of a core scaffolding protein assembly in addition to peripheral proteins involving weaker protein-protein interactions.[165, 166] The core of the complex was found to be comprised of the first three enzymes of the pathway,

PPAT, GART and FGAMS, whereas PAICS, ADSL and ATIC were defined as peripheral proteins (**Figure 12**). In addition, proteomic studies uncovered interactions between proteins of the purinosome , with most of the proteins found to interact with one another.[165-168] In addition to the six enzymes of the *de novo* purine biosynthetic pathway, ADSS and IMPDH, the enzymes responsible for the conversion of IMP into AMPS and XMP, respectively, were found to also be part of the purinosome, although no protein-protein interactions with the enzymes of the *de novo* pathway were found.[169]

Although PAICS, ADSL and ATIC have been defined as peripheral proteins, they remain essential for the stability of the complex. Purinosome formation was found to be decreased in fibroblasts from patients suffering from ADSL-deficiency and AICAr-ribosiduria (ATIC deficiency), suggesting that the structure and activity of these two peripheral proteins impact upon purinosome formation.[170] To further confirm this, it was shown that in CRISPR-Cas9 HeLa cell lines, each deficient for one of the *de novo* purine pathway (except PPAT which was not assessed), the formation of purinosomes was disrupted, indicating that each enzyme of the pathway is required for the stability of the complex.[171]

To further understand the organisation of this complex, the oligomeric states of each enzyme were studied. PAICS was found to be an octamer, ADSL a tetramer and both GART and ATIC were described as dimer, although ATIC exists as an equilibrium between the monomeric and dimeric forms, with the dimer being predominant in presence of the enzyme's substrate and cofactor.[172-177] No information about the structures of FGAMS and PPAT are available for the human proteins, but comparison with homologous enzymes from other species suggests that FGAMS and PPAT exist as monomer and tetramer, respectively (**Figure 12**).

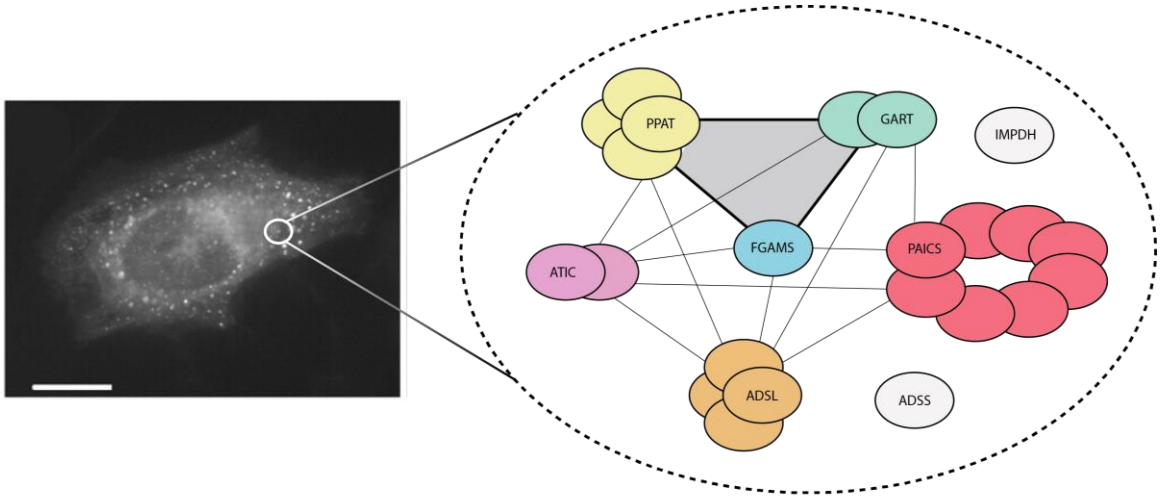

Figure 12. Schematic representation of the oligomeric states of the *de novo* purine enzymes and their interactions within the purinosome network. The purinosome network is comprised of a core scaffold assembly (grey triangle) and peripheral proteins. The core proteins tetrameric PPAT, dimeric GART and monomeric FGAMS strongly interact with each other (thick lines), whereas the peripheral proteins (dimeric ATIC, tetrameric ADSL and octameric PAICS) display weaker protein interactions with the other members of the complex (thin lines). IMPDH and ADSS are known to be part of the complex although no protein-protein interactions with other purinosome proteins have been described.

Studies based on particle analysis showed that the size of a purinosome cluster can vary from 0.2 to 0.9 µm (0.56 µm on average) and that 50-1000 entities can be found per cell.[178] Purinosomes were first discovered using transient transfection which artificially leads to increased protein levels. To ensure that the observed clusters were not stress bodies resulting from protein aggregation, various control experiments were carried out to specifically characterise purinosomes and demonstrate that they are a unique entity clearly distinct from already reported cellular bodies. Indeed, the transfection of fluorescently-tagged stress granule marker Ras GTPase-activating protein-binding protein (G3BP), as well as GFP250 and GFP170 aggresome markers simultaneously with FGAMS did not show any colocalisation between the proteins, confirming that purinosomes are distinct from stress bodies and aggresomes.[179] In addition, both stress granules and aggresomes displayed different physical characteristics compared to purinosomes, as their sizes were 0.4-5.0 µm for the stress granules and 2-10 µm for the aggresomes.[180] Moreover, only 5-30 stress granules and 1 aggresome were observed within a single cell, suggesting a smaller number of entities per cell compared to purinosomes.

Altogether, the above-mentioned observations about the purinosome complex enabled its qualification as a unique cellular entity. As an additional feature, the purinosome was shown to

not be a static metabolon as its formation is reversible upon purine supplementation.[164] This characteristic demonstrates that purinosomes form when cells experience high purine demand but that their formation follows the metabolic requirements of the cells. This finding raised the possibility that purinosome formation might be modulated by many more cellular components and/or metabolic stimuli.

1.3.3 Function of the purinosome

As the purinosome is defined as a metabolon, it was highly expected to observe a significant increase in *de novo* production of purines in conditions that favour purinosome formation. In fact, when cells were placed under purine-depleted conditions, a 50% increase in the rate of the pathway was observed, leading to a final three-fold increase in IMP formation.[169] To further support this, analyses were carried out in fibroblasts derived from patients suffering from the Lesch-Nyhan syndrome.[181] In these cells, the HPRT enzyme is deficient, indicating that the formation of IMP solely relied on *de novo* purine biosynthesis. In this pathological condition, the cells displayed a 25% increase in purinosome formation compared to normal cells. This data supports that purinosome formation is correlated with an up-regulation of the *de novo* purine biosynthesis.

In order to understand the biological relevance of this metabolon, different studies were carried out, and a link between the cell cycle and the purinosome was hypothesised. Purinosome formation has been reported to be dependent on the cell cycle phase, with the number of purinosome-positive cells being at its maximum in G1 phase.[178] On a biological point of view, this phase-dependent increase in purinosome formation is consistent with the fact that cells need to increase their nucleotide pool before DNA duplication in S phase. Following this increase, purinosome formation was shown to decrease as cells were progressing through S and G2/M phase. Consistent with this observation, studies in HCT116 cells showed a five-fold increase in purine synthesis when cells were progressing from G1 to S phase, supporting the correlation between purinosome formation and an increased metabolic flux through the pathway.[182] Unsurprisingly, this increase was accompanied by a three-fold increase in PRPP levels, the first substrate of the *de novo* synthesis of purines, indicating that the increase in the *de novo* purine synthesis is likely a downstream effect of increased substrate and cofactor availability from the input pathways.

As an increase in substrate levels of the *de novo* pathway seemed to correlate with enhanced *de novo* purine biosynthesis, links between the input metabolic pathways and the purinosome were investigated. Recently, the enzymes of glycolysis were shown to form a metabolon called a

glucosome which was interestingly found to be spatially located next to the purinosome.[183] Although the characteristics of the spatial organisation between the glucosome and the purinosome require further investigation, it is hypothesised that the close proximity between these two clusters facilitates the channelling of the molecules from one pathway into another.

1.3.4 Modulation of purinosome formation

The different characteristics of the purinosome complex, such as its size, its stepwise formation and its transient nature, suggested that other proteins and/or auxiliary proteins might be involved in the support and formation of the complex.

Immunoprecipitation of FGAMS demonstrated that the protein was interacting with many chaperones, including the Hsp70/Hsp90 machinery.[179] Chemical inhibition of these chaperones with specific inhibitors (i.e. Pifithrin-μ and MKT-077 for Hsp70, and 17-AAG and NVP-AUY922 for Hsp90) led to a total disassembly of the purinosome complexes. In the same way, removal of these inhibitors from the cell media induced a resurgence of purinosome, indicating that the Hsp70/90 complex is necessary for purinosome formation. Further studies investigating the role of Hsp90 in purinosome formation determined that the chaperone was not responsible for the stabilisation of the whole complex as such. The first two enzymes of the pathway, PPAT and FGAMS, were shown to be client proteins of Hsp90 which acts by processing them prior to complexation within the purinosome complex, whereas Hsp90 was not found to interact with the four remaining enzymes of the pathway.[184]

In cells containing purinosomes, the complexes were physically distributed throughout the cell cytoplasm. Following the hypothesis that the organisation of enzymes into a metabolon was linked to cytoskeletal structures, the formation of purinosomes was found to be partly linked to microtubules. In fact, purinosome complexes formed under purine-depleted conditions were found to be embedded into the microtubule network and an inhibition of microtubule formation using nocodazole led to a dissociation of the complexes coupled to a decreased production of purines.[185]

The role of the microtubule network in purinosome formation and function was further uncovered a few years later. A combination of microscopy techniques showed that microtubules ensured the trafficking of purinosomes, partly in order to send them to the mitochondria.[186] The functional link between the purinosome and the mitochondria was further demonstrated by inhibiting either the electron transport using antimycin A or the oxidative phosphorylation using oligomycin. In both cases, the number of cells containing purinosomes was found to increase.[187] In addition, inhibition of purinosome formation by small molecules correlated with a decrease in the

mitochondrial activity (assessed by measuring the production of malate) whereas the stimulation of purinosome formation resulted in increased malate production. Altogether, this demonstrates that there is a physical and functional link between the purinosome and the mitochondria.

Although the exact nature of the link between the purinosome and the mitochondria remains to be explored, several hypotheses can be generated to explain the close proximity between these two entities. First, the *de novo* pathway requires five molecules of ATP to produce one molecule of IMP. The localisation of the purinosome complex next to the mitochondria would ensure a constant flux of ATP into the *de novo* pathway thus ensuring a proper function of the pathway. In addition, formate, the precursor of 10-formyltetrahydrofolate (10-f-THF), a cofactor used by two enzymes of the *de novo* synthesis of purine (i.e GART and ATIC), is exported from the mitochondria. Thus, a close proximity between the two entities would ensure the proper activity of these two purinosome enzymes.

The nature of the relationship between purinosome formation and mitochondrial activity was further assessed using a screening of the human kinome. The mammalian target of rapamycin (mTOR), known for its implication in modulating mitochondrial physiology as well as regulating nucleotide metabolism, was found to affect the colocalisation of the purinosome with the mitochondria, with the inhibition of mTOR using rapamycin disrupting this colocalisation.[187-190]

In addition to mTOR, other kinases and signalling pathways have been found to modulate purinosome formation. As an example of such, the core proteins of the purinosome, PPAT, GART and FGAMS, were found as potential substrates of casein kinase II (CK2).[191] The involvement of the kinase was determined by inhibiting it with specific small molecules which resulted in purinosome formation, although a different inhibitor of CK2 was, in contrast, found to disrupt purinosome formation. The mechanisms by which CK2 and its inhibitors modulate purinosome formation remain mostly unclear but this data suggests that CK2-mediated pathways might reversibly regulate purinosome formation. In the same way, purinosome assembly and disassembly was found to be modulated by the activation of the $G\alpha_i$-coupled protein receptors, suggesting that the formation of the complex might be resulting from GPCR signalling.[192]

Overall, since its discovery in 2008, the purinosome complex has been found to interact with many other cellular components (organelles, cytoskeleton proteins, chaperone proteins, etc.) and its formation to be modulated by the cellular environment. It now seems clear that the purinosome complex requires interactions with these cellular components in order to function and ultimately synthesise purines, as previously described. The mechanism by which the purinosome forms would provide insight into how such a complex works. In pathophysiological conditions, the purinosome could be of high therapeutic interest as purines, and to a larger extent

nucleotide synthesis, is a process that has been extensively studied and targeted in various pathologies that involve enhanced or uncontrolled DNA and RNA synthesis, especially in diverse types of cancers.

1.4 Aims of the project

Due to its high occurrence in cancer tumours, hypoxia has been widely studied over the last few decades. Cancer cells have developed many ways to adapt and survive to these low oxygen environments including metabolic reprogramming. The metabolic adaptation of hypoxic cancers cells involves many alterations at the gene expression level, most of which are regulated by the Hypoxia-inducible Factors (HIFs). The HIF-1 transcription factor has been shown to induce the upregulation of many metabolic genes from pathways such as glycolysis, ultimately aiming at providing nutrients and metabolites to ensure cell growth and proliferation in low oxygen conditions. Upregulation of glycolysis provides substrates for diverse downstream pathways, all of which provide substrates and cofactors for nucleotide synthesis. For years, it has been hypothesised that upregulated pathways in hypoxia would lead to increased nucleotide synthesis, but currently very little is known about the effect of hypoxia on nucleotide biosynthesis.[193]

In parallel, in 2008, a protein macro-complex composed of the six enzymes of the *de novo* purine biosynthetic pathway was characterised for the first time and was referred to as the purinosome.[164] Later, this complex has been shown to coincide with an increased rate of the *de novo* production of the purines.[169] Such a metabolon is of high therapeutic interest as inhibiting its formation could prevent the increased formation of purines and downstream nucleic acid synthesis thus limiting cell growth and proliferation.

As healthy cells are known to mostly rely on salvage purine synthesis, determining whether hypoxic cancer cells preferentially use the *de novo* purine biosynthesis as a way to refill their purine pool could enable to distinguish them from their healthy counterparts and to specifically target them.[141-143] Indirect inhibitors of the nucleotide biosynthesis such as antifolates (e.g methotrexate) have been used for years but present the disadvantage to be unspecific towards nucleotide synthesis as folate species have other functions in the cell metabolism.[153,154] In a pathological context such as cancers, tumour hypoxia represents a challenging target as it remains resistant to radiotherapy. If the purinosome complex is found to be a feature of hypoxic cancer cells, it can be thought that development of inhibitors of purinosome formation would enable to directly target hypoxic cancer cells by inhibiting their *de novo* purine biosynthesis. These inhibitors could be used in combination to radiotherapy as a treatment against cancerous tumours.

As such, this work will focus on deciphering the impact of hypoxia on purinosome formation and purine nucleotide synthesis in hypoxic cancer cells. Preliminary work within the Tavassoli Lab suggested an increased formation of these complexes in hypoxic cancer cells compared to normoxic conditions (unpublished data). This project will involve a multidisciplinary approach, using a variety of biochemical and cell based tools. Experiments including gene knockouts, colocalisation assays, proteomics and metabolomics approaches as well as gene and protein expression assays will be conducted to characterise for the first time the formation of purinosomes in hypoxia and its impact on the pool of purines in cancer cells.

The first step of this project will be to fully characterise the formation of purinosomes in hypoxia using microscopy techniques on cancers cells. These experiments will involve transiently expressed fluorescently tagged purinosome enzymes in addition to the analysis of endogenous proteins using label-free techniques. Following this, the involvement of HIF-1α in this process will be probed in order to understand the role of the transcription factor in this process. In addition, the effect of hypoxia on the purine pool will be assessed in order to determine any potential link between the purinosome complex and purine biosynthesis.

Chapter 2 Results and Discussion

2.1 Probing and characterising the formation of purinosome complexes

In regards to all of the metabolic changes occurring in cancer cells experiencing hypoxia, it was hypothesised that the synthesis of purines could also be affected in low oxygen environments. As the formation of purinosome complexes has previously been shown to correlate with increased *de novo* purine biosynthesis (in purine-depleted conditions)[169], the first step into this project was to assess purinosome formation in hypoxic cancer cells. Preliminary work carried out by Dr Ishna Mistry within the Tavassoli Lab (University of Southampton, UK), suggested an increased formation of these clusters in hypoxia compared to normoxia (unpublished data).

From this promising preliminary work, it was decided that these experiments would be repeated and that the formation of these complexes would be further characterised, first by observing the formation of the clusters in hypoxia using diverse microscopy techniques, then by deciphering the processes underlying this hypoxia-induced formation.

2.1.1 Characterising the formation of purinosomes using microscopy techniques

To initiate the project, enzymes of the *de novo* purine biosynthesis, tagged with a fluorescent protein, were expressed into cervical cancer (HeLa) cells. For this purpose, DNA plasmids encoding for FGAMS-mCherry and ADSL-GFP (obtained from Prof. Stephen Benkovic Lab, Penn State University, USA) were used.

First, a plasmid encoding mCherry-tagged FGAMS, the fourth enzyme of the pathway and one of the core proteins of the purinosome, was transiently transfected into HeLa cells. The cells were then incubated for 24 h in normoxia or hypoxia (1% oxygen) and were subsequently observed and imaged by confocal microscopy. When cultured in normoxic conditions for 24 h, the enzyme was found to be evenly distributed throughout the cell cytoplasm as indicated by the homogenous fluorescence in the cell cytoplasm (**Figure 13a**). However, when cells were incubated in hypoxic conditions for 24 h, the phenotype observed in normoxia changed to a fluorescently clustered distribution where each fluorescent cluster is likely to constitute a single purinosome complex (**Figure 13b**).

It is to mention that, although the homogenous fluorescence phenotype was largely predominant in normoxia, a small number of cells containing purinosomes was observed in presence of oxygen. If, as hypothesised, the formation of purinosome complexes reflects the activity of the *de novo*

purine biosynthesis pathway, it would be expected to observe cells containing purinosomes in normoxia. Indeed, although in physiological conditions most of the purine pool originates from the salvage pathway, a small fraction of the purine pool remains produced via the *de novo* synthesis in culture media containing purines.[141-143] The presence of purinosomes as well as a basal rate of the *de novo* synthesis of purines has previously been observed in HeLa cells cultured in presence of purines.[169, 187]

In order to determine the extent to which the formation of purinosomes was increased in hypoxia, HeLa cells were transfected with a plasmid encoding FGAMS-mCherry and were subsequently incubated in normoxia or hypoxia (1% oxygen) for 24 h. For each condition, the number of purinosome-positive cells were counted and normalised to the total number of transfected cells counted (purinosome-positive and purinosome-negative). The results are presented as a relative purinosome formation compared to normoxia (**Figure 13c**). After 24 h in hypoxia, when considering the percentages of purinosome-positive cells in both conditions, 19% of transfected HeLa cells were found to display purinosomes in normoxia compared to 40% in hypoxia, thus representing a 2.1-fold increase in purinosome formation in hypoxic conditions.

As a comparison, purinosome formation was also assessed in the conditions that first enabled the discovery of the purinosome complex. These culture conditions, where the cell media was deprived of purines, are referred to as purine-depleted conditions. As previously reported, cells had to be kept in purine-depleted conditions for seven days prior to purinosome counting. When the number of purinosome-positive cells was assessed in these conditions, a 2.3-fold increase compared to normoxia was observed (44% of purinosome-positive cells in purine-depleted conditions), similar to the increase observed in hypoxic conditions (**Figure 13c**). Together, this data suggests that hypoxia triggers purinosome formation.

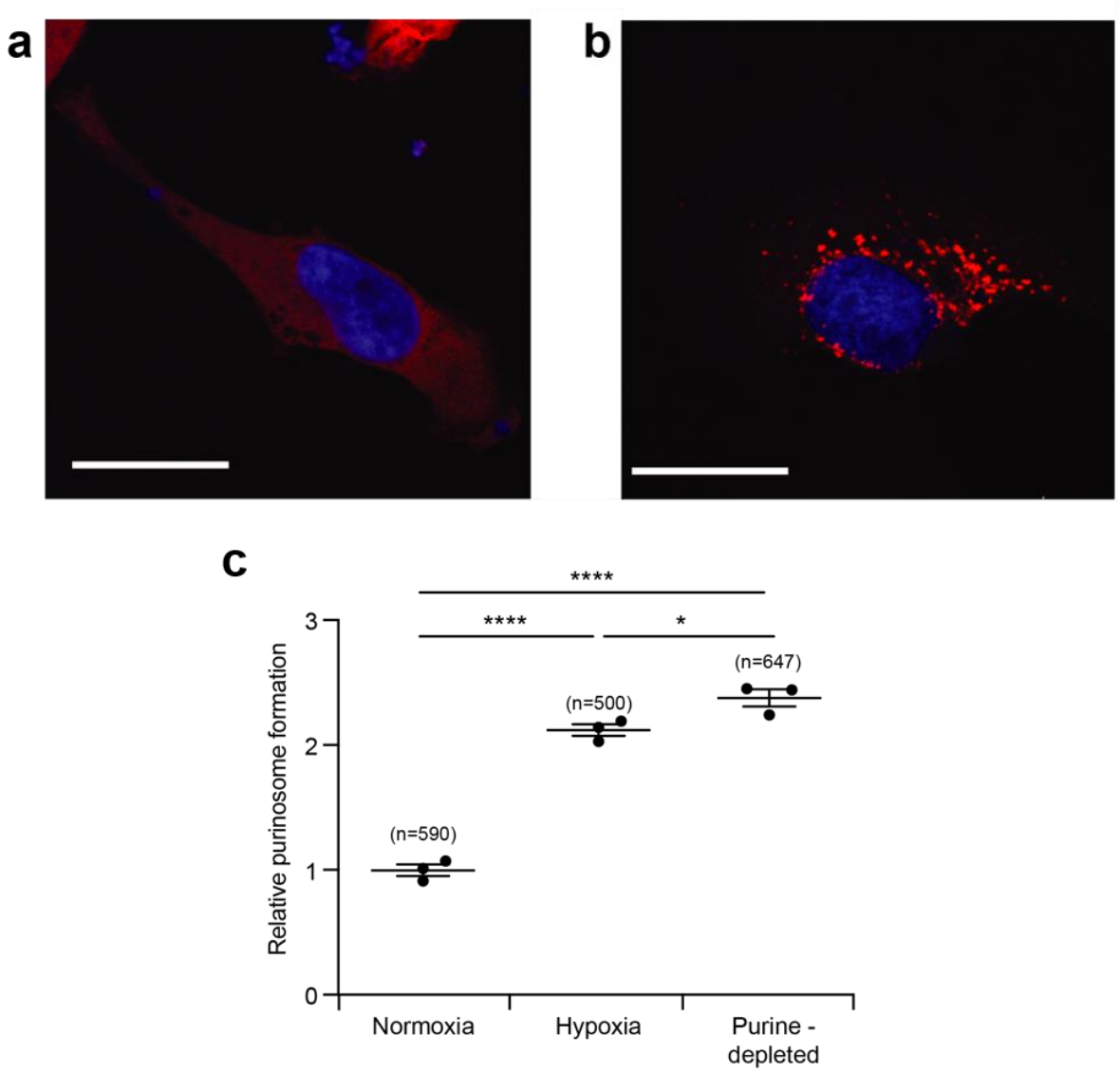

Figure 13. Purinosome formation in HeLa cells transfected with FGAMS-mCherry encoding plasmid. (a) When cultured in normoxia for 24 h, cells displayed a homogenous fluorescence indicating that the fluorescently tagged protein is evenly distributed throughout the cytoplasm. **(b)** Incubation in hypoxia (1% oxygen) for 24 h induced the formation of a clustered fluorescent pattern within the cytoplasm. Scale bar represents 25 µm. Blue channel represents DAPI staining. Red channel represents FGAMS-mCherry. **(c)** HeLa cells transfected with FGAMS-mCherry displayed a 2.1-fold increase in the number of purinosome-positive cells in hypoxia compared to normoxia after 24 h of incubation. Cells cultured in purine-depleted conditions also displayed a 2.3-fold increase compared to normoxia. Data are means (n=3) ± SEM. Significance was determined using unpaired Student t test, **** $p < 0.0001$, * $p < 0.05$. The number in brackets indicates the number of cells counted per condition.

To ensure that the observed clusters were not the result from mCherry aggregation and that the clustering formation was not only observed with FGAMS, the same transient transfection was repeated using another *de novo* purine enzyme tagged with a different fluorescent protein. Therefore, a plasmid encoding for a GFP-tagged ADSL, a peripheral purinosome enzyme that catalyses the eighth step of the pathway, was transiently transfected into HeLa cells.

Similar results to the ones obtained with FGAMS-mCherry were observed with the ADSL-GFP fusion construct (**Figure 13** and **Figure 14**, respectively). After 24 h in normoxic conditions, the cells displayed an homogenous fluorescence throughout the cytoplasm (**Figure 14a**), whereas in hypoxic conditions, the fluorescence was observed in isolated clusters (**Figure 14b**). These results suggest that the fluorescent clusters are due to the co-compartmentalisation of the relative *de novo* enzymes and not due to the aggregation of the fused fluorescent tags (mCherry and GFP).

To further assess purinosome formation in hypoxia, the counting of purinosome-positive cells was carried out using a construct encoding ADSL-GFP. Following an incubation in normoxia and hypoxia for 24 h, the number of purinosome-positive cells was determined in the same way as with the FGAMS-mCherry construct. Consistent with the results obtained from the transfection of the plasmid encoding FGAMS-mCherry, a 2-fold increase in purinosome formation was observed in hypoxic cells (31%) transfected with ADSL-GFP when compared to normoxic cells (15%) (**Figure 14c**). This data is in line with the increased purinosome formation previously observed in hypoxic HeLa cells transfected with FGAMS-mCherry (**Figure 13c**), thus strengthening the hypothesis that purinosome formation is enhanced in hypoxic conditions.

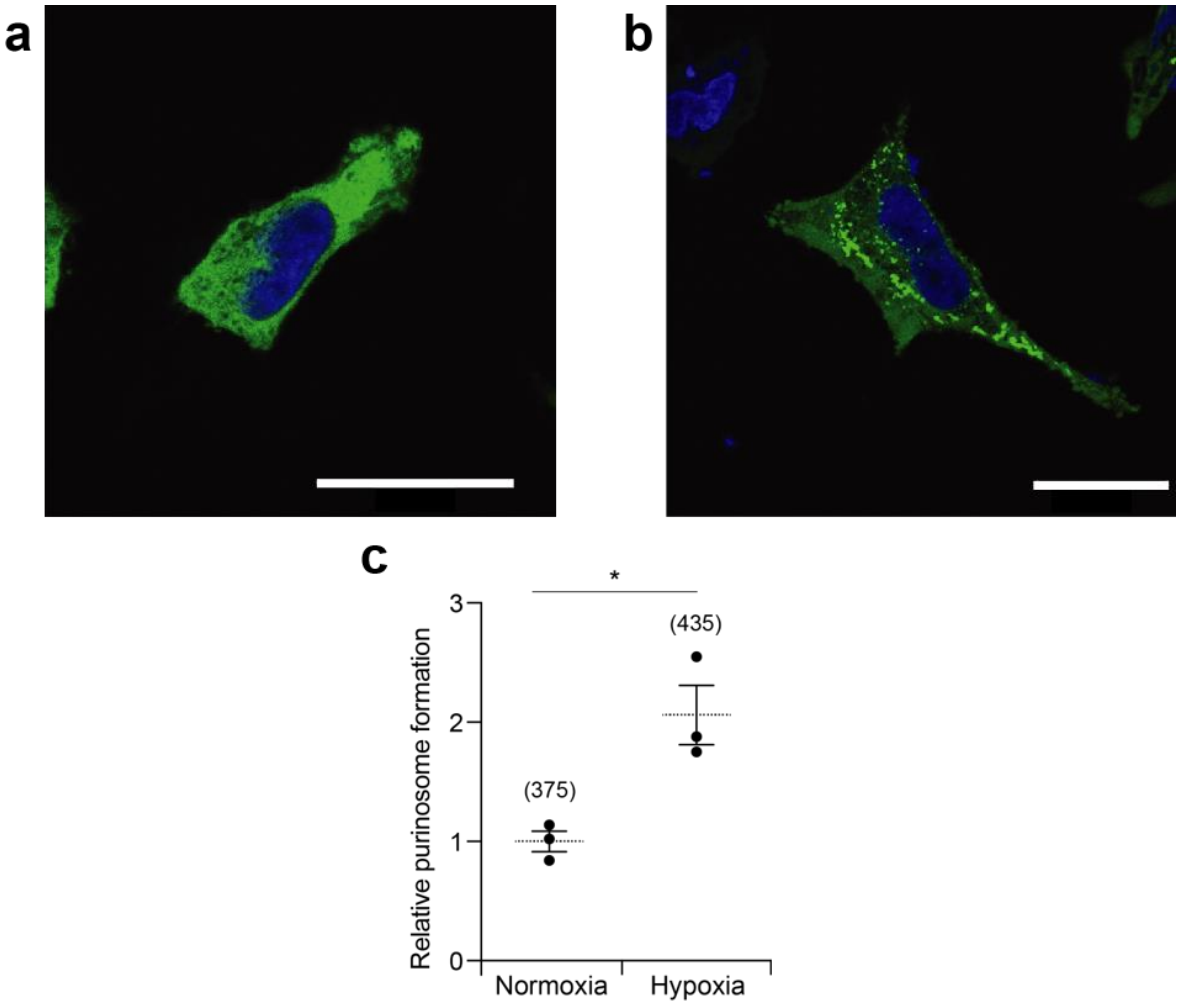

Figure 14. Purinosome formation in HeLa cells transfected with ADSL-GFP encoding plasmid. **(a)** When cultured in normoxia for 24 h, cells displayed a homogenous fluorescence indicating that the fluorescently tagged protein is evenly distributed throughout the cytoplasm. **(b)** Incubation in hypoxia (1% oxygen) for 24 h induced the formation of a clustered fluorescent pattern within the cytoplasm. Scale bar represents 25 µm. Blue channel represents DAPI staining. Green channel represents ADSL-GFP **(c)** HeLa cells transfected with ADSL-GFP displayed a 2-fold increase in the number of purinosome-positive cells in hypoxia compared to normoxia after 24 h of incubation. Data are means (n=3) ± SEM. Significance was determined using unpaired Student t test, * $p < 0.05$. The number in brackets indicates the number of cells counted per condition.

In order to ensure that the hypoxia-induced formation of purinosome was not cell type specific, the formation of the complexes, which in the above-mentioned experiments was described in cervical cancer cells HeLa, was then probed and counted in a breast cancer cell line, MDA-MB-231 (**Figure 15**). Similarly to HeLa cells, a 2-fold increase in purinosome formation was observed in these cells compared to normoxic conditions, thus suggesting that the hypoxic purinosome formation is not cell type specific and can occur in different tissues.

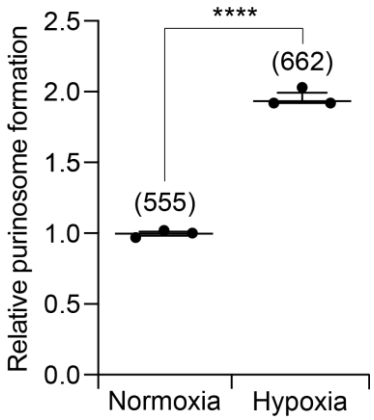

Figure 15. Relative purinosome formation in hypoxic and normoxic MDA-MB-231 cells. Hypoxic conditions (1% oxygen) induced a 2-fold increase in the number of purinosome-positive cells compared to normoxia after 24 h of incubation. Data are means (n=3) ± SEM. Significance was determined using unpaired Student t test, **** $p < 0.0001$. The number in brackets indicates the number of cells counted per condition.

Purinosome formation was previously quantified by transfecting two individual constructs encoding two fluorescently-tagged purinosome enzymes into HeLa cells (**Figure 13** and **Figure 14**. As a result, the formation of the complex was found to be increased by 2-fold in hypoxia for both FGAMS-mCherry and ADSL-GFP constructs, reaching a maximum of 40% of positive cells in hypoxic HeLa cells transfected with FGAMS-mCherry. This heterogeneity observed within the cell population (i.e 60% of the hypoxic cells not displaying purinosomes), raised the question of whether the hypoxic formation of the complex could depend upon cell cycle phases as previously described in purine-depleted conditions.[178] Indeed, cells maintained in purine-depleted conditions were found to display a purinosome formation that varied depending on the phase of the cell cycle, with a maximum of positive cells observed in G1 phase. As such, HeLa cells were synchronised in G1 phase and the purinosome formation was quantified following incubation in normoxia and hypoxia. As a result, the total percentages of purinosome-positive cells remained similar to non-synchronised cells (i.e 15% and 28.5% in normoxia and hypoxia, respectively), thus leading to a 2-fold increase in hypoxia as previously observed without synchronisation (**Figure 16**). This data suggests that hypoxic purinosome formation is not a function of the cell cycle.

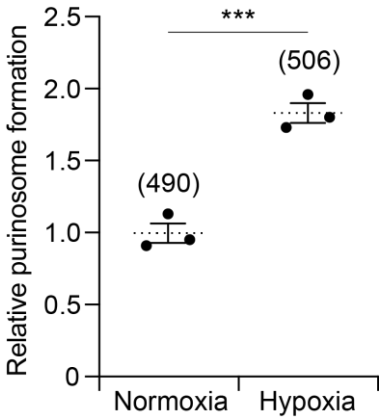

Figure 16. Relative purinosome formation in HeLa cells synchronised in G1 phase and incubated in normoxia and hypoxia. HeLa cells were transfected with FGAMS-GFP and subsequently incubated in normoxia and hypoxia (1% oxygen) for 16 h in media containing 0.5 mM of dibutyryl-cAMP (db-cAMP). Data are means (n=3) ± SEM. Significance was determined using unpaired Student t test, *** $p < 0.001$. The number in brackets indicates the number of cells counted per condition.

The individual transient transfections of two different plasmids, each encoding one enzyme of the *de novo* purine biosynthesis pathway, led to the formation of clusters likely to be purinosomes in both cases (**Figure 13** and **Figure 14**). In order to further assess whether the observed clusters were purinosomes, additional analyses were required.

As previously reported, the purinosome complex is comprised of the six enzymes of the *de novo* pathway. The simultaneous transient transfection of two plasmids encoding for two enzymes of the *de novo* purine pathway is a strategy that had been previously used to observe the colocalisation of the two proteins within the purinosome complex.[164]

This way, in order to assess whether the hypoxia-induced clusters observed as a result of transfection of plasmids encoding ADSL-GFP and FGAMS-mCherry were purinosomes, the two plasmids encoding these proteins were transiently co-transfected into HeLa cells. The cells were then incubated for 24 h in normoxia or in hypoxia and were subsequently observed (**Figure 17**). When incubated in normoxia both fluorescently tagged proteins exhibited a diffuse cytoplasmic distribution, indicating that both proteins were being expressed and homogenously distributed throughout the cytoplasm. When the two fluorescent channels were overlaid, the resulting merged image displayed an orange homogenous fluorescence indicating that both proteins were expressed simultaneously and did not display any particular compartmentalisation within the cell. The incubation in hypoxia of co-transfected cells revealed the presence of a clustered pattern for both FGAMS-Cherry and ADSL-GFP (**Figure 17**). When the two channels were overlaid, the

clustered pattern found for FGAMS-mCherry matched the one found for ADSL-GFP, indicating a high degree of colocalisation between the two proteins.

In order to determine the degree of this colocalisation, the pictures acquired under hypoxic conditions were analysed using ImageJ software and the Pearson's coefficient was calculated. The Pearson's coefficient translates the level of colocalisation between two entities, with no colocalisation between the analysed proteins resulting in a coefficient equal to 0, whereas a perfect colocalisation results in a Pearson's coefficient of 1. In the case of the hypoxic clusters formed by FGAMS-mCherry and ADSL-GFP within the same cell (**Figure 17**), the coefficient was found to be 0.83 (after 200 iterations of Coste's approximation), indicating a very high level of co-localisation between the two proteins, thus suggesting that the observed clusters were purinosome complexes. In addition, it should be notes that the Pearson's coefficient value obtained was consistent with the literature reporting the colocalisation of these same two enzymes within the purinosome complex in purine-depleted conditions.[164]

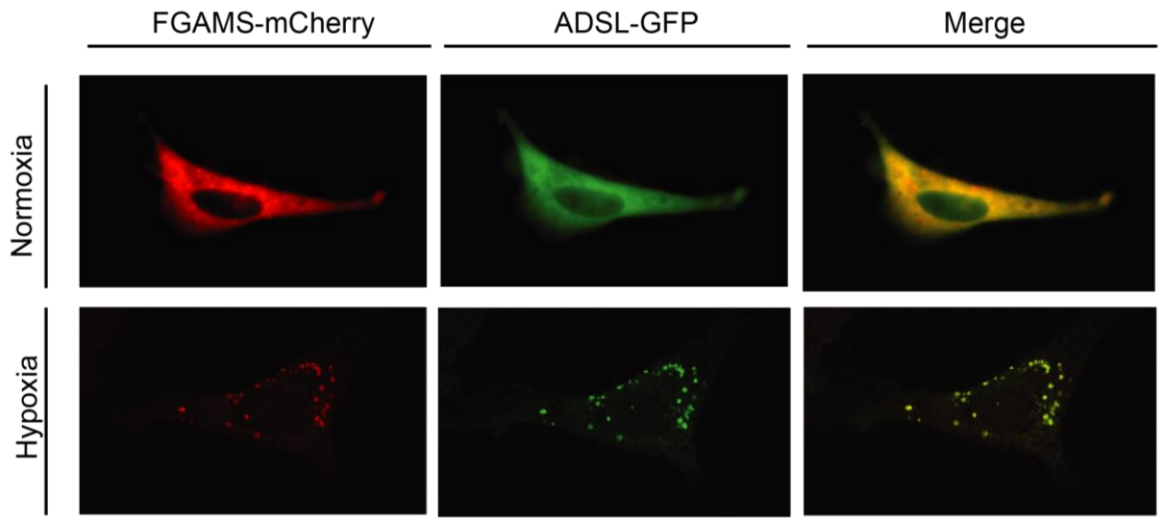

Figure 17. Colocalisation of FGAMS-mCherry and ADSL-GFP in HeLa cells cultured for 24 h in normoxia or hypoxia. FGAMS-mCherry was co-transfected with ADSL-GFP and the two channels were merged. Co-transfection of the two proteins exhibited diffuse cytoplasmic distribution in normoxia and purinosome formation in hypoxia, where the two enzymes colocalised with a Pearson's coefficient of 0.83 (after 200 iterations of Coste's approximation).

To further characterise the colocalisation between FGAMS-mCherry and ADSL-GFP within the purinosome complexes, the HeLa cell incubated in hypoxia for 24 h presented in **Figure 17** was analysed using Z-scan imaging in confocal microscopy. Fifteen images were acquired at different focal planes throughout the entire volume of the cell. These planes, also referred to as stacks, were acquired from the top to the bottom of the cell following the z axis. The 2D view of the

analysed cell is presented in **Figure 18a** where the x and y axis are displayed in red and green lines, respectively.

The acquisition of 15 stacks enabled the observation of the cell in three dimensions: x-y plane (**Figure 18a**), x-z plane (**Figure 18b**) and y-z plane (**Figure 18c**). As observed on the x-y plane, only one cluster is present at the intersection of the x and y axis. When observed in the x-z plane (**Figure 18b**), the deconvolution of this single purinosome cluster along the z axis clearly shows that the green fluorescence is present on precisely the same x-y coordinates as the red fluorescence. Similarly, in the y-z plane (**Figure 18c**), two clusters are visible and they both display a green fluorescence on top of the red florescent signal. These fluorescent signals clearly indicate that ADSL-GFP and FGAMS-mCherry are located together, in this case with ADSL located on a higher z coordinate than FGAMS. This observation is coherent with the purinosome organisation into which the two proteins are located together within the complex. A volume reconstruction of the cell, made from the 15 stack images, displays the fluorescence distribution along the z axis (**Figure 18d**). This 3D volume enabled the detection of the clusters within the cell cytoplasm, where each isolated peak represents an individual purinosome complex.

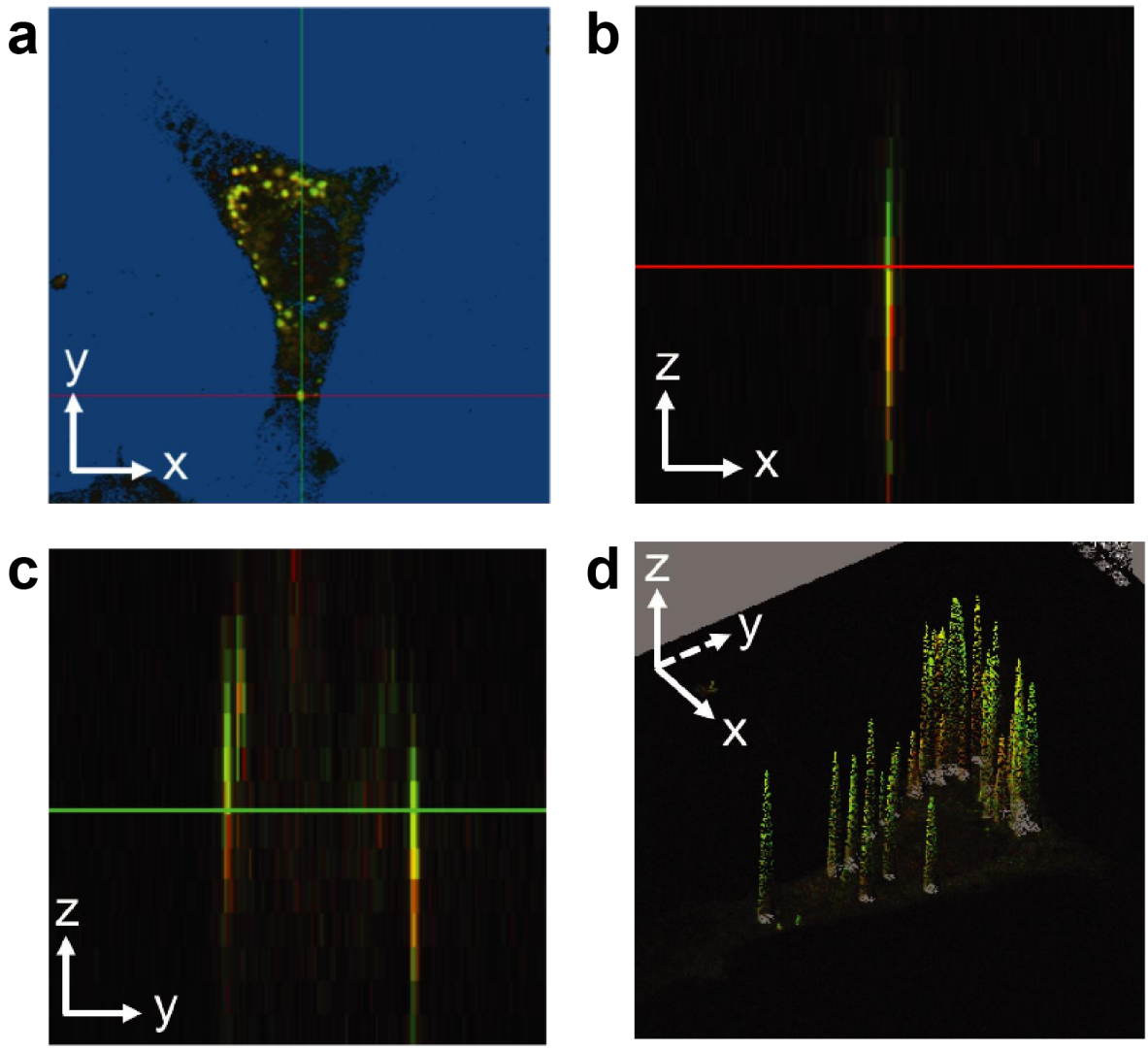

Figure 18. Z-stack imaging in confocal microscopy presenting FGAMS-mCherry and ADSL-GFP co-clustering within the cytoplasm. HeLa cell, co-transfected with plasmids encoding FGAMS-mCherry and ADSL-GFP, cultured in hypoxia for 24 h displayed a co-clustering of the two enzymes within purinosome complexes. **(a)** Overlay of 15 stacks in a 2D representation following the x-y plane. **(b)** x-z plane view from panel (a). One purinosome aligned on the x axis. **(c)** y-z plane view from panel (a). Two purinosomes aligned on the y axis. The fluorescent signals displayed green fluorescence in high z values and red fluorescence in low z values indicating that the two enzymes were located on the same x-y location but on different z-stacks. **(d)** Volume reconstitution of the cell from 15 stacks. The co-transfection of plasmids encoding fluorescently tagged proteins confirmed that the clusters observed firstly with FGAMS-mCherry and secondly with ADSL-GFP in HeLa cells exposed to hypoxia were purinosomes as the two proteins were found to colocalise.

To further confirm that the observed clusters were purinosomes and that these entities were distinguishable from other cellular bodies, a marker of cellular stress bodies tagged with GFP was transfected into HeLa cells so as to compare the physical characteristics of the two different complexes and ensure that they were distinct from one another.

To first probe this, a plasmid encoding Ras GTPase-activating protein-binding protein (G3BP), a stress body marker, fused to GFP, was transiently transfected into HeLa cells which were subsequently observed by fluorescence microscopy. As a result, two cellular phenotypes were observed within the cell population. G3BP-GFP was found to be either homogenously distributed with the cell cytoplasm (**Figure 19a**) or to cluster into stress bodies (**Figure 19b**).

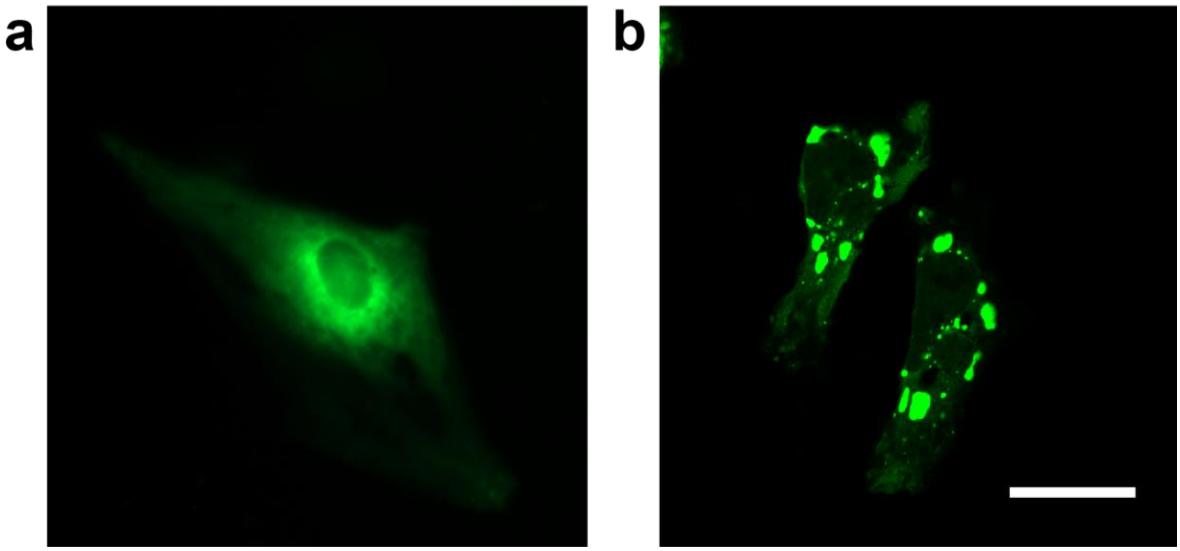

Figure 19. HeLa cells expressing G3BP-GFP. HeLa cells were transiently transfected with a plasmid encoding the stress body marker G3BP fused to fluorescent protein GFP. G3BP-GFP was found to be either homogenously distributed throughout the cytoplasm **(a)** or to cluster into stress bodies **(b)**. Scale bar represents 25 µm.

To determine whether stress bodies and purinosomes were two distinct cellular bodies, two plasmids encoding FGAMS-mCherry and G3BP-GFP, respectively, were co-transfected into HeLa cells that were further maintained in hypoxia for 24 h. Following the hypoxic incubation, the cells were observed by confocal microscopy as before and a Z-stack imaging was a carried out to analyse the localisations of the different complexes. Purinosomes were observed with FGAMS-mCherry (**Figure 20a**) and stress bodies were formed with G3BP-GFP, the latter displaying a morphology clearly distinct from the purinosomes as previously reported (**Figure 20b**).[178] When the two channels were overlaid, the clusters formed from each fluorescently tagged protein did not colocalise (**Figure 20c**). The Pearson's coefficient between the two proteins was found to be -0.003 after 200 Coste's approximations, indicating that the two proteins did not colocalise. In addition, the 3D reconstruction of the cell volume clearly showed that the red clusters and the

green clusters were distinct from one another, strengthening the fact that purinosomes and stress bodies are two distinct entities that do not colocalise (**Figure 20d**).

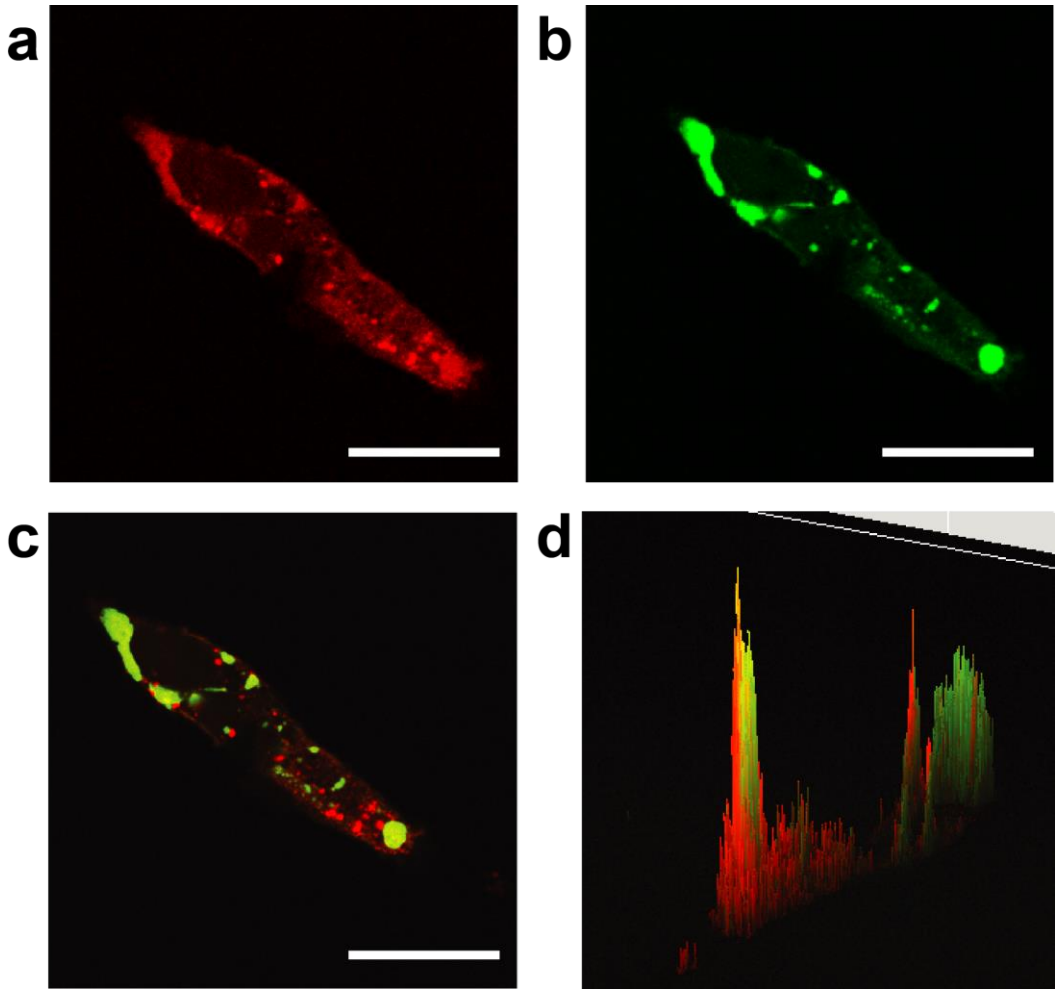

Figure 20. Confocal fluorescence microscopy presenting the co-transfection of FGAMS-mCherry and G3BP-GFP. HeLa cells co-transfected with FGAMS-mCherry and G3BP-GFP encoding plasmids displayed purinosomes following 24 h of hypoxic incubation (1% oxygen) **(a)** and stress bodies **(b)**. Overlay of the two channels indicated that the two proteins did not colocalise (-0.003 Pearson's coefficient after 200 Coste's approximations) **(c)**. Reconstruction of the 3D volume of the cell showed that the red clusters and the green clusters were found at different localisations within the cell cytoplasm **(d)**. Scale bar represents 25 µm.

Although the co-expression of G3BP-GFP and FGAMS-mCherry into HeLa cells indicated that stress bodies and purinosomes were different cellular bodies, it remained ensure whether the formation of the purinosome clusters resulted from a hypoxia-induced stress or if this was the consequence of an actual metabolic adaptation.

In order to probe this, the number of cells containing stress bodies was quantified in HeLa cells transfected with the plasmid coding for G3BP-GFP following an incubation in normoxia or hypoxia

for 24 h (**Figure 21**). As a result, approximately 20% of HeLa cells were found to display stress bodies, both in normoxia and hypoxia, without any significant difference between the two conditions. This way, as hypoxia did not induce an increased formation of stress bodies in cells, it could be concluded that the hypoxic increase in purinosome formation was not resulting from cellular stress.

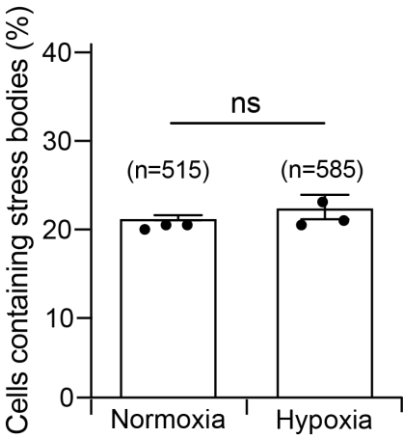

Figure 21. Quantification of HeLa cells containing stress bodies in normoxia and hypoxia. HeLa cells transfected with G3BP-GFP were observed by fluorescence microscopy and the number of cells containing stress bodies was normalised to the total number of cells transfected, i.e displaying green fluorescence. No significant difference in the number of cells containing stress bodies was observed between normoxia and hypoxia (1% oxygen) following 24 h of incubation. Data are means (n=3) ± SEM. Significance was determined using unpaired Student t test. The number in brackets indicates the number of cells counted per condition.

Despite clear evidence of the co-clustering of ADSL and FGAMS in hypoxia (**Figure 17** and **Figure 18**), the possibility that this clustering was the result of aggregation of the fluorescent proteins themselves (GFP and mCherry) had to be ruled out. Indeed, the aggregation of fluorescently labelled proteins is a known phenomenon, and the use of label-free techniques was thus required to strengthen the evidence in favour of hypoxic purinosome formation.[194]

The first label-free technique used in this study was immunofluorescence and enabled the determination of the cellular localisation of the previously studied purinosome proteins ADSL and FGAMS. HeLa cells were incubated with primary antibodies specific for ADSL and FGAMS, followed by an incubation with secondary antibodies coupled to fluorophores Alexa 488 or Alexa 568, respectively. The presence of the fluorophores enabled the imaging of the cells by fluorescence microscopy and the determination of the localisation of the proteins of interest within the cell. As a result, an homogenous fluorescent pattern was observed for both ADSL and FGAMS, regardless of the oxygen conditions (**Figure 22**).

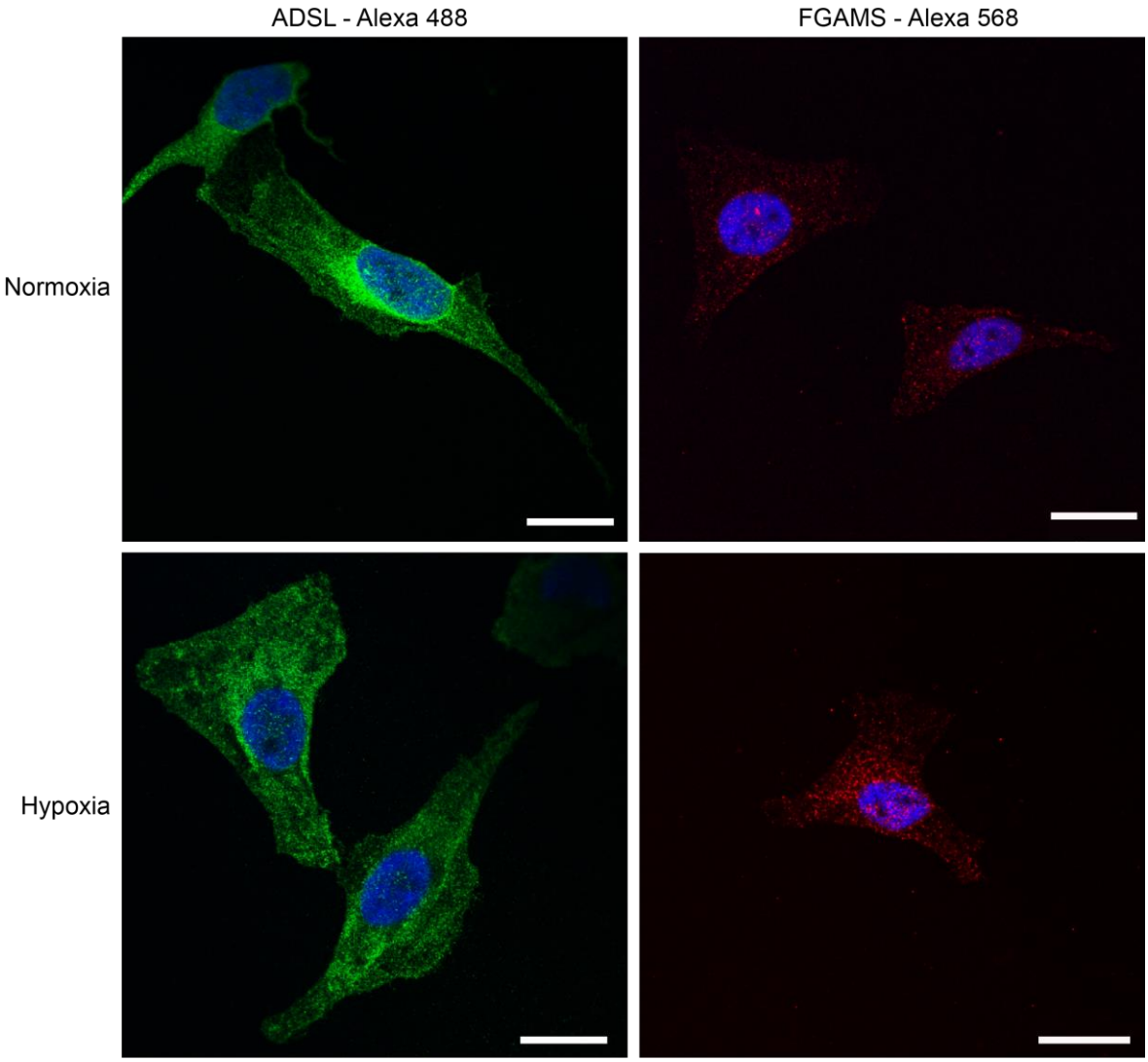

Figure 22. Detection of ADSL and FGAMS by immunofluorescence in HeLa cells incubated in normoxia and hypoxia. HeLa cells were maintained in normoxia or hypoxia (1% oxygen) for 24 h and were subsequently incubated with primary antibodies specific for ADSL or FGAMS. Secondary antibodies conjugated to Alexa 488 and Alexa 568 were used to detect and localise ADSL and FGAMS, respectively. Cells were stained with DAPI. Scale bar represents 25 µm.

Clustering of the enzymes could be expected in hypoxia in order to reveal purinosome complexes, but no such fluorescent clusters were observed. Different hypothesis can be raised regarding the absence of visible fluorescent clusters by immunofluorescence. Firstly, it can be hypothesised that despite clustering in purinosome complexes, there are still remaining free purinosome enzymes within the cell cytoplasm. The presence of these individual proteins (i.e not present in a purinosome cluster), would result in fluorescence throughout the cytoplasm thus yielding a high fluorescent background sufficient to hide the presence of the clusters. Furthermore, as a primary antibody recognises an epitope of the protein of interest, it could be thought that depending on the orientation of the protein of interest within the purinosome complex, the epitope might be

less accessible to the primary antibody, thus limiting the detection. In addition, if multiple copies of a given protein are present within the purinosome, their orientation/organisation in the complex might vary from one copy to another which would result in not all the copies being detectable by immunofluorescence. Finally, as the stoichiometry of the complex is unknown, it is likely that at least some of the purinosome complexes contain only one copy of each protein. As such, the recognition by the antibody of an enzyme within the purinosome complex would not be distinguishable from a "free" cytoplasmic purinosome enzyme.

In order to enable the detection of purinosome complexes based on endogenous proteins levels and according to the fact that these clusters were not detectable using immunofluorescence, another label free immunostaining-based technique was used: Proximity Ligation Assay (PLA) (**Figure 23.**).[195] PLA is an *in cellulo* immunoassay similar to immunofluorescence that enables the detection of a close proximity between two proteins of interest, thus making it an extremely valuable assay when studying protein macro-complexes. In this assay, the cells are cultured under specific conditions and subsequently fixed, permeabilised and treated with two primary antibodies targeting two proteins of interest, A and B (step 1). The primary antibodies are then recognised by two different secondary antibodies linked to DNA probes (step 2). Following this, consecutive addition of ligase and polymerase enzymes enable the two DNA probes to bind to each other and to be amplified (step 3). Fluorescently-labelled complementary oligonucleotides are then added so as to bind the amplified DNA. The formed "ball" of DNA is detectable by microscopy as it emits a red fluorescent signal (step 4). If the two proteins of interest are close to each other (i.e less than 40 nm distance) (**Figure 23.a**) the two DNA probes are able to bind and amplify, thus inducing a PLA signal. However, if the proteins of interest are too far away from one another, no PLA signal is detected (**Figure 23.b**). The advantage of this assay compared to immunofluorescence is that, regardless of the stoichiometry of the complex, if two purinosome enzymes are in close proximity, their colocalisation will be detected.

To ensure that no non-specific interactions occurred, control experiments were carried out (not shown). Each primary antibody used was tested on its own in the presence of both secondary antibodies to ensure that no non-specific red signal appeared. In addition, secondary antibodies were also tested in the cells in the absence of primary antibodies to ensure that they did not display any non-specific binding to any protein within the cell (as indicated by the absence of red signal).

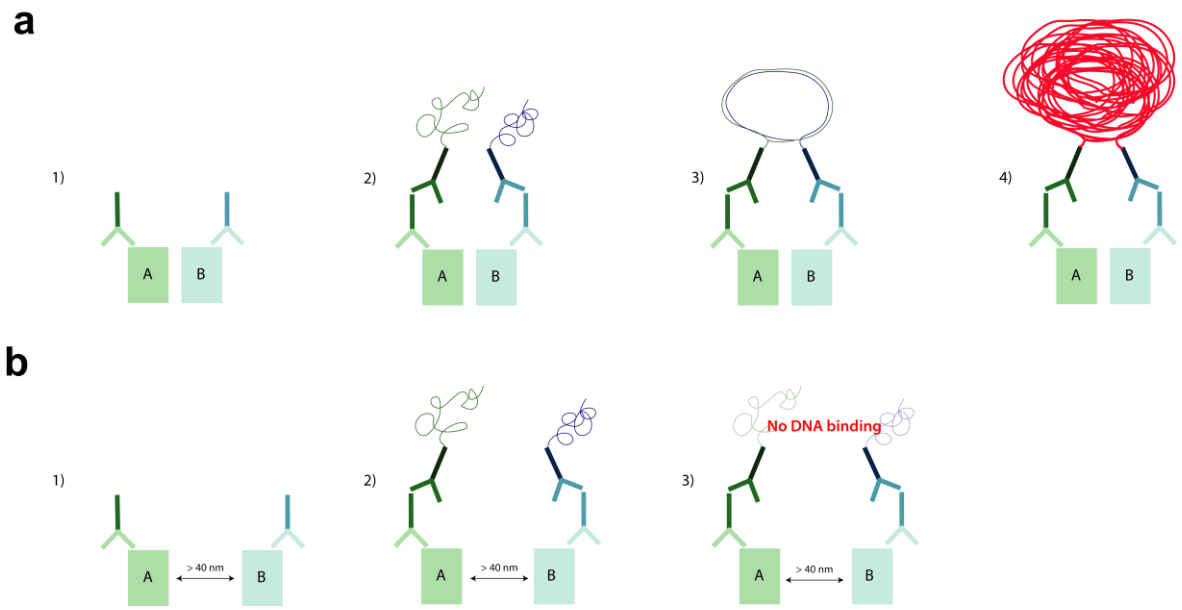

Figure 23. **Mechanism of the Proximity Ligation Assay technique**. Step 1) Two proteins A and B are recognised by two specific primary antibodies. Step 2) Addition of two secondary antibodies linked to DNA probes that recognise the primary antibodies. Step 3) Addition of ligase induces the binding of the two DNA probes to each other if these two are in close proximity (< 40 nm). Step 4) Addition of polymerase induces an amplification of DNA and apparition of a red fluorescent signal. **(a)** The close proximity of the two proteins of interest A and B is indicated by a red fluorescent signal when observed under a microscope. **(b)** If the two proteins A and B are more than 40 nm away from each other, no PLA signal is detected.

In order to study the colocalisation of the purinosome enzymes, the PLA technique was applied to the previously investigated enzymes, ADSL and FGAMS. Cells were incubated for 24 h, either in normoxia or in hypoxia, and subsequently used for the PLA assay. In this case, no PLA signal was detected in normoxia (**Figure 24a**). However, after incubation in hypoxia for 24 h, PLA signals were observed within the cytoplasm of the cells, indicating a colocalisation between ADSL and FGAMS (**Figure 24b**). As a positive control, the colocalisation of these two enzymes was also assessed in purine-depleted conditions, into which the two enzymes are known to colocalise (**Figure 24c**). In absence of purines, PLA signals were observed within the cells in the same extent as the signals observed in hypoxic conditions, confirming a colocalisation between ADSL and FGAMS both in purine-depleted conditions and in hypoxia.

Following this, pictures obtained from the PLA experiment presented in **Figure 24a-c** were used to quantify the colocalisation between ADSL and FGAMS in normoxia, hypoxia and normoxia in purine-depleted conditions (**Figure 24d**). In normoxic HeLa cells, 10% of the cells were found to be purinosome-positive. This number increased to 88% in hypoxia and 87% in purine-depleted

conditions, yielding to a 8.8-fold and 8.7-fold increase in purinosome formation compared to hypoxia, respectively.

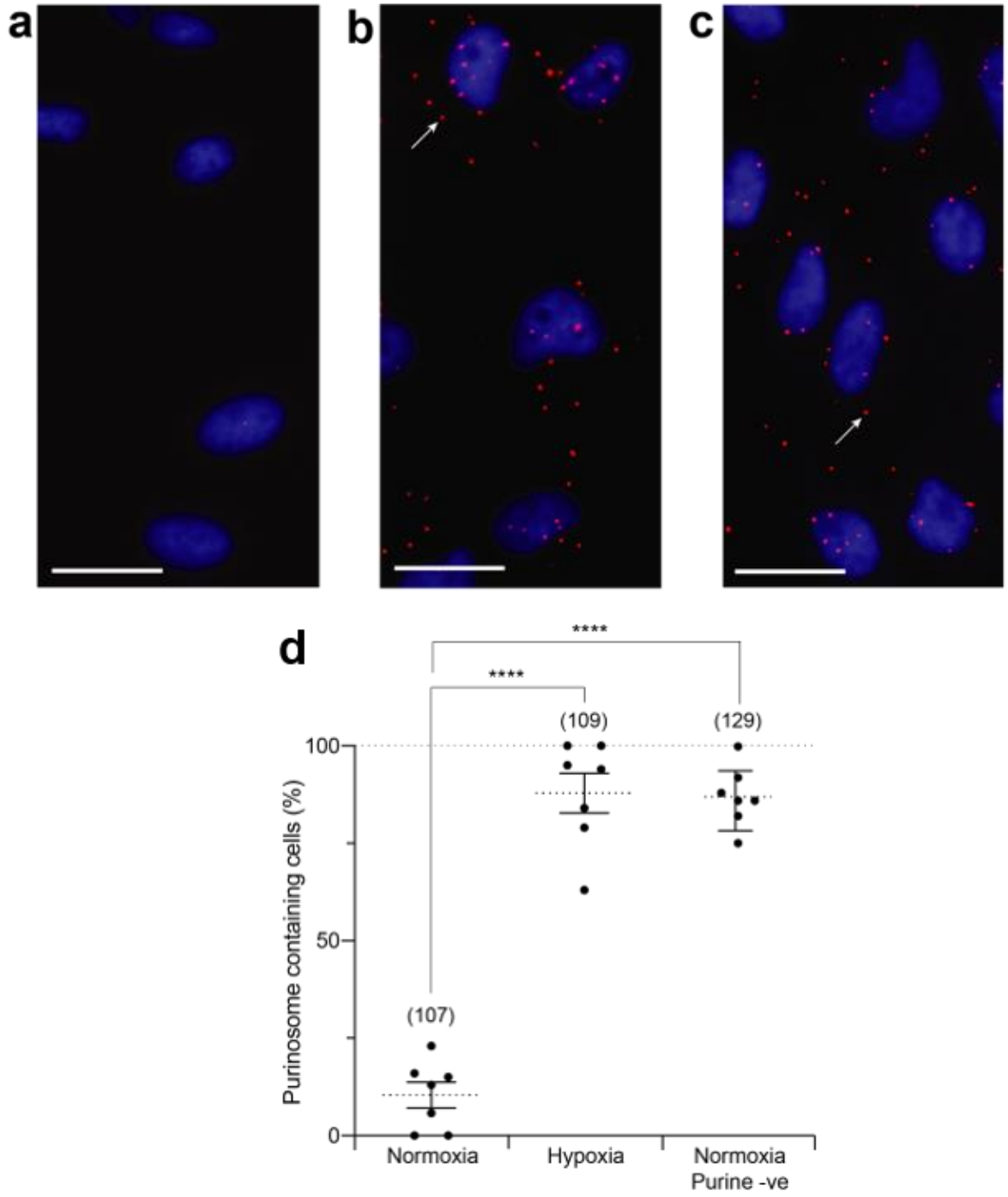

Figure 24. Proximity Ligation Assay between ADSL and FGAMS in HeLa cells. (a) HeLa cells cultured in normoxia for 24 h. **(b)** HeLa cells cultured in hypoxia (1% oxygen) for 24 h. **(c)** HeLa cells cultured in purine-depleted conditions. PLA signals were observed in hypoxia and purine-depleted conditions indicating a colocalisation between ADSL and FGAMS in these conditions. The PLA signals appear as red dots. White arrows point to individual PLA signal. Cells were stained with DAPI. Scale bar represents 25 µm. **(d)** Quantification of the colocalisation between ADSL and FGAMS by PLA in HeLa cells

maintained in normoxia, hypoxia and purine-depleted conditions (purine -ve). The number of cells containing PLA signals in each condition was quantified using 7 individual pictures per condition. Data are means (n=7) ± SEM. Significance was determined using unpaired Student t test, **** $p < 0.0001$. The number in brackets indicates the number of cells counted per condition.

It should be noted that the decision of whether a cell should be considered as purinosome-positive during the PLA experiment was based on previous data. Indeed, previous experiments carried out within the laboratory by Dr Ishna Mistry helped determine the physical characteristics of the hypoxic purinosome complexes. In this experiment, HeLa cells were transfected either with FGAMS-mCherry or ADSL-GFP and the number of clusters per cell was determined. The number of clusters per cell was found to vary between 6 and 220 with the median being 42 clusters per cell (**Figure 25**). In regard of this data, it was decided that a cell would be considered as positive if it contained at least six PLA signals.

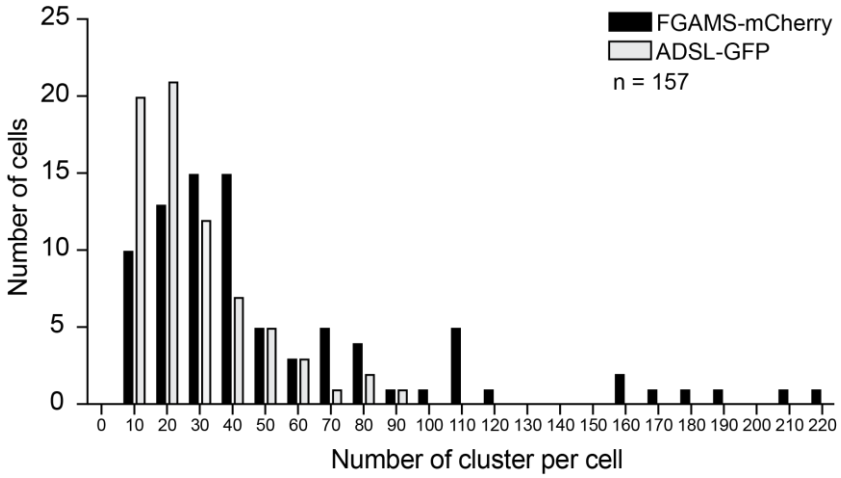

Figure 25. Number of purinosome clusters per cell transfected with FGAMS mCherry and ADSL-GFP. HeLa cells were transfected with plasmids encoding FGAMS-mCherry or ADSL-GFP and the number of clusters per cell was quantified in hypoxia (1% oxygen, 24 h).

In order to further confirm that the clusters observed were purinosomes, the PLA analysis was extended to a third enzyme of the pathway, GART. The colocalisation between GART and FGAMS was assessed, both in normoxic and hypoxic conditions in HeLa cells cultured for 24 h (**Figure 26**). As previously observed between ADSL and FGAMS, very little colocalisation was observed in normoxia (**Figure 26a**). However, the number of PLA signals was found to increase in hypoxia, suggesting an enhanced occurrence of the colocalisation between GART and FGAMS in this condition (**Figure 26b**).

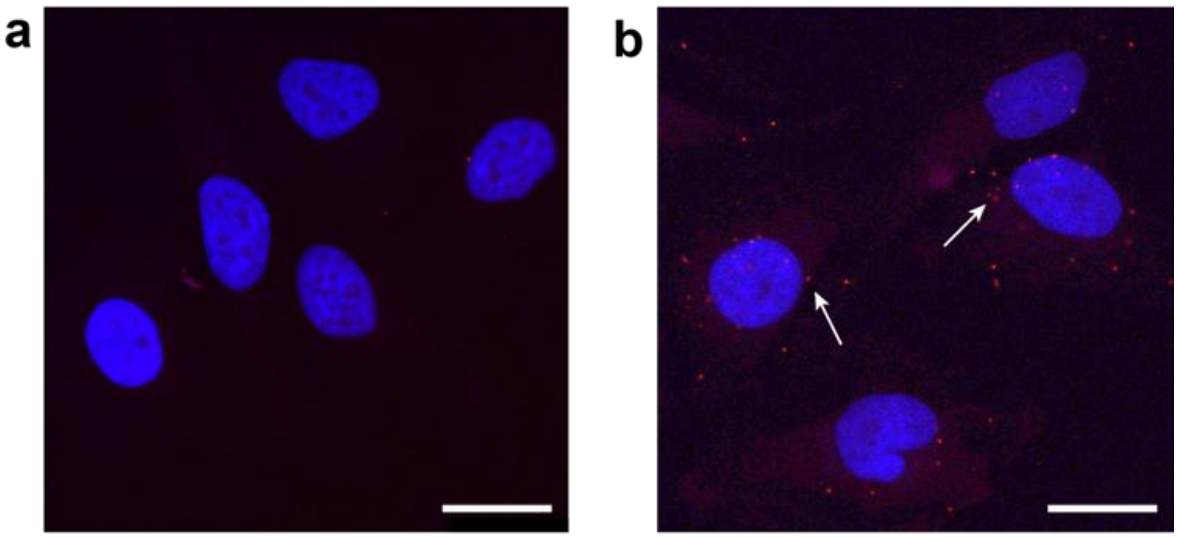

Figure 26. Proximity Ligation Assay between FGAMS and GART in HeLa cells. (a) HeLa cells cultured in normoxia for 24 h. **(b)** HeLa cells cultured in hypoxia (1% oxygen) for 24 h. PLA signals were observed in hypoxia indicating a colocalisation between GART and FGAMS in this condition. The PLA signals appear as red dots. White arrows point to individual PLA signal. Cells were stained with DAPI. Scale bar represents 25 µm.

Using fluorescently-labelled proteins and label-free techniques, ADSL and FGAMS as well as FGAMS and GART have been shown to colocalise in HeLa cells maintained in hypoxia, thus strengthening the evidence of enhanced hypoxic purinosome formation. Although a maximum of 40% of the transfected cells were found to contain purinosomes following transfection, 88% were found to be purinosome-positive when looking at endogenous protein colocalisation. This difference in number of positive cells between the two techniques could be the result of diverse variables. For example, when considering purinosome counting in transfected cells, it can be thought that although the protein of interest is overexpressed and observable thanks to its fluorescent protein tag, there is still endogenous protein present within the cell. As a result, while purinosome complexes are formed, any of these two types of proteins can join the complex. In the case of an endogenous protein clustering with the purinosome, the resulting complex would not be seen as no fluorophore would be part of the purinosome. Furthermore, it is to note that so far, no data related to the stoichiometry within the complex is available. As such, if it is hypothesised that the stoichiometry within the complex is one copy of each protein of the pathway, the complex would not be visible as a fluorescently tagged enzyme comprised within the purinosome would not be distinguishable from an isolated fluorescent signal within the cytoplasm. From this, it can be hypothesised that the clusters observed as a result of transfection contain more than one copy of the protein of interest. In contrast, PLA is a technique aiming at indicating the close proximity between two endogenous proteins of interest. Using this technique, it can be thought that any colocalisation between two proteins of the purinosome complex would

be detectable, thus revealing a number of purinosome-positive cells closer to the real occurrence of endogenously formed purinosome complexes.

Although PLA showed that most of the hypoxic HeLa cells contained purinosomes, due to the limitations of the technique such as the complexity in quantifying the number of PLA signals and considering that the cells are fixed (thus limiting the interpretation of a live occurring phenomenon), transfection of fluorescently-labelled purinosome proteins was used in the next steps of this work as a quantification technique.

So far, purinosomes were quantified and observed in hypoxic cells maintained in low oxygen environments for 24 h. In order to determine the time-course of purinosome formation in hypoxia, a set-up of hypoxic live microscopy was developed in order to record purinosome formation over time.

As such, a gas bottle containing a hypoxic gas mixture (1% oxygen, 5% carbon dioxide, 94% nitrogen) was used (**Figure 27**, **panel 1**). The gas bottle was plugged into a gas regulator in order to control the output pressure of gas into the tubing, with the input pressure coming from the gas bottle being kept at its minimum (**Figure 27**, **panel 2**). In order to further control the gas flow, the gas tubing was plugged to a flowmeter set on its minimum gas flow speed (20 mL/minute) (**Figure 27, panel 3**). The extremity of the gas tube coming from the flowmeter was placed into a sealed 35 mm cell culture dish. To enable this, the lid of the cell culture dish had previously been perforated on both sides, with an inlet diameter of approximately 4 mm so as to enable the proper fitting of the gas tubing and an outlet measuring approximately 1-2 mm (**Figure 27, panel 4**). The cell culture dish was then subsequently placed onto a DeltaVision Elite live imaging microscope equipped with a 37 °C incubator (**Figure 27, panel 5**).

To ensure high quality imaging, HeLa cells were plated onto a glass-bottom dish and were transfected with FGAMS-mCherry one day prior to recording.

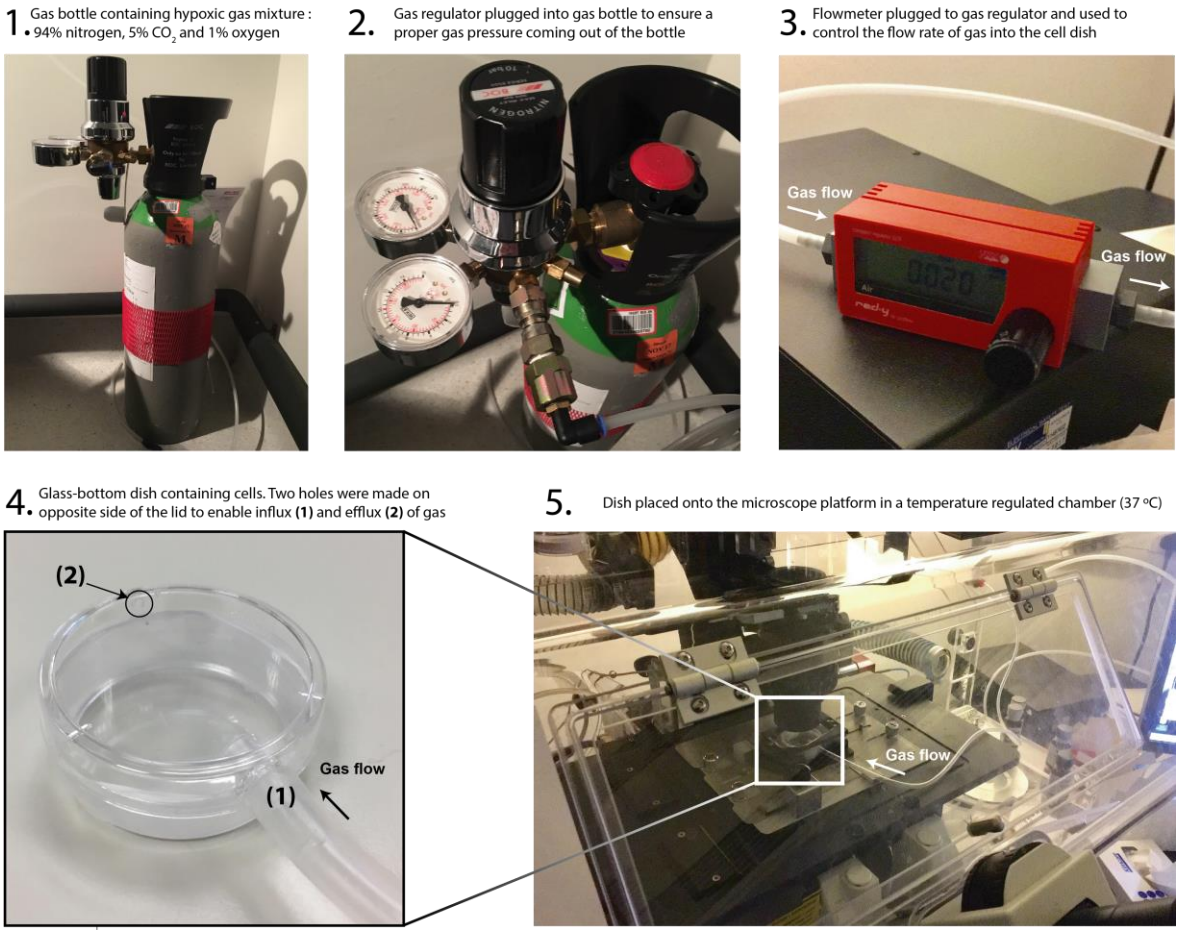

Figure 27. Equipment set up for live recording of purinosome formation. A gas bottle containing a hypoxic gas mixture **(1)** was plugged into a gas pressure regulator in order to control the output gas flow **(2)**. To further decrease the gas flow, gas tubing was plugged into a flowmeter to ensure a flow rate of 20 mL per minute **(3)**. The outgoing gas tubing was placed into the lid of a sealed 35 mm glass-bottom cell culture dish containing HeLa cells previously transfected with FGAMS-mCherry **(4)**. The dish was then placed onto the platform of a DeltaVision Elite live imaging microscope equipped with a 37°C incubator **(5)**.

To initiate the live cell recording, HeLa cells that were transfected with FGAMS-mCherry and displayed an homogenous fluorescence were selected and their coordinates on the dish were saved in order to image each of them at different time points. Pictures were acquired every 15 minutes for 4 hours for each selected cell. Image analysis enabled the reconstitution of the live formation of purinosomes by following the cellular fluorescence and associated localisation of FGAMS within the cell cytoplasm (**Figure 28**). As observed, the purinosome complexes start to appear at approximately 2 hours and 15 minutes. However, it should be noted that due to the time required to set up the experiment, the hypoxia gas flow had been opened and running

through the dish for approximately 15 minutes prior beginning of imaging, explaining the absence of a picture at time 0 h.

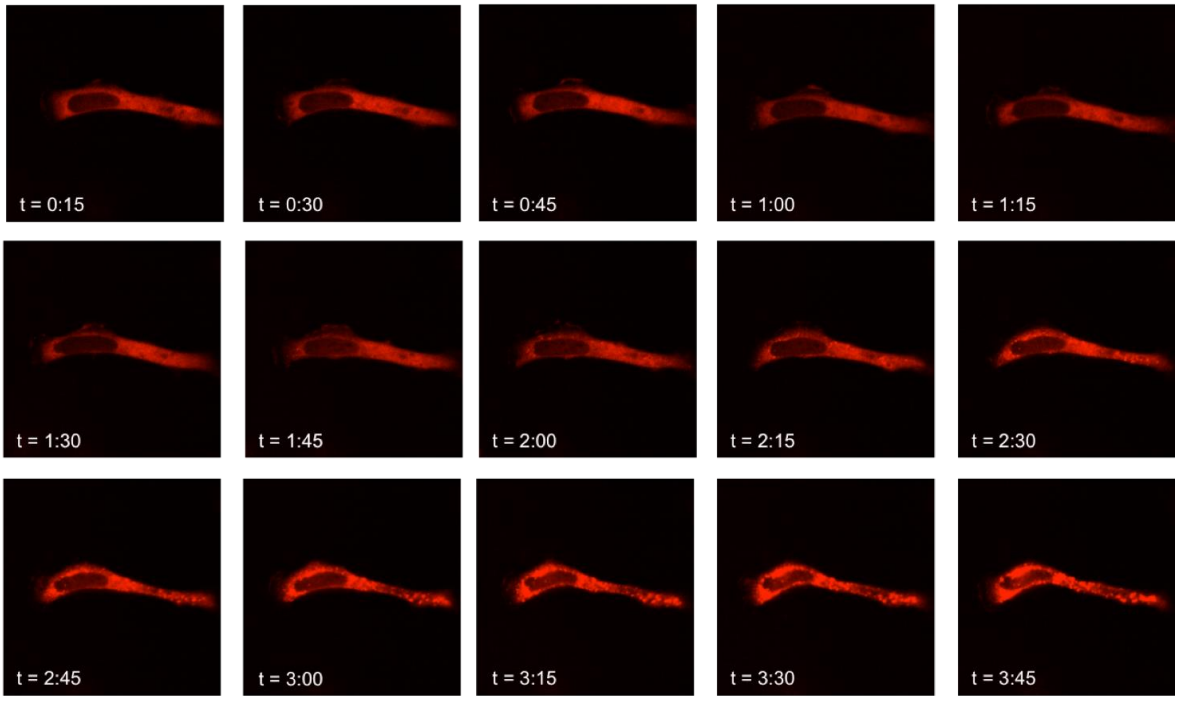

Figure 28. Purinosome formation in hypoxic HeLa cells recorded by live microscopy and observed using FGAMS-mCherry. HeLa cells transfected with FGAMS displayed an homogenous fluorescence at the beginning of the live recording. Hypoxic gas mixture was sent through the cell culture dish in order to maintain the cells in a low oxygen environment. Recording of the cellular localisation of FGAMS over time enabled the observation of the formation of purinosomes within the cell cytoplasm from approximately 2 hours and 15 minutes. Purinosome complexes remained formed until the end of the recording.

To further assess the rate of the purinosome formation over time in hypoxia, the number of purinosome-positive cells was counted at different time points. HeLa cells were transiently transfected with a plasmid encoding for FGAMS-mCherry as before and were subsequently incubated in hypoxia for 1 h, 2 h, 3 h, 4 h, 6 h, 8 h and 10 h (**Figure 29**).

From 0 h to 2 h of incubation in hypoxia, the proportion of purinosome-positive cells significantly dropped to approximately 0.6-fold change compared to normoxia. This decrease in the number of purinosome-containing cells is not unexpected as it is known that some cell lines start responding to hypoxia within 30 minutes of incubation. This early decrease could reflect an adaptation of HeLa cells to the deprivation of oxygen, requiring them to adapt their metabolisms to their new environment. This way, it could be hypothesised that two hours represents the time required for the cells to initiate their response to hypoxia. At 2 h, the number of purinosome-positive cells was

found to be at its lowest level, before increasing from 3 h until reaching a plateau at 10 h of incubation. From 10 h onwards, the number of purinosome-positive cells did not significantly change, and no significant difference was observed between 10 h and 24 h.

The increase in purinosome formation starting between 2 h and 3 h correlates with the data obtained from live recording of purinosome formation in hypoxia where the clustering of FGAMS occurred at 2 hours and 15 minutes.

It has previously been reported that purinosomes forming under purine-depleted conditions are reversible and disrupt upon purine supplementation. In the case of hypoxia-induced formation, if hypoxia represents the stimuli triggering purinosome formation, a reoxygenation of the cells containing complexes would be expected to lead to a disruption of those complexes. To probe this, HeLa cells transfected with FGAMS-mCherry were incubated in hypoxia for 10 h and subsequently reoxygenated for 2 h (**Figure 29**). When the number of purinosome-positive cells were counted in these conditions, it was found that the levels of purinosome formation had reversed back to normoxic levels. This data suggests that the purinosome complex that is triggered by a hypoxic environment is transient and reversible upon reoxygenation, thus suggesting that the cells might use the purinosomes only in certain environmental conditions and can modulate its formation depending on their purine need.

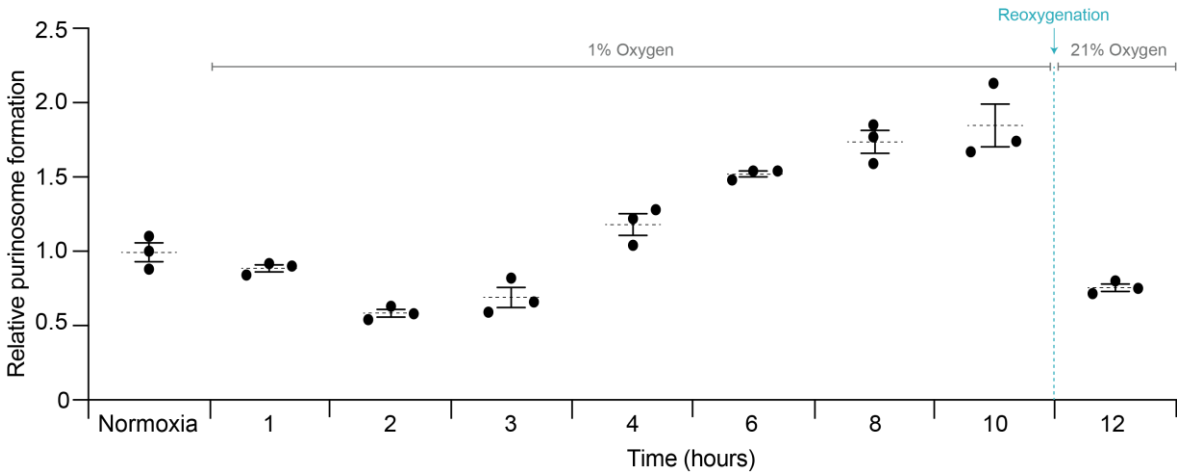

Figure 29. Time lapse of hypoxia-induced purinosome formation in HeLa cells. HeLa cells cultured in hypoxia (1% oxygen) from 0 h to 2 h displayed a decrease in the total number of purinosome positive cells. From 3 h, the number of positive cells started to increase until reaching a maximum at approximately 6 h. From 6 h to 10 h, the number of positive cells did not significantly change and reached a plateau. Data are means (n=3) ± SEM. At least 400 cells were counted for each time point.

2.1.2 Role of HIF-1α in the formation of purinosomes in hypoxia

In the first part of this work, hypoxia was shown to induce a significant increase in purinosome formation, which was found to occur gradually over time whilst cells were incubated in hypoxia. In order to understand how this formation was triggered, the role of the main regulator of the response to hypoxia, HIF-1α, was assessed. To probe whether HIF-1α was involved in purinosome formation, the first step was to assess purinosome formation whilst knocking out the *hif1a* gene.

As such, HeLa cells were treated with a HIF-1α small interfering RNA (siRNA), which is a small RNA fragment that specifically binds the HIF-1α mRNA and induces its degradation via the Dicer/RISC machinery, thus leading to the silencing of the gene.[196] Here, HeLa cells were co-transfected with a plasmid coding for FGAMS-mCherry and HIF-1α siRNA and were subsequently incubated in hypoxia for 24 h. The number of purinosome-positive cells was counted, and it was found that HeLa cells treated with HIF-1α siRNA displayed a drop in the number of positive cells compared to hypoxic untreated cells (Student t-test **, $p < 0.01$) (**Figure 30**). The decrease in purinosome formation led to a relative purinosome number comparable to normoxic levels (Student t-test, no statistical difference), indicating that silencing the *hif1a* gene completely prevents the hypoxia-induced formation of the complexes. It should be noted that the efficiency of HIF-1α siRNA in decreasing HIF-1α expression was assessed by qPCR and is presented in **Figure 38**.

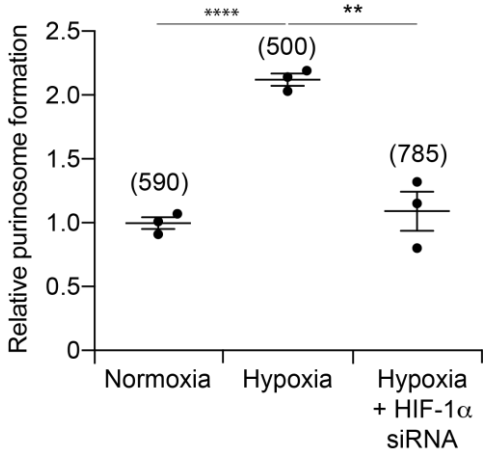

Figure 30. Effect of the knocking down of HIF-1α on the number of purinosome-positive cells. Cells treated with HIF-1α siRNA and incubated in hypoxia displayed a percentage of positive cells similar to normoxic conditions (no statistical difference) indicating that depriving the cells of HIF-1α prevents the hypoxia-induced formation of purinosomes. The data shown for normoxia and hypoxia are the same as in **Figure 13** but are presented here for the comparison. Data are means (n=3) ± SEM. Significance was determined using unpaired Student t test, **** $p < 0.0001$, ** $p < 0.01$. The number in brackets indicates the number of cells counted per condition.

To further confirm that the hypoxia-induced formation of purinosomes was mediated by HIF-1α another control experiment was required. As previously described in **section 1.1.2**, HIF-1α is constantly being degraded in the presence of oxygen due to the activity of PHD enzymes that use oxygen as substrate. As such, in order to mimic the effects of hypoxia, inhibitors of the PHD proteins can be used, thus preventing the degradation cascade of HIF-1α.[197] One of the most commonly used inhibitors of the PHDs is deferoxamine (DFX), that acts as an iron chelator competing the endogenous iron(II) required for PHD activity. Addition of DFX to normoxic cells is referred to as chemically-induced hypoxia.[198]

Prior to assessing the effect of DFX on purinosome formation, a viability test was carried out to ensure that treating the cells with 100 μM of DFX did not induce cell toxicity. The viability of the treated HeLa cells was measured by trypan blue exclusion test. Briefly, in this test cells are resuspended and mixed with a trypan blue dye. If the treatment causes damage to the cells, the membrane is likely to lose its integrity and become permeable, thus enabling the dye to enter the cells and stain them blue. The cell suspension is then placed in a haemocytometer and the number of stained cells, as well as the total number of cells, are counted and the percentage of viable cells (not stained) is calculated.[199]

This viability test was carried out on cells incubated in normoxia, hypoxia and DFX-treated (100 μM) in normoxia for 24 h (**Figure 31**). All three conditions were found to result in cell viability above 98% indicating that none of these treatments were toxic or harmful to the cells.

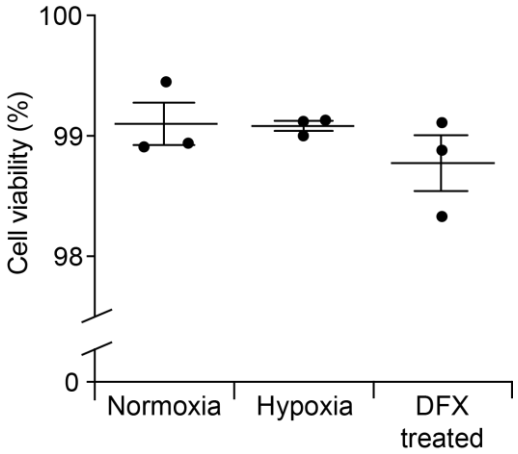

Figure 31. Assessment of the cell viability of HeLa cells treated with DFX using trypan blue exclusion test. HeLa cells were incubated in normoxia, hypoxia or normoxia with 100 μM DFX for 24 h. Number of live cells (not stained) was normalised to the total number of cells and represented as percentages of cell viability. Treatment is considered as not harmful or toxic if cell viability is above 95%. Data are means (n=3) ± SEM.

As DFX is known to enable the stabilisation of HIF-1α, HeLa cells were treated with 100 µM of DFX for 24 h in normoxic conditions and protein levels were analysed by western blot (**Figure 32**). In normoxia, HIF-1α protein levels are low and multiple degradation bands were observed. However, in hypoxia, the levels of HIF-1α were higher than in normoxia, and treatment with DFX under normoxic conditions led to even higher protein levels.

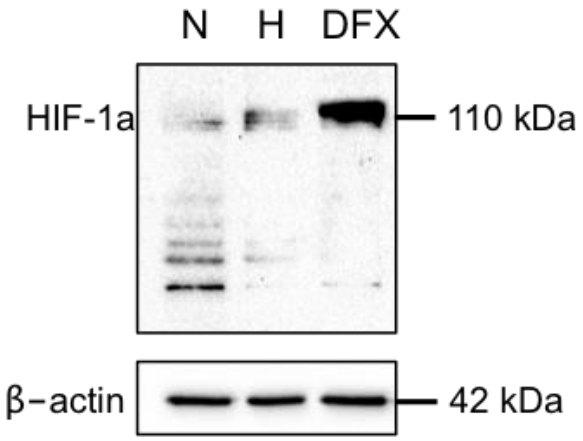

Figure 32. Effect of deferoxamine on HIF-1α analysed by western blot. The protein level of HIF-1α in normoxic cells (N) was low and degradation products were observed. Environmental hypoxia (H, 1% oxygen) and chemically-induced hypoxia (DFX) induced the up-regulation of HIF-1α. β-actin was used as an internal loading control.

To further confirm that the hypoxic formation of purinosomes was mediated by HIF-1α, HeLa cells were transiently transfected with the plasmid encoding FGAMS-mCherry as before and were subsequently treated with 100 µM DFX for 24 h in normoxia (**Figure 33**). As expected, the number of purinosome-positive cells observed in DFX-treated cells increased by approximately 2-fold, thus reaching a level similar to hypoxic conditions (no significant difference by Student t-test). This data confirmed that the hypoxia-induced formation of purinosomes is mediated by HIF-1α and is not dependent upon oxygen levels directly.

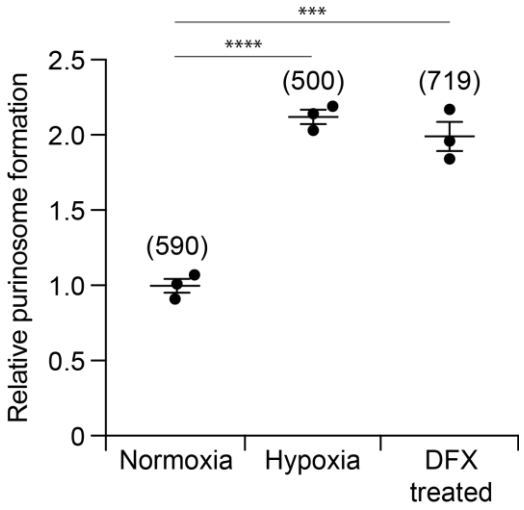

Figure 33. Effect of DFX treatment on the number of purinosome-positive HeLa cells cultured in normoxic conditions. Cells treated with DFX and incubated in normoxia for 24 h displayed a number of positive cells similar to hypoxic conditions (no statistical difference), indicating that the stabilisation of HIF-1α by DFX leads to the same results as environmental hypoxia on purinsome formation. The data shown for normoxia and hypoxia are the same as in **Figure 13** but are presented here for comparison. Data are means (n=3) ± SEM. Significance was determined using unpaired Student t test, **** $p < 0.0001$, *** $p < 0.001$. The number in brackets indicates the number of cells counted per condition.

Both inhibition of HIF-1α in hypoxia and its chemical stabilisation in normoxia were found to impact upon purinosome formation. These results indicate that the transcription factor is likely to be a key element responsible for the purinosome formation in response to hypoxia.

In order to understand how HIF-1α is linked to purinosome formation, a time-course on the protein levels of the transcription factor was carried out at the same time points as the ones used in the overtime measurement of purinosome formation (**Figure 29**). It was found that the protein levels of HIF-1α over time increased in hypoxia until reaching a maximum at 3 h. It should be noted that after 3 h, the protein levels of HIF-1α gradually decreased which is consistent with previous reports.[200, 201]

When looking at hypoxic purinosome formation, it was found that the number of cells-containing complexes started to increase from approximately 3 h, which highly correlates with HIF protein levels. Although HIF-1α levels decrease after 3 h, the purinosome formation was in contrast found to keep increasing, likely because the downstream effects of HIF activation persist.

The correlation between the time at which HIF-1α levels peak and the initiation of purinosome formation represents additional evidence of a link between these two processes.

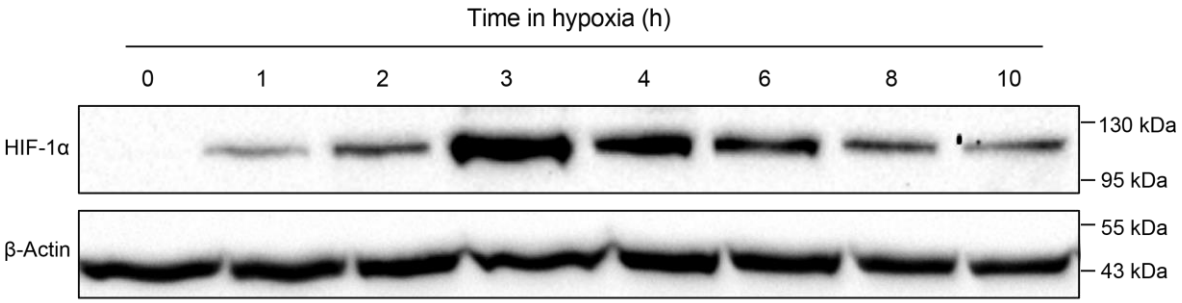

Figure 34. Protein levels of HIF-1α over time in hypoxia. HeLa cells were cultured in hypoxia (1% oxygen) for different incubation times and the levels of HIF-1α protein at each time point was analysed. β-actin was used as loading control. HIF-1α protein levels increased until reaching a maximum at 3 h and then gradually decreased to remain stable from approximately 8 h of hypoxic incubation.

To further probe the involvement of HIF-1α in the hypoxic purinosome formation, the formation of the complex was assessed in the renal cell adenocarcinoma cell line 786-O, which does not express HIF-1 (**Figure 35**).[63] The cells were transfected with a plasmid encoding FGAMS-mCherry and placed in hypoxia for 24 h. When purinosome formation was assessed in these cells, no increase was observed under hypoxic conditions. However, when cells were placed in purine-depleted conditions, a 6.6-fold increase in purinosome formation was observed, suggesting that 786-O cells are able to make purinosomes but the lack of HIF-1 prevents the formation of the complexes in hypoxic conditions.

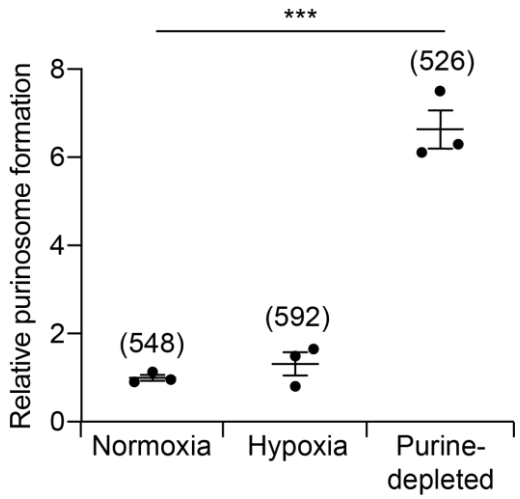

Figure 35. Relative purinosome formation in 786-O cells cultured in hypoxia and purine-depleted conditions. Hypoxic conditions (1% oxygen) did not induce any increase in the number of purinosome-positive cells compared to normoxia. Cells in purine-depleted conditions displayed a 6.6-fold increase in purinosome formation. Data are means (n=3) ± SEM. Significance was determined using unpaired Student t test, *** $p < 0.005$. The number in brackets indicates the number of cells counted per condition.

It has been shown that HIF-1α plays a pivotal role in triggering purinosome formation in cells experiencing hypoxia. However, the presence of the protein within the purinosome complex remained to be assessed. As such, a proximity ligation assay (PLA) was carried to probe the colocalisation of HIF-1α and ADSL (**Figure 36**). HeLa cells were incubated in normoxia and hypoxia for 24 h and treated as before for this assay. When observed by confocal microscopy, red signals were observed in both normoxia and hypoxia (**Figure 36 a** and **b**, respectively). The presence of PLA signal in normoxia can likely be considered as background signals, as HIF-1α is known to be degraded in the presence of oxygen. The fact that the primary antibody specific for HIF-1α recognises only a small epitope within the entire protein can partly explain this background recognition by the antibody. In addition, no difference in the number of red signals was observed between normoxia and hypoxia thus suggesting that HIF-1α does not preferentially interact with ADSL in one condition over the other. This data suggests that the transcription factor is not part of the purinosome complex. Moreover, HIF-1α is known to be translocated into the nucleus in hypoxia indicating that a positive PLA signal involving an interaction with HIF-1α would be expected to be found within the nucleus and a colocalisation between the cytoplasmic ADSL and HIF-1α would be unexpected.[202] As the purinosomes are cytoplasmic clusters, it would therefore be unlikely to find HIF-1α within the purinosome complex.

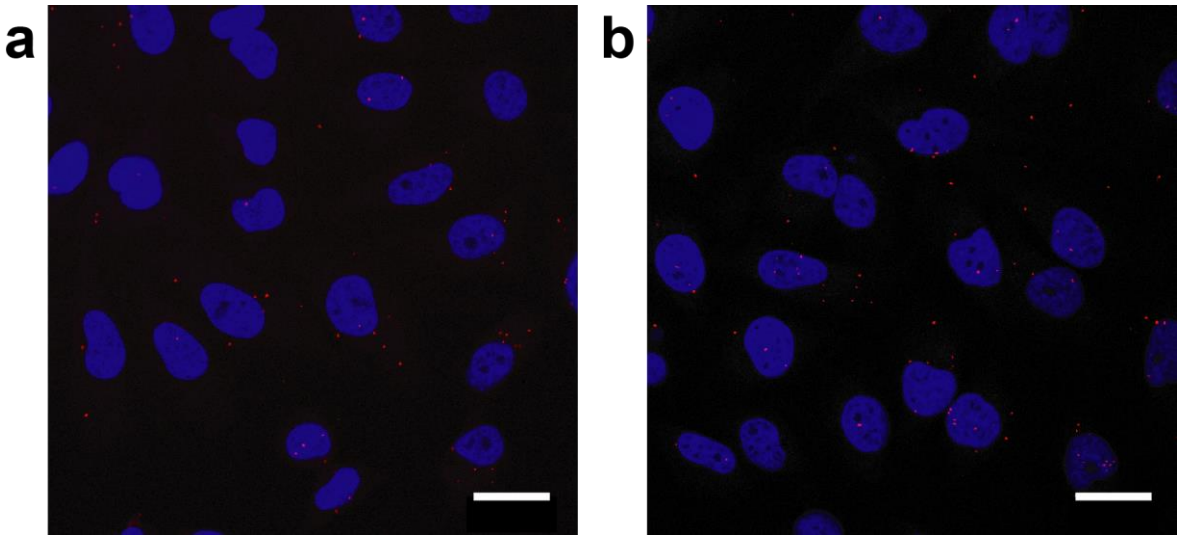

Figure 36. Proximity Ligation Assay between ADSL and HIF-1α in normoxia and hypoxia. (a) Cells cultured in normoxia for 24 h. **(b)** Cells cultured in hypoxia (1% oxygen) for 24 h. PLA signals appear in both normoxia and hypoxia indicating a background signal. No increase in the number of PLA signals in hypoxia indicates that HIF-1α is unlikely to be part of the purinosome complex. The PLA signals appear as red dots. Cells were stained with DAPI. Scale bar represents 25 μm.

The chemical stabilisation of HIF-1α using DFX was found to induce purinosome formation under normoxic condition and in contrast, the inhibition of HIF-1α using siRNA in hypoxia prevented purinosome formation. In addition, the protein levels of HIF-1α were found to correlate with the overtime rate of formation of the purinosome complexes. Altogether, this data presents HIF-1α as a modulator of purinosome formation in hypoxia, although the transcription factor has not been found as part of the complex. Despite observations indicating that HIF-1α triggers purinosome formation in hypoxia, its mechanism of action remains unclear. Additional experiments were carried out in order to decipher the role of HIF-1α in hypoxic purinosome formation and will be presented and discussed in the next section of this work.

2.1.3 Effects of hypoxia on mRNA and protein levels of purine synthesis associated proteins

As a transcription factor, HIF-1α acts by modulating the regulation (increase or decrease) of downstream target genes. As such, the first hypothesis regarding the mode of action of HIF-1α in purinosome formation was that HIF-1α could directly impact upon the gene expression of the purinosome enzymes themselves. To probe this, quantitative PCR (qPCR) was carried out on complementary DNA (cDNA) reverse-transcribed from mRNA previously extracted from HeLa cells cultured for 24 h in hypoxia and normoxia.

First, in order to ensure that the cells were responsive to the hypoxic environment, the gene expression of HIF-1α and VEGF, a target gene of HIF known to be up-regulated in hypoxia, was quantified in normoxia and hypoxia (**Figure 37**).[203] To improve the reliability of the normalisation, all gene expressions obtained from qPCR analysis were normalised to two reference genes, 18S and β-actin, that were measured and averaged. The gene expression in hypoxia was normalised to the gene expression normoxia in order to report the change in gene expression between the two conditions as a fold-change. After 24 h in hypoxia, the gene expression of *hif1a* was found to slightly increase in hypoxia with no statistical significance compared to normoxic conditions, as previously reported.[204] As such, the impact of hypoxia on HIF-1α is mostly reflected on a protein level as previously seen in **Figure 32**. In parallel, the gene expression of *vegf* was found to significantly increase in hypoxia (3.8 fold-change, Student t-test ****, $p < 0.0001$). This significant increase in *vefg* gene expression confirmed that the hypoxic conditions into which the cells were cultured were effective and that the cells were properly responding to this low oxygen environment.

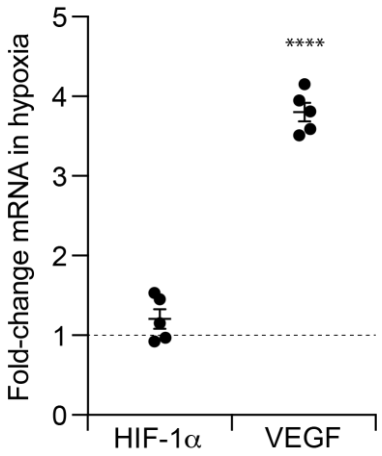

Figure 37. Relative mRNA expression of HIF-1α and VEGF in normoxia and hypoxia. Gene expression was normalised to the average of reference genes 18S and β-actin expression. Gene expression in hypoxia was normalised to normoxia. Data are means (n=3) ± SEM. Significance compared to normoxia was determined using unpaired Student t test, **** $p < 0.0001$.

In order to assess whether the purinosome formation was a consequence of HIF-1α upregulating the gene expression of the enzymes of the *de novo* pathway, qPCR analysis was carried out as before on the six genes encoding for these six enzymes (**Figure 38**). As for HIF-1α and VEGF, the gene expression was measured after 24 h of incubation in normoxia or hypoxia. The gene expression in hypoxia was normalised to normoxia and was expressed as fold-change. Overall, no significant change was found in the gene expression of the purinosome enzymes with the exception of FGAMS which was found to slightly decrease in hypoxia (0.75 fold-change). If the purinosome formation was a consequence of a HIF-induced upregulation of the gene expression of the *de novo* enzymes, the gene expression of at least one or more enzymes would be expected to increase.

Earlier in this study, an siRNA specific for HIF-1α was used to show that purinosome formation was modulated by HIF-1α. In order to ensure that the knockout of HIF-1α was efficient and that the decrease in the purinosome number observed when cells were treated with this siRNA was not due to a downregulation of the gene expression of the *de novo* enzymes, qPCR analysis was carried out to determine the level of gene expression of the six purinosome enzymes under HIF-1α knock-out conditions. HeLa cells were cultured in hypoxia with HIF-1α siRNA for 24 h and the gene expression of all above-mentioned proteins was determined (**Figure 38**).

First, the results suggest that the silencing of the *hif1α* gene was efficient, as its mRNA expression was found to be extremely low following siRNA treatment (0.2-fold compared to normoxia). In addition, the expression of VEGF was found to significantly decrease in the presence of HIF-1α siRNA (1.6-fold in hypoxia with HIF-1α siRNA vs. 3.8-fold in hypoxia untreated), thus indicating

that the downstream upregulation of the target genes of HIF-1α is mostly inhibited in these conditions. The gene expression of the enzymes of the *de novo* purine biosynthetic pathway remained mostly similar to normoxia. FGAMS which was found to slightly decrease in hypoxia (0.75-fold) displayed a slightly further decrease when the cells were treated with HIF-1α siRNA (0.6-fold-change, ** significance compared to normoxia). Although this decrease in FGAMS gene expression seems to be significant, the reasons for this remain unclear.

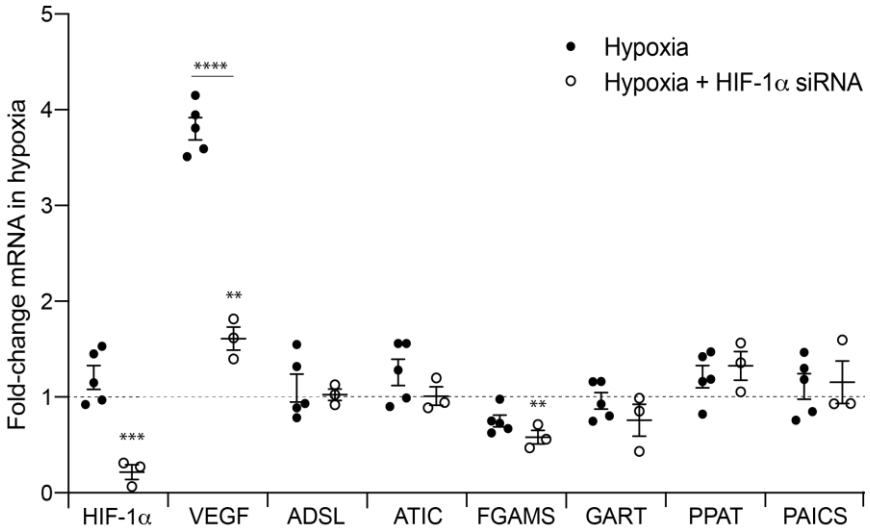

Figure 38. Relative mRNA expression of the enzymes of the *de novo* purine biosynthetic pathway in normoxia and hypoxia and effect of HIF-1α siRNA. The gene expressions of the purinosome enzymes in hypoxia remained mostly similar to their expression in normoxic conditions. FGAMS seemed to slightly decrease (**). HIF-1α siRNA down-regulates the gene expression of HIF-1α (0.2-fold compared to normoxia, ***) and VEGF (1.6-fold in hypoxia with HIF-1α siRNA, ** significance compared to normoxia,**** significance compared to hypoxia). However, HIF-1α siRNA did not affect the gene expression of the purinosome enzymes. FGAMS, that slightly decreased in hypoxia, shows a decrease when treated with siRNA in hypoxic conditions (0.6-fold change,** compared to normoxia). Gene expression was normalised to the average of reference genes 18S and β-actin expression. Gene expression of hypoxia and hypoxia with HIF-1α siRNA treatment was normalised to normoxia. Data are means (n=3 in hypoxia + HIF-1α siRNA or n=5 in hypoxia) ± SEM. Significance was determined using unpaired Student t test, ** $p < 0.01$, , *** $p < 0.005$, **** $p < 0.0001$. Data for HIF-1α and VEGF in normoxia and hypoxia are from **Figure 37** and are used for comparison only.

As the qPCR analyses enabled the observation that HIF-1α was not impacting the gene expression of most of the purinosome enzymes, the next key point was to control the protein levels of these enzymes in hypoxia. An increase in the protein levels of the *de novo* enzymes could result in the

formation of purinosomes. To probe this, HeLa cells were cultured in normoxia and hypoxia as before, and the protein content of the cells was extracted in order to be further analysed by western blot (**Figure 39**). Unsurprisingly, the protein levels matched the corresponding gene expression for each target protein. HIF-1α, presented as a positive control of the hypoxic conditions, clearly increased in low oxygen environments, further supporting the efficiency of the cell response under hypoxic conditions. Furthermore, all the purinosome enzymes displayed similar protein levels between normoxia and hypoxia, with the exception of ATIC that displayed a small increase in hypoxia, although no explanation for this has been found. In addition, the decreased gene expression of FGAMS previously observed in hypoxia did not reflect on the protein levels.

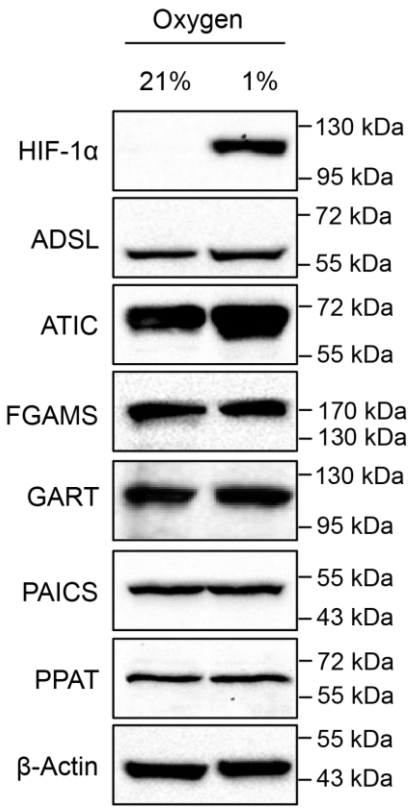

Figure 39. Western blots of the *de novo* purine biosynthetic pathway enzymes and HIF-1α in normoxia and hypoxia. HIF-1α protein level displayed a clear increase in hypoxia. Five out of six *de novo* enzymes did not display any change in protein levels following hypoxia incubation. ATIC appeared to slightly increase in hypoxia. β-actin was used as an internal loading control. 25 or 50 μg of proteins were loaded per lane depending on the target protein. Blots were repeated at least twice to ensure the reproducibility of the results.

Despite minors changes encountered in the gene expressions and the protein levels of the six purinosome enzymes, it is clear that hypoxic conditions have no effect on the general expression

of the enzymes, suggesting that the hypoxic purinosome formation does not result from gene or protein upregulation of the *de novo* purine biosynthetic enzymes.

In cells, the purine pool is maintained by the coordination of two pathways, the *de novo* biosynthesis and the salvage pathway, as previously described (**Figure 10**). Although it is clear that hypoxia and HIF-1α did not affect the expression of the enzymes of the *de novo* pathway, an effect of hypoxia on the expression of the salvage enzymes can be hypothesised. In fact, if purinosome formation does not result from the upregulation of the *de novo* enzymes, a decrease in the expression of the salvage enzymes and downstream synthesis of purines via this pathway could hypothetically lead to purinosome formation to maintain the purine pool.

As such, the effect of hypoxia on the gene expression and protein levels of the two salvage enzymes, APRT and HPRT, was assessed (**Figure 40**). After 24 h of incubation in hypoxia, no change in gene expression was observed for any of the two enzymes compared to normoxic levels (**Figure 40a**). In the same way, no change in protein levels was observed between hypoxic and normoxic conditions (**Figure 40b**).

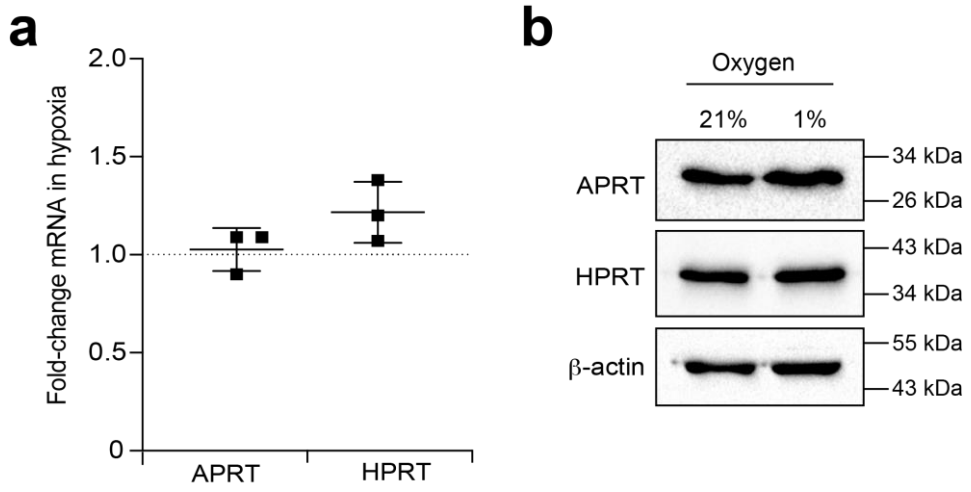

Figure 40. qPCR and western blot analysis of the purine salvage enzymes APRT and HPRT. (a) The gene expressions of the salvage enzymes were not affected in hypoxia compared to normoxia (no statistical difference). **(b)** Similarly, no difference was observed for the protein levels between normoxia and hypoxia. For the qPCR analysis, significance compared to normoxia was determined using unpaired Student t test. Blots were repeated three times to ensure reproducibility of the results.

To conclude this first section, it was determined that the formation of purinosomes is enhanced in hypoxia by 2-fold when utilising transiently transfected fluorescently-tagged enzymes, and by 8.8-fold when observing endogenous colocalisation of purinosome enzymes. This process was found

to be mediated by HIF-1α and, despite clear evidence that the transcription factor is responsible for the clustering of the six *de novo* purine biosynthesis enzymes, its mode of action has been shown to be indirect as no direct effect on the expression of the purinosome enzymes and salvage enzymes was found. The formation of the complex was found to occur in different cell types thus supporting the idea that the biological relevance of the complex is applicable to different tissues.

Although the link between HIF-1α and the purinosome is established but remains so far unclear, it is strongly hypothesised that this mechanism involves intermediate actors. Previous reports showed that different proteins, such as chaperones from the Heat Shock Proteins (HSP) family, have been reported to interact with the purinosome in purine-depleted conditions.[179] As such, in the next section of this work, the role of different members of the HSP family in the purinosome formation in hypoxia, as well as their link to HIF-1α will be assessed and discussed.

In addition, as the purinosome was shown to be a transient complex that disrupts upon reoxygenation, different conditions aiming at modulating the hypoxic purinosome formation were assessed so as to provide further insight into the functioning of the complex.

2.2 Uncovering the cellular processes affecting the hypoxia-mediated purinosome formation

2.2.1 Involvement of members of the HSP family in purinosome formation

In 2013, French *et al*. reported the involvement of two members of the HSP family in purinosome formation when purines were depleted from the media.[179] These two chaperones, namely Hsp90 and Hsp70 isoform 1, also referred to as HspA1 or Hsp70-1, were found to be involved in the maintenance of the purinosome complex. Inhibition of either of them, separately or simultaneously, led to the disruption of the complex. A few years later, further studies investigated the role of Hsp90 in the process of purinosome formation and it was found that Hsp90 interacts with only two enzymes of the complex, PPAT and FGAMS, and is responsible for processing them prior to complexation within the purinosome complex.[184] In parallel, in 2009, Hsp70 isoform 2, also known as HspA2 or Hsp70-2, was reported to be up-regulated by HIF-1α in hypoxia.[205]

In regards to this data , the role of these three HSPs was investigated in the hypoxic purinosome formation. First, the gene expression of the three chaperones was assessed in order to determine whether they were affected by low oxygen environments. As such, HeLa cells were cultured in normoxia and hypoxia for 24 h and the mRNA levels of Hsp70-1, Hsp70-2 and Hsp90 were measured (**Figure 41**). Although Hsp70-1 and Hsp90 did not display any significant difference in their hypoxic gene expression compared to normoxic conditions, Hsp70-2 was found to significantly increase in hypoxia (2.5-fold change) compared to normoxia, in line with previous reports.[205]

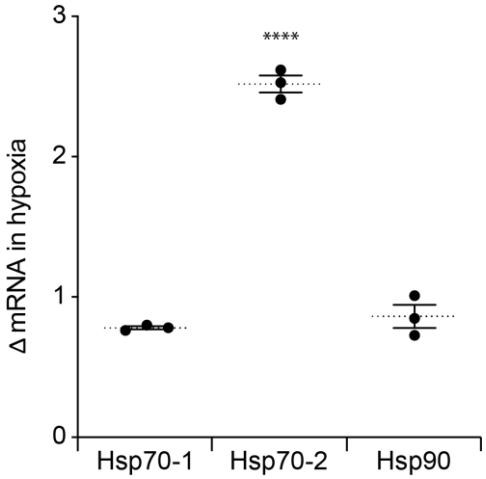

Figure 41. Relative mRNA expression of three members of the HSP family in hypoxia compared to normoxia. The gene expression of Hsp70-1 and Hsp90 in hypoxia (1% oxygen) remained similar to their expression in normoxic conditions. However, a significant increase was observed for Hsp70-2 in hypoxia (****). Gene expression was normalised to the average of reference genes 18S and β-actin expression. Gene expression in hypoxia was normalised to normoxia. Data are means (n=3) ± SEM. Significance was determined using unpaired Student t test, **** $p < 0.0001$.

To further probe the effect of hypoxia on the three HSPs, their protein levels were assessed by western immunoblotting following incubation of HeLa cells in normoxia and hypoxia for 24 h (**Figure 42**). No change in the protein levels of Hsp90 and Hsp70-1 was observed in hypoxia and only Hsp70-2 was found to increase, consistent with their previously observed gene expression.

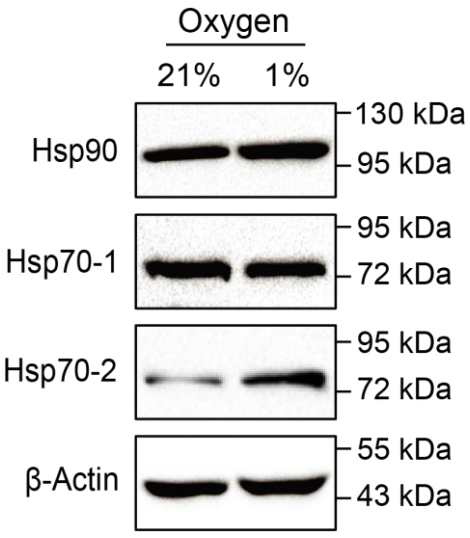

Figure 42. Western immunoblotting of Hsp70-1, Hsp70-2 and Hsp90 in normoxia and hypoxia. The protein levels of Hsp90 and Hsp70-1 remained unaffected in hypoxia (1% oxygen). Consistent with the qPCR data, Hsp70-2 protein levels increased in hypoxia. β-actin was used as an internal loading control. 25 µg of proteins were loaded per

lane. Blots were repeated two or three times to ensure the reproducibility of the results.

As Hsp70-2 was found to be the only chaperone to be upregulated in hypoxia out of the three HSPs studied, the effect of HIF-1α siRNA treatment on the gene expression of Hsp70-2 was assessed in order to determine whether the observed hypoxia-induced increase was the result of HIF activity (**Figure 43**). Upon HIF-1α knockout in hypoxia, the gene expression of Hsp70-2 significantly decreased compared to untreated hypoxic cells, indicating that its upregulation in hypoxia is HIF-1α dependent. It is to note that a significant difference in the gene expression was observed for Hsp70-2 between normoxia and hypoxia with HIF-1α siRNA (***, $p < 0.001$ by Student t-test) with the gene expression in hypoxia treated with HIF-1α siRNA displaying lower levels than in normoxic conditions. It can be hypothesised that the expression level of HIF-1α in normoxia, even if low, partly regulates the basal expression of Hsp70-2.

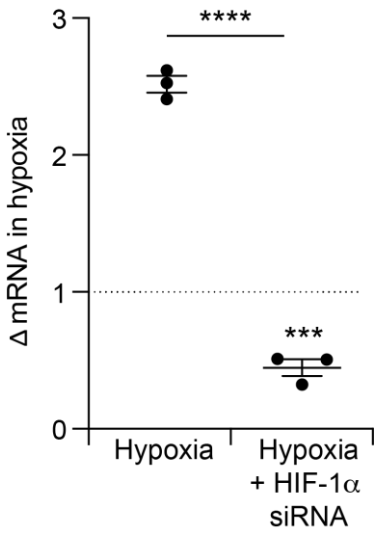

Figure 43. **Relative mRNA expression of Hsp70-2 in cells treated with HIF-1α siRNA in hypoxia.** In cells treated with HIF-1α siRNA, the gene expression of Hsp70-2 dropped to 0.44-fold compared to normoxia (***). HIF-1α siRNA significantly prevents the hypoxia-induced increase in the gene expression of Hsp70-2 (****). The data presented for the hypoxic gene expression of Hsp70-2 are reused from **Figure 41** for comparison. Gene expression was normalised to the average of reference genes 18S and β-actin expression. Gene expression in hypoxia was normalised to normoxia. Data are means (n=3) ± SEM. Significance was determined using unpaired Student t test, , *** $p < 0.001$, **** $p < 0.0001$.

Following these observations and based on previous litterature, it was then hypothesised that the three HSPs could be part of the purinosome complex in hypoxia. Although Hsp90 and Hsp70-1 were known to be part of the purinosome complex in purine-depleted conditions, the involvement of Hsp70-2 was yet to be determined.[179] To assess the presence of these proteins within the purinosome complex, PLA experiments were carried out.

The first chaperone studied was Hsp70-2 and its potential colocalisation with ADSL was assessed by PLA (**Figure 44**). In HeLa cells cultured in normoxia for 24 h, no PLA signal was observed suggesting that the two proteins were not in close proximity in this condition (**Figure 44a**). However, when cells were cultured under hypoxic conditions (**Figure 44b**), many PLA signals were present, revealing a high colocalisation between ADSL and Hsp70-2. In order to determine whether this colocalisation was a characteristic specific to hypoxia, the same experiment was repeated in purine-depleted conditions (known to induce purinosome formation) (**Figure 44c**). Surprisingly, only a small number of PLA signals were detected when compared to hypoxic conditions. This last observation suggests that Hsp70-2 is present within the purinosome complex in both purine-depleted conditions and hypoxia, although the chaperone seems to interact with the complex preferentially in hypoxia.

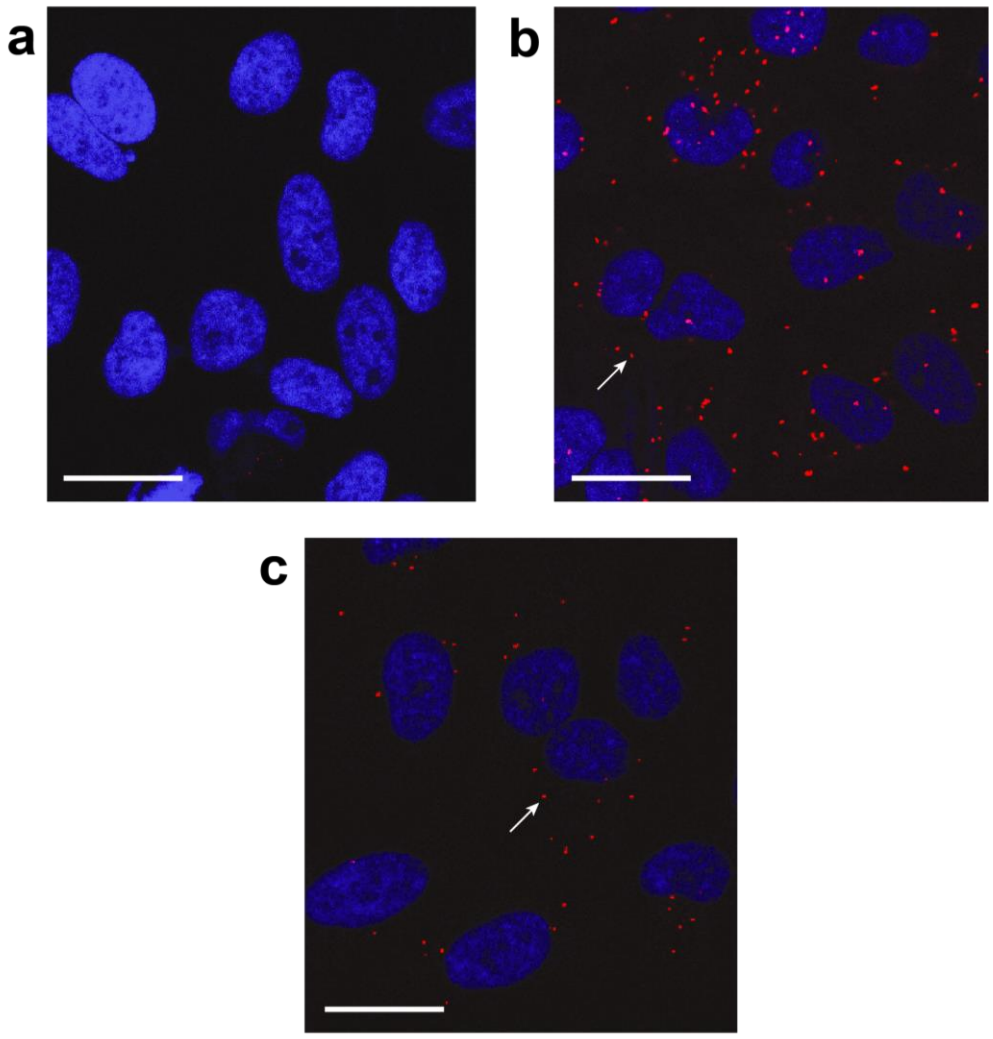

Figure 44. Proximity Ligation Assay between ADSL and Hsp70-2 in normoxia, hypoxia and purine-depleted conditions. (a) HeLa cells cultured in normoxia for 24 h did not display PLA signals **(b)** HeLa cells cultured in hypoxia (1% oxygen) for 24 h displayed a high number of PLA signals suggesting a colocalisation between the two proteins. **(c)** HeLa cells cultured in purine-depleted media for 24 h displayed some PLA signals suggesting a colocalisation between the two proteins but to a lesser extent when compared to hypoxia. The PLA signals appear as red dots. Cells were stained with DAPI. White arrows point towards individual PLA signal. Scale bar represents 25 µm.

To determine whether Hsp70-1 and Hsp90 were present in the hypoxic purinosome as previously reported in purine-depleted conditions, a PLA experiment was carried out between Hsp70-1 and ADSL (**Figure 45**). When cells were cultured in normoxia, a low number of PLA signals was observed suggesting a low degree of colocalisation between the proteins in this condition (**Figure 45a**). However, when cells were placed in hypoxia, the number of PLA signals observed increased compared to normoxia, suggesting an enhanced colocalisation between the two proteins of interest in low oxygen environments (**Figure 45b**).

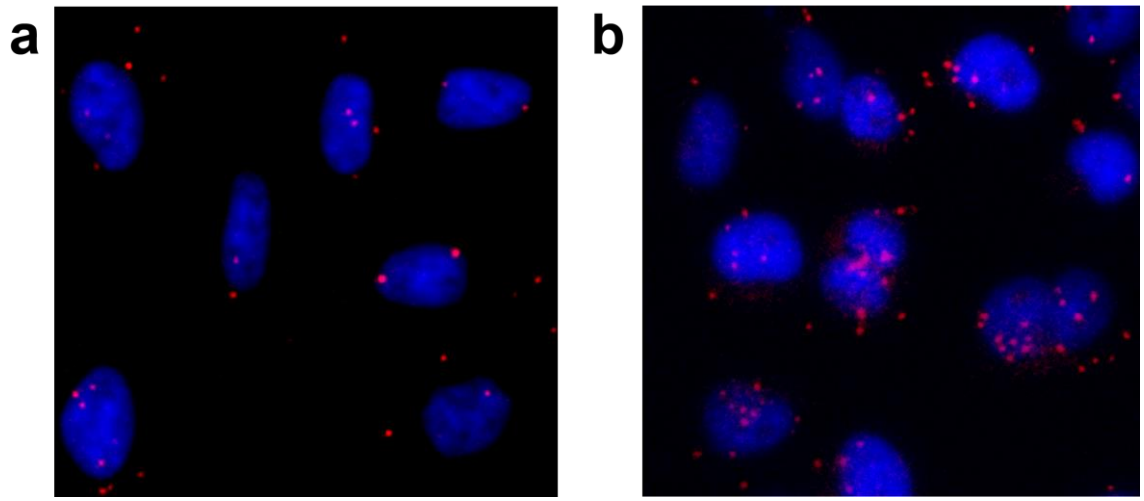

Figure 45. Proximity Ligation Assay between ADSL and Hsp70-1 in normoxia and hypoxia. (a) HeLa cells cultured in normoxia for 24 h. **(b)** HeLa cells cultured in hypoxia (1% oxygen) for 24 h. Few PLA signals were detected in normoxia while a larger number of PLA signals were detected in hypoxia, indicating that the colocalisation between Hsp70-1 and ADSL was enhanced in this condition. The PLA signals appear as red dots. Cells were stained with DAPI.

In the same way, the colocalisation between FGAMS and Hsp90 was assessed by PLA in HeLa cells cultured in normoxia and hypoxia for 24 h (**Figure 46**). As previously observed between ADSL and Hsp70-1, a small number of PLA signals was detected in normoxia (**Figure 46a**). The presence of positive PLA signals in normoxia can be explained by the fact that Hsp90 is a chaperone responsible for the folding and stabilisation of a large number of proteins in physiological conditions, including FGAMS.[184] When the cells were cultured in hypoxia, many more PLA signals were observed indicating an increased colocalisation between the two proteins compared to normoxia, supporting the hypothesis that Hsp90 is present within the hypoxic purinosome complex (**Figure 46b**).

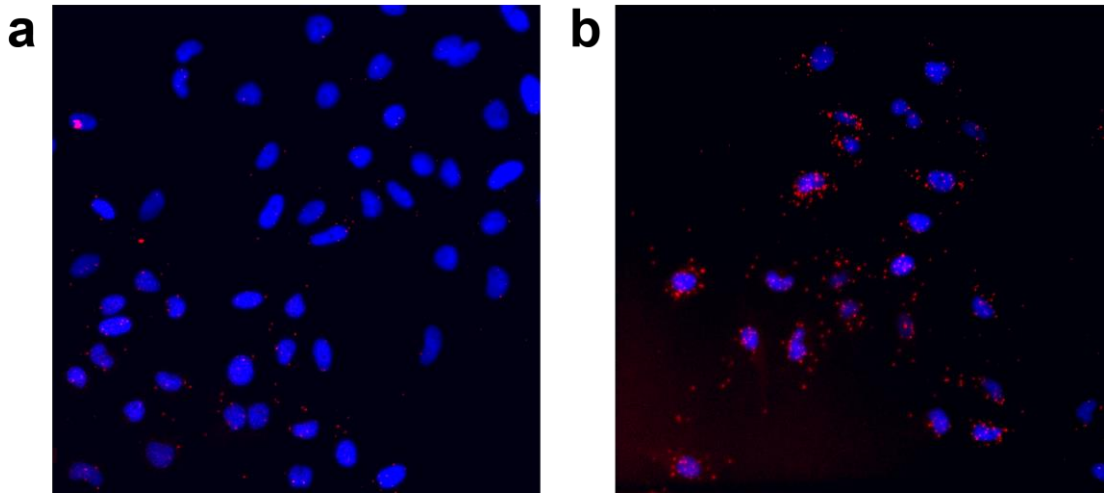

Figure 46. Proximity Ligation Assay between FGAMS and Hsp90 in normoxia and hypoxia. (a) HeLa cells cultured in normoxia for 24 h. **(b)** HeLa cells cultured in hypoxia (1% oxygen) for 24 h. A small number of signals were detected in normoxia while a more significant number of signals were detected in hypoxia, suggesting a high colocalisation of the two proteins in hypoxia. The PLA signals appear as red dots. Cells were stained with DAPI.

Hsp90, Hsp70-1 and Hsp70-2 have all been shown to colocalise with proteins of the purinosome in hypoxia. Although Hsp90 and Hsp70-1 were already known to be involved in the purinosome complex in purine-depleted conditions, there is now strong evidence that they also interact with the complex in hypoxia. Furthermore, Hsp70-2 was shown to highly interact with ADSL in hypoxia but significantly less in purine-depleted media thus suggesting that Hsp70-2 might be interacting with the purinosome preferentially in hypoxia.

When conducting a PLA experiment, the positive red signals reflect the close proximity between the two proteins of interest. In the previous experiments, it was shown that Hsp90, Hsp70-1 and Hsp70-2 were colocalising with purinosome enzymes in hypoxia, however this does not imply that the chaperones are required for the support/formation of the purinosome complex.

In order to probe this, the hypoxic formation of purinosomes was assessed in hypoxia in the presence of siRNAs specific for Hsp90, Hsp70-1 and Hsp70-2 (**Figure 47**). If the chaperones are necessary for the formation/maintenance of the complex, it would be expected that their knockout prevents the hypoxic purinosome formation. As such, it was found that when HeLa cells were treated with any of the three siRNA, the relative purinosome formation compared to hypoxic non-treated cells significantly decreased. Silencing of the genes encoding Hsp90 and Hsp70-1 induced a relative purinosome formation comparable to normoxic levels. Silencing of Hsp70-2 induced a significant decrease in purinosome formation compared to hypoxic conditions although this decrease did not reach to normoxic levels. The overall purinosome formation in

hypoxic cells treated with Hsp70-2 siRNA remained slightly above normoxic levels (* $p < 0.05$ significance by Student t test). The origin of the difference of effect on purinosome formation of Hsp70-2 siRNA compared to Hsp90 and Hsp70-1 siRNAs remains unknown however.

To summarise, all three studied members of the HSP family are required to ensure the hypoxia-induced purinosome formation.

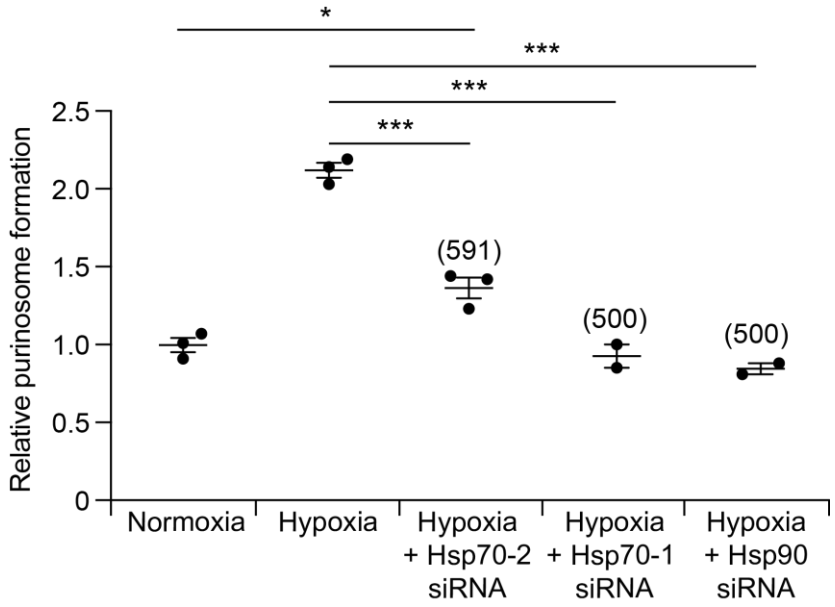

Figure 47. Relative purinosome formation in HeLa cells cultured in hypoxia in the presence of siRNAs specific for Hsp70-2, Hsp70-1 and Hsp90. HeLa cells maintained in hypoxia (1% oxygen) and treated with Hsp90 and Hsp70-1 siRNA displayed a number of positive cells similar to normoxic conditions (no statistical difference). Cells cultured with Hsp70-2 siRNA in hypoxia also displayed a decrease when compared to hypoxia untreated (***), but the number of purinosome-positive cells remained higher than in normoxia. The data shown for normoxia and hypoxia are the same as in **Figure 13** but are presented here for comparison. Data are means (n= at least 2) ± SEM. Significance was determined using unpaired Student t test, * $p < 0.05$, *** $p < 0.001$. The number in brackets indicates the number of cells counted per condition.

In order to evaluate whether the observed effects of the siRNAs targeting the three chaperones were specific to hypoxic purinosomes, especially in the case of Hsp70-2 which was found to preferentially colocalise with ADSL in hypoxia compared to purine-depleted conditions, the same experiment using siRNAs was repeated in purine-depleted conditions (**Figure 48**). In line with previous reports which indicated that an inhibition of Hsp90 and Hsp70-1 led to a 2-fold decrease in relative purinosome formation in purine depleted conditions, the same effect was observed here using siRNAs instead of small molecule inhibitors.[179] In purine-depleted media, siRNA treatments against Hsp90 and Hsp70-1 led to a 1.5-fold and 1.6-fold decrease, respectively,

compared to hypoxic untreated cells. However, it was surprisingly found that Hsp70-2 siRNA also induced a decrease in purinosome formation (1.7-fold change compared to hypoxia untreated). This last result was unexpected due to the fact that by PLA, Hsp70-2 was not colocalising as much with ADSL in purine-depleted media when compared to hypoxia (**Figure 44**).

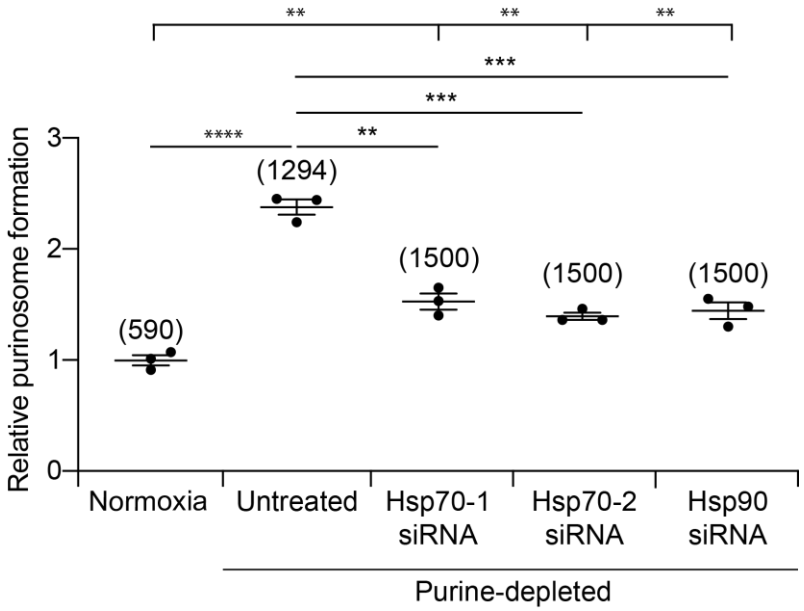

Figure 48. Relative purinosome formation in HeLa cells treated with Hsp90, Hsp70-1 and Hsp70-2 siRNAs in purine-depleted conditions. Purine-depleted conditions induced a 2.4-fold increase in the number of purinosome-positive cells compared to normoxia. Treatment with Hsp70-1 siRNA, Hsp70-2 siRNA and Hsp90 siRNA induced significant decreases in the number of purinosome-positive cells (1.64-fold, 1.7-fold and 1.55-fold, respectively). Data are means (n=3) ± SEM. Significance was determined using unpaired Student t test, ** $p < 0.01$, *** $p < 0.001$, **** $p < 0.0001$. The number in brackets indicates the number of cells counted per condition.

Due to the increase in PLA signals between ADSL and Hsp70-2 in hypoxia, it can be hypothesised that the previously determined hypoxia-induced upregulation of Hsp70-2 is partly responsible for the increased purinosome formation in hypoxia. The increased availability of the chaperone can potentially trigger purinosome formation in hypoxia by contributing to the stabilisation of the complex. To probe this, purinosome formation was assessed in normoxic cells into which Hsp70-2 was up-regulated by transient plasmid transfection. To do so, first a control experiment was carried out where a plasmid encoding Hsp70-2 fused to GFP was transfected into HeLa cells (**Figure 49a**). Following normoxic incubation, a clear fluorescence was observed in the cells suggesting that the fusion protein was properly expressed.

Following this, the same construct encoding Hsp70-2 without GFP was transfected into HeLa cells that were subsequently incubated in normoxia for 24 h. As a second means of control of the

proper expression of Hsp70-2 in these cells, Hsp70-2 protein levels were assessed (**Figure 49b**). As such, western immunoblotting was carried out on Hsp70-2 from HeLa cells transfected with the Hsp70-2-encoding construct which were compared to mock transfect cells (i.e endogenous Hsp70-2 levels). In cells transfected with the Hsp70-2-encoding construct, a clear increase in protein levels was observed, thus suggesting an increase in the expression of the chaperone as a result of the transfection.

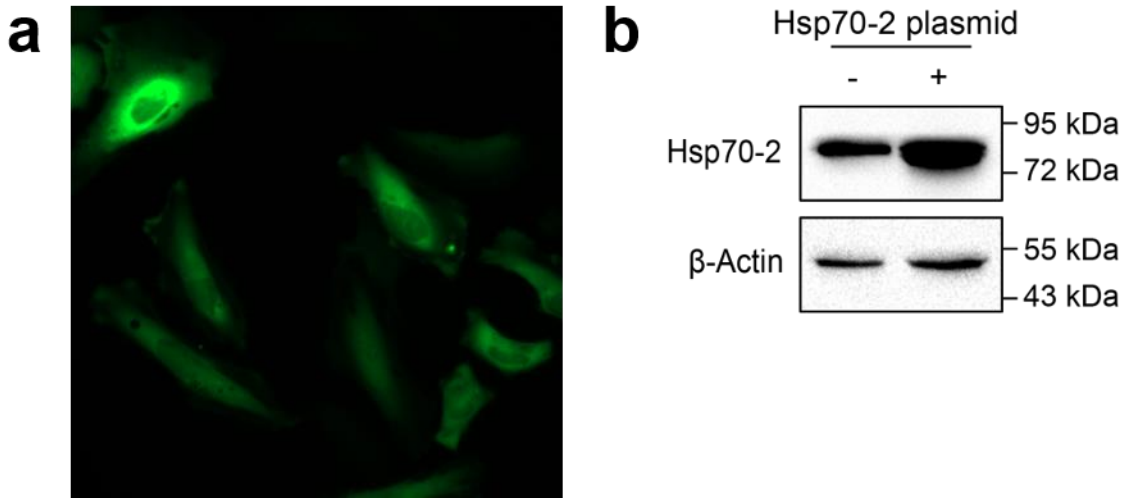

Figure 49. **Upregulation of Hsp70-2 in HeLa cells. (a)** HeLa cells were transiently transfected with a plasmid encoding Hsp70-2 fused to fluorescent protein GFP. The cells displayed green fluorescence indicating that Hsp70-2 was properly expressed. **(b)** Western immunoblotting of Hsp70-2 with and without transfection of a Hsp70-2 encoding plasmid. The protein levels of Hsp70-2 increased in cells transfected with plasmid encoding Hsp70-2 (+) compared to mock transfected cells (-). β-actin was used as an internal loading control. 25 µg of proteins were loaded per lane. Blots were repeated twice to ensure the reproducibility of the results.

As it was confirmed that the transfection of a Hsp70-2-encoding plasmid enabled the proper up-regulation of the protein, HeLa cells were then either co-transfected with this construct and a plasmid encoding FGAMS-mCherry or transfected with FGAMS-mCherry alone. Following normoxic incubation for 24 h, purinosome formation was assessed in HeLa cells and no increase was observed in cells transfected with the Hsp70-2 construct (**Figure 50**). Although Hsp70-2 is up-regulated in hypoxia in a HIF-1α-dependent manner, its artificial upregulation in normoxic conditions was not sufficient to induce purinosome formation.

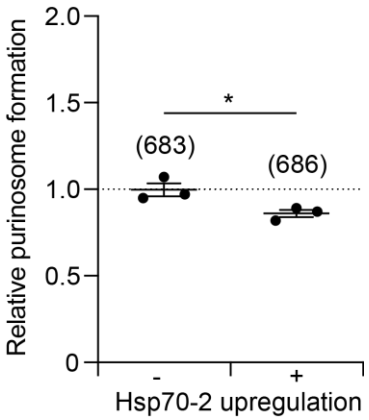

Figure 50. Relative purinosome formation in normoxia with or without Hsp70-2 upregulation. HeLa cells were either mock transfected (-) or transfected with a plasmid encoding Hsp70-2 (+) and subsequently maintained in normoxia for 24 h. The number of cells containing purinosome was assessed and a small decrease was observed in the treated cells compared to untreated (*) suggesting that the upregulation of Hsp70-2 did not induce purinosome formation in normoxia. Data are means (n=3) ± SEM. Significance was determined using unpaired Student t test, * $p < 0.05$. The number in brackets indicates the number of cells counted per condition.

Following these observations, many assumptions can be made about the roles of the HSPs in the hypoxic purinosome formation. It is now clear that each of Hsp90, Hsp70-1 and Hsp70-2 are required for the formation of the purinosome complex in hypoxia. Although Hsp70-2 was thought to be exclusively found in the purinosome in hypoxia, its silencing in purine-depleted media also led to a decrease in purinosome formation, indicating that this chaperone is involved in the purinosome formation / maintenance in these conditions (**Figure 48**). However, this result is in contrast with the PLA experiment where it was found that Hsp70-2 was colocalising with ADSL preferentially in hypoxia compared to purine-depleted conditions. (**Figure 44**).

Different causes for this phenomenon can be hypothesised. As Hsp70-2 has been reported to interact with both Hsp70-1 and Hsp90, it can be thought that a silencing of Hsp70-2 is likely to prevent the proper activity of its chaperone partners, thus inducing a decrease in purinosome formation.[168,206] Although this hypothesis can be viable for both purine-depleted conditions and hypoxia, the increased number of PLA signals in hypoxia compared to purine-depletion supports the hypothesis that Hsp70-2 is prevalently involved in the hypoxia-induced purinosome complex. However, despite being necessary for the complex to form in hypoxia, the HIF-mediated upregulation of Hsp70-2 is not the origin of the hypoxic purinosome formation as upregulating the protein in normoxia did not trigger purinosome formation.

Overall, all three HSPs can be found within the hypoxic purinosome complex and constitute an important factor in its formation. Although required in the assembly of the complex in hypoxia, the above-mentioned data suggests that the HSP proteins are not at the origin of the purinosome formation. It can be strongly hypothesised that other hypoxia-related factors and / or mechanisms are involved in the process of hypoxic purinosome formation.

To further determine how the hypoxic purinosome functions and on what features its assembly relies, different conditions aiming at modulating the hypoxic purinosome formation were investigated. As such, various conditions were assessed in order to modify the environment of the purinosome proteins to further understand the relationship between the multi-enzyme complex and its environment.

2.2.2 Inhibiting the formation of purinosomes

The purinosome complex was first described in artificial cellular conditions where cells had been cultured in purine-depleted media. Few cases of purinosome formation in "natural" conditions have been reported since then, one being in fibroblasts derived from a patient suffering from AICA-ribosiduria.[170] This extremely rare and severe pathology results from a deficiency of the last enzyme of the *de novo* purine biosynthesis, ATIC.[207] When purinosome formation was studied in these cells maintained in purine-depleted conditions, no purinosome was observed although their healthy fibroblast counterparts cultured in the same conditions contained purinosomes. This data suggested that the formation of the purinosome complex likely required all the enzymes of the pathway to be present and structurally intact. This hypothesis was further probed and confirmed by the same research group a few years later. In their later work, the authors used CRISPR-knockout HeLa cells and deleted each enzyme of the *de novo* purine pathway individually.[171] Upon culturing in purine-depleted conditions, it was found that a deficiency in any enzyme of the *de novo* pathway induced a disruption of the purinosome formation.

Following the hypothesis that purinosome formation requires the presence of all purinosome enzymes, HeLa ATIC CRISPR-KO cells were used to probe the purinosome formation in hypoxia. The previously reported cells were obtained from Dr M. Zikanova's lab (Charles University, Prague, Czech Republic) and were previously controlled by western immunoblotting to show the absence of ATIC in this cell line.[171]

These cells were transfected with a plasmid encoding FGAMS-GFP and were incubated in normoxia untreated or in the presence of 100 µM DFX in order to chemically induce hypoxic conditions (**Figure 51**). Compared to untreated cells in normoxia, treatment with DFX did not induce purinosome formation in ATIC-KO HeLa cells, although the same treatment was found to

result in purinosome formation in wild-type HeLa cells (**Figure 33**). This data suggests that the hypoxic purinosome formation relies, like in purine-depleted conditions, on the presence and structural integrity of ATIC, and likely of all six purinosome enzymes.

It is to note that the observation of these cells in low oxygen conditions was attempted multiple times but consistently resulted in poor fluorescence for unknown reasons, thus explaining the choice of DFX treatment instead.

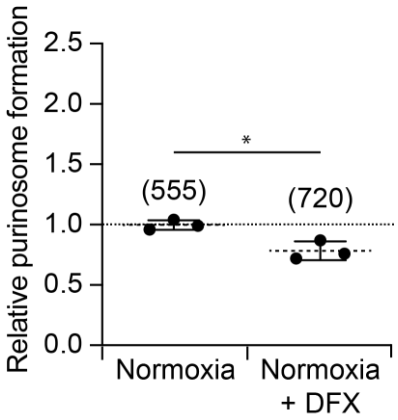

Figure 51. Relative purinosome formation in ATIC knockout HeLa cells. ATIC KO HeLa cells were transfected with a construct encoding FGAMS-GFP and were subsequently cultured in normoxia untreated or in the presence of DFX (100 µM) for 24 h. Although DFX induced purinosome formation in WT HeLa cells (**Figure 33**), no increase was observed in ATIC KO cells. Data are means (n=3) ± SEM. Significance was determined using unpaired Student t test, * $p < 0.05$. The number in brackets indicates the number of cells counted per condition.

After it was found that the presence of ATIC was required for the formation of the purinosome in hypoxia, whether ATIC had to be functional for the complex to form remained unknown. In order to probe this, the formation of purinosomes was assessed in HeLa cells treated with a small molecule inhibitor of ATIC named Compound 14 (Cpd14). In 2012, this small molecule was found to inhibit the homodimerisation of the ATIC enzyme, resulting in increased levels of monomeric ATIC.[208] Further studies demonstrated that an inhibition of the homodimerisation of ATIC using Cpd14 prevented the enzymatic reaction from occurring, thus leading to an accumulation of ATIC's substrate (i.e AICAR).[209]

As such, Cpd14 was used to inhibit ATIC and the resulting effect on hypoxic purinosome formation was assessed. The first step was to determine any potential cytotoxic effect of the compound on HeLa cells. To determine this, a cytotoxicity assay was carried out on HeLa cells cultured in normoxia and hypoxia with compound 14 at different doses (**Figure 52**). As the final DMSO concentration in cells treated with Cpd14 was 0.5%, a DMSO alone control was also included.

Cpd14 was dosed at 50 µM, 100 µM and 250 µM, and no cytotoxic effect was observed even at the highest dose (no significant different by Student t test). Similarly, the DMSO control did not display any cytotoxicity.

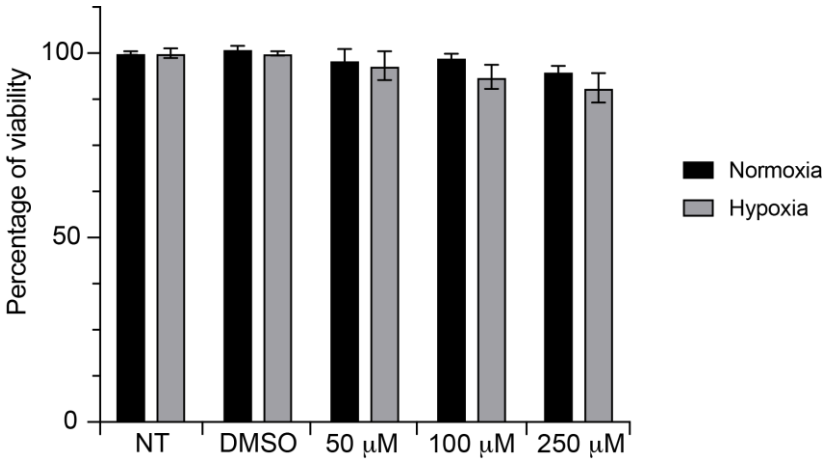

Figure 52. Cytotoxicity of Cpd14 in HeLa cells incubated in normoxia and hypoxia and treated at different doses for 24 h. HeLa cells were either untreated, treated with 0.5% DMSO (DMSO control) or treated with Cpd14 at 50 µM, 100 µM and 250 µM. No cytotoxic effect was observed for the DMSO control compared to untreated cells. No cytotoxic effect was observed for Cpd14 at any of the doses studied. Data are means (n=3) ± SEM. Significance was determined using unpaired Student t test. No significant difference between untreated cells and the other conditions was observed.

As a result, in order to assess purinosome formation in hypoxic HeLa cells treated with Cpd14, the compound was used at 250 µM. HeLa cells were transfected with the plasmid encoding FGAMS-GFP as before and were subsequently maintained in normoxia untreated, hypoxia untreated, and hypoxia with Cpd14 for 24 h following transfection (**Figure 53**). As a result, compared to untreated normoxic cells, untreated hypoxic cells displayed the same increase in purinosome formation as previously observed (**Figure 13**), whereas the treatment with Cpd14 in hypoxic cells was found to drive the number of purinosome-positive cells back to normoxic levels, indicating that Cpd14 prevents purinosome formation in hypoxia. This data suggests that purinosome formation relies not only on the presence of ATIC (and likely every purinosome enzyme), but potentially on its ability to function.

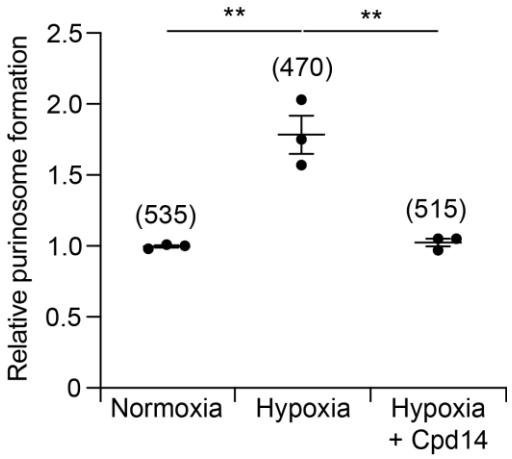

Figure 53. Effect of Cpd14 on relative purinosome formation in hypoxic HeLa cells. HeLa cells were transfected with a plasmid encoding FGAMS-GFP and were subsequently placed in normoxia untreated as well as hypoxia (1% oxygen), untreated and treated with Cpd14 (250 µM), for 24 h. Treatment with Cpd14 prevented the hypoxia-induced purinosome formation. Data are means (n=3) ± SEM. Significance was determined using unpaired Student t test, ** $p < 0.01$. The number in brackets indicates the number of cells counted per condition.

The previously obtained data in cells treated with Cpd14 suggested that the proteins of the purinosome have to be functional in order to enable the formation of the complex. As a metabolon, it is to be expected that the formation of the multi-enzyme purinosome complex is related to the metabolism of the *de novo* purine biosynthesis. As such, if the formation of the hypoxic purinosome formation correlates with the ability of the *de novo* pathway to function, alterations within the purine metabolism would be expected to impact upon purinosome formation. Such experiments have been carried out in cells lacking one of the salvage enzymes, HPRT (artificially knocked out or pathologically deficient).[181, 210] In purine-rich conditions these cells displayed an enhanced purinosome formation compared to wild-type cells, suggesting that when the salvage pathway is not functional (i.e synthesis of purines solely relies on the *de novo* pathway), the formation of purinosomes is triggered. In these cells, the formation of purinosomes was shown to enable the compensation for the purine loss induced by salvage deficiency.

To probe whether the purinosome complexes in hypoxia were also responsive to alterations within the purine metabolism, the salvage pathway was stimulated by supplementing the cell media with hypoxanthine, the base transformed into IMP by the HPRT enzyme.[211] If the hypothesis that hypoxic purinosome formation occurs in response to purine demand and correlates with an enhanced rate of the *de novo* pathway is accurate, then stimulating the salvage pathway should induce a downregulation of the *de novo* pathway, ultimately resulting in a disruption of the purinosome complexes.

To assess this, hypoxanthine was added to the culture media of HeLa cells maintained in hypoxia (**Figure 54**). Following 24 h of incubation, untreated hypoxic cells displayed an ~2-fold increase in purinosome formation as previously observed. However, when cells were cultured in the presence of hypoxanthine, no increase in purinosome formation was observed, suggesting that supplementation with the purine base prevents the formation of the complex in hypoxia. This is likely caused by the upregulation of the salvage pathway which ultimately maintains the purine pool, thus making the *de novo* synthesis of purines and associated purinosome formation dispensable.

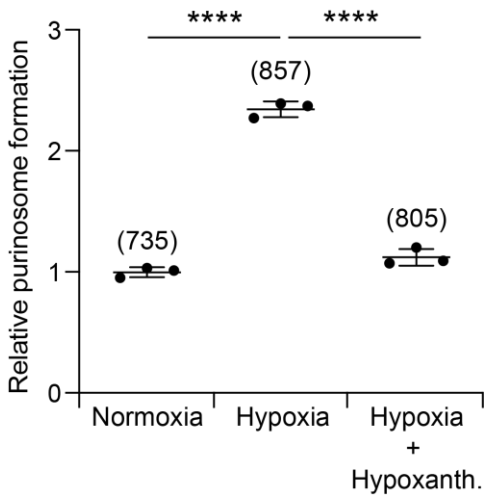

Figure 54. Effect of hypoxanthine on relative purinosome formation in hypoxic HeLa cells. HeLa cells were transfected with a construct coding for FGAMS-mCherry and were subsequently placed in normoxia and hypoxia (1% oxygen) untreated and treated with hypoxanthine (60 µM) for 24 h. Treatment with hypoxanthine prevented the hypoxia-induced purinosome formation. Data are means (n=3) ± SEM. Significance was determined using unpaired Student t test, **** $p < 0.0001$. The number in brackets indicates the number of cells counted per condition.

In the second section of this work, various cellular processes and components were found to impact upon the hypoxic purinosome formation. Three members of the HSP family, Hsp90, Hsp70-1 and Hsp70-2 were found to colocalise with the purinosome complex in hypoxic cells. Although Hsp70-2 was found to be upregulated in a HIF-dependent manner in hypoxia, this increase in protein levels was not sufficient to trigger purinosome formation as an artificial upregulation of the chaperone in normoxia did not induce purinosome formation. As previously described in purine-depleted conditions using small molecules inhibitors, the inhibition of Hsp90 and Hsp70-1 in hypoxia using siRNA prevented purinosome formation.[179] In addition to these two chaperones, inhibition of Hsp70-2 by siRNA was also found to prevent the assembly of the purinosome complex. Whether Hsp70-2 plays a direct role on individual *de novo* purine biosynthesis enzymes

or whether its involvement in the purinosome complex relies on its ability to partner with other chaperones remains unknown. To summarise, it is clear that the purinosome complex, for its formation / maintenance, requires interactions with the three above-mentioned chaperones, although the exact mechanism is yet to be determined.

The use of ATIC KO HeLa cells enabled the determination that a deficiency in one enzyme of the pathway prevents the formation of the complex, as previously observed in different conditions.[170, 171] In addition, in wild-type HeLa cells expressing all six enzymes of the pathway, chemical inhibition of the previously knocked out ATIC enzyme using Cpd14 also resulted in the disruption of the purinosome complex. Together, this data suggests that the formation of the complex relies on all six enzymes of the pathway to be present and functional. This feature of the purinosome formation was described using only one enzyme of the pathway but this experiment could be extended to the other five enzymes, although a similar disruption of the complex would be expected, as previously observed in purine-depleted conditions.[171]

Finally, based on the hypothesis that the purinosome complex forms in response to an adaptation of the purine metabolism, it was found that stimulating the salvage pathway by addition of hypoxanthine resulted in the disruption of the complex in hypoxia. This data supports the idea that the hypoxic formation of the purinosome reflects metabolic changes in the purine metabolism, more specifically, that it correlates with an upregulated *de novo* purine biosynthesis, as previously reported in purine-depleted conditions.[169]

The responsiveness of the purinosome formation to the addition of hypoxanthine raises the hypothesis that many more metabolic stimuli might impact and/or trigger purinosome formation. The *de novo* biosynthesis of purines relies on the availability of many substrates and co-factors provided by parallel metabolic pathways. Such pathways involve, for example, glycolysis and the pentose phosphate pathway, as well as the *de novo* serine biosynthesis and the one-carbon metabolism. As most of these metabolic pathways are known to be up regulated in hypoxia (see **section 1.1.4**), it is therefore highly possible that their upregulation, and thus the increased availability of substrates and co-factors for the *de novo* purine biosynthesis, affects the formation of the purinosome complex in hypoxia.

The next section of this work will focus on defining the links between the *de novo* purine biosynthesis and parallel metabolic pathways, as well as understanding how these pathways can impact upon purinosome formation in hypoxia.

2.3 Determining the nature of the link between purine synthesis and parallel metabolic pathways in hypoxic cancer cells

Following the observation that addition of hypoxanthine prevented the purinosome formation in hypoxia, further investigations were carried out to determine the nature of the link between the complex and various pathways that feed into the *de novo* purine biosynthesis.

2.3.1 Alterations in metabolic pathways linked to the *de novo* purine biosynthetic pathway affect purinosome formation

The glycolysis pathway is responsible for converting the incoming glucose molecules into pyruvate in the cell cytoplasm (**Figure 55**, pink pathway). Intermediates of this pathway are commonly rewired into other metabolic pathways such as the pentose phosphate pathway and the serine biosynthesis (**Figure 55**, green and orange pathway, respectively), all of which provide substrates and co-factors to the *de novo* purine biosynthesis (**Figure 55**, blue pathway).

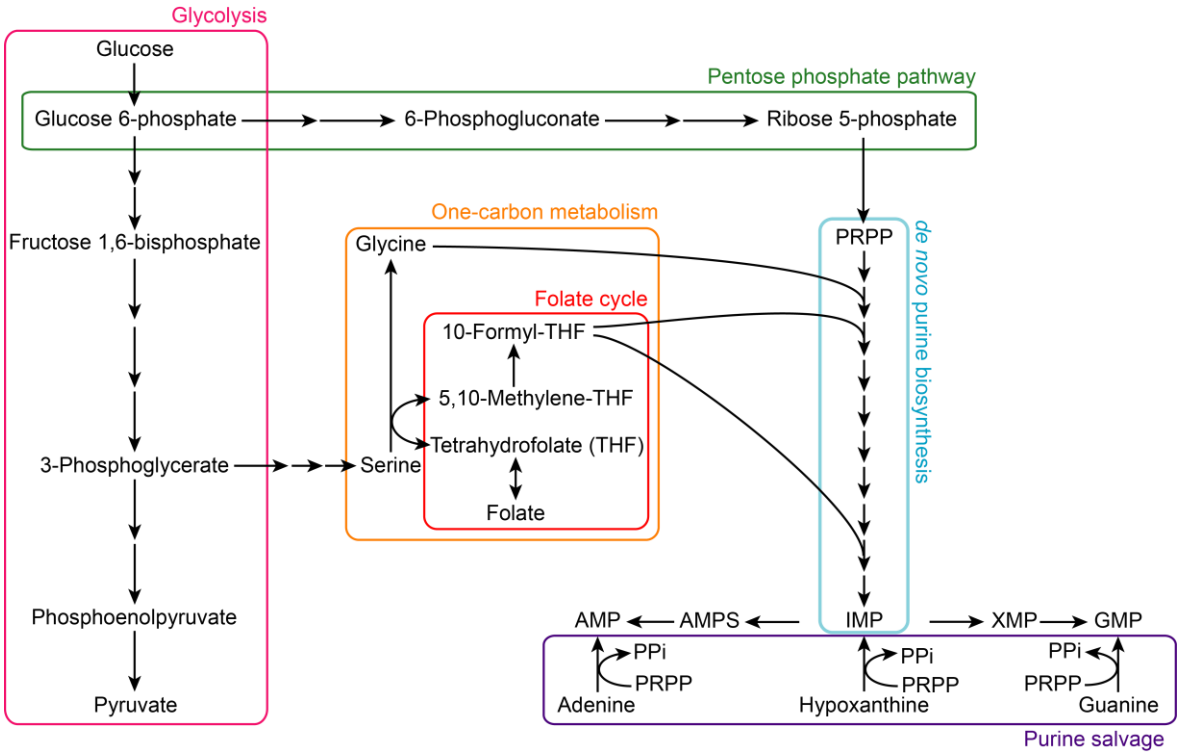

Figure 55. Scheme representing the interconnections between the *de novo* purine biosynthesis and associated metabolic pathways.

As such, due to its main role in providing metabolites to the *de novo* purine biosynthesis pathway and considering its upregulation in hypoxia, the role of the glycolysis pathway in the hypoxic purinosome formation was first assessed.

In order to determine whether the hypoxia-induced glycolysis was impacting the formation of the purinosome complex in low-oxygen environments, the first enzyme of the pathway, hexokinase (HK), was inhibited using 2-deoxyglucose (2-DG).[212] The effect of this inhibition was probed by assessing the relative purinosome formation in normoxic and hypoxic cells treated with 5 mM of 2-DG compared to untreated cells (**Figure 56**). When cells were treated with 2-DG in hypoxia, the purinosome formation was prevented with a relative purinosome formation similar to the one observed in normoxic untreated cells. 2-DG treatment did not display any effect on basal normoxic purinosome formation. Altogether, this data suggests that a functional glycolysis pathway is required for purinosome formation to occur in hypoxia.

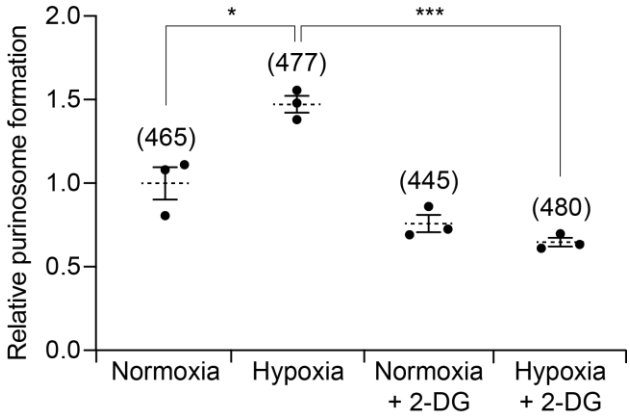

Figure 56. Effect of 2-deoxyglucose on relative purinosome formation in HeLa cells maintained in normoxia and hypoxia. HeLa cells were transfected with FGAMS-GFP and were subsequently placed in normoxia and hypoxia (1% oxygen) untreated and treated with 2-deoxyglucose (2-DG, 5 mM) for 6 h. Treatment with 2-DG prevented the hypoxia-induced purinosome formation. Data are means (n=3) ± SEM. Significance was determined using unpaired Student t test, * $p < 0.05$, *** $p < 0.001$. The number in brackets indicates the number of cells counted per condition.

As purinosome formation was found to depend on a functional glycolysis pathway, the involvement of other metabolic pathways in the formation of the complex was assessed. The glycolysis metabolism is at the origin of downstream branched metabolic pathways that use glycolytic intermediates as substrates. As an example of such, the pentose phosphate pathway uses glucose-6-phosphate, the product of the first reaction of the glycolysis, to produce ribose-5-phosphate, the sugar unit used as substrate in the *de novo* purine biosynthesis. This way, the PPP is a crucial metabolism for the *de novo* purine biosynthesis to occur. As the PPP is also partly upregulated in hypoxia, and according to the reliance of purinosome formation on glycolysis, the link between a functional PPP and purinosome formation in hypoxia was assessed.

To do so, purinosome formation was assessed in HeLa cells treated with 6-aminonicotinamide (6-AN), a small molecule inhibitor of the PPP (**Figure 57**). 6-AN is known to inhibit two enzymes of the PPP, the first enzyme, G6PD, as well as the third enzyme of the pathway 6-phosphogluconate dehydrogenase (PGD). [213-215] Upon treatment with 6-AN, hypoxic HeLa cells displayed a significant decrease in purinosome formation compared to untreated hypoxic cells. The resulting relative purinosome formation was found to be even lower than untreated normoxic cells. In the same way, treatment of normoxic cells with 6-AN also decreases the purinosome formation compared to untreated normoxic cells. This data suggests that not only does 6-AN prevent the hypoxic purinosome formation, but it also, to some extent, decreased purinosome formation compared to basal normoxic levels. Although this phenomenon does not have a defined explanation, different hypothesis can be raised. First, this decrease in normoxic purinosome formation upon treatment with 6-AN can result from the fact that normoxic purinosomes, despite being present in less cells than in hypoxia, still rely on the substrate availability provided by the PPP to form. In addition, 6-AN is known to inhibit two PPP enzymes which could induce an enhanced inhibitory effect on purinosome formation compared to the inhibition of a single enzyme.

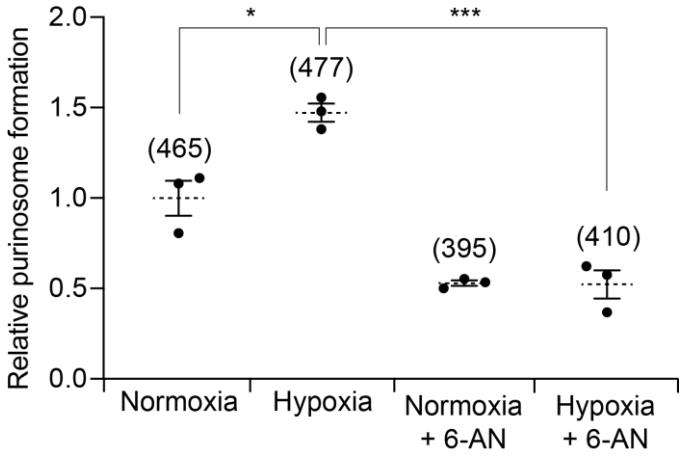

Figure 57. Effect of 6-aminonicotinamide on relative purinosome formation in HeLa cells maintained in normoxia and hypoxia. HeLa cells were transfected with FGAMS-GFP and were subsequently placed in normoxia and hypoxia (1% oxygen) untreated and treated with 6-aminonicotinamide (6-AN, 1 mM) for 6 h. Treatment with 6-AN prevented the hypoxia-induced purinosome formation. Data are means (n=3) ± SEM. Significance was determined using unpaired Student t test, * $p < 0.05$, *** $p < 0.001$. The number in brackets indicates the number of cells counted per condition.

To further analyse the effect of inhibiting the PPP on hypoxic purinosome formation, another approach was used. Instead of inhibiting PPP enzymes using a small molecule inhibitor like 6-AN, only one enzyme, G6PD, was knocked out using a specific siRNA. This approach enabled the

targeting of only one enzyme and can be compared to the previous data obtained with 6-AN treatment.

As such, purinosome formation was assessed as before in HeLa cells co-transfected with a plasmid encoding FGAMS-mCherry and a construct encoding either G6PD siRNA or a G6PD siRNA scramble sequence as a negative control (**Figure 58**). These two constructs were built by Dr Anthony Pedley (Pennsylvania State University, USA) using shRNA sequences against G6PD (and scramble) that were previously reported and tested for their efficiency in inducing a knock down of G6PD expression.[216] To ensure that only the cells expressing the siRNAs were taken into account in the purinosome counting, a gene encoding the GFP protein was incorporated into the G6PD siRNA encoding constructs, so that only green fluorescent cells were analysed for their purinosome content. As a result, HeLa cells transfected with only FGAMS-mCherry displayed an increased purinosome formation in hypoxia as previously observed. However, in cells co-transfected with G6PD siRNA, this hypoxic purinosome formation was prevented. In contrast, the negative control scramble G6PD siRNA did not prevent the hypoxic purinosome formation, suggesting a specific effect of the G6PD siRNA towards inhibiting purinosome formation. Altogether, this data suggests that hypoxic purinosome formation is prevented when one of the PPP enzyme, in this case G6PD, is not present, likely because of a decreased availability of *de novo* purine biosynthesis substrates provided by the PPP. This data is in line with previously observed results in HeLa cells treated with 6-AN (**Figure 57**).

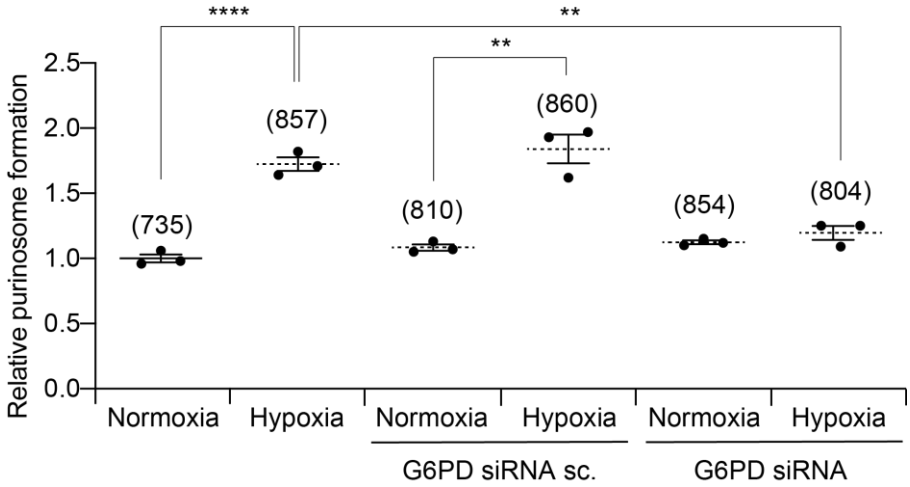

Figure 58. Relative purinosome formation in HeLa cells treated with G6PD siRNA and scramble G6PD siRNA. HeLa cells were transfected with FGAMS-mCherry alone, co-transfected with FGAMS-mCherry and psiRNA-G6PD or co-transfected with FGAMS-mCherry and psiRNA-G6PD-scramble. Cells were subsequently placed in normoxia and hypoxia (1% oxygen) for 24 h. G6PD siRNA prevented hypoxia-induced purinosome formation whereas its scramble counterpart did not have any effect. Data are means (n= 3) ± SEM. Significance was determined using unpaired Student t test, ** $p < 0.01$, **** p

< 0.0001. The number in brackets indicates the number of cells counted per condition.

Inhibition of metabolic pathways that feed into the *de novo* purine biosynthesis, either by using small molecule inhibitors or siRNA, determined that the hypoxic purinosome formation requires the pathways upstream of the *de novo* purine biosynthesis to be functional. This data strongly suggests that the hypoxic purinosome formation relies on the availability of substrates and co-factors provided by glycolysis and PPP and that the formation of the multi-enzyme complex is highly modulated and responsive to metabolic stimuli received by the cell.

2.3.2 Physical proximity between the purinosome and enzymes from functionally associated pathway

Purinosome formation was found to be modulated by alterations of metabolic pathways linked to the *de novo* purine biosynthesis, thus linking the formation of the complex to the functionality of the *de novo* biosynthetic pathway. Although it seems clear that the purinosome complex requires the glycolysis and PPP to be functional in order to form, the nature of the link between the pathways requires further unravelling.

The purinosome complex is referred to as a metabolon, a protein macro-complex comprised of enzymes that belong to the same pathway, in this case, the *de novo* biosynthesis of purines. However, the purinosome was not the first metabolon reported. Its discovery was inspired by other already existing metabolons from different metabolic pathways, with one of the most commonly studied being the glycolysis pathway. Over the years, macro-complexes containing enzymes of glycolysis have been reported in different organisms and mammalian cell types.[217-219] The first evidence of a human glycolytic metabolon was found in human erythrocytes where GAPDH, PFK, PK and LDH enzymes were co-clustering on the cell membrane.[220] Following this, in 2017, a glycolytic metabolon was characterised in human cancer cells, thus broadening the understanding of how cancer cells might use metabolons to regulate the metabolite flux in metabolic pathways.[221] This metabolon, referred to as the glucosome, was found to be comprised of all rate-limiting glycolytic enzymes (i.e PFK liver isoform (PFKL), FBPase and PK). The co-transfection of two constructs encoding for FGAMS fluorescently tagged with orange fluorescent protein (OFP) and PFKL-GFP, enabled the visualisation of the two metabolons, glucosome and purinosome, simultaneously in the cell cytoplasm. Interestingly, preliminary microscopy analysis in this study suggested that the two complexes were localised next to one another, thus suggesting a physical/functional relationship between the two entities and ultimately, between

the two pathways. In parallel, *in vitro* studies carried out using a microfluidic device showed that the first four enzymes of glycolysis assemble by substrate-driven chemotaxis.[222]

In regard of these findings, and according to the high responsiveness of the hypoxic purinosome to metabolic alterations within glycolysis and the PPP, it was hypothesised that individual enzymes of glycolysis and the PPP might be colocalising with the purinosome complex. The colocalisation of enzymes belonging to pathways that feed into the *de novo* purine biosynthesis with the purinosome complex would reflect an efficient protein localisation aiming at facilitating and improving the metabolic flux from one pathway to another. The next section of this work will describe how the close proximity between the purinosome complex and enzymes from associated pathways was assessed in hypoxic cells.

In order to probe the colocalisation of the purinosome complex with other proteins, a pull-down assay was carried out. The ultimate aim of this assay was to determine any localisation between proteins from other pathways and the purinosome, obtain a qualitative list of the proteins that were interacting with the purinosome in hypoxia in order to guide the next steps of this work into more specific assays such as fluorescent microscopy and PLA.

As such, in this assay, FGAMS, which is known to interact with every other enzymes of the *de novo* pathway within the purinosome complex, was used as bait. It is to note that the commonly used name of this protein is FGAMS but it can also be referred to as PFAS, in line with the name of its encoding gene *pfas*. As such, as the next steps of this work involved searches in protein databases into which the protein is referred to PFAS instead of FGAMS, the protein will be referred to as PFAS in the next part of this work.

To carry out the pull-down experiment, a construct encoding for PFAS fused to a tandem StrepTagII tag (PFAS-2xStrepTagII) was transfected into HeLa cells. Following 24 h of incubation, the cells were further incubated for 24 h in normoxia or hypoxia.

As a first control, the presence and expression level of PFAS-2xStrepTagII was assessed in the lysates of HeLa cells in order to ensure that the protein was expressed equally in normoxia and hypoxia. As a result, PFAS-2xStrepTagII was detected by western immunoblotting using an anti-StrepTagII antibody (**Figure 59**). Protein levels of PFAS-2xStrepTagII were found to be similar in normoxia and hypoxia, indicating that the protein is equally expressed in both conditions, regardless of the oxygen levels.

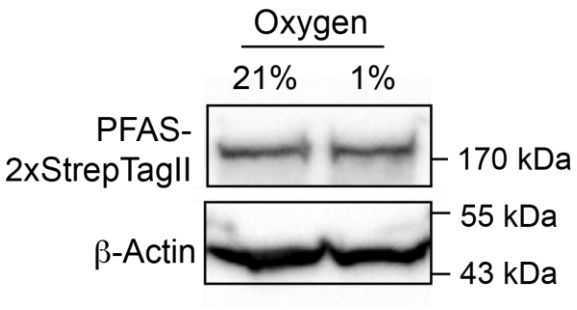

Figure 59. Western immunoblotting to assess expression of PFAS-2xStrepTagII in HeLa cells maintained in normoxia and in hypoxia. Following transfection, HeLa cells were incubated in normoxia for 24 h and subsequently incubated for a further 24 h in normoxia and hypoxia (1% oxygen). Lysates were used to assess expression of PFAS-2xStrepTagII using anti-StrepTagII antibody. The protein levels of PFAS-2xStrepTagII were found to be similar in normoxia and hypoxia. β-actin was used as an internal loading control.

As PFAS-2xStrepTagII was found to be similarly expressed in both normoxia and hypoxia, the next level of control in the pull-down assay was to determine whether the quantity of PFAS-2xStrepTagII isolated by pull-down in each condition was affected by oxygen levels. As such, the same transfection and incubation process with lysate samples was used for a subsequent pull-down assay using streptavidin coated magnetic beads. Using western immunoblotting, PFAS-2xStrepTagII was detected in both normoxic and hypoxic conditions with more protein detected in hypoxia (**Figure 60a**). Band intensities were measured and revealed a 3-fold increase in the protein levels of the bait in hypoxia compared to normoxia (**Figure 60b**).

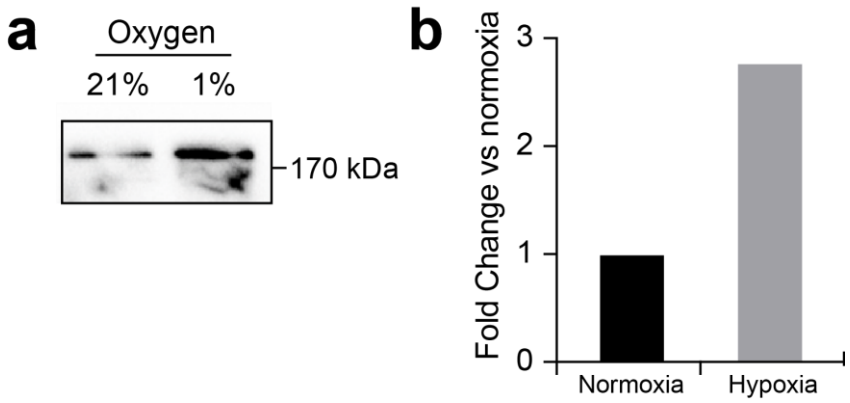

Figure 60. Expression of pulled down PFAS-2xStrepTagII assessed by western immunoblotting. Samples resulting from pull-down assay were taken for western immunoblotting analysis using anti-StrepTagII antibody to detect PFAS-2xStrepTagII. **(a)** The bait was detected in both normoxia and hypoxia (1% oxygen). **(b)** Band intensity measurements carried out on western blot in **Figure 60a** indicated a 3-fold increase

in protein levels in hypoxia compared to normoxia. The western blot was repeated at least twice to ensure the reproducibility of the results.

Together, these two controls suggest that although the protein is being expressed similarly in HeLa cells maintained in normoxia and hypoxia, three times as much PFAS-2xStrepTagII protein is being pulled-down in hypoxia compared to normoxia. This data suggest that one PFAS protein clusters with more copy of PFAS, likely in a 3 to 1 ratio in hypoxia compared to normoxia, according to the band intensity measurements. This result is not unexpected as the purinosome is known to be a complex comprised of the six enzymes of the *de novo* biosynthetic pathway of purines where more than one copy of each protein that compose the cluster can be expected, although no report have established the stoichiometry within the complex yet.

So far, the pull-down assay proved to be working as the bait, PFAS-2xStrepTagII was found to be properly caught. However, it was yet to be determined whether any prey proteins could be captured using this assay. As such, in order to carry out a broad screening of any potential prey being present in normoxic and hypoxic conditions, samples resulting from the pull-down assay were prepared as before (with the exception that the proteins were kept attached on the beads instead of being eluted). These were subsequently sent for mass spectrometry proteomics analysis to the Centre for Proteomic Research at the Institute for Life Sciences (IfLS) (University of Southampton).

As a result of this proteomic analysis, 554 different proteins were detected in normoxia, and 710 proteins in hypoxia. 92 proteins were found to be detected in normoxia only and 248 proteins were detected exclusively in hypoxia. In order to analyse this data, each protein was referred to as its Uniprot number and the lists of proteins were submitted to the online STRING database for analysis. The STRING database enables the creation of networks between proteins using reported data issued from experiments or computational predictions.

The first analysis was carried out on the 92 proteins specific to normoxia. Amongst these 92 proteins, 39 were found to be related to the cell cytoskeleton including 24 that were structural proteins involved in intermediate filaments (e.g keratin). These 39 proteins can presumably be accounted for as non-specific proteins as no previous data suggested an interaction between PFAS and intermediate filaments. In addition to these, 20 proteins were found to be individual nodes, indicating that they do not have any previously reported interactions with any other proteins present within the same list. Finally, the overall view of the network highlighted that only one sub-network was present when looking at these 92 proteins (composed of the above-mentioned cytoskeleton-related proteins), indicating that the proteins exclusive to normoxia do

not have any special interactions between one another and likely result from non-specific interactions with PFAS or the strep-tag.

Following this, the list of 248 proteins exclusive to hypoxia was submitted to the STRING database and analysed. A sub-network containing 64 proteins was found. All of these proteins were part of the same network as they were purine nucleotide-binding proteins, with most of them (45 out of 64) being GTP-binding proteins such as small GTPases and G-alpha protein subunits from the Ras family. The presence of that many purine nucleotide-binding proteins was unexpected but rather interesting, although no definite explanation for this is known. This can hypothetically be explained by the fact that they would perhaps be located close to the purine production site within the cell cytoplasm in order to bind to their corresponding nucleotide faster than if they were randomly distributed throughout the cell. However, this phenomenon, which could happen to be a random coincidence, would need further investigation to determine whether the presence of purine nucleotide-binding proteins in close proximity to PFAS was an actual hypoxia-specific phenomenon, or simply a random non-specific event caused by the high number of proteins caught in the hypoxic pull-down samples (i.e 710 proteins in total).

The main aim of this proteomics analysis was to determine whether any interaction between PFAS and proteins from associated pathway was enhanced or exclusive to hypoxic conditions, known to be favourable for purinosome formation. As such, the analysis was then orientated towards proteins belonging to the cell metabolism. The entire list of proteins present in hypoxia (710 proteins) as well as the list of protein present in normoxia (554 proteins) were submitted to the string database and analysed for the presence of proteins belonging to pathways related to the purine metabolism.

As such, proteins belonging to the purine biosynthesis, the pentose phosphate pathway (PPP), the glycolysis pathway and the one-carbon metabolism were detected. In addition, members of the HSP family, previously reported to be involved in the hypoxic purinosome formation, were detected and studied. Overall, 28 pulled down prey proteins belonging to these pathways or families were detected and are presented as a network in **Figure 61**. All these proteins were detected in hypoxia including 11 that were only detected in these low-oxygen conditions and not pulled down in normoxia. As a result, when using PFAS as bait, 4 proteins of the purine biosynthesis (including PFAS) (green box), 14 proteins from glycolysis (red box), 4 proteins from the PPP (blue box), 3 proteins from the one-carbon metabolism (yellow box) and 3 proteins from the HSP family (grey box) were pulled down in hypoxia using PFAS as bait. It should be noted that more members of the HSP family were detected in the proteomics analysis but only Hsp90

(HSP90AA1), Hsp70-1 (HSPA1A) and Hsp70-2 (HSPA2) were considered due to their previously demonstrated involvement in the hypoxic purinosome formation.

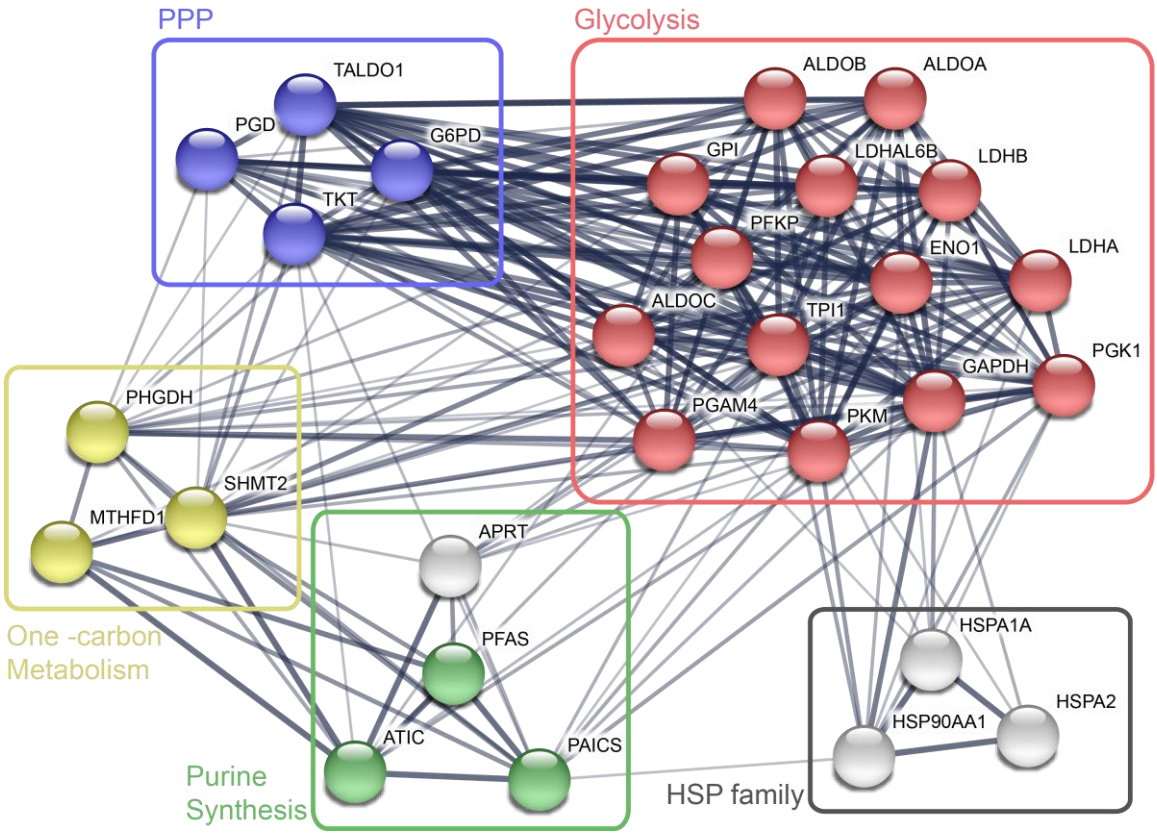

Figure 61. STRING network of proteins pulled down in hypoxic HeLa cells using PFAS as bait. PFAS (central green node in green box) was used as bait and enabled the pull-down of 3 other purine biosynthesis related proteins (green box). Proteins from the PPP (blue box), glycolysis (red box), the one-carbon metabolism (yellow box) and three members of the HSP family (grey box) were detected in hypoxia. Each protein is presented as a node labelled with the name of the protein of interest.

From this broad proteomics screening, it was determined that the pull-down assay using PFAS as bait enabled the isolation and detection of prey proteins, including proteins from pathways linked to the *de novo* purine biosynthesis.

In addition to listing the proteins detected in a given pull-down sample, the proteomics analysis also provided quantitative data and enabled the quantification of each detected protein in each sample. As such, the quantity of each protein, reported in nanograms, was used to determine the change in protein levels between normoxia and hypoxia. For each protein, the quantity of protein detected in the hypoxic sample was normalised to that of the normoxic sample and fold-changes were calculated for the 28 proteins studied. These proteins were then classified by pathway or family as presented in **Figure 61**, and their fold-changes presented in heat-maps that will be further discussed.

2.3.2.1 Further assessing purinosome formation in hypoxia and the involvement of Hsp proteins.

The first pathway of interest is the purine biosynthesis pathway. PFAS was found to be three times as abundant in hypoxia as in normoxia (**Figure 62**), consistent with the previously observed western immunoblotting analysis (**Figure 60**), thus reinforcing the hypothesis that PFAS clusters with itself in hypoxia. As previously suggested following the analysis on the pull-down sample (**Figure 60**), this 3-fold increase in PFAS levels in hypoxia might reflect the stoichiometry of this protein within the complex as the detected protein here is the total level of PFAS protein, both endogenous and StrepTagII-tagged.

In addition, proteins of the purinosome complex, ATIC and PAICS were pulled-down exclusively in hypoxia (**Figure 62**), suggesting a strong interaction between the bait, PFAS, and these two proteins. No interaction between PFAS and these two proteins was observed in normoxia. This is in line with the previous results suggesting that the purinosome formation is substantially enhanced in hypoxia. Although it can seem surprising to only pull down two out of the five remaining purinosome enzymes in hypoxia, these results are in line with previous reports into which the same experiment was carried out in purine-depleted conditions and enabled the detection of ATIC and PAICS only when PFAS was used as bait.[179]

Interestingly, the salvage enzyme that convers adenine into AMP, namely adenine phosphoribosyl transferase (APRT), was also found to be pulled down in hypoxia and to be absent in normoxia using PFAS as bait. This result was unexpected but could suggest that, although the purinosome complex forms in hypoxia (suggesting an upregulation of the *de novo* purine biosynthesis)[169], the salvage pathway may still be efficient in these conditions, and so the enzymes that compose this pathway may be in close proximity to the purinosome. Assessing the close proximity between the salvage enzymes and the purinosome complex would require further investigation.

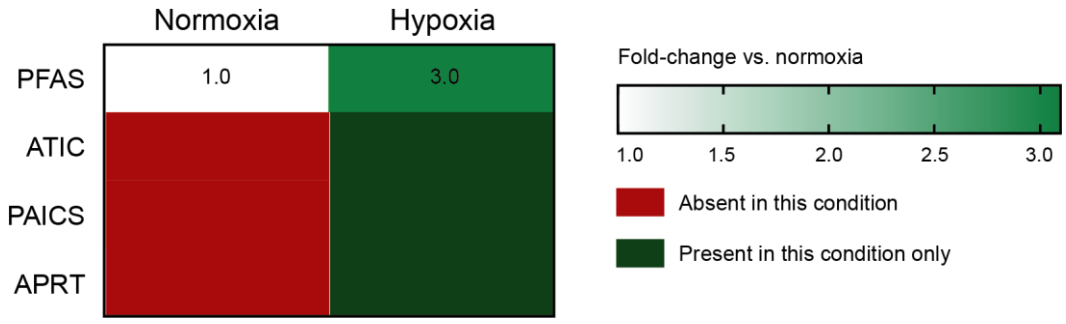

Figure 62. Heat-map presenting the levels of proteins belonging to the purine metabolism, determined from proteomics analysis carried out in normoxia and hypoxia from a pull-down assay. Fold-changes were calculated by normalising the amount of protein in nanograms in hypoxic conditions to that measured in normoxic conditions. Red box indicates that the protein of interest is absent in this condition. Dark green box indicates that the protein is present only in this condition. Fold-changes are indicated in their corresponding box, coloured according to the fold-change base colour gradient.

In order to determine whether the results observed in the proteomics analysis were reliable, the pull-down experiment was repeated as before and the samples were analysed by western immunoblotting instead of mass spectrometry. The presence of some of the prey proteins determined in the pull-down list was assessed. As such, immunoblotting against PAICS and ATIC was carried out. Although ATIC was not detectable, likely due to the detection limit of western immunoblotting, PAICS was however detected in both normoxia and hypoxia (**Figure 63**). In line with the observation made from the proteomics results (**Figure 62**), PAICS was found to be more present in the hypoxia sample than in normoxia, thus supporting the results previously obtained by proteomics.

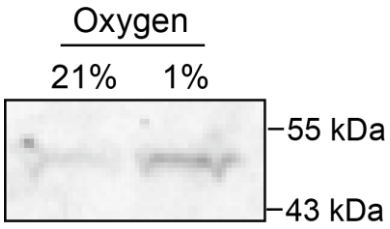

Figure 63. Expression of pulled down PAICS using PFAS-2xStrepTagII as bait assessed by western immunoblotting. Samples resulting from pull-down assay were taken for western immunoblotting analysis using anti-PAICS antibody. The prey was detected more in hypoxia (1% oxygen) than in normoxia.

Following this finding, it could be of interest in the context of future experiments, to carry out a similar western immunoblotting analysis on the three remaining purinosome enzymes PPAT, GART and ADSL despite these not being detected in the list of pulled down proteins in hypoxia.

As Hsp70-1, Hsp70-2 and Hsp90 were previously shown to interact with the hypoxic purinosome complex, the presence of these three chaperones was assessed in the pulled down samples. All three proteins were detected in the hypoxic samples, where Hsp90 and Hsp70-1 displayed a 2.9 and 2.3-fold increase in hypoxia, respectively, compared to normoxic conditions (**Figure 64**). In addition, Hsp70-2 could not be detected in normoxia and was only present in hypoxia, suggesting that the interaction between PFAS and Hsp70-2 is specific to hypoxia (**Figure 64**). This result is in line with previously observed data collected from the PLA analysis between ADSL and Hsp70-2 where normoxic cells did not contain any PLA signals compared to hypoxic cells that displayed a high number of PLA signals (**Figure 44**). Together, this data suggests that the interaction between the purinosome and Hsp70-2 is substantially enhanced in hypoxia and potentially even specific to these low oxygen environments. Further experiments would be required to further assess this. In the same way, the enhanced interaction between Hsp90 or Hsp70-1 with PFAS (**Figure 64**) is in line with the results previously observed by PLA where a stronger PLA signal was observed in hypoxic conditions compared to normoxia for both the PFAS/Hsp90 (**Figure 46**) and ADSL/Hsp70-1 (**Figure 45**) interactions.

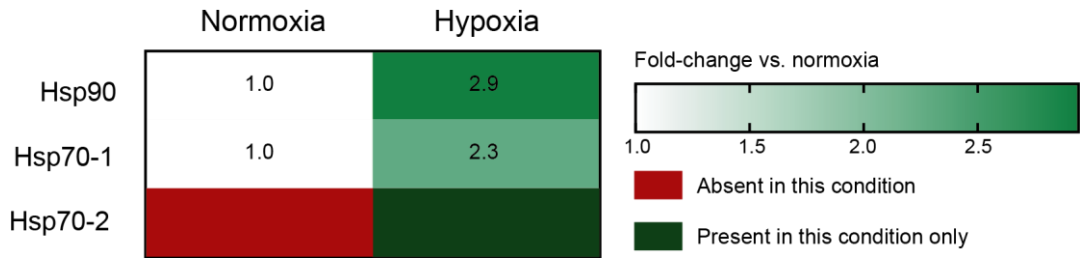

Figure 64. Heat-map presenting the levels of proteins belonging to the HSP family, determined from proteomics analysis carried out in normoxia and hypoxia from a pull-down assay. Fold-changes were calculated by normalising the amount of protein in nanograms in hypoxic conditions to that measured in normoxic conditions. Red box indicates that the protein of interest is absent in this condition. Dark green box indicates that the protein is present only in this condition. Fold-changes are indicated in their corresponding box, coloured according to the fold-change base colour gradient.

The data resulting from the pull-down assay provided further evidence of an enhanced purinosome formation in hypoxia, as suggested by the presence of purinosome proteins (ATIC and PAICS). The presence of the three members of the Hsp family that were previously found to be

required and present within the hypoxic purinosome complex was also observed and found to be enhanced or exclusive to hypoxic conditions, in line with the previously observed data (**section 2.2.1**).

2.3.2.2 Assessing the close proximity between purinosome enzymes and proteins from glycolysis

The second pathway of interest in this proteomics analysis is glycolysis. Fourteen proteins belonging to this pathway were detected in hypoxia, with four of them being undetectable in normoxic conditions and one of them being less present in hypoxia (**Figure 65**). As such, analysis of the glycolytic proteins pulled down in normoxia and hypoxia suggests that glycolytic enzymes displayed an enhanced interaction with PFAS in hypoxic conditions as 13 out of 14 displayed an increased fold-change in hypoxia. This strengthens the hypothesis of an enhanced close proximity between the purinosome and glycolytic enzymes in low oxygen environments.

The proteins that were more present in hypoxia displayed a 2.0 to 4.5-fold increase compared to normoxic conditions. In addition, four proteins were found to be exclusively detected in hypoxic conditions : aldolase B (ALDOB), lactate dehydrogenase A-like isoform 6B (LDHAL6B), phosphoglycerate mutase isoform 4 (PGAM4) and phosphofructokinase platelet isoform (PFKP). Interestingly, it was the platelet isoform of PFK that was detected in the hypoxic samples. The liver isoform of this enzyme (PFKL) has been reported to form “glycolytic bodies” under hypoxic stress in HepG2 cells, and to form the glucosome complex in cells transfected with a PFKL-GFP construct. [222,221] Although both isoforms have been reported to be upregulated in hypoxia, only PFKL has so far been described to form glycolytic complexes.[224] This data suggests that, in this pull-down, PFKP seems to preferentially interact with the purinosome in hypoxic conditions, although this hypothesis requires further investigation.

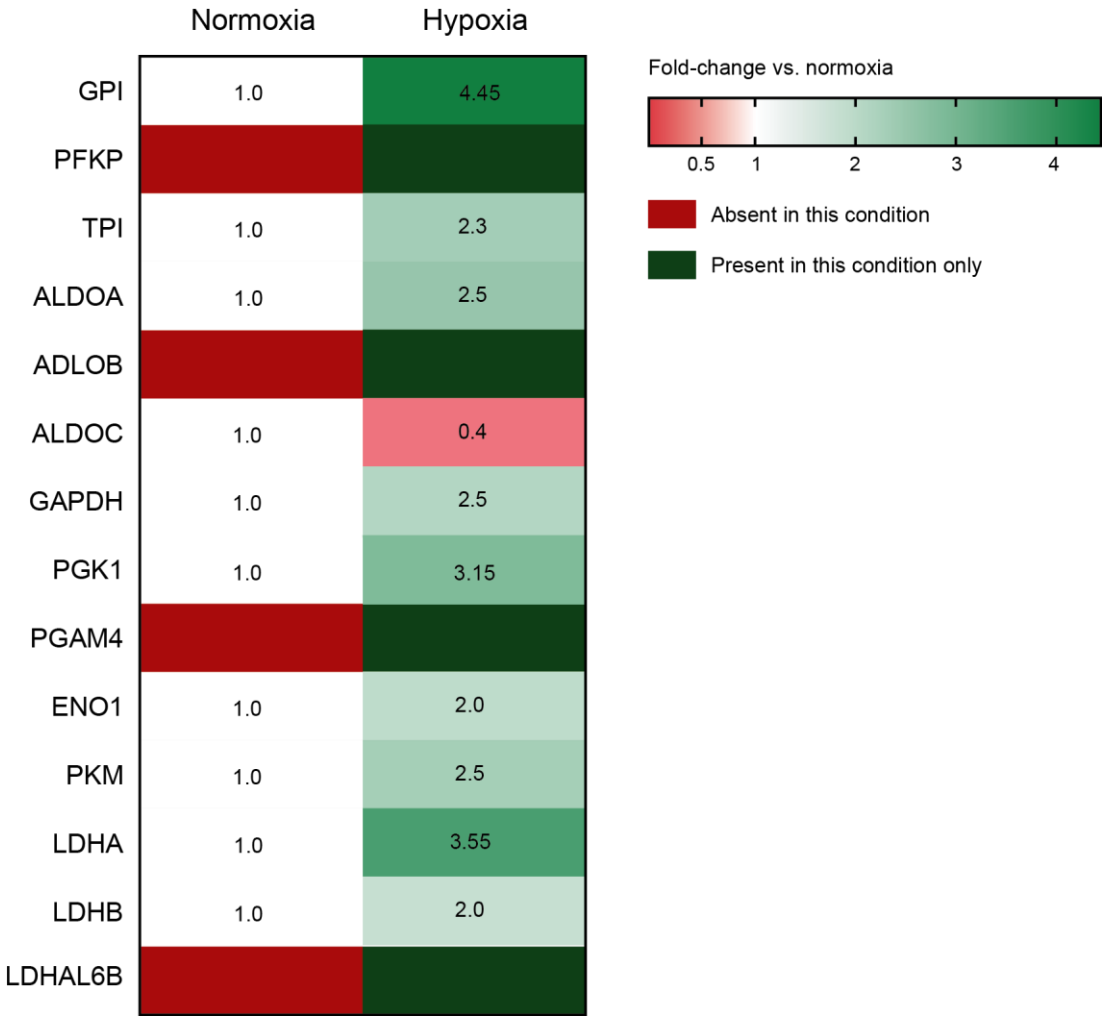

Figure 65. Heat-map presenting the levels of proteins belonging to the glycolysis pathway, determined from proteomics analysis carried out in normoxia and hypoxia from a pull-down assay. Fold-changes were calculated by normalising the amount of protein in nanograms in hypoxic conditions to that measured in normoxic conditions. Red box indicates that the protein of interest is absent in this condition. Dark green box indicates that the protein is present only in this condition. Fold-changes are indicated in their corresponding box, coloured according to the fold-change base colour gradient. Glycolytic enzymes are listed from top to bottom in their order of occurrence within the pathway.

Following this wide proteomics screening, the colocalisation of different proteins was assessed using PLA in order to verify the data obtained from the proteomics analysis. This was used to determine whether the interactions observed in the proteomics analysis were reflecting actual protein interactions within the cells

As observed in the proteomics analysis, although PFKL is the isoform of PFK reported to form glycolytic complexes, it was determined that the platelet isoform (PFKP) was present exclusively in the hypoxic sample, thus suggesting a strong interaction with the bait (**Figure 65**). As such, the

colocalisation between PFAS and PFKP was assessed by PLA, both in normoxic and hypoxic cells. Although the two proteins seem to interact in normoxia as shown by the presence of PLA signals (**Figure 66a**), a substantially higher number of PLA signals can be observed in hypoxic cells (**Figure 66b**). This result is consistent with the data obtained from the proteomics analysis and suggests an enhanced interaction between PFAS and PFKP in hypoxic cells. It should be noted that although PFKP was not detected in the normoxic pull-down sample by proteomics analysis, some PLA signals are still detected in normoxic cells when looking at this protein-protein interaction, which might suggest that the quantity of PFKP pulled down in normoxia was below the detection limit of the mass spectrometry equipment.

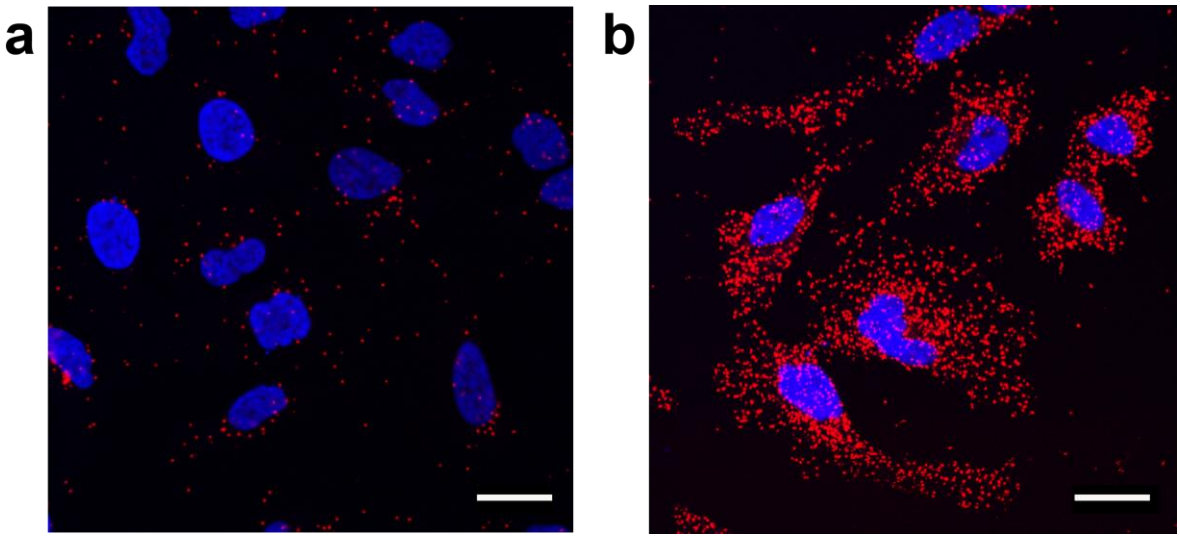

Figure 66. **Proximity ligation assay between PFAS and PFKP. (a)** HeLa cells cultured in normoxia for 24 h. **(b)** HeLa cells cultured in hypoxia (1% oxygen) for 24 h. A small number of signals was detected in normoxia while a higher number of signals was detected in hypoxia suggesting a high colocalisation of the two proteins in hypoxia. The PLA signals appear as red dots. Cells were stained with DAPI. Scale bar represents 25 µm.

As PFKP was found to highly interact with PFAS in hypoxic cells, the interaction between PFAS and the PFKL isoform was next assessed in order to determine whether the interaction between PFK and the purinosome was isoform specific. Both normoxic and hypoxic cells displayed some PLA signals (**Figure 67a** and **67b**, respectively) but no difference in the number of signals was observed. The number of signals was comparable to the normoxic interaction between PFAS and PFKP (**Figure 66a**), thus indicating little interaction between PFAS and PFKL. This data suggests that although PFKL was found to slightly interact with PFAS, this interaction is not enhanced in a low oxygen environment.

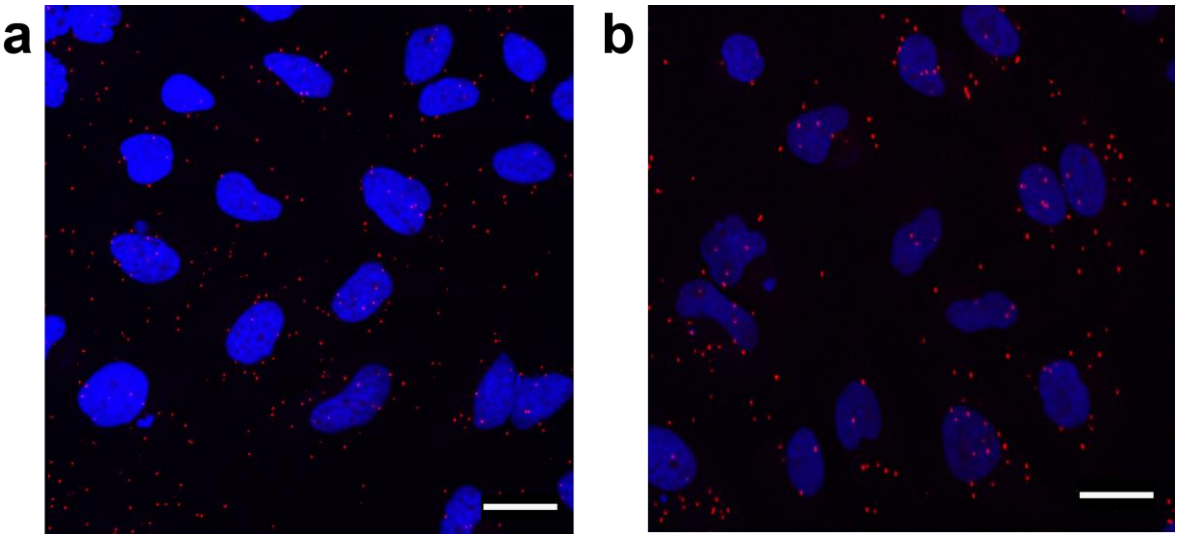

Figure 67. Proximity ligation assay between PFAS and PKFL. (a) HeLa cells cultured in normoxia for 24 h. **(b)** HeLa cells cultured in hypoxia (1% oxygen) for 24 h. A small number of signals was detected in normoxia with a similar number of signals observed in hypoxia suggesting that the colocalisation between the two proteins is not enhanced in hypoxia. The PLA signals appear as red dots. Cells were stained with DAPI. Scale bar represents 25 µm.

The PLA data obtained from the PFAS-PFKP and PFAS-PFKL interactions confirmed what was previously observed in the proteomics analysis (**Figure 65**). Together, this data suggests that the observed increase in interaction between PFAS and PFKP in hypoxia (**Figure 65** and **Figure 66**) is specific to the platelet isoform of PFK and not applicable to the liver isoform. It can thus be hypothesised that the 13 glycolytic proteins that displayed an enhanced interaction with PFAS in hypoxia by proteomics (**Figure 65**) are also in close proximity with PFAS, and to some extent with the purinosome complex, in these conditions.

Overall, 14 glycolytic enzymes were found in the list of proteins pulled down in hypoxia. The PLA assay confirmed that PFAS was preferentially interacting with PFKP and not PFKL and that this interaction was enhanced in hypoxia.

2.3.2.3 Assessing the close proximity between purinosome enzymes and proteins from the pentose phosphate pathway (PPP)

Following the analysis of the glycolysis pathway, proteins from the pentose phosphate pathway (PPP) were analysed in the pull-down samples. Four proteins belonging to this pathway were detected with one of them, phosphogluconate dehydrogenase (PGD), being absent in normoxia (**Figure 68**). A small decrease in fold-change was observed in hypoxia for the transaldolase (TALDO) enzyme (0.9-fold change in hypoxia compared to normoxia). The two remaining

enzymes, glucose-6-phosphate dehydrogenase (G6PD) and transketolase (TKT), were both found to increase in hypoxia at a 2.3 and 3.4-fold change, respectively. Together, this data suggests that enzymes of the PPP are preferentially pulled down in hypoxia compared to normoxia, thus indicating an enhanced interaction between PFAS and proteins from the PPP in these conditions.

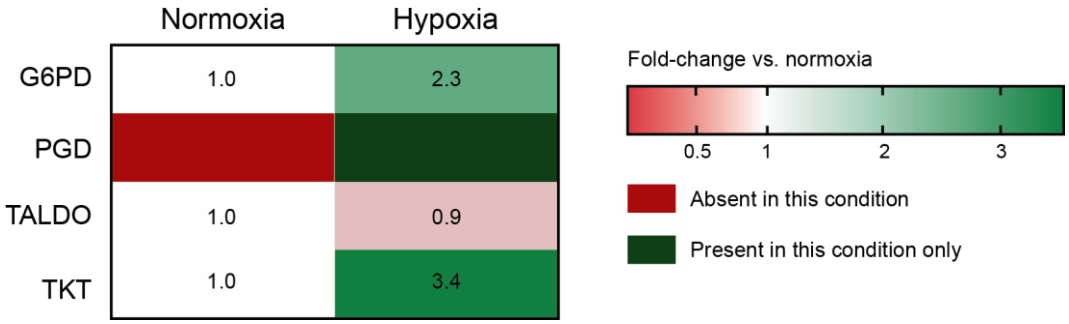

Figure 68. Heat-map presenting the levels of proteins belonging to the PPP, determined from proteomics analysis carried out in normoxia and hypoxia from a pull-down assay. Fold-changes were calculated by normalising the amount of protein in nanograms in hypoxic conditions to that measured in normoxic conditions. Red box indicates that the protein of interest is absent in this condition. Dark green box indicates that the protein is present only in this condition. Fold-changes are indicated in their corresponding box, coloured according to the fold-change base colour gradient. PPP enzymes are listed from top to bottom in their order of occurrence within the pathway.

To further assess the reliability of this proteomics data, the pull-down experiment was repeated as before and the presence of one of the prey proteins from the PPP found within the list generated from the proteomics analysis was assessed by western immunoblotting. As such, the samples resulting from the pull-down were used to probe for the presence of G6PD, both in normoxic and hypoxic conditions. In line with the results obtained from the mass spectrometry proteomics (**Figure 68**), G6PD was found to be significantly more present in the hypoxia sample compared to the normoxic one (**Figure 69**).

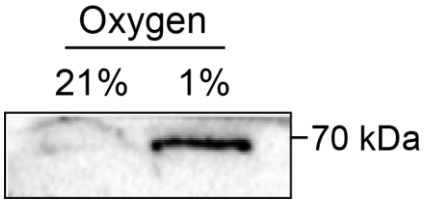

Figure 69. Expression of pulled down G6PD using PFAS-2xStrepTagII as bait assessed by western immunoblotting. Samples resulting from the pull-down assay were taken for western immunoblotting analysis using anti-G6PD antibody. The prey was detected more in hypoxia (1% oxygen) than in normoxia.

Following this, the close proximity between purinosome proteins and proteins from the PPP was assessed by PLA. According to the pull-down assay data, PGD was found exclusively in hypoxia and the levels of G6PD were found to be increased by 2.3 fold in hypoxia (**Figure 68**). This result was particularly interesting as inhibition of these two proteins using a small molecule inhibitor (6-aminonicotinamide) or siRNA was previously shown to prevent the hypoxic purinosome formation (**Figure 57** and **Figure 58**). As such, in order to confirm the enhanced interaction between the purinosome and G6PD found by pull-down assay in hypoxia, the close proximity between G6PD and GART, a core enzyme of the purinosome, was assessed. Normoxic cells did not display PLA signals (**Figure 70a**), however, many PLA signals were observed in hypoxia (**Figure 70b**). This result is in line with the previously observed pull-down data suggesting an enhanced interaction between the purinosome and G6PD in hypoxia.

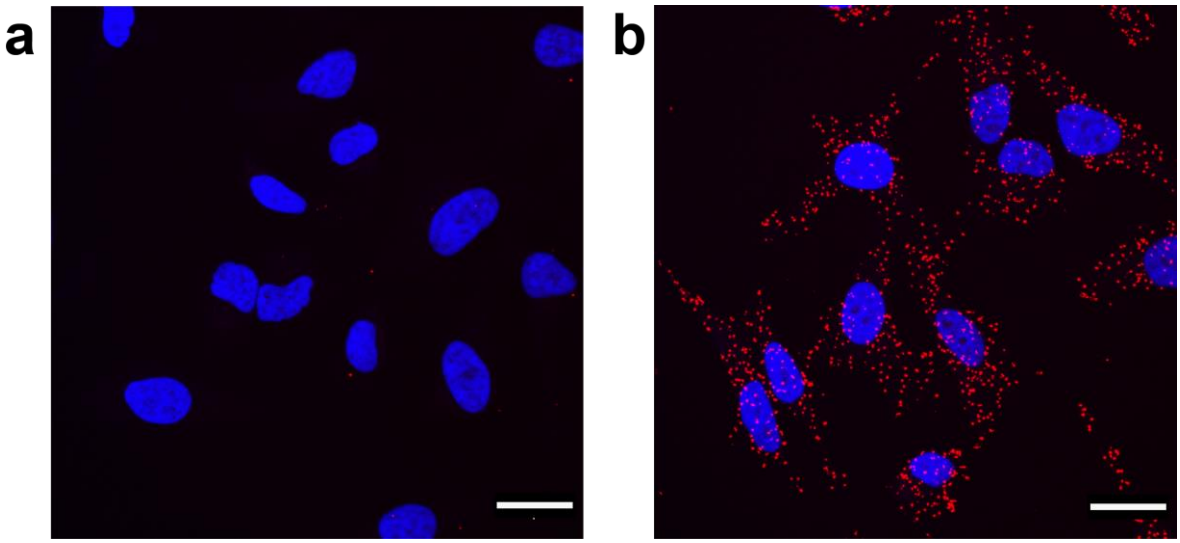

Figure 70. **Proximity ligation assay between GART and G6PD. (a)** HeLa cells cultured in normoxia for 24 h. **(b)** HeLa cells cultured in hypoxia (1% oxygen) for 24 h. A small number of signals was detected in normoxia while a larger number of signals was detected in hypoxia suggesting an enhanced colocalisation of the two proteins in hypoxia. The PLA signals appear as red dots. Cells were stained with DAPI. Scale bar represents 25 µm.

In addition, to further probe the results obtained from the pull-down analysis, the colocalisation between GART and PGD, another protein from the PPP, was assessed. Very few PLA signals were observed in normoxic cells (**Figure 71a**). In contrast, a high number of PLA signals was observed in hypoxia, suggesting an increased colocalisation between GART and PGD in hypoxic conditions (**Figure 71b**). This result supports the data previously obtained from the pull-down assay where PGD was only caught in hypoxic conditions.

Together, this data suggests that proteins from the PPP (i.e G6PD and PGD) display enhanced interactions with proteins from the purinosome in hypoxia.

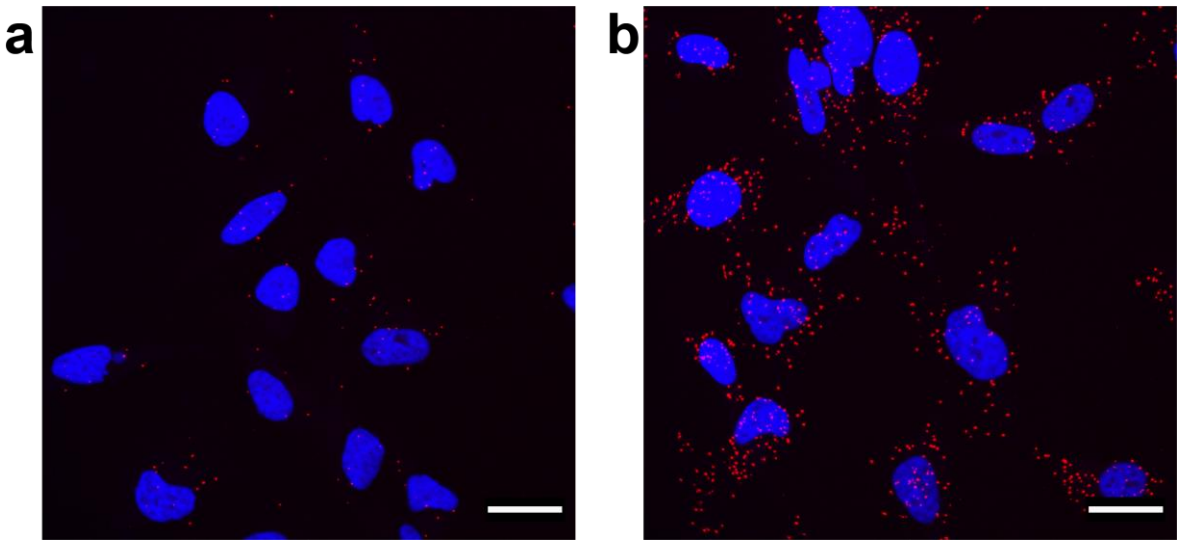

Figure 71. **Proximity ligation assay between GART and PGD. (a)** HeLa cells cultured in normoxia for 24 h. **(b)** HeLa cells cultured in hypoxia (1% oxygen) for 24 h. A small number of signals was detected in normoxia while a higher number of signals was detected in hypoxia suggesting a high colocalisation of the two proteins in hypoxia. The PLA signals appear as red dots. Cells were stained with DAPI. Scale bar represents 25 µm.

It is interesting to note that proteins from both glycolysis and the PPP have been pulled down in hypoxia using a protein from the purinosome as bait. In addition to these proteins, there are more enzymes required in the synthesis of substrates and co-factors used in the *de novo* purine biosynthesis that did not get caught in the pull-down experiment. One of them is the enzyme enabling the synthesis of the first substrate of the *de novo* and salvage purine biosynthesis, namely phosphoribosyl pyrophosphate (PRPP). PRPP is synthesised from ribose-5-phosphate, the final product of the PPP, by PRPP synthase, also known as PRPS1 (**Figure 72**). This enzyme does not belong to either the PPP or the purine biosynthesis pathway but links the two pathways and is indispensable for purine biosynthesis to function.

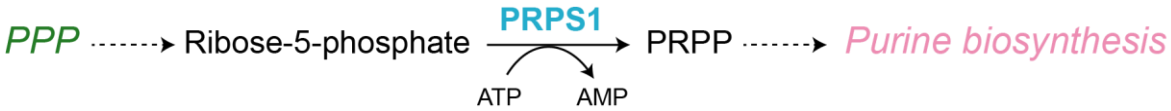

Figure 72. **Synthetic pathway of PRPP.** Phosphoribosyl pyrophosphate (PRPP) is synthesised by conversion of ribose-5-phosphate issued from the pentose phosphate pathway (PPP) by PRPP synthase (PRPS1). PRPP is then used as substrate into purine biosynthesis (both salvage and *de novo*).

As such, the close proximity between PRPS1 and the purinosome was next assessed using PLA between PRPS1 and GART, a core enzyme of the purinosome complex. When cells were maintained either in normoxia (**Figure 73a**) or in hypoxia (**Figure 73b**), a small number of PLA signals was observed with no obvious difference in their number between the two conditions, suggesting a weak colocalisation between the two proteins of interest independently of the oxygen levels.

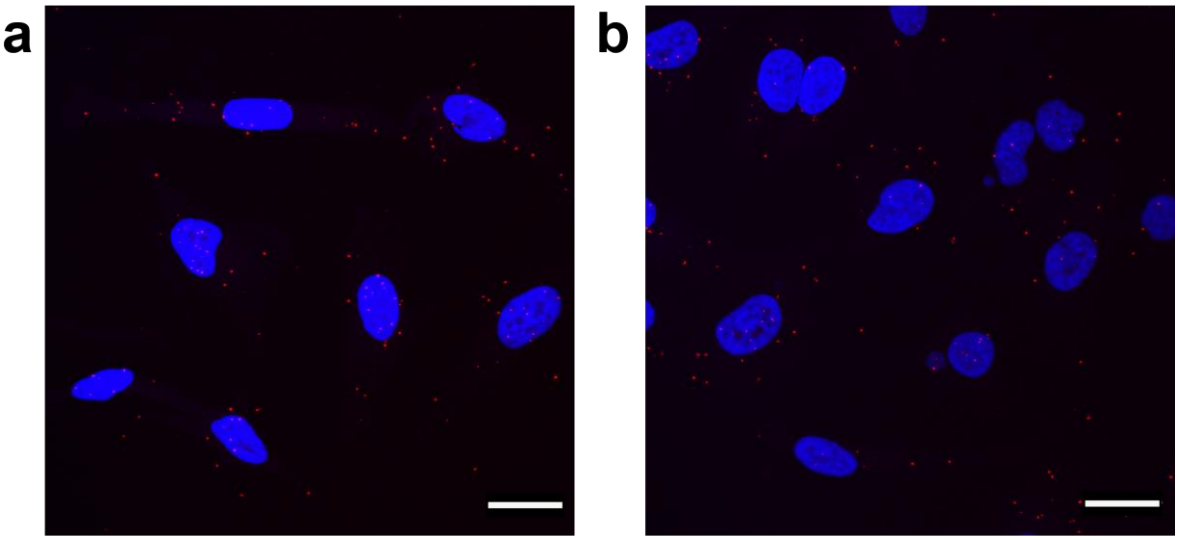

Figure 73. Proximity ligation assay between GART and PRPS1. (a) HeLa cells cultured in normoxia for 24 h. **(b)** HeLa cells cultured in hypoxia for 24 h. A small number of signals was detected in normoxia with a similar number of signals observed in hypoxia suggesting that the colocalisation between the two proteins is not enhanced in hypoxia. The PLA signals appear as red dots. Cells were stained with DAPI. Scale bar represents 25 µm.

Although PRPS1 did not display an enhanced colocalisation with GART in hypoxia compared to normoxia, the close proximity of PRPS1 with proteins of the purinosome was further assessed by probing the colocalisation of PRPS1 and PPAT by PLA. PPAT is the first enzyme of the *de novo* purine biosynthesis and catalyses the conversion of PRPP into phosphoribosyl amine (PRA). As PPAT uses the product of PRPS1 as substrate, it could be hypothesised that the two enzymes are in close proximity when channelling the metabolite from one enzyme to another. As such, when analysing the colocalisation between PPAT and PRPS1, normoxic cells were found to display a small number of PLA signals suggesting some colocalisation between the two proteins in these conditions (**Figure 74a**). However, a subsequent increase in the number of PLA signals was observed in hypoxia, suggesting an enhanced colocalisation between the two proteins of interest in this condition (**Figure 74b**).

Similarly to proteins from glycolysis and the PPP, PRPS1 was found to display an enhanced colocalisation with proteins from the purinosome, although only its colocalisation with PPAT was enhanced. As PPAT is the first enzyme of the *de novo* purine biosynthesis, it can be thought that its colocalisation with PRPS1 occurs independently of the purinosome complex and that PPAT is in close proximity with PRPS1 prior to joining the purinosome.

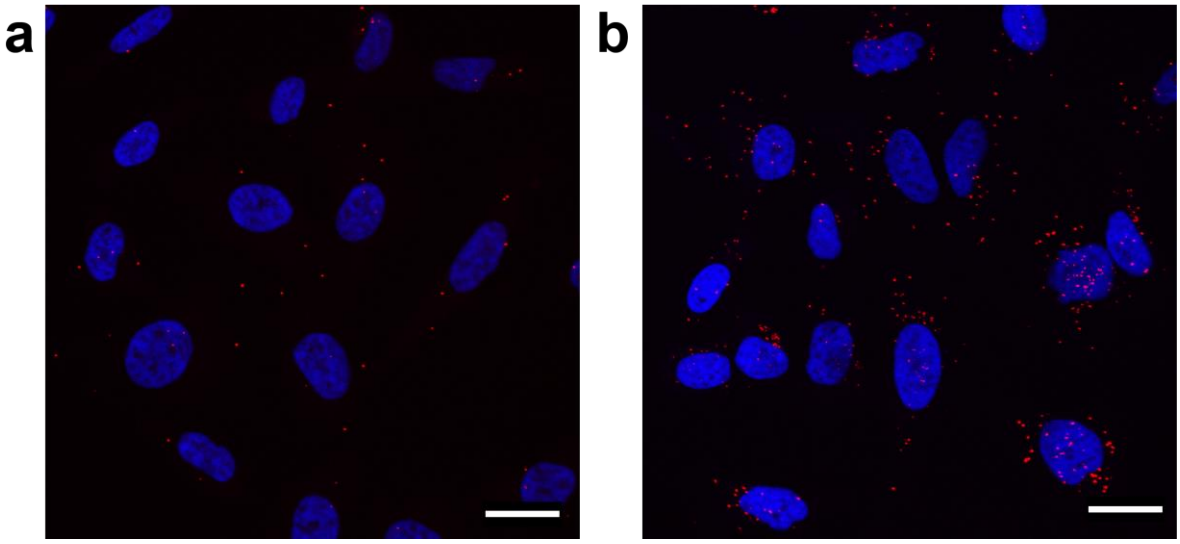

Figure 74. **Proximity ligation assay between PPAT and PRPS1. (a)** HeLa cells cultured in normoxia for 24 h. **(b)** HeLa cells cultured in hypoxia for 24 h. A small number of signals was detected in normoxia while a higher number of signals was detected in hypoxia suggesting an increased colocalisation of the two proteins in hypoxia. The PLA signals appear as red dots. Cells were stained with DAPI. Scale bar represents 25 µm.

To summarise, enzymes from the PPP were found to preferentially or exclusively interact with PFAS in hypoxia. This has been further assessed and confirmed using PLA where two enzymes of the pathway, G6PD and PGD, showed an increased colocalisation with the core purinosome enzyme GART in hypoxia. In addition, PRPS1, the enzyme that links the PPP to the purine biosynthesis by ensuring the synthesis of PRPP was also shown to display an enhanced co-localisation with the first enzyme of the *de novo* purine biosynthesis, PPAT. However, no increase in the colocalisation between PRPS1 and GART was observed in hypoxia. This last result suggests that the hypoxia-induced increase in colocalisation between PPAT and PRPS1 might occur independently of the purinosome complex or that PRPS1 is in close proximity with the purinosome complex but the organisation of the complex itself places the two proteins far away from each other, thus preventing the appearance of a PLA signal. The summary of the interactions determined by PLA are summarised in **Table 1**

Table 1. Summary of protein-protein interactions detected by PLA between purinosome proteins and proteins from associated pathways. Green boxes indicate that the interaction was enhanced in hypoxia (1% oxygen, 24 h) compared to normoxia (21% oxygen, 24 h). Red boxes indicate that the interaction between the two proteins was similar in hypoxia and in normoxia (no increase). *N/A* indicates that the given interaction was not assessed by PLA.

Purinosome proteins / Associated proteins	PFAS	GART	PPAT
PFKP		*N/A*	*N/A*
PFKL		*N/A*	*N/A*
G6PD	*N/A*		*N/A*
PGD	*N/A*		*N/A*
PRPS1	*N/A*		

2.3.2.4 Assessing the close proximity between purinosome enzymes and proteins from the one-carbon metabolism (OCM)

Another pathway that was found to be of interest when studying the *de novo* synthesis of purines is the one-carbon metabolism (OCM). Comprised of the *de novo* synthesis of serine as well as the folate cycle, the OCM is a major source of co-factors required for the *de novo* purine biosynthesis, as previously described in **section 1.1.4**. As such, the presence of enzymes from the OCM was investigated in the list of proteins pulled down by PFAS in hypoxia, and three enzymes of the OCM were detected in the hypoxic pull-down samples (**Figure 75**). The first OCM protein detected was phosphoglycerate dehydrogenase (PHGDH) which constitutes the first enzyme of the *de novo* serine biosynthesis and uses 3-phosphoglycerate, a glycolytic intermediate, as substrate (as previously described in **section 1.1.4**). PHGDH was detected in both normoxia and hypoxia but displayed a 3.6 fold increase in hypoxia, suggesting an enhanced interaction with PFAS in these conditions. In addition, two enzymes from the folate cycle, serine hydroxymethyltransferase isoform 2 (SHMT2, mitochondrial isoform of SHMT) and methylenetetrahydrofolate dehydrogenase 1 (MTHFD1, cytoplasmic isoform of MTHFD) were detected exclusively in hypoxic conditions. It is interesting that both cytosolic and mitochondrial proteins from the folate cycle were detected, as it correlates with previous reports suggesting that the purinosome colocalises with the mitochondria.[186, 187] It can be thought that this proximity between the purinosome complex and the mitochondria is also a feature of the hypoxia-induced purinosome and that this

facilitates the exchange of co-factors (e.g 10-f-THF) between the mitochondria and the purinosome in order to feed into the *de novo* purine biosynthesis.

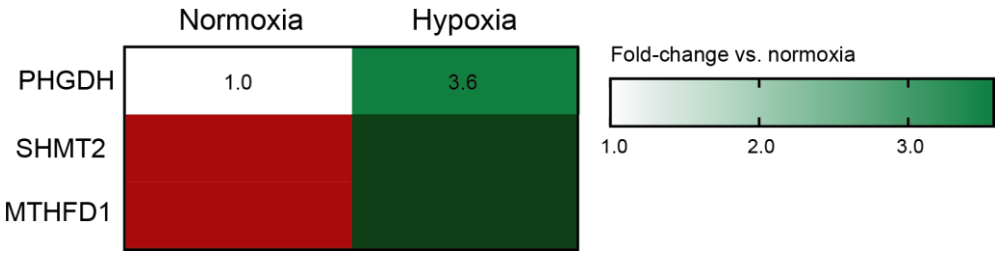

Figure 75. Heat-map presenting the levels of proteins belonging to the one-carbon metabolism, determined from proteomics analysis carried out in normoxia and hypoxia from a pull-down assay. Fold-changes were calculated by normalising the amount of protein in nanograms in hypoxic conditions to that measured in normoxic conditions. Red box indicates that the protein of interest is absent in this condition. Dark green box indicates that the protein is present only in this condition. Fold-changes are indicated in their corresponding box, coloured according to the fold-change based colour gradient.

In order to further confirm the enhanced proximity between PFAS and enzymes from the OCM in hypoxia, the colocalisation between PFAS and MTHFD1 was assessed by PLA. Some PLA signals were detected in normoxic conditions (**Figure 76a**) suggesting that the two enzymes tend to colocalise a little in this condition. However, when the cells were cultured in hypoxia, the number of PLA signals substantially increased indicating an enhanced colocalisation between these two proteins in low oxygen environments, thus confirming the observation made in the proteomics results (**Figure 76b**).

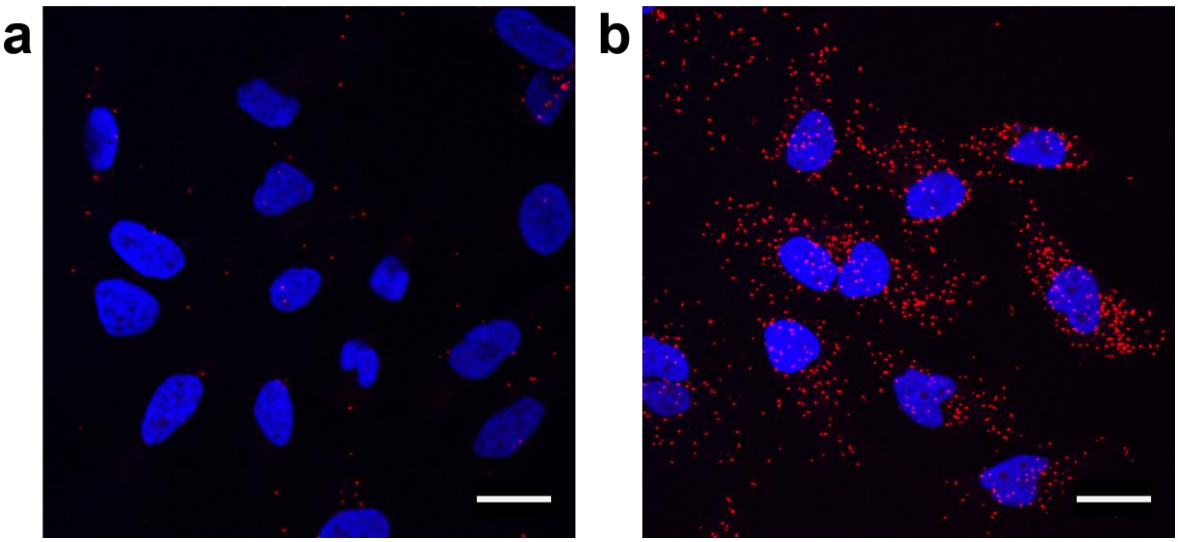

Figure 76. Proximity ligation assay between PFAS and MTHFD1. (a) HeLa cells cultured in normoxia for 24 h. **(b)** HeLa cells cultured in hypoxia (1% oxygen) for 24 h. A small number of signals was detected in normoxia while a higher number of signals was detected in hypoxia suggesting an increased colocalisation of the two proteins in hypoxia. The PLA signals appear as red dots. Cells were stained with DAPI. Scale bar represents 25 µm.

Altogether, this data suggests an enhanced interaction between proteins from the one-carbon metabolism and PFAS in hypoxic conditions. It can be hypothesised that this close proximity enables a facilitated transport of metabolites between the one-carbon metabolism and the *de novo* purine biosynthesis.

Overall the proteomics analysis revealed an interaction between PFAS and other proteins of the purinosome only in hypoxic conditions, thus strengthening the previously observed results suggesting an enhanced purinosome formation in hypoxia compared to normoxia. In addition, many proteins from related pathways (i.e glycolysis, PPP, one-carbon metabolism) were found to interact with PFAS preferentially, and in some cases exclusively, in hypoxia, thus suggesting a close proximity between these proteins and the purinosome complex in low oxygen conditions. The presence of proteins belonging to pathways that feed into the *de novo* pathway strengthens the hypothesis that proteins cluster or get in close proximity in order to render the metabolite flux more efficiently between pathways.

Such a broad screening provided an insight into the nature of the proteins that would be in close proximity with the hypoxic purinosome, but this analysis on its own is rather preliminary and requires further investigation. Although the proteomics analysis provided much information regarding potential protein-protein interactions, the data presented in this analysis were issued from one replicate (one normoxic and one hypoxic sample). Despite many attempts, the observed

results could not be repeated, although western immunoblotting analysis on PFAS-2xStrepTagII in pull-down samples, as previously presented in **Figure 60**, still enabled the detection of the bait. As such, although the assay was still efficient, the proteomic analysis did not enable the generation of a list of prey proteins.

2.3.3 Assessing the colocalisation of the purinosome with mitochondria

In 2016, the purinosome complexes were first reported to spatially colocalise with the mitochondrial network in purine-depleted conditions.[187] The association between these two entities was determined using a fluorescently tagged FGAMS-mEos2 and an immunofluorescence targeting a mitochondrial protein, TOM20. This colocalisation was found to be mTOR-mediated thus suggesting the presence of a functional link between the mitochondria and the nucleotide metabolism.

As two OCM enzymes were detected in the hypoxic pull-down sample with one being mitochondrial (i.e SHMT2), it was then hypothesised that the hypoxic purinosome might also colocalise with the mitochondria.

In order to assess this, the close proximity between a purinosome enzyme, PFAS, and TOM20, a protein located on the outer mitochondrial membrane which points into the cytoplasm, was probed using a PLA assay. HeLa cells were cultured in normoxia and hypoxia in normal purine conditions, as well as in normoxia in purine-depleted conditions, the latter being used as positive control. Few PLA signals were detected in normoxia suggesting a very low level of colocalisation between the two proteins of interest in this condition (**Figure 77a**). However, when cells were cultured in hypoxic conditions, the number of PLA signals substantially increased indicating an enhanced colocalisation of PFAS and TOM20 in low oxygen environments (**Figure 77b**). Cells in purine-depleted conditions also displayed a high number of PLA signals (**Figure 77c**), in line with previous reports indicating the colocalisation of PFAS-mEos2 and TOM20.[187] The number of PLA signals detected in hypoxia was similar to that observed in purine-depleted conditions, thus indicating that the close proximity between PFAS and the mitochondria occurs in a very similar manner in hypoxia compared to previously reported purine depleted conditions.

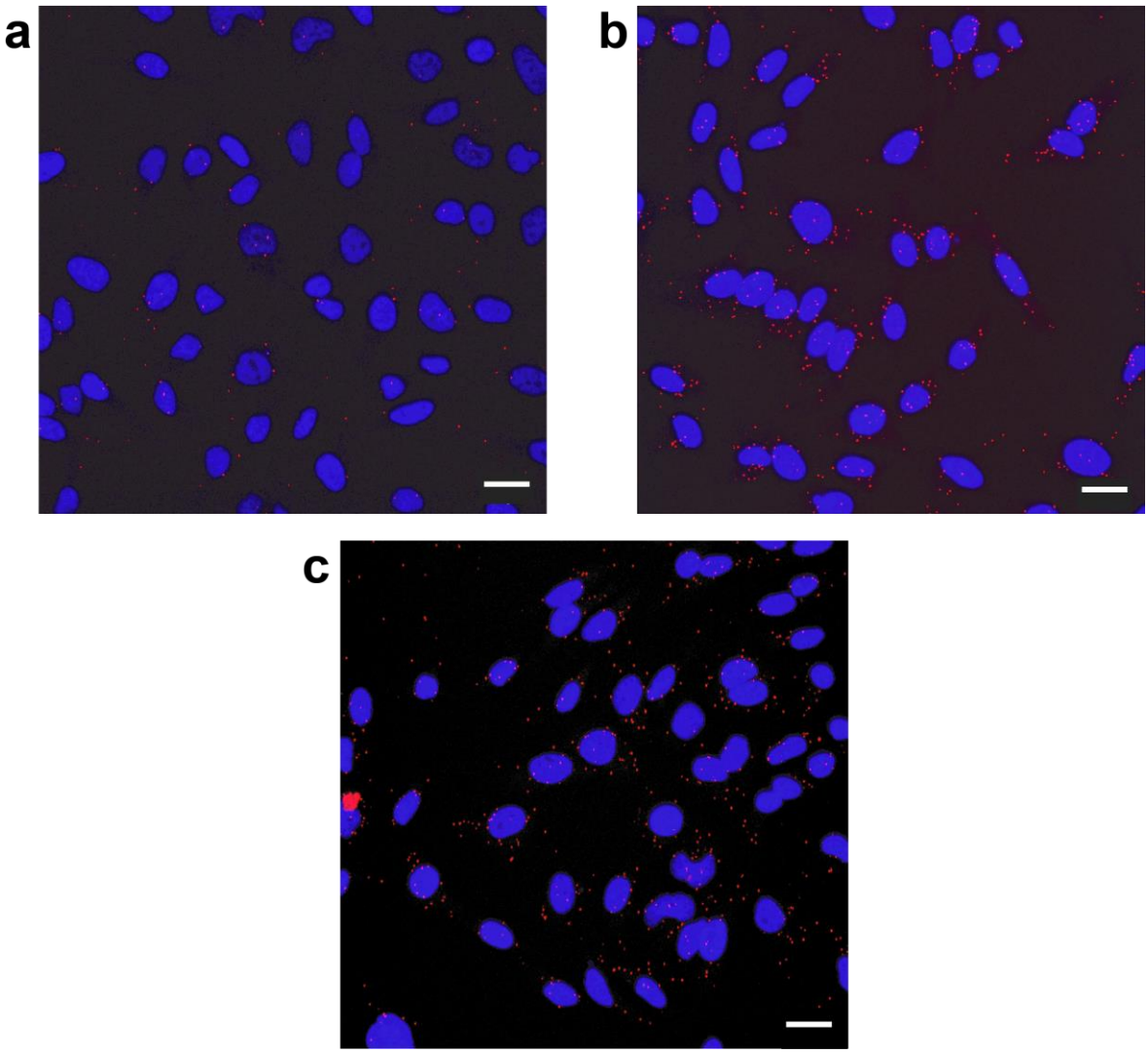

Figure 77. Proximity Ligation Assay between PFAS and TOM20. (a) HeLa cells cultured in normoxia for 24 h. **(b)** HeLa cells cultured in hypoxia (1% oxygen) for 24 h. **(c)** HeLa cells cultured in normoxia in purine-depleted conditions for 24 h. A small number of signals was detected in normoxia while a higher number of signals was detected in hypoxia and normoxia purine-depleted, suggesting a high colocalisation of the two proteins in these two last conditions. The PLA signals appear as red dots. Cells were stained with DAPI. Scale bar represents 25 µm.

To further analyse the close proximity between the hypoxic purinosome and the mitochondria, additional microscopy analyses were carried out. As such, HeLa cells were transfected with a construct encoding FGAMS-GFP and were subsequently incubated in hypoxia for 24 h. The mitochondria was then stained using a MitoTracker Deep Red dye. Following fixing, the cells were observed on a confocal microscope. Both the mitochondrial network (**Figure 78a**) and the purinosomes (**Figure 78b**) were detected.

In order to obtain high resolution imaging, the cells were imaged in a different way to traditional confocal microscopy, referred to as Super-Resolution Radial Fluctuations (SRRF). This imaging technique is based on confocal imaging but involves the processing of the pictures in an ImageJ plugin called NanoJSRRF that enables the reduction of the fluorescent background in order to achieve a higher resolution image, currently down to approximately 150 nm for GFP.[226]

As the background reduction is based on the emission fluctuations of the fluorophore, 100 image frames need to be acquired in the shortest possible time so as to then be processed via the above-mentioned plugin, resulting in the pictures presented in **Figure 78**. Overlay of the SRRF-processed red channel (**Figure 78a**) and green channel (**Figure 78b**) provided a merged picture showing the cellular localisation of the mitochondria and the purinosome complexes simultaneously (**Figure 78c**). The small region of interest (ROI) within the cell displayed in **Figure 78c** was zoomed in (8.3-fold compared to original picture) and is presented in **Figure 78d**. In this ROI, the red fluorescence of the mitochondria can nicely be seen in extremely close proximity to the green fluorescence, strengthening the hypothesis that the hypoxic purinosomes, like their purine-depleted counterparts, localise near the mitochondria.

To strengthen this observation, a Pearson's colocalisation coefficient was calculated to determine the degree of colocalisation between the two fluorophores, Mitotracker Deep Red and GFP. Following 200 Coste's iterations, the colocalisation coefficient was found to be of 0.525, indicating that the cellular localisation of each fluorophore is not random and that FGAMS-GFP and Mitotracker Deep Red display a significant colocalisation in hypoxic cells. This reinforces the observations made in **Figure 78** that purinosomes colocalise with the mitochondria in hypoxia.

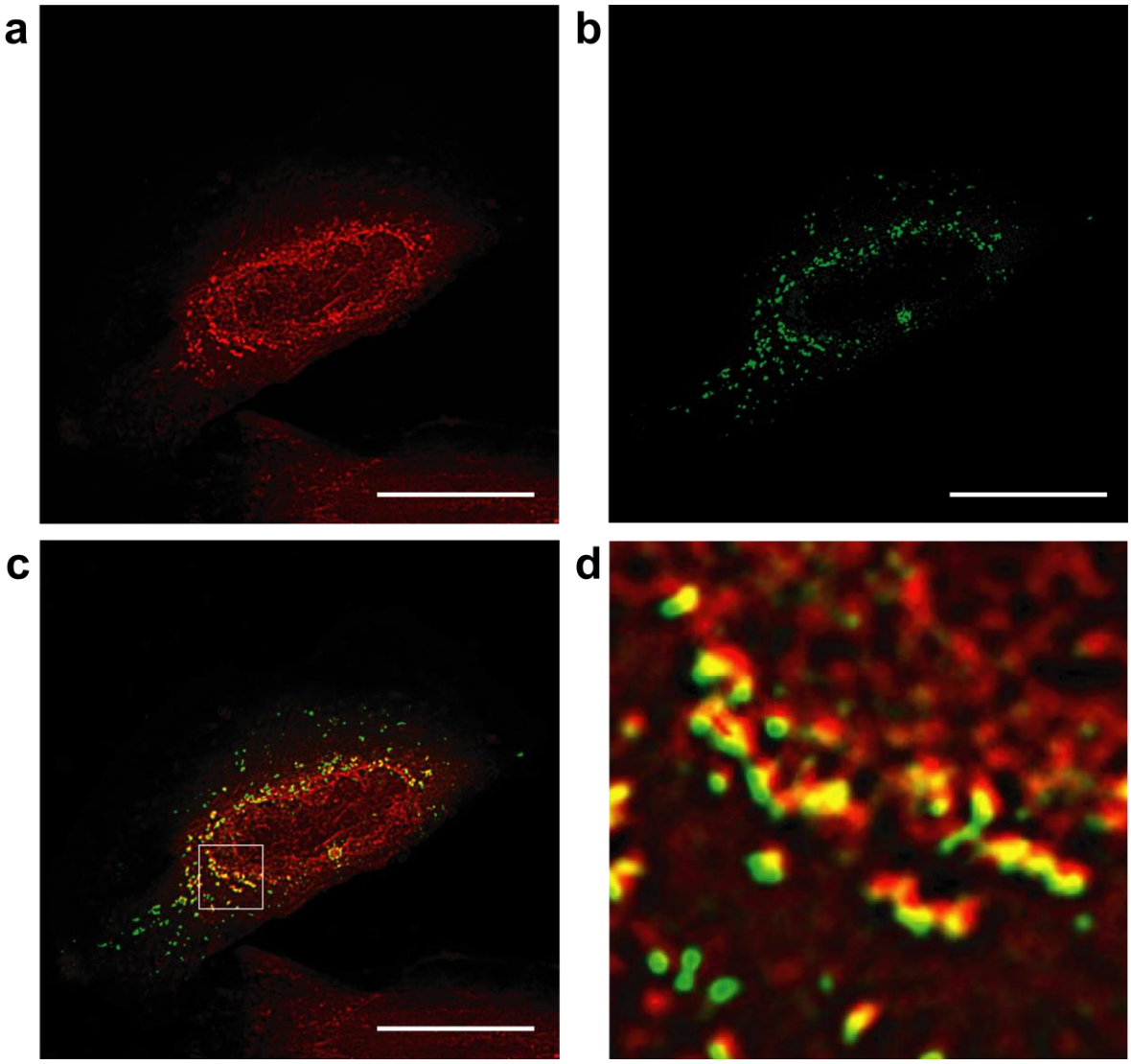

Figure 78. High resolution imaging of purinosomes and mitochondria in hypoxic HeLa cells. Hypoxic HeLa cells (1% oxygen) transfected with FGAMS-GFP and stained for their mitochondria using MitoTracker Deep Red were imaged using confocal imaging coupled to SRRF. **(a)** Mitochondria was observed using MitoTracker Deep Red. **(b)** Cells were transfected with FGAMS-GFP and incubated in hypoxia, leading to purinosome formation. **(c)** Merge of (a) and (b). **(d)** Zoom on ROI represented as a white square in (c), 8.3-fold zoom factor. Purinosomes (green) were localised near mitochondria filaments (red). Scale bar represents 25 µm.

Taken together, the data obtained from the pull-down analysis and the microscopy experiments strongly suggest that the purinosome protein PFAS (FGAMS), and to a larger extent the purinosome complex, colocalises with the mitochondria in hypoxic conditions. The summary of the different results suggesting this close proximity are presented in **Figure 79**.

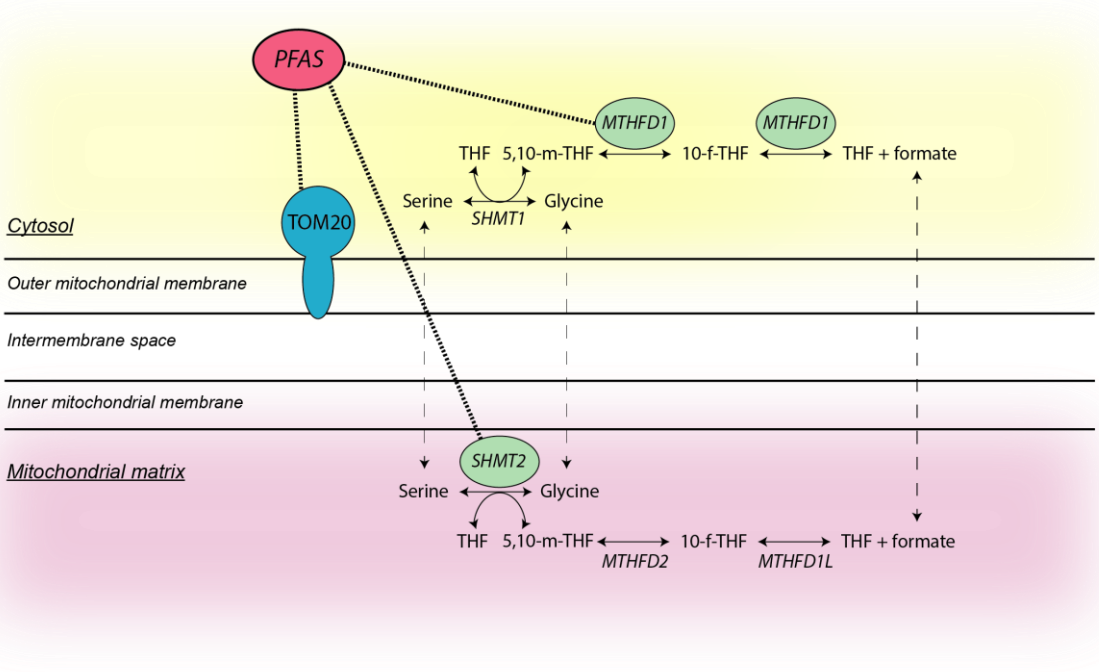

Figure 79. Scheme summarising the interactions between PFAS and the mitochondria-related proteins. The purinosome enzyme PFAS (in red) was found to colocalise with TOM20 (in blue) using a PLA experiment. In addition, pull-down analysis showed that in hypoxia PFAS interacted with cytosolic and mitochondrial enzymes of the one-carbon metabolism MTHFD1 and SHMT2, respectively (in green), with the increased PFAS-MTHFD1 interaction in hypoxia further supported by PLA data.

In addition to its close proximity with the mitochondrial protein TOM20 (**Figure 79**, blue protein), PFAS (**Figure 79**, red protein) was found to interact with SHMT2 and MTHFD1 by pull-down analysis in hypoxia (**Figure 79**, green proteins), results later strengthened by the increased number of PLA signals between PFAS and MTHFD1 in hypoxia compared to normoxic conditions.

It is of high interest to observe metabolic enzymes such as MTHFD1 and SHMT2 being pulled down using purinosome enzymes in hypoxia, as this could indicate that the observed close proximity between purinosomes and mitochondria reveals a metabolic link between the two entities, as previously suggested for the purinosome/mitochondria association in purine-depleted conditions.[187] MTHFD1 and SHMT2 are part of a metabolism called the one-carbon metabolism (OCM), and more specifically the folate cycle, which plays a major role in providing co-factors for multiple pathways such as the *de novo* purine biosynthesis, methionine synthesis and dTMP synthesis.

Although the data presented in this section strongly suggested the presence of potential interactions between the *de novo* purine biosynthesis and other metabolic pathways (glycolysis,

PPP, OCM), the nature of the functional link between purinosomes and enzymes from associated metabolic pathways (both cytosolic and mitochondrial) is yet to be determined.

As such, the next and last section of this work will focus on understanding the hypoxic metabolism of purine synthesis using metabolomics experiments based on isotope labelling. The main aims were i) to determine whether the formation of the purinosome complex in hypoxia correlates with increased purine biosynthesis via the *de novo* pathway ii) whether the pathways associated with the *de novo* purine biosynthesis are altered in hypoxic conditions and if so, how does this affect the *de novo* purine biosynthesis.

2.4 Tracing metabolite synthesis into the purine *de novo* pathway using isotope labelling.

The use of metabolomics analysis for the understanding of metabolic pathways and interconnections between various metabolisms has become widely utilised and optimised over the last few years. Isotope incorporation into metabolites extracted from cells is a powerful tool used to unravel yet unknown reactions, enzymatic mechanisms and pathway adaptations to various cellular conditions. The incorporation of isotope-labelled molecules into the cell media enables the tracing of the newly formed metabolites, as these will be easily detectable by mass spectrometry analysis due to the mass incorporation that will distinguish them from their unlabelled counterparts.

In this work, the initial hypothesis was that as purinosome formation was found to be significantly enhanced in hypoxia, their formation would correlate with an increased purine synthesis via the *de novo* pathway, as previously observed and reported in purine-depleted conditions.[169] In order to probe this, three different isotope-labelling experiments were carried out to obtain a wide range of complementary data, ultimately used to understand the metabolism around the hypoxic purine synthesis. The common aim of these experiments was to determine whether *de novo* purine synthesis was carried out in hypoxia, determine whether the rate of the pathway was increased or decreased and finally, determine how the pathways associated with the *de novo* purine biosynthesis were affected by hypoxic conditions.

These three different approaches utilised either ^{13}C labelling or ^{15}N labelling and are presented in **Figure 80**, where carbon atoms are represented as circles and nitrogen atoms as squares. These three experiments were carried out independently and utilised three isotope-labelled molecules, each of them being represented by a different colour and enabling the formation of different possible isotopes. The blue labelling represents the experiment involving the supplementation of cell media with glucose uniformly labelled on the six carbons using ^{13}C, referred to as $^{13}C_6$-glucose. The resulting isotope-labelled metabolites can be directly traced into glycolysis and in the *de novo* purine biosynthesis, leading to additional masses of up to M+9 for IMP, AMP and GMP. The pink labelling represents the incorporation of labelled ^{15}N-glutamine, a co-factor used twice during the 10-step synthesis leading to IMP, thus enabling the formation of M+1 and M+2 isotopologues for IMP and AMP (pink labelling, **Figure 80**). In addition, glutamine is used once in the conversion of IMP into GMP, thus leading to the formation of M+3 GMP species (pink labelling, **Figure 80**). Finally, the third approach involved the use of ^{15}N-serine (**Figure 80**, green labelling), which via its conversion into glycine, enables the incorporation of one labelled nitrogen atom into the purine ring at the second step of the pathway, leading to M+1 nucleotide monophosphate species.

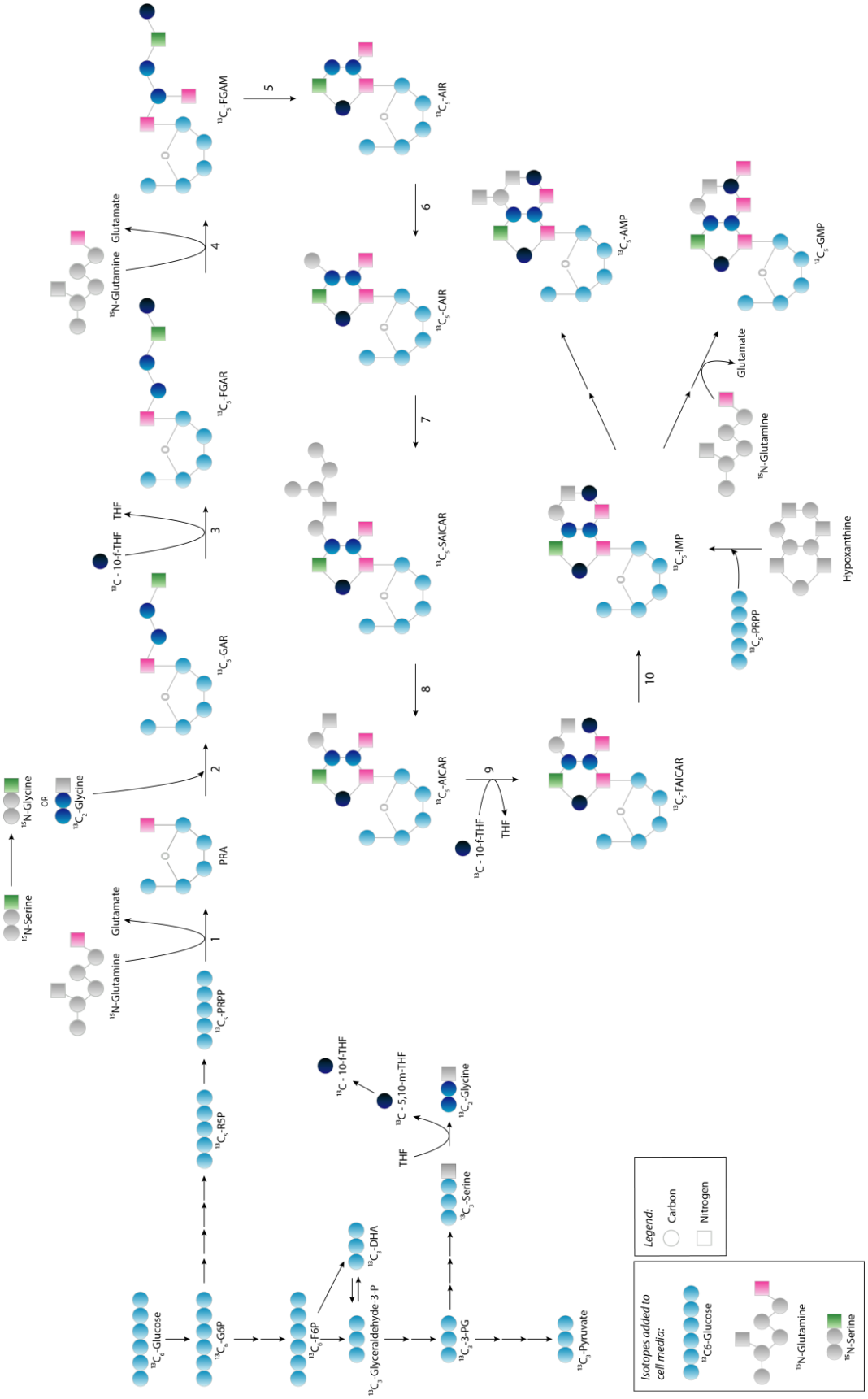

Figure 80. Scheme tracing isotope incorporation into the *de novo* purine biosynthesis pathway. Different isotope-labelled molecules were added individually and separately to the cell media during different experiments: $^{13}C_6$-Glucose, ^{15}N-Serine and ^{15}N-Glutamine (amide). All possibilities of resulting metabolites are presented.

2.4.1 Using ^{15}N-(amide)-glutamine to assess isotope incorporation into nucleotide monophosphates.

The first approach used in this study was based on the use of ^{15}N(amide)-glutamine (**Figure 80**, pink squares). This amino acid is of particular interest when studying the *de novo* purine biosynthesis as it is used twice as a co-factor in the pathway. First by PPAT (step 1) and then by GART (step 4), thus leading to a +2 mass incorporation in the final product IMP (referred as M+2 IMP). In addition, glutamine is also used in the synthesis of GMP from IMP, enabling the incorporation of a third isotope-labelled nitrogen atom, thus making the newly formed GMP detectable with a +3 in mass (M+3) compared to the unlabelled GMP molecule. In parallel, the newly synthesised AMP molecule, like its precursor IMP, would be detectable via the formation of its M+2 isotopologue.

It should be noted that although glutamine is used twice in the pathway (10 steps leading to IMP), unlabelled endogenous glutamine is still present in the cell and can be incorporated in the newly synthesised nucleotide monophosphates, resulting in the appearance of M and M+1 isotopologues.

In this experiment, HeLa cells were placed in hypoxia for 12 h prior to the isotope pulse. This time point was chosen as it was previously determined to be the time at which purinosome formation reaches its maximum. Cells were placed in hypoxia or normoxia for 12 h (in the presence of purines, referred to as P+), or in normoxia with no purines in the media (referred to as P-). Normoxia P- was used as a positive control as this condition was previously demonstrated to induce *de novo* purine biosynthesis (coupled to purinosome formation).[169] Cells were subsequently cultured in a growth media supplemented with ^{15}N-(amide)-glutamine for 4 h whilst being maintained in normoxia P+, hypoxia P+ and normoxia P-. Following this, the cells were collected for downstream metabolite analysis.

Before analysing the isotope incorporation into the nucleotide monophosphates, the total abundance of IMP, AMP and GMP was assessed in all three conditions in order to determine whether hypoxic conditions induced a change in the total availability of the purine monophosphates. As a result, no significant difference in total metabolite abundance was observed for IMP, AMP or GMP between hypoxic and normoxic conditions (P+) (**Figure 81**). However, culturing the cells in purine-depleted conditions (normoxia P-) induced an increase in the total abundance of IMP and AMP, likely generated by the increased *de novo* purine synthesis, in line with previous reports.[169]

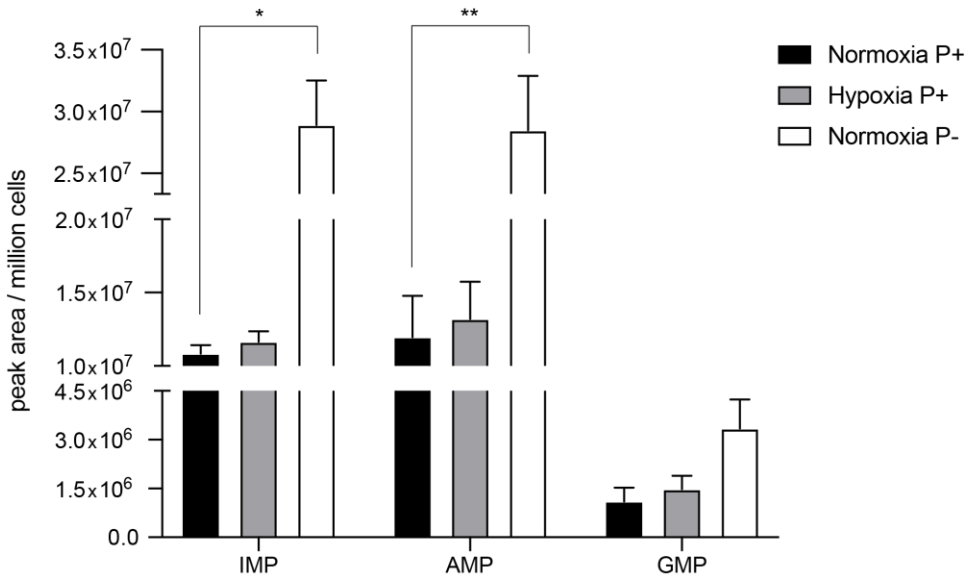

Figure 81. Total abundance of purine nucleotide monophosphates in normoxia (P+), hypoxia (P+), and normoxia in purine-depleted conditions (P-). The total abundance of IMP, AMP, and GMP was measured in HeLa cells maintained in hypoxia (P+) (1% oxygen), normoxia (P+) and normoxia purine-depleted conditions (P-) for 16 h. No statistical difference was observed for any of the three nucleotide monophosphates between normoxic and hypoxic conditions (P+). Normoxia P- induced an increase in total abundance of IMP and AMP. Data are means (n=3) ± SEM. Significance was determined using unpaired Student t test, * $p < 0.05$, ** $p < 0.01$.

Although the total metabolite abundance is normalised to cell number, the cell proliferation rate between normoxic and hypoxic cells was assessed to determine whether the following metabolomics results could be biased by a significant difference in cell proliferation. A decreased cell proliferation could be associated with a decreased metabolite consumption, which could then impact upon the interpretation of isotope incorporation.

As such, to ensure that hypoxic cell proliferation was not affected compared to normoxic cells, the cell growth of HeLa cells was assessed. No difference was observed after 24 h of culture between normoxia and hypoxia, suggesting that HeLa cells do not slow down their proliferation in low oxygen environments (

Figure 82). This data suggests that the cells are likely to display similar metabolite consumption in both oxygen conditions and that all of the metabolomics obtained result strictly from metabolic differences between normoxic and hypoxic cells.

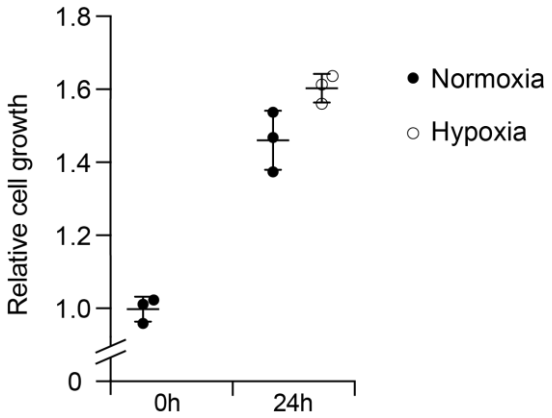

Figure 82. Cell growth of HeLa cells after 24 h of incubation in normoxia and hypoxia. The number of cells were measured after 24 h of incubation in normoxia or hypoxia (1% oxygen) and normalised to the number of cells at time 0 h. Data are means (n=3) ± SEM.

Following this, the mass incorporation resulting from the ^{15}N-glutamine pulse was determined by analysing the isotopologue profiles of the nucleotide monophosphates. If the *de novo* pathway is upregulated, incorporation of ^{15}N-glutamine should lead to the synthesis of M+2 IMP molecules and M+2 AMP molecules (**Figure 80**, pink squares). In addition, the *de novo* synthesis of GMP should lead to the formation of an M+3 species as one molecule of glutamine is used in the conversion of IMP into GMP. Based on this, it should be noted that in the case of a salvage synthesis of GMP, the precursor IMP molecule would be unlabelled (resulting from a conversion of hypoxanthine) and the IMP to GMP conversion would lead to the incorporation of singly labelled nitrogen atom from glutamine into the newly synthesised GMP molecule, resulting in an M+1 isotopologue formation.

This way, in this experiment, the isotopologue profile of IMP revealed that in normoxia after 4 h isotope pulse, the total pool of IMP was still comprised of more than 95% of unlabelled molecule (97%), consistent with a normoxic purine biosynthesic process mostly reliant on the salvage pathway (**Figure 83a**). However, it was rather surprising to observe the same isotopologue repartition in hypoxic conditions after 4 h isotope pulse as this indicates that in hypoxia too, the synthesis of IMP relies mostly on the salvage pathway (97% of unlabelled IMP in the total pool) (**Figure 83a**). Neither normoxia P+ nor hypoxia P+ enabled the detection of the M+2 IMP isotopologue, suggesting no activity of the *de novo* pathway in these conditions. However, when determining the isotope incorporation into IMP in purine-depleted conditions (normoxia P-), the significant appearance of M+2 IMP isotopologues after 4 h of isotope pulse was observed (38% of total IMP pool), consistent with previous reports indicating that in these conditions, the *de novo* purine biosynthesis is upregulated (**Figure 83a**).[169]

Similarly, the isotopologue profile of AMP revealed the same trend, with most of the normoxic and hypoxic AMP pool remaining unlabelled after 4 h isotope pulse (both displaying 98.5% of unlabelled AMP), thus indicating that regardless of the oxygen levels, AMP is synthesised via the salvage pathway in these two conditions (**Figure 83b**). However, when cells were cultured in normoxia in the absence of purines (normoxia P-), the appearance of an M+2 AMP species was detected (33% of total AMP pool), indicating an increased *de novo* biosynthesis in these conditions (**Figure 83b**), consistent with previous reports and in line with the similar observations made with IMP in normoxia P- (**Figure 83a**).[169]

Following this, the isotopologue profile of GMP was analysed. In normoxia and hypoxia (P+), 57% of the total pool was composed of M+1 GMP species after 4 h pulse, consistent with a salvage synthesis of the molecule (**Figure 83c**). It is to note that this large fraction of M+1 was detected after 4 h isotope pulse but was extremely low prior to the isotope pulse (0 h), indicating that the M+1 GMP molecules detected after 4 h isotope pulse result from newly synthesised molecules that incorporated a labelled nitrogen atom. In parallel, as the M+1 GMP isotopologue results from the salvage with incorporation of labelled glutamine, the unlabelled GMP molecules (M fraction) also result from the salvage pathway but this time with the incorporation of an unlabelled glutamine molecule instead of ^{15}N-glutamine, hence the absence of labelling. In normoxia P-, 50% of the total fraction of GMP was found to be the M+3 GMP isotope after 4 h pulse, consistent with a *de novo* mode of synthesis of the molecule in this condition (**Figure 83c**).

As a control, the isotope incorporation was also studied in uridine monophosphate (UMP). UMP is a pyrimidine nucleotide monophosphate that can be synthesised *de novo* from a glutamine molecule in a six-step reaction.[225] As such, isotope incorporation from ^{15}N-glutamine can also be traced into UMP in the case of *de novo* synthesis of this nucleotide. Here, when tracing labelled nitrogen incorporation, it was found that a very low fraction of UMP was labelled (M+1) after 4 h isotope pulse in normoxia (15%) and hypoxia (14%) (P+) (**Figure 83d**). However, a significant increase in the fraction of M+1 UMP was observed in purine-depleted conditions (60% of total UMP pool), consistent with an increased synthesis of UMP in this condition (**Figure 83d**).

It should be noted that increased UMP synthesis via the *de novo* pathway in purine-depleted conditions has, to the best of our knowledge, not been reported in the literature so far. However, the composition of the culture media used in “purine-depleted conditions” is composed of culture media supplemented with dialysed FBS. Dialysed FBS is of particular interest when studying metabolic pathways because of the absence of small molecules in the serum. In the case of this work, it is used for the deprivation of purines, but additionally, this serum is also deprived of pyrimidines. As such, it can be hypothesised that depriving the cells of pyrimidines (like they are

deprived of purines for the purpose of this work) triggers *de novo* pyrimidine formation, in the same way that it triggers d*e novo* purine synthesis. To support this, a previous study reported that L1210 cells switch off the *de novo* pyrimidine synthesis when exogenous uridine is available.[227] As such, it can be hypothesised that when using dialysed serum, the lack of DNA bases induces an upregulation of the *de novo* pyrimidine biosynthesis in order to maintain the pyrimidine pool in cells.

Overall, the use of ^{15}N-glutamine enabled the determination that the hypoxic synthesis of purines is not different to the normoxic synthesis of purines and mostly relies on the salvage pathway whereas, as previously reported, purine-depleted conditions resulted in the upregulation of the d*e novo* pathway.[169]

This absence of *de novo* upregulation in hypoxia was rather unexpected as the formation of the purinosome complex has previously been reported to correlate with an upregulation of the *de novo* purine biosynthesis pathway in purine-depleted conditions.[169]

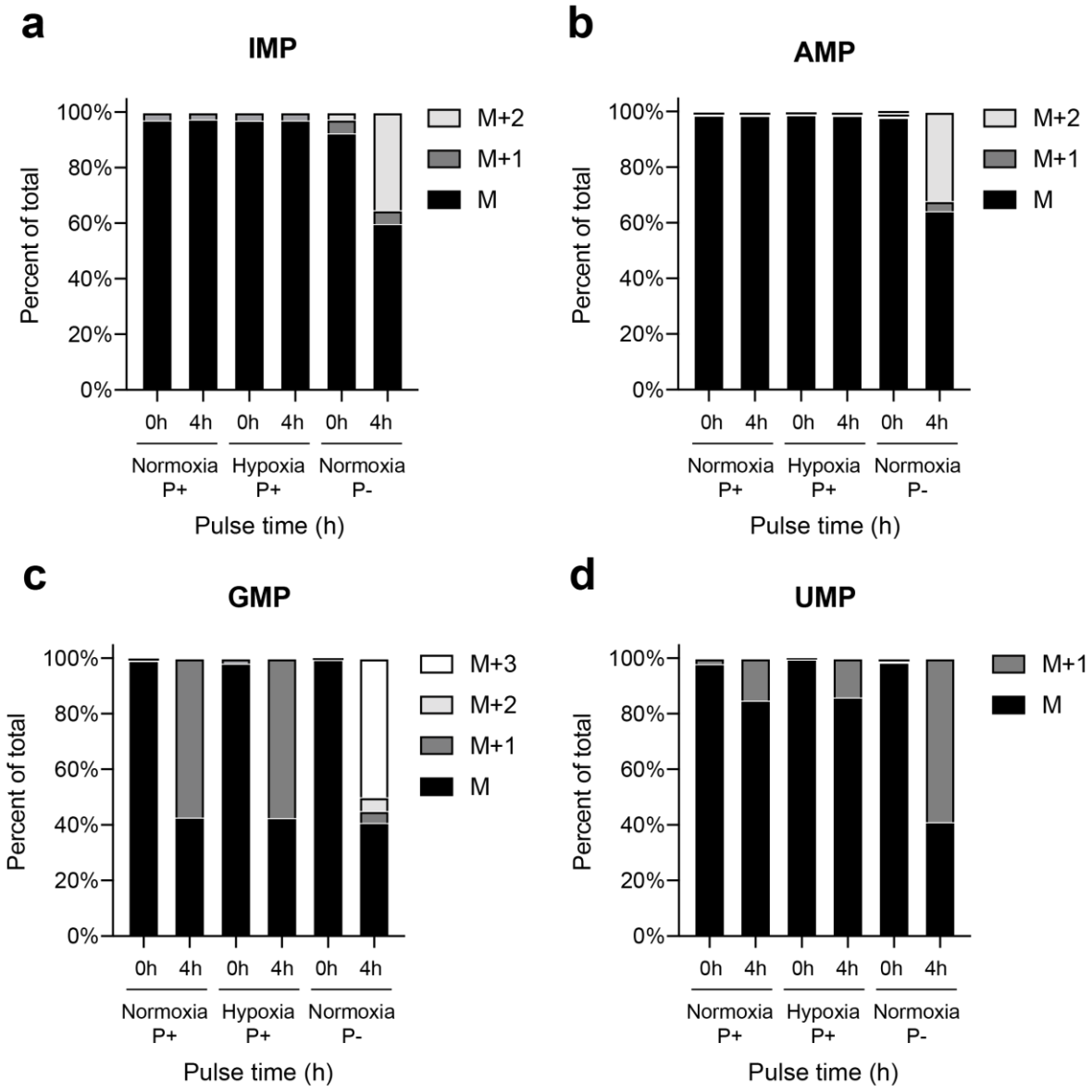

Figure 83. Isotopologue profiles of nucleotide monophosphates after ^{15}N-(amide)-glutamine labelling. HeLa cells were cultured in normoxia or hypoxia P+ (1% oxygen) and normoxia P- for 12 h and were subsequently pulsed with ^{15}N-glutamine for 4 h. Isotopologue profiles of **(a)** IMP, **(b)** AMP and **(c)** GMP revealed that the purine monophosphates are synthesised via the salvage pathway in normoxia and hypoxia (P+). However, as previously reported, cells cultured in normoxia P- displayed increased fractions of labelled purine monophosphates revealing the upregulation of *de novo* purine biosynthesis in these conditions (IMP M+2, AMP M+2 and GMP M+2 and M+3).[169] **(d)** Isotope incorporation into UMP revealed that the pyrimidine monophosphate was not synthesised *de novo* from glutamine in normoxia and hypoxia (P+) but that its *de novo* synthesis was upregulated in P- conditions. Data are means (n=3).

2.4.2 Using ^{15}N-serine to assess isotope incorporation into nucleotide monophosphates

To further understand the metabolism of purines in hypoxic conditions, another isotope-based approach was used with HeLa cells placed in a growth media supplemented with ^{15}N-serine. This metabolite is a good marker to trace *de novo* purine biosynthesis as it is converted into ^{15}N-glycine which can be directly incorporated into the purine ring during the second step of the pathway. This way, an increased rate of the *de novo* pathway would enable the formation of M+1 species of the nucleotide monophosphates. In the case of a salvage-driven synthesis, only the unlabelled species (M) would be observed.

As such, following 4 h ^{15}N-serine pulse in hypoxia, normoxia (P+) and purine-depleted conditions (normoxia P-), the incorporation of labelled nitrogen into AMP was analysed. A very low fraction of labelled AMP was observed in both normoxic and hypoxic conditions with no significant increase in labelled nitrogen incorporation in hypoxia compared to normoxia (1.5% in both conditions) (**Figure 84a**). This result indicates that the synthesis of AMP via the *de novo* pathway is low in normoxia and is not increased in hypoxia, suggesting a salvage biosynthesis of AMP in both oxygen conditions. In purine-depleted conditions (normoxia P-), the fraction of labelled AMP was significantly increased compared to normoxia P+ (24% of total AMP pool in P- conditions), suggesting, once again, an upregulated *de novo* synthesis of AMP in this condition (**Figure 84a**).

In order to further understand the causes of this non-increase in the rate of the *de novo* pathway, the levels of ^{15}N-serine and ^{15}N-glycine were analysed following the 4 h isotope pulse. No significant increase in ^{15}N-serine was observed between normoxia and hypoxia (5% and 4% of total pool, respectively), suggesting a comparable metabolite uptake from the extracellular environment between the two oxygen conditions (**Figure 84b**). However, a substantial increase in intracellular ^{15}N-serine was observed in purine depleted conditions (34% of total serine pool) suggesting an important increase in metabolite uptake in this condition (**Figure 84b**).

Similarly, the intracellular levels of ^{15}N-glycine were analysed in all three studied conditions in order to determine the impact of the culture environment on the serine to glycine conversion. A small increase in ^{15}N-glycine levels were observed in hypoxia compared to normoxic conditions (8% and 9% of total pool, respectively), suggesting a minor increase in the serine to glycine conversion after 4 h of hypoxia incubation (**Figure 84c**). In line with the trend observed for the intracellular levels of ^{15}N-serine, a substantial increase was observed in intracellular levels of ^{15}N-glycine in purine-depleted conditions (20% of total glycine pool), suggesting that the uptaken ^{15}N-serine is largely converted into ^{15}N-glycine (**Figure 84c**).

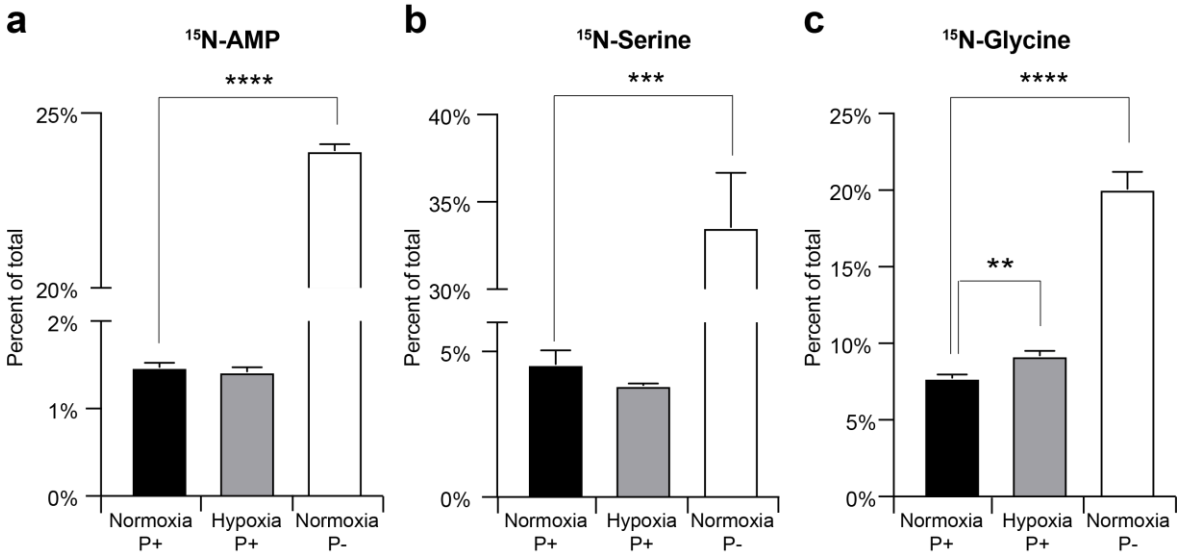

Figure 84. Intracellular levels of ^{15}N-AMP, ^{15}N-serine and ^{15}N-glycine in HeLa cells cultured in normoxia (P+), hypoxia (P+) and purine-depleted conditions (normoxia P-) following 4 h ^{15}N-serine isotope pulse. HeLa cells were cultured in normoxia or hypoxia P+ (1% oxygen), and normoxia P-, in the presence of ^{15}N-serine for 4 h. **(a)** Intracellular levels of ^{15}N-AMP reveals no upregulation of the *de novo* purine biosynthetic pathway in hypoxia (P+) compared to normoxia (P+) but a strong increase was observed in normoxia P-. **(b)** Intracellular levels of ^{15}N-serine reveal no increase in the uptake of the metabolite in hypoxia compared to normoxia, and a significant increase in purine-depleted conditions. **(c)** Intracellular levels of ^{15}N-glycine reveal a small increase in serine to glycine conversion in hypoxia after 4 h and a substantial increase in ^{15}N-glycine levels in normoxia P-. Data are means (n=3) ± SEM. Significance was determined using unpaired Student t test, *** $p < 0.001$, **** $p < 0.0001$.

Altogether, this data suggests that the synthesis of AMP via the *de novo* pathway is extremely low in normoxia and that this pathway is not upregulated after 4 h of hypoxic incubation. However, it was determined that the uptake of serine remained similar in hypoxia compared to normoxia with the conversion to glycine marginally enhanced in hypoxic conditions.

Interestingly, in addition to the increased *de novo* synthesis of AMP in purine-depleted conditions, it was found that the serine uptake and its subsequent conversion to glycine are also substantially enhanced in purine-depleted conditions. It can be hypothesised that this increased serine uptake and resulting glycine availability contributes to the increased rate of the *de novo* purine biosynthesis in purine-depleted conditions.

Altogether, these results are in line with the data obtained from the ^{15}N-glutamine labelling. It should be noted that the glutamine labelling experiment was carried out for a total incubation time of 16 h; 12 h in the presence of unlabelled glutamine in order to induce the hypoxia response in the cells, followed by a 4 h isotope pulse while keeping the cells in hypoxia. In the serine-labelled experiment, the cells were placed in hypoxia at the same time as the beginning of the isotope pulse. Both conditions were assessed in order to determine whether pre-incubating the cells in hypoxia for 12 h, thus enabling maximum purinosome formation and the establishment of the hypoxia response, would impact upon the rate of the *de novo* purine biosynthetic pathway. Together, the results obtained from these two isotope labelling approaches suggest that regardless of whether the hypoxia response had been established prior to the isotope pulse or not, no increase in the rate of the *de novo* purine biosynthesis was observed following 4 h of isotope pulsing.

To further understand the metabolism underlying purine synthesis in hypoxic conditions, a final labelling approach was attempted. This experiment was carried out using HeLa cells cultured in the presence of uniformly labelled $^{13}C_6$-glucose for 24 h in normoxia and in hypoxia (in the presence of purines in media), and will be discussed in the next section of this work.

2.4.3 Using $^{13}C_6$-glucose to assess the metabolic link between *de novo* purine biosynthesis and the mitochondrial metabolism.

The final labelling approach used in this study involved the use of $^{13}C_6$-glucose in order to directly trace labelled carbon incorporation into nucleotide monophosphates and into metabolites associated with the synthesis of purines.

For this purpose, HeLa cells were cultured in normoxia and hypoxia for 24 h in the presence of $^{13}C_6$-glucose after which the cells were collected and the metabolites analysed.

As previously presented in **Figure 80**, labelled glucose (M+6) is catabolised via the glycolysis pathway which enables the formation of labelled glycolytic intermediates such as glucose-6-phosphate which is used as a substrate for the pentose phosphate pathway, leading to the formation of ribose-5-phosphate and the downstream synthesis of phosphoribosyl pyrophosphate (PRPP), the main substrate of both *de novo* and salvage purine synthesis. As such, a newly synthesised PRPP molecule resulting from $^{13}C_6$-glucose labelling would display a +5 in mass incorporation ($^{13}C_5$-PRPP, **Figure 80**).

In addition, amongst the different labelled glycolytic intermediates that can be formed following $^{13}C_6$-glucose supplementation, $^{13}C_3$-3-phosphoglycerate ($^{13}C_3$-3-PG) is also of interest when

studying *de novo* purine synthesis as its carbon labelling can be traced into co-factors used in the pathway. Indeed, 3-phosphoglycerate is the first substrate of the *de novo* serine pathway and thus the newly formed $^{13}C_3$-3-PG can be used for the synthesis of $^{13}C_3$-serine (**Figure 80**). As part of the one-carbon metabolism, $^{13}C_3$-serine can be converted downstream into $^{13}C_2$-glycine enabling the simultaneous production of labelled 5,10-methyleneTHF (^{13}C-5,10-mTHF) (**Figure 80**). This newly formed molecule can subsequently enter the folate cycle and be converted into ^{13}C-10-f-THF, a co-factor required in two independent steps of the *de novo* purine biosynthesis (**Figure 80**, steps 3 and 9). In parallel, the newly formed $^{13}C_2$-glycine can also be used as a co-factor during the second step of the *de novo* purine biosynthesis, leading to a +2 in mass incorporation into the final nucleotide monophosphates (**Figure 80**).

Overall, if all newly synthesised labelled species are used as co-factors during the *de novo* purine biosynthesis, different masses of isotopes would be expected : each of ^{13}C-10-f-THF molecules would enable a +1 in mass incorporation, and $^{13}C_2$-glycine would enable a +2 in mass incorporation. In addition, the newly synthesised $^{13}C_5$-PRPP would contribute to a +5 mass incorporation into the final nucleotide. It should be noted that unlabelled metabolites will likely remain available for the *de novo* purine synthesis and can also be incorporated into the purine ring. As a summary, nucleotide monophosphate species ranging from M to M+9 could be expected following $^{13}C_6$-glucose labelling (**Figure 80**).

It should be noted that, as PRPP is the first substrate of the *de novo* and salvage purine synthesis pathways, an increase in M+5 nucleotide monophosphate species would not enable to determine whether the observed species are synthesised *de novo* or from salvage. As such, an increase in the levels of higher mass species (M+6 to M+9) would reflect an increased rate of the *de novo* purine biosynthetic pathway. Alternatively some increase in smaller mass species could be expected in the situation where labelled co-factors such as ^{13}C-10-f-THF and $^{13}C_2$-glycine are incorporated into a *de novo* synthesis initiated with a non-labelled PRPP substrate.

This way, the first metabolite analysed following $^{13}C_6$-glucose supplementation was PRPP. Analysis of the isotopologue profile of PRPP indicated that both normoxic and hypoxic cells displayed the formation of the M+5 PRPP isotopologue, with no significant difference between the two conditions after 24 h of incubation (**Figure 85a**). In addition, a significant fraction of the PRPP pool was composed of unlabelled molecules (M), that were either already present prior to the isotope pulse or that were likely resulting from the catabolism of unlabelled glucose (**Figure 85a**). Together, this data suggests that the synthesis rate of PRPP from glucose is not affected by hypoxic conditions and occurs similarly in both oxygen conditions.

Following this, the isotopologues profile of IMP was analysed following 24 h incubation with $^{13}C_6$-glucose. The formation of an M+5 IMP species was observed in both normoxic and hypoxic conditions, with no significant difference between the two conditions (**Figure 85b**). Very low fractions of ^{13}C-IMP and $^{13}C_2$-IMP were detected in both normoxia and hypoxia with no significant difference between the two conditions. The levels of ^{13}C-IMP were found to be similar to the natural abundance of isotope, indicating that the labelled carbon incorporation into ^{13}C-IMP in normoxia and hypoxia likely resulted from natural abundance and was independent from the isotope pulse (**Figure 85b**). In addition, no high mass IMP species (M+6 and above) were detected in neither normoxia nor hypoxia, suggesting that no co-factors (i.e ^{13}C-10-f-THF and $^{13}C_2$-glycine) were incorporated into the purine ring containing $^{13}C_5$-PRPP (**Figure 85b**). Together, this data suggests that IMP is mostly synthesised from the salvage pathway, as an upregulated *de novo* synthesis in hypoxia would be reflected by increased levels of labelled IMP species (other than M+5) due to the incorporation of labelled co-factors.

Similarly, the isotopologue profile of AMP was analysed and a small increase in the levels of $^{13}C_5$-AMP (M+5 AMP) was observed in hypoxia compared to normoxia, although as previously mentioned, the M+5 species does not indicate from which pathway the nucleotide originated (**Figure 85c**). As such, when looking at high mass species, the presence of M+6 and M+7 AMP molecules could be detected in both normoxia and hypoxia indicating a *de novo* synthesis of the molecule (**Figure 85c**). However, for both isotope species, the levels were found to be lower in hypoxia than in normoxia, indicating that the *de novo* synthesis of AMP is less efficient in hypoxic conditions (**Figure 85c**). Accordingly, increased levels of unlabelled AMP (M) were observed in hypoxia compared to normoxia suggesting that in the total pool of AMP, the fraction resulting from the *de novo* pathway is smaller in hypoxia than in normoxia, once again supporting the idea that *de novo* purine biosynthesis is not upregulated in hypoxia as previously hypothesised (**Figure 85c**).

Finally, the carbon incorporation was analysed in GMP isotpologues. As previously observed for IMP (**Figure 85b**), similar levels of M+5 GMP were observed in normoxia and hypoxia and no high mass species (above M+6) were observed (**Figure 85d**). The presence of small fractions of M+1 and M+2 GMP were detected in both normoxia and hypoxia with no significant difference between the two conditions (**Figure 85d**). As such, this isotopologue profile suggests that GMP, like IMP and AMP, does not display an enhanced synthesis via the *de novo* pathway in hypoxia compared to normoxia.

Altogether, this data is in line with the previous results obtained form ^{15}N-glutamine and ^{15}N-serine supplementation, and indicate, that purine monophosphates were not synthesised as a result of an upregulated *de novo* pathway in hypoxia.

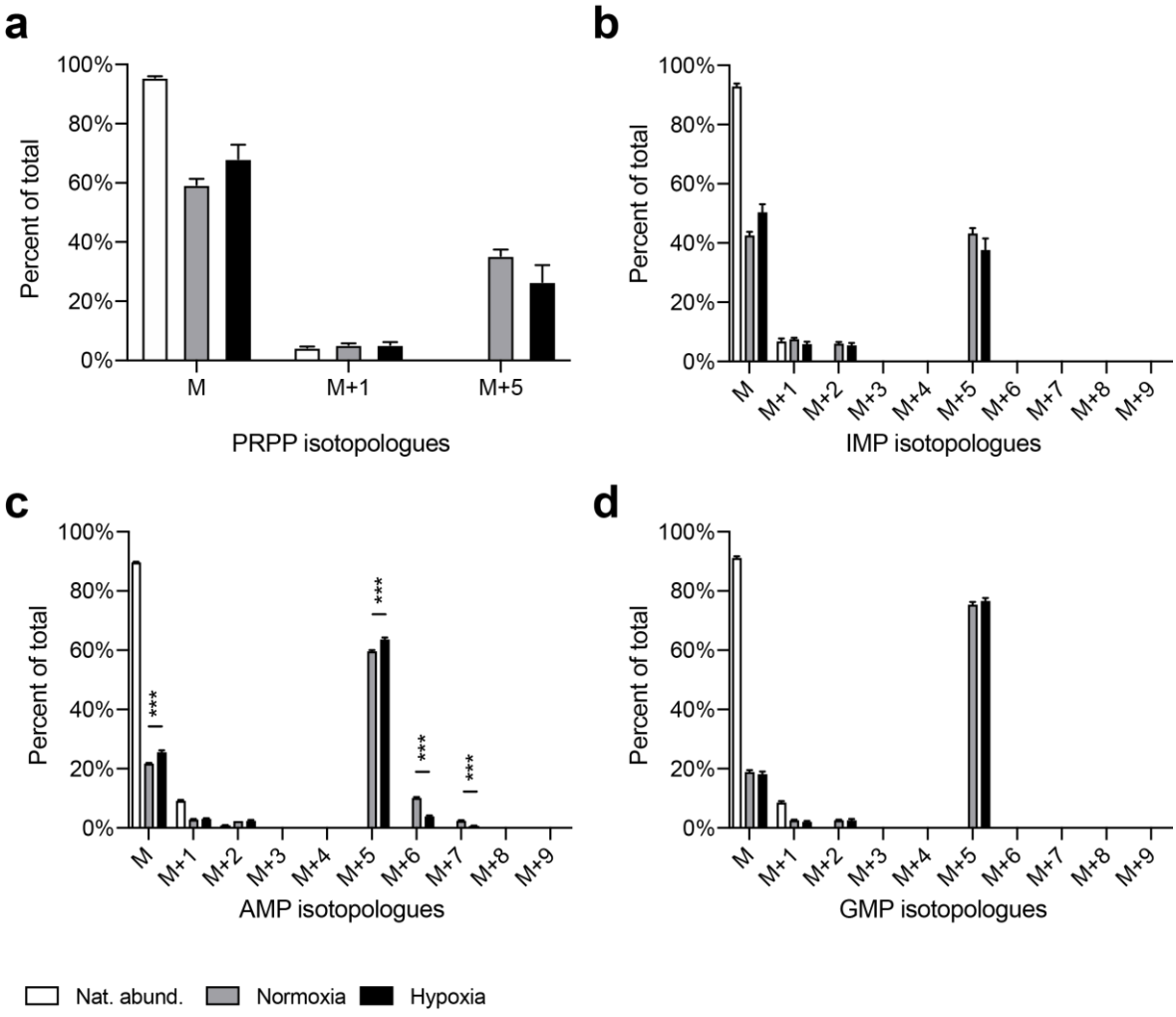

Figure 85. Isotopologue profiles of PRPP and nucleotide monophosphates after labelling with $^{13}C_6$-glucose. HeLa cells were cultured in normoxia or hypoxia (1% oxygen) for 24 h in the presence of $^{13}C_6$-glucose. Isotopologue profiles of **(a)** PRPP, **(b)** IMP, **(c)** AMP and **(d)** GMP revealed that the purine monophosphates did not display an enhanced *de novo* synthesis in hypoxia compared to normoxia as indicated by the absence of high mass species (M+6 and above). Data are means (n=4) ± SEM.

By using three different isotope approaches, no change in the rate of the *de novo* synthesis of purines was observed in hypoxia despite purinosome formation being upregulated in this condition. As such, in order to further understand the effect of hypoxia on the availability of co-factors required for the *de novo* purine synthesis, metabolites from the one-carbon metabolism were analysed following $^{13}C_6$-glucose supplementation. $^{13}C_6$-glucose can be directly traced into the one-carbon metabolism as its catabolism via glycolysis leads to the formation of $^{13}C_3$-

phosphoglycerate ($^{13}C_3$-PG) and subsequent synthesis of $^{13}C_3$-serine, used as substrate in the one-carbon metabolism (**Figure 86**). Conversion of $^{13}C_3$-serine into $^{13}C_2$-glycine will then yield ^{13}C labelled one-carbon-derived molecules.

The one-carbon metabolism which is mostly centred around the folate cycle, is known to occur in two cellular compartments, the cytoplasm and the mitochondria, with every enzyme of the metabolism being present as two isoforms, cytosolic and mitochondrial. This metabolism involves numerous metabolite exchanges between the two compartments, hence the necessity for both cytosolic and mitochondrial isoforms to be present (**Figure 86**). As such, following $^{13}C_6$-glucose supplementation, different metabolites were analysed in regards to their cellular localisation in the one-carbon metabolism in order to further understand how this pathway is affected.

HeLa cells have been shown to use the mitochondrial arm of the one-carbon metabolism over the cytosolic one for the synthesis of one-carbon units.[228] As such, as described in **Figure 86**, serine is transported from the cytoplasm into the mitochondrial matrix where it can be converted into glycine and 5,10-mTHF via the activity of SHMT2. Following this, 5,10-mTHF can be further converted by MTHFD2 into 10-f-THF which is itself used as co-factor in the mitochondrial synthesis of formylmethionine (fMet) or transformed into THF and formate. Formate can subsequently be sent back to the cytoplasm where it gets converted back into cytosolic 10-f-THF, which can then be incorporated into the purine ring during *de novo* purine biosynthesis. It was found that in the case of a malfunctioning mitochondrial folate cycle (i.e deficiency of one of the mitochondrial one-carbon metabolism enzymes), the one-carbon metabolism would then be processed in reverse whereby serine, instead of being transported into the mitochondria, would directly be converted into glycine and 5,10-mTHF via the activity of SHMT1 in the cytoplasm.[228] The resulting 5,10-mTHF can therefore be subsequently be used as co-factor for the synthesis of methionine and dTMP or be converted into 10-f-THF via MTHFD1, with the resulting metabolite then available for incorporation into the purines.

This way, following $^{13}C_6$-glucose supplementation in the cell culture media, carbon labelling can be easily traced into metabolites of the one-carbon metabolism (**Figure 86**). Analyses of carbon incorporation into methionine, dTMP and formylmethionine synthesis would therefore facilitate the understanding of how the one-carbon metabolism works and would allow the identification of any aberrant function.

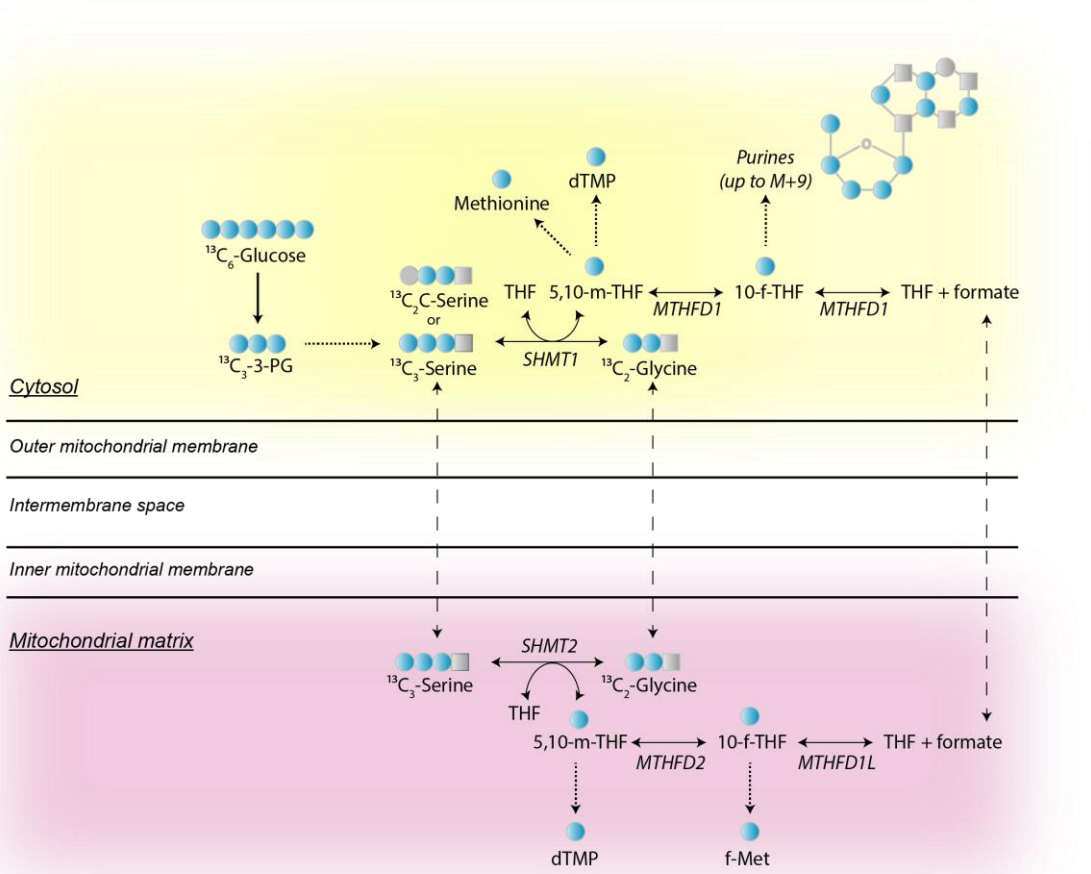

Figure 86. Expected labelling incorporation into the folate cycle and associated metabolites from $^{13}C_6$-glucose. Labelled glucose leads to the formation of $^{13}C_3$-PG which is then converted into $^{13}C_3$-serine, which can subsequently enter the mitochondrial folate cycle when all mitochondrial enzymes are functional. In case of a malfunction of one of the mitochondrial enzymes, the folate cycle occurs in the cytoplasm. Depending on the cellular localisation of the one-carbon metabolism, the carbon labelling can be traced into downstream metabolites such as methionine (cytoplasm), dTMP (cytoplasm and mitochondria) and formylmethionine (fMet, mitochondria).

In order to understand how hypoxia impacted the one-carbon metabolism, the incorporation of labelled carbon from $^{13}C_6$-glucose was traced in a linear fashion from glycolysis to one-carbon-derived metabolites, starting from the glycolytic intermediate 3-PG, first substrate of the *de novo* serine synthesis pathway (SSP). Analysis of the isotopologue profile of 3-PG showed the formation of an M+3 species, both in normoxia and hypoxia (64% and 75%, respectively), suggesting an efficient glycolytic process, slightly increased in hypoxia although no statistical difference was observed (**Figure 87a**). The presence of unlabelled 3-PG (M) was detected in both normoxic and hypoxic conditions, with a slight increase in normoxia compared to hypoxia (34% and 24%,

respectively), consistent with the levels of M+3 observed, and suggesting a slightly enhanced glycolytic rate in a low oxygen environment, in line with previous reports (**Figure 87a**).[102, 229]

As a result of an increased glycolytic rate towards 3-PG in hypoxia, it was then hypothesised that more $^{13}C_3$-serine could be synthesised in low oxygen environments. To probe this, the isotopologue profile of serine was analysed. Although an M+3 serine species was observed in both normoxia and hypoxia, no difference in the levels of the metabolite was observed between the two oxygen conditions (**Figure 87b**). In addition, both M+1 and M+2 serine species were observed in normoxia and hypoxia (**Figure 87b**). As previously described, $^{13}C_3$-serine can be converted into $^{13}C_2$-glycine and ^{13}C-5,10-mTHF. The back conversion of $^{13}C_2$-glycine with unlabelled 5,10-mTHF into serine would enable the formation of $^{13}C_2$-serine. Similarly, in the case of a back conversion of unlabelled glycine and ^{13}C-5,10-mTHF into serine, a ^{13}C-serine isotopologue would be formed.

Here, both ^{13}C-serine (M+1) and $^{13}C_2$-serine (M+2) displayed decreased levels in hypoxia compared to normoxia (**Figure 87**). As such, it can be suggested that these decreases are the result of a decreased back conversion of glycine into serine.

To further probe the origin of this decreased retro-conversion, the isotopologue profile of glycine was analysed. A clear decrease in the hypoxic levels of $^{13}C_2$-glycine (M+2) was observed in hypoxia compared to normoxia, suggesting a decreased conversion of serine into glycine in this condition (6% in normoxia and 4% in hypoxia, **Figure 87c**). Decreased levels of $^{13}C_2$-glycine in hypoxia could be the origin of the decreased levels of ^{13}C-serine and $^{13}C_2$-serine, as less $^{13}C_2$-glycine and by association, less ^{13}C-5,10-mTHF are formed in hypoxia. In line with these observations, decreased levels of labelled species correlated to increased levels of unlabelled serine and glycine in hypoxia (**Figure 87b** and **c**), thus supporting a decreased *de novo* synthesis of serine from $^{13}C_3$-3-PG and a decreased downstream serine to glycine conversion.

It is to note that as a result of ^{15}N-serine supplementation, a small increase was observed in the conversion of ^{15}N-serine into ^{15}N-glycine following 4 h of hypoxic incubation (**Figure 84c**). When using $^{13}C_6$-glucose, after 24 h of incubation in hypoxia the conversion of $^{13}C_3$-serine to $^{13}C_2$-glycine was found to be downregulated, suggesting that longer incubation times in hypoxia alters the serine to glycine conversion and thus reduces the downstream availability of glycine (**Figure 87c**).

In order to further understand how the folate cycle functions in hypoxia, labelled carbon incorporation was determined in metabolites that utilise folate derivatives as co-factors. As an example, cytosolic 5,10-mTHF is used as a precursor for 5-methylTHF (5-mTHF), substrate in the synthesis of methionine. If the decreased $^{13}C_3$-serine to $^{13}C_2$-glycine conversion is due to a decreased activity of the cytosolic enzyme responsible for this conversion (SHMT1) less cytosolic

^{13}C-5,10-mTHF would be produced, which would be reflected by a decreased incorporation of carbon labelling into methionine. As such, isotope incorporation into methionine was analysed. No difference in incorporation was observed between normoxia and hypoxia (5% of total pool), but these levels were also found to be similar to the isotope incorporation resulting from natural abundance, highly suggesting that no ^{13}C-5-mTHF (resulting from ^{13}C-5,10-mTHF) is incorporated into methionine as a result of $^{13}C_6$-glucose supplementation (**Figure 87d**). This result is unsurprising as HeLa cells are known to use the mitochondrial folate cycle rather than the cytosolic one to produce their one-carbon unit.[227] The absence of increased labelled methionine in both normoxia and hypoxia likely reveals that no cytosolic ^{13}C-5,10-mTHF is produced after 24 h of an isotope pulse, indicating that the cytosolic one-carbon metabolism does not run, or runs to a negligible level.

As the cytosolic folate cycle seems to not function or functions at very low rates, it can be hypothesised that the decreased serine to glycine conversion previously observed in hypoxia (**Figure 87c**) is the result of a decreased activity of the mitochondrial enzyme responsible for the conversion, SHMT2.

As such, the labelled carbon incorporation was then traced into deoxythymidine monophosphate (dTMP) which can be synthesised in the cytoplasm and the mitochondria with 5,10-mTHF used as co-factor during the synthesis. Increased levels of M+1 dTMP was observed in both normoxic and hypoxic conditions compared to the natural isotopic abundance, suggesting a significant labelled carbon incorporation following the isotope pulse (**Figure 87e**). No significant difference in ^{13}C-dTMP levels were observed in hypoxia compared to normoxia (11% and 12%, respectively), suggesting that the mitochondrial synthesis of 5,10-mTHF is not affected by low oxygen levels (**Figure 87e**).

Finally, a third metabolite was analysed to determine the fate of labelled carbon through the mitochondrial one-carbon metabolism. Formylmethionine (fMet) works as an acceptor of mitochondrial-derived formate, as its synthesis uses mitochondrial 10-f-THF as a co-factor. Incorporation of labelled carbon into fMet was analysed in normoxia and hypoxia, and M+1 fMet species were detected in both conditions and were found to be at higher levels than natural abundance (5% of total pool), suggesting a significantly increased label incorporation into the metabolite following the isotope pulse (**Figure 87f**). Lower metabolite levels were detected in hypoxia compared to normoxia (16% and 20% of total fMet pool, respectively), suggesting a decreased incorporation of ^{13}C from ^{13}C-10-f-THF in low oxygen environments (**Figure 87f**). As the ^{13}C atom incorporated into fMet can only originate from mitochondrial production of 10-f-THF,

the decreased levels of ^{13}C-fMet (M+1) in hypoxia suggests a decreased ^{13}C-10-f-THF production in the mitochondria, likely as a result of decreased mitochondrial activity of the folate cycle.

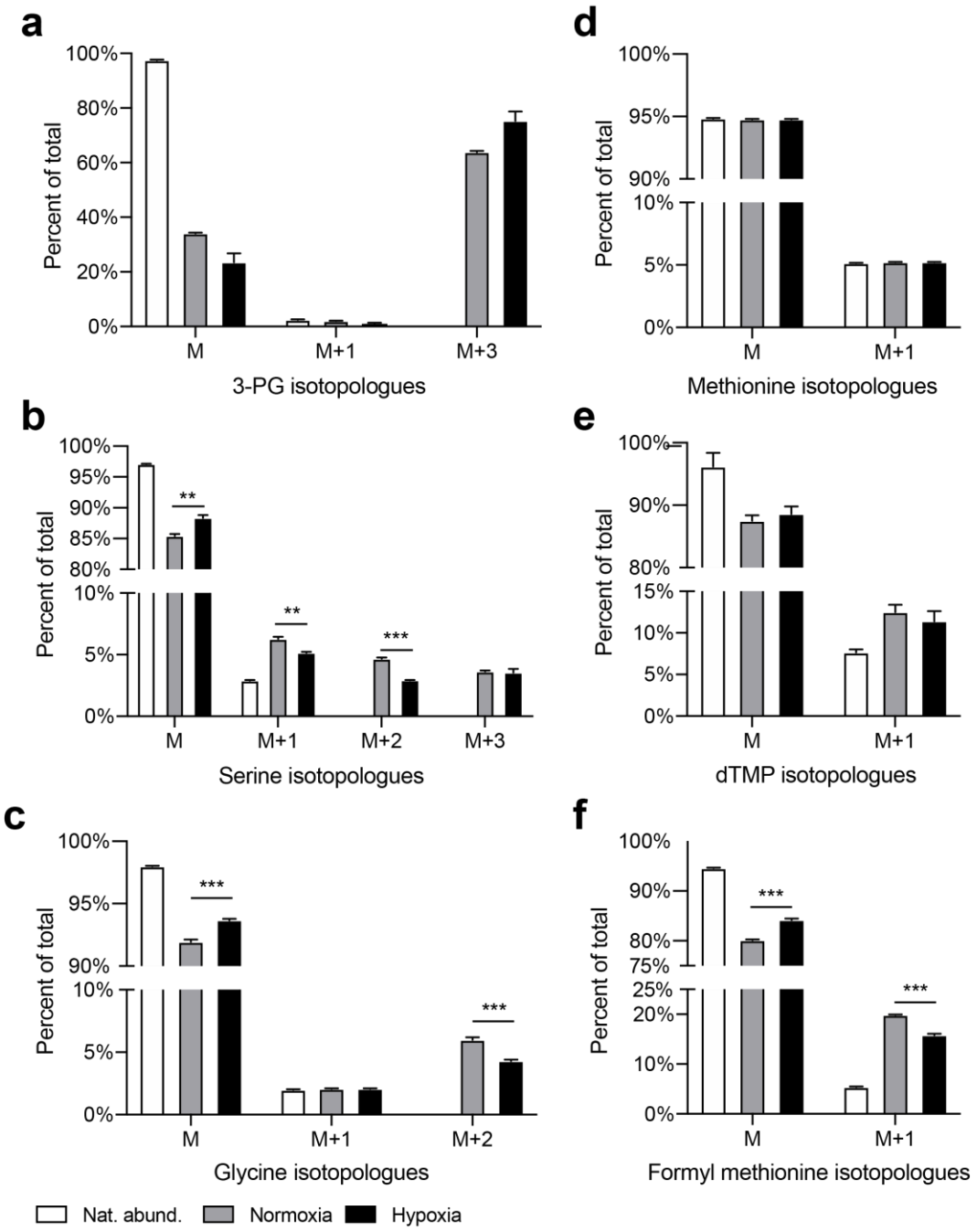

Figure 87. Isotopologue profiles of metabolites from the folate cycle and associated pathways after labelling with $^{13}C_6$-glucose. HeLa cells were cultured in normoxia or hypoxia (1% oxygen) for 24 h in the presence of $^{13}C_6$-glucose. Isotopologue profiles of **(a)** 3-phosphoglycerate (3-PG), **(b)** Serine, **(c)** Glycine, **(d)** Methionine, **(e)** dTMP and **(f)** Formylmethionine were established to determine the impact of hypoxia on the one-carbon metabolism. Data are means (n=4) ± SEM. Significance was determined using unpaired Student t test, ** $p < 0.01$, *** $p < 0.001$.

Altogether, this data suggests that the cytosolic folate cycle does not function in HeLa cells in normoxia, in line with previous reports, and that hypoxia does not induce this cytosolic process, as determined by the absence of label incorporation into methionine (**Figure 87d**).[228] As such, it can be hypothesised that the decreased $^{13}C_3$-serine to $^{13}C_2$-glycine conversion observed is a result of the decreased activity of the mitochondrial enzymes of the folate cycle. Two main enzymes are responsible for the mitochondrial folate cycle activity: SHMT2, which converts mitochondrial serine into glycine and 5,10-mTHF, and MTHFD2 which converts 5,10-mTHF into 10-f-THF. A significant decrease in ^{13}C-fMet was observed in hypoxia compared to normoxia, suggesting a decreased availability of labelled mitochondrial ^{13}C-10-f-THF in this condition (**Figure 87f**), consistent with the decreased serine to glycine conversion. However, it was surprising to see that the ^{13}C incorporation into dTMP was not affected in hypoxic conditions (**Figure 87e**)**.** Indeed, the absence of incorporation into methionine suggests that dTMP can only be synthesised using one-carbon units from the mitochondrial one-carbon metabolism. The decreased ^{13}C incorporation into glycine, supported by a decreased isotope incorporation into fMet, suggested a reduced availability of mitochondrial units which was expected to be reflected as a decrease in ^{13}C-dTMP levels in hypoxia.

Taken together, these results could reflect a decreased activity of SHMT2 and/or MTHFD2 in hypoxic conditions. Further experiments would be required in order to further probe the effect of hypoxia on the enzymatic activity of these two proteins.

In HeLa cells, the production of one-carbon units required for cytosolic synthesis is ensured by the mitochondrial side of the one-carbon metabolism, where transport of serine into the mitochondrial matrix and its downstream conversion into glycine fuels the folate cycle. This ensures the mitochondrial production of formate, itself transported back into the cytoplasm for further conversion into 10-f-THF, subsequently utilised in the *de novo* purine synthesis.[228] According to the data obtained from the $^{13}C_6$-glucose labelling experiment, if, as hypothesised, the mitochondrial activity of the cycle is decreased in hypoxia, then a decreased production of mitochondrial one-carbon unit is to be expected, subsequently resulting in decreased mitochondrial formate synthesis and a downstream decrease in cytosolic 10-f-THF synthesis. As such, a decreased activity of the one-carbon metabolism would ultimately lead to decreased availability of substrates for the *de novo* purine biosynthesis. In addition to an eventual decrease in the availability of cytosolic 10-f-THF, the above-mentioned results indicated a decreased conversion of serine into glycine, thus leading to a decreased availability of cytosolic glycine, required as a co-factor in the second step of the *de novo* purine biosynthesis.

Overall, the data obtained suggest that a hypoxic environment somehow induces a decreased production of one-carbon units via the mitochondrial one-carbon metabolism, ultimately leading to a decreased availability of co-factors required in the *de novo* purine biosynthesis. Further experiments would be required to better understand whether this decreased mitochondrial activity is responsible for the absence of upregulation of the *de novo* purine biosynthetic pathway in hypoxia. Although multiple processes might be responsible for this absence of upregulation of biosynthesis despite purinosome formation, it can be hypothesised that this altered mitochondrial metabolism constitutes one of these causes.

It is interesting to note that in hypoxia, SHMT2 has been reported to be upregulated although only in Myc-amplified cells.[111] It is to note that HeLa cells do not express N-Myc and possess low levels of c-Myc expression, suggesting that this cell line does not upregulate SHMT2 in hypoxia. As such, it can be hypothesised that in Myc-amplified cells such as the neuroblastoma KELLY cells (N-Myc amplified), the upregulation of SHMT2 would enable the downstream synthesis of the one-carbon-derived co-factors required for the *de novo* purine biosynthesis (i.e glycine and 10-f-THF), although this hypothesis would need to be further examined experimentally.[230-232]

As a summary, the use of isotope-labelled metabolites in cell culture media and the subsequent tracing of isotope incorporation into the resulting metabolites shed some light on the effect of hypoxia on purine metabolism. The use of ^{15}N-glutamine and ^{15}N-serine showed that purine nucleotide monophosphates are mostly synthesised via the salvage pathway in both normoxia and hypoxia in HeLa cells cultured in the presence of purines for 24 h (**Figure 84** and **Figure 83**). As a control, the same analysis was carried out in normoxic cells cultured in the absence of purines (purine-depleted, normoxia P-) and an increased *de novo* purine biosynthesis was observed, as previously reported (**Figure 83** and **Figure 84**).[169] Furthermore, the use of $^{13}C_6$-glucose confirmed that the *de novo* pathway was not upregulated in hypoxia (**Figure 85**). In addition, this last experiment revealed that the one-carbon metabolism was slightly downregulated in hypoxia, as indicated by the decreased serine to glycine conversion (**Figure 87c**). It was found that after 24 h of incubation, the cytosolic branch of the one-carbon metabolism was not active in HeLa cells in normoxia (consistent with previous reports), nor in hypoxia, and that the mitochondrial branch was downregulated in hypoxic conditions, as suggested by the decreased isotope incorporation into fMet (**Figure 87f**).

Chapter 3 Conclusions

For the first time, the formation of the multi-enzyme purinosome complex has been described in hypoxic cancer cells. The use of plasmid DNA encoding enzymes of the purinosome tagged with fluorescent proteins enabled the transient expression of these fluorescent proteins and their subsequent detection and analysis using confocal microscopy. In normoxic conditions, the majority of the cells displayed an homogenous fluorescent pattern suggesting an evenly distributed protein throughout the cytoplasm. However, when placed in hypoxic conditions, the number of cells displaying clusters increased by more than 2-fold, indicating an enhanced purinosome formation in this condition. The use of two independent purinosome enzymes tagged with two different fluorescent enzymes (mCherry and GFP) enabled the simultaneous co-expression of the two proteins within the same cell. Confocal microscopy enabled the characterisation of the colocalisation of these two proteins and showed that in hypoxic HeLa cells, the two proteins were located together within the purinosome complex.

Although the use of transiently expressed fluorescently-tagged purinosome enzymes showed a 2-fold increase in hypoxic cancer cells, it should be noted that unlabelled endogenous purinosome enzymes were present in the cytoplasm, thus able to join the purinosome complex. As such, it was hypothesised that following transient transfection, not all purinosome complexes could be detected. To challenge this, another approach was used. Instead of determining purinosome formation using one fluorescent enzyme, the colocalisation between two purinosome proteins was assessed using proximity ligation assay. This technique enabled the determination that the colocalisation between purinosome proteins was enhanced in hypoxic HeLa cells and that up to 88% of the cells were displaying purinosomes, whereas only 10% of the normoxic cells were.

Following this, the molecular determinants underlying the hypoxic purinosome formation were analysed. The role of HIF-1α was investigated in this process, and the formation of the hypoxic purinosome was found to be HIF-1 mediated as a knockout of the transcription factor in hypoxic conditions completely prevented the hypoxia-induced formation of the complex. The time-dependent formation of the purinosome complexes was analysed during hypoxic incubation and was found to correlate with HIF-1α protein levels. In addition, when the formation of the purinosome was analysed in a cell line which expresses HIF-2 but not HIF-1, no increase was observed in purinosome formation upon hypoxic incubation, suggesting that HIF-1 but not HIF-2 is involved in the complexation of the enzymes of the *de novo* purine biosynthesis.

The molecular processes involved in the hypoxic formation of the purinosome were probed and three members of the Heat Shock Protein (HSP) family, Hsp90, Hsp70-1 and Hsp70-2 were found

to colocalise with the purinosome complex in hypoxia. These were found to be required for its formation as a knockout of any of these three chaperones using siRNA prevented the hypoxic purinosome formation. Hsp70-2 was found to be of particular interest in the hypoxic purinosome formation as its gene transcription and protein expression were found to be upregulated in hypoxia in a HIF-dependent manner. In addition, Hsp70-2 was found to display an enhanced colocalisation with the purinosome in hypoxia compared to purine-depleted conditions, suggesting a preferential interaction of the chaperone with the complex in low oxygen environments. However, although Hsp70-2 is upregulated in hypoxia and seemed to be preferentially involved in the hypoxic purinosome complex compared to that observed in purine-depleted conditions, it was found that the upregulation of Hsp70-2 on its own is not sufficient to induce purinosome formation, suggesting that the hypoxic purinosome formation relies on a different mechanism.

The purinosome was firstly characterised in purine-depleted conditions and its formation was found to correlate with an increased rate of the *de novo* purine biosynthesis.[164, 169] From the hypothesis that the hypoxic purinosome might ensure the same cellular function, it was thought that in the context of a protein macro-complex forming to fulfil metabolic requirements, any impact or alterations of the cell metabolism would impact upon purinosome formation. As such, various metabolic stimuli were applied on hypoxic HeLa cells in order to determine how these were altering the formation of the purinosome complex. It was found that the inhibition of a glycolytic enzyme, a PPP enzyme or a stimulation of the salvage pathway prevented purinosome formation. In hypoxia, metabolic pathways upstream of the *de novo* purine biosynthesis such as glycolysis and the PPP have been shown to be upregulated in various cell types. These pathways are crucial to ensure the functioning of the *de novo* purine biosynthesis as they provide substrates and co-factors required at different steps of the pathway. Here, it was shown that inhibition of these hypoxia-induced pathways resulted in a prevention of the hypoxic purinosome formation.

To further probe the link between the purinosome and enzymes from associated pathways, a pull-down assay was carried out in hypoxic and normoxic cells using one of the purinosome enzymes, PFAS, as bait. As a result of this pull-down, many proteins belonging to pathways related to the *de novo* purine biosynthesis (i.e glycolysis, PPP and one-carbon metabolism) were detected in the list of prey proteins, with most of them being either increased or exclusively present in hypoxia. The results from this pull-down analysis were further supported by assessing the colocalisation between some of the proteins detected preferentially in the hypoxic sample and one purinosome enzyme using a proximity ligation assay. Most of the protein combinations tested confirmed the results previously obtained by pull-down, suggesting an enhanced interaction between the purinosome proteins and enzymes from glycolysis, PPP and the one-carbon metabolism in hypoxic

conditions. Although further experiments would be required to confirm and understand the role of such colocalisation between enzymes of different pathways, it can be hypothesised that the close proximity between enzymes that belong to pathways that exchange substrates and co-factors is a strategy used by the cells to facilitate the metabolite flux between pathways.

In 2016, the purinosome complex was found be located near the mitochondria, which was thought occur in order to facilitate the exchange of metabolites between the two entities, including ATP and one-carbon units generated by the mitochondrial one-carbon metabolism.[187] As such, the close proximity between the hypoxic purinosomes and the mitochondria was assessed and this colocalisation was also confirmed to occur in hypoxia, suggesting another common feature between hypoxic purinosomes and purinosomes in purine-depleted conditions.

Finally, the ultimate aim of this project was to determine whether the observed purinosome clusters were, like their purine-depleted counterparts, correlating with an increased rate of the *de novo* purine biosynthesis. Three different isotope labelling approaches, involving nitrogen and carbon labelling coupled to metabolomic analyses, were used in order to determine the isotope incorporation into the purine nucleotides. The methods used were validated using purine-depleted conditions as a positive control, conditions in which the *de novo* synthesis of purines was found to be upregulated.[169] However, despite the approach enabling the detection of upregulated *de novo* purine synthesis in purine-depleted conditions, no increase in the rate of the pathway was observed in hypoxic conditions, suggesting that HeLa cells synthesise their purines using the salvage pathway in low oxygen environments. This finding was extremely surprising as the presence of purinosomes in hypoxic cells was expected to correlate with an increased rate of the pathway. As a result, further investigations were carried out and the isotopologue profiles of different metabolites were analysed. The *de novo* purine biosynthesis is known to utilise various co-factors from diverse pathways, among which two are produced in the one-carbon metabolism (i.e glycine and 10-f-THF). As such, other metabolites that also use one-carbon units as co-factors in their synthesis were analysed in order to determine whether the one-carbon metabolism was affected in hypoxia. The initial use of $^{13}C_6$-glucose enabled the tracing of carbon incorporation directly into serine, glycine and downstream one-carbon units. As a result, no activity of the cytosolic one-carbon metabolism was detected, as indicated by the lack of isotope incorporation into the cytoplasmically synthesised methionine. In addition, a decreased activity of the mitochondrial branch of the one-carbon metabolism was observed, as suggested by the decreased isotope incorporation into the mitochondrial formylmethionine.

In physiological conditions, HeLa cells rely on the mitochondrial branch of the one-carbon metabolism to produce their one-carbon units,[228] and the last finding of this work indicates a

decreased activity of the mitochondrial one-carbon metabolism in HeLa cells after 24 h of hypoxic incubation, thus suggesting a decreased production of the co-factors required for the *de novo* purine biosynthesis. Whether this decreased co-factor production is one of the causes of the absence of *de novo* purine synthesis upregulation is yet to be determined.

In conclusion, the initial aims of the project were met. The enhanced formation of the purinosome complex was described and characterised in cancer cells maintained in hypoxic conditions. This process was found to be mediated by HIF-1, requires the presence of Hsp proteins and is responsive to metabolic stimuli, thus suggesting the existence of a link between the formation of the complex and the metabolism of hypoxic cells. Although the presence of purinosomes in hypoxic HeLa cells was expected to correlate with an increased rate of *de novo* purine biosynthesis, it was determined that instead, HeLa cells synthesise their purines using the salvage pathway, at least during the first 24 h of hypoxic incubation. The observed effect of hypoxia on the one-carbon metabolism of HeLa cells raised the hypothesis that purinosome formation and purine synthesis might occur independently in HeLa cells, raising the possibility of a new, yet undiscovered secondary role for the purinosome complex. In addition, it can be hypothesised that the pathway utilised to synthesise purines in hypoxia is cell type dependent, suggesting that a broader study in multiple cell lines could potentially reveal a different outcome regarding purine synthesis. Finally, it can be hypothesised that in hypoxic HeLa cells, purinosome formation occurs in the first hours of incubation in hypoxia by a yet unknown mechanism and that the upregulation of the *de novo* purine biosynthesis does not occur simultaneously to complex formation but is triggered later. To probe this last hypothesis, longer study times could be envisaged. Overall, all these suggestions open new avenues of investigation which would lead to a better understanding of the function of the purinosome complex in HeLa cells and the effect of hypoxia on purine synthesis in other cancer types.

Chapter 4 Further work

This study described for the first time the formation of the purinosome complex in the pathological context of hypoxic cancer cells. Although it has been shown that in HeLa cells, the purinosomes do not function by upregulating the *de novo* purine biosynthesis after 24 h in hypoxia, it can be thought that the complexes fulfil another yet unknown function. In addition, it can be hypothesised that, although purinosome formation occurs during the early phase of the hypoxia response, the *de novo* purine biosynthesis might require longer incubation times to be upregulated. As such, it would be of interest to analyse both purinosome formation and purine synthesis in HeLa cells maintained in hypoxia for longer incubation times.

Regardless of the function of the purinosome complex, the cause at the origin of their formation remains to be determined. It was found that the formation of the hypoxic purinosome was mediated by HIF-1 and not HIF-2, but the exact mechanism behind this formation is yet unknown. A recent study revealed the presence of multiple post-translational modifications (PTMs) within the purinosome enzymes in cells cultured under purine-depleted conditions, and these PTM patterns were found to be different from cells cultured under purine-rich conditions.[233] As a result, it has been hypothesised that theses PTMs play a significant role in regulating the enzymes activity and in altering their ability to cluster into a purinosome complex. It could be hypothesised that such PTMs would also occur on the purinosome enzymes in hypoxic conditions, ultimately regulating the purinosome formation and / or enzyme activity. As such, screening for the presence of various PTMs on enzymes of the *de novo* purine biosynthesis in hypoxic conditions could provide a mechanistic explanation for the clustering of these enzymes. In addition, it can be thought that hypoxia-induced PTMs could occur and result in a lack of enzymatic activity, explaining the observed low rate of the *de novo* pathway in HeLa cells.

The variety of techniques used as well as the numerous controls carried out provided strong evidence that the clusters observed in this study were purinosomes. In addition, the robustness of the metabolomic experiment confirmed that the *de novo* biosynthesis of purines is not upregulated in HeLa cells cultured in hypoxia for 4 to 24 h. In addition to investigating longer incubation times in HeLa cells, another approach can be utilised. Over the last years, multiple cancer cell lines have been reported to upregulate the one-carbon metabolism in hypoxic conditions. As an example, a report showed that breast cancer cells upregulate the gene expression of the enzymes of the *de novo* serine biosynthesis (SSP) and enzymes from the mitochondrial one-carbon metabolism in a HIF-dependent manner. The authors found that the metabolism of glucose was reprogrammed further away from the PPP towards the SSP, and that

this adaptation was playing a major role in maintaining the redox homeostasis of cancer cells, especially via the production of NADPH.[98] In addition, another study reported that in hypoxia, cancer cells that were MYC-amplified were upregulating the expression of the mitochondrial enzyme responsible for the serine to glycine conversion, SHMT2, and that this upregulation was mediated by HIF-1.[111] It is interesting to see that hypoxia can upregulate the one-carbon metabolism in some cancer cell types but not all, as these observations made in myc-amplified cells and breast cancer cells, are in contrast with the results obtained in this study in HeLa cells. Although very little is known about the adaptation of the one-carbon metabolism in hypoxic HeLa cells it has been reported that HeLa cells display a decreased expression of myc (c-myc) when cultured in severe hypoxia (0.1%) for 24 h.[234] In addition, a separate study showed that upon glucose deprivation, glutamine deprivation or serine deprivation, HeLa cells induce the upregulation of c-myc which results in the upregulation of enzymes from the SSP and the one-carbon metabolism.[235] As such, as myc has been shown to drive the upregulation of genes encoding enzymes of the one-carbon metabolism, it can be thought that the hypoxia-induced downregulation of myc in HeLa cells is involved in the observed downregulation of their mitochondrial one-carbon metabolism.

Further investigations would be required to probe this hypothesis. First, myc could be transiently expressed into HeLa cells and the impact on purine synthesis (and purinosome formation) analysed as a result of this upregulation. It can be hypothesised that “rescuing” myc in HeLa cells could be sufficient to restore the metabolic flux through the one-carbon metabolism and therefore enable the synthesis of the co-factors required for *de novo* purine biosynthesis. Metabolomic analysis would assess whether the mitochondrial one-carbon metabolism is restored upon myc overexpression and if so, does this allow to induce the *de novo* purine synthesis? If the answer to this second hypothesis is no, then the absence of an upregulation of *the novo* pathway in HeLa cells likely originates from a different issue than the downregulation of the mitochondrial one-carbon metabolism.

In parallel, further work could involve probing purinosome formation and downstream *de novo* purine biosynthesis in cell lines that have previously been used to display an upregulated SSP and one-carbon metabolism in hypoxic conditions (e.g N-MYC amplified KELLY cells or MDA-MB-231, with the latter known to display an increased purinosome formation in hypoxia, as described in this work).[98, 111] This way, it can be thought that the upregulation of these pathways will likely provide enough co-factors (i.e glycine and 10-f-THF) for the *de novo* purine biosynthesis to function. From these experiments, if the results suggest that the purinosome complexes form in these cells but do not synthesise purines then this might indicate either a new unknown function

of the purinosome complex in hypoxia or that the absence of *de novo* upregulation has another origin than the downregulated one-carbon metabolism.

By completing these experiments, one could obtain further information about the cellular processes underlying purine biosynthesis in hypoxic cancer cells and gain further understanding of how various cancer cell types adapt their biosynthetic purine pathways in hypoxic conditions. Such understanding would enable the development of therapeutic strategies aiming at decreasing the synthesis of nucleotides, especially the purines, to specifically target hypoxic cancer cells.

Chapter 5 Experimental

5.1 Equipment

5.1.1 Cell culture and cell imaging

All mammalian cells were maintained in a HeraCell 150I incubator (Fisher Scientific, UK). Experiments in hypoxia were carried out in a H35 Hypoxystation (Don Whitley Scientific). Centrifugations of mammalian cell cultures were carried out in a Heraeus Biofuge Primo Centrifuge (ThermoScientific).

Fluorescence microscopy was carried out using a Zeiss Axio Vert.A1 microscope fitted with a HXP 120V light box as well as 10X, 20X and 40X phase contrast objectives (Carl Zeiss Microscopy). Three Zeiss fluorescence filter sets were used (excitation/emission) : Filter set 02 (365/420), Filter set 46 (500/535) and filter set 31 (565/620). Image acquisition was done using ZEN software (Carl Zeiss Microscopy). Confocal microscopy was carried out on a Leica SP8 Inverted scanning confocal microscope fitted with a Nikon plan apochromat 63x oil-immersion objective. Live recording was carried out using a Deltavision Elite live imaging system.

5.1.2 Molecular Biology and Assay Development

All media and glassware were sterilised using a Touchclave-R autoclave (LTE Scientific Ltd., UK). A pH meter was used to measure the pH of buffers.

Bacterial cell cultures were incubated in a Thermo Scientific MaxQ 600 (Thermo Scientific, UK) shaking incubator. Agar plates were incubated in a Thermo Scientific Heratherm incubator (Thermo Scientific, UK). Room temperature or refrigerated centrifugation below 2,500 g was carried out in a Heraeus Biofuge Primo R centrifuge (Thermo Scientific, UK). Centrifugation of samples in microcentrifuge tubes was carried out in an accuSpin Micro17 centrifuge (Fisher Scientific). DNA purification was carried out using GeneJET miniprep and GeneJet Maxiprep (Thermo Scientific, UK). DNA, RNA and protein concentrations were measured using a NanoDrop ND-1000 Spectrophotometer (NanoDrop Technologies, USA).

All SDS-PAGE electrophoresis and western blot transfers onto membranes were carried out in a Mini-PROTEAN Tetra Cell set up using a BioRad Power Pac Basic (BioRad Laboratories Ltd., UK). Gels and membranes were imaged using a ChemiDoc Imaging system linked to Image Lab 4.0 software (BioRad Laboratories Ltd., UK). RT-qPCR were run on a CFX Connect Real Time PCR

System linked to a CFX Connect Software (BioRad Laboratories Ltd., UK). Absorbance in 96-well plates were measured using a ClarioStar plate reader (BMG Labtech, UK).

5.2 Materials

5.2.1 Chemicals

All chemicals were purchased from Fisher Scientific (UK) and Sigma-Aldrich, unless otherwise stated. RNA purification and reverse transcription reagents were purchased from Promega (UK). Western blotting reagents were purchased from GE Healthcare and BioRad Laboratories Ltd. (UK). Mammalian cell culture reagents were purchased from Life Technologies (UK). All solvents used were HPLC grade and purchased from Fisher Scientific (UK).

Deferoxamine (DFX, D9533), 2-deoxyglucose (2-DG, D6134), 6-aminonicotinamide (6-AN, A68203) and hypoxanthine (H9636) were purchased from Sigma-Aldrich.

5.2.2 Plasmids

hFGAMS-GFP, hFGAMS-mCherry, hADSL-GFP, G3BP-GFP, pC1-Neo-hPFAS-2xStrep, psiRNA-G6PD and psiRNA-G6PD-sc constructs were generously provided as gifts from Prof. Stephen Benkovic (Penn State University, Pennsylvania, USA). pcDNA5/FRT/TO HSPA2 (Addgene plasmid #19485) and pcDNA5/FRT/TO GFP HSPA2 (Addgene plasmid #19458) were gifts from Harm Kampinga.

5.2.3 siRNA

Small interfering RNA (siRNA) targeting HIF-1α (S6539), Hsp90 (121532), Hsp70 isoform 1 (145248), Hsp70 isoform 2 (145384) and Negative Control (4390846) were purchased from ThermoFisher Scientific (UK).

5.2.4 Antibodies

Table 2. List of antibodies

Target protein	Supplier	Reference
Antibody Anti-β-actin HRP-conjugated	Sigma-Aldrich	A3854-200UL
Antibody Anti-ADSL	Novus Biologicals	NBP2-03107
Antibody Anti-APRT	Novus Biologicals	NBP1-89519

Antibody Anti-ATIC	Novus Biologicals	NBP2-01941
Antibody Anti-FGAMS	Novus Biologicals	NBP1-84691
Antibody Anti-G6PD	Novus Biologicals	NBP1-89804
Antibody Anti-GART	Novus Biologicals	H00002618-M01
Antibody Anti-Glut1	Santa Cruz Biotechnology	Sc-377228
Antibody Anti-HIF-1α	Novus Biologicals	NB100-449
Antibody Anti-HPRT	Novus Biologicals	NBP1-33527
Antibody Anti-HspA1	Novus Biologicals	NBP2-46806
Antibody Anti-HspA2	Novus Biologicals	NBP1-86185
Antibody Anti-Hsp90	Abcam	Ab13492
Antibody Anti-MTHFD1	Santa Cruz Biotechnology	sc-271412
Antibody Anti-Mouse HRP-conjugated	Thermo Fisher Scientific	35502
Antibody Anti-Mouse Alexa 488-conjugated	Thermo Fisher Scientific	A11001
Antibody Anti-PAICS	Novus Biologicals	NBP2-02817
Antibody Anti-PFKL (rabbit)	Novus Biologicals	NBP1-85934
Antibody Anti-PFKL (mouse)	Santa Cruz Biotechnology	Sc-393713
Antibody Anti-PFKP	Novus Biologicals	H00005214-B01P
Antibody Anti-PGD	Novus Biologicals	NBP1-31589
Antibody Anti-PPAT	Novus Biologicals	NBP2-02056
Antibody Anti-PRPS1	Novus Biologicals	NBP1-31654
Antibody Anti-Rabbit HRP-conjugated	Cell Signalling	7074P2
Antibody Anti-Rabbit Alexa 568-conjugated	Thermo Fisher Scientific	A11011
Antibody Anti-StrepTagII	Abcam	Ab76949
Antibody Anti-TOMM20	Abcam	Ab56783

5.2.5 Gene expression assay probes

Table 3. List of qPCR probes

Target gene	Supplier	Reference
TaqMan Gene expression 18S	Thermo Fisher Scientific	Hs99999901_s1
TaqMan Gene expression Beta actin	Thermo Fisher Scientific	Hs99999903_m1
TaqMan Gene expression HIF-1α	Thermo Fisher Scientific	Hs00153153_m1
TaqMan Gene expression Hsp90	Thermo Fisher Scientific	Hs00743767_sH
TaqMan Gene expression ADSL	Thermo Fisher Scientific	Hs01075808_m1
TaqMan Gene Expression APRT	Thermo Fisher Scientific	Hs00356991_m1
TaqMan Gene expression ATIC	Thermo Fisher Scientific	Hs00269671_m1
TaqMan Gene expression FGAMS (PURL)	Thermo Fisher Scientific	Hs00389822_m1
TaqMan Gene expression GART	Thermo Fisher Scientific	Hs00894582_m1
TaqMan gene Expression HPRT	Thermo Fisher Scientific	Hs02800695_m1
TaqMan Gene expression HspA1	Thermo Fisher Scientific	Hs00359163_s1
TaqMan Gene expression HspA2	Thermo Fisher Scientific	Hs00745797_s1
TaqMan Gene expression PAICS	Thermo Fisher Scientific	Hs00935017_gH
TaqMan Gene expression PPAT	Thermo Fisher Scientific	Hs00601264_m1
TaqMan Gene expression VEGF	Thermo Fisher Scientific	Hs00900055_m1

All qPCR reagents and probes were purchased from ThermoFisher Scientific; TaqMan Universal Master Mix (4369016).

5.3 Preparation of materials and buffers

5.3.1 Lysogeny Broth (LB)

LB powder (2.5 g) was added to deionised water (100 mL) and autoclaved at 115 °C for 20 minutes using the liquid media cycle. Media was allowed to cool down at room temperature before use.

5.3.2 LB Agar Plates

LB Agar powder (10 g) was dissolved in deionised water (250 mL) and autoclaved at 115 °C for 20 minutes using the liquid media cycle. Media was then allowed to cool down to 50 °C before addition of required antibiotics at the following concentrations: kanamycin (50 µg/mL) and carbenicillin (100 µg/mL). The media / antibiotic mixture was slowly swirled to prevent formation of bubbles and subsequently poured into sterile petri dishes (25 mL/dish). Once the gel was set, plates were dried at 37 °C for 30 minutes before use.

5.3.3 SOC Super Optimal broth with Catabolite repression

SOC media was prepared by combining 500 µL of 20% (w/v) glucose solution, 500 µL of 1 M $MgCl_2$, 500 µL of 2 M $MgSO_4$ and 48.5 mL of freshly autoclaved LB. All solutions were previously prepared with autoclaved deionised water. SOC media was then filtered through a 0.22 µm sterile filter (Millipore, UK) and stored at 4 °C.

5.3.4 Antibiotics

Antibiotic stock solutions were prepared using autoclaved deionised water to a final concentration of 100 mg/mL. The solutions were filtered through a 0.22 µm sterile filter (Millipore, UK) and stored at 4 °C until needed.

5.3.5 TBF I Buffer

TBF I buffer solution was made up by mixing the components in **Table 4**.

Table 4. Composition of TBF I buffer

Component	Final concentration	Quantity
Potassium acetate	30 mM	0.59 g
Rubidium chloride	100 mM	2.42 g
Calcium chloride	10 mM	0.29 g
Manganese chloride	50 mM	2.00 g
Glycerol	15% (v/v)	30 mL

The pH of the solution was adjusted to 5.8 with 1% acetic acid and made up to 200 mL using autoclaved deionised water. The solution was filtered through a 0.22 µm sterile filter and stored at -80 °C.

5.3.6 TBF II Buffer

TBF II Buffer solution was made up by mixing the components in **Table 5**.

Table 5. Composition of TBF II buffer

Component	Final concentration	Quantity
3-(N-morpholino) propansulfonic acid (MOPS)	10 mM	0.21 g
Rubidium chloride	10 mM	0.12 g
Calcium chloride	75 mM	1.10 g
Glycerol	15% (v/v)	15 mL

The solution was adjusted to pH 6.5 with 5 M NaOH and made up to 100 mL with autoclaved deionised water. The solution was then filtered through a 0.22 µm sterile filter and stored at -80 °C.

5.3.7 Making Chemical Competent Cells

A small amount of frozen stock of cells was added to 10 mL of LB broth and incubated at 37 °C overnight with shaking. From this, a 1% subculture was made in LB broth (250 µL of culture into

25 mL of LB broth) and this was incubated at 37 °C with shaking until OD_{600} reached 0.5-0.7. The culture was then centrifuged at 2,000 g for 15 minutes at 4 °C. The supernatant was discarded and the cell pellet was resuspended in 5 mL of TBF I buffer (see section **5.3.5** - **Table 4**). The centrifugation was repeated and supernatant discarded, followed by the resuspension of the cell pellet in 1 mL of TBF II buffer (see section **5.3.6** – **Table 5**). This solution was divided into 100 µL aliquots in PCR tubes on dry ice and stored at -80 °C until needed.

5.3.8 Agarose Gels

1 % agarose gels were made by adding 1 g of agarose powder to 100 mL of Tris-acetate-EDTA (TAE) (1X) buffer and subsequent heating in microwave until powder was dissolved. The mixture was allowed to cool down to room temperature for 2 minutes and 15-20 µL of ethidium bromide was added to the solution (0.625 mg/mL). Solution was homogenised by gentle swirling and subsequently poured into a gel cast and left to set for 30 to 60 minutes at room temperature.

5.3.9 SDS-PAGE Gel preparation

Resolving gels were prepared by mixing all components as indicated in **Table 6**. The solution was mixed ammonium persulfate was added followed by TEMED. Gel solution was mixed and poured between the two glass slides maintained by the gel cast. 200 µL of isopropanol was subsequently added on top to keep the gel meniscus flat. Resolving gel was let to set. Isopropanol was then removed and resolving gel was rinsed with plenty of water. All components for the stacking gel were mixed, finishing with ammonium persulfate and TEMED as before (**Table 7**). Stacking gel was then poured on top of resolving gel and a 10-well comb was placed between the two slides. Gel was let to set up at room temperature.

Table 6. Composition of SDS-PAGE Resolving gels

Component	Quantity per 8% SDS	Quantity per 10% SDS	Quantity per 12% SDS
Tris-Base 1.5 M pH 8.8	1.875 mL	1.875 mL	1.875 mL
Acrylamide / Bisacrylamide (40% / 0.8%) (w/v)	1.5 mL	1.875 mL	2.25 mL
SDS 10% Solution	75 µL	75 µL	75 µL
TEMED	5 µL	5 µL	5 µL
Ammonium Persulfate	37.5 µL	37.5 µL	37.5 µL
dH_2O	4 mL	3.65 mL	3.25 mL

Table 7. Composition of SDS-PAGE Stacking Gel

Component	Quantity per gel
Tris-Base 1.5 M pH 6.8	0.625 mL
Acrylamide / Bisacrylamide (40% / 0.8%) (w/v)	315 µL
SDS 10% Solution	25 µL
TEMED	2.5 µL
Ammonium Persulfate	12.5 µL
dH_2O	1.55 mL

5.3.10 SDS-PAGE Loading buffer (2X) or Laemmli Buffer

Before being loaded onto SDS-PAGE Gel, protein samples were mixed in a 1:1 volume ratio to a 2X SDS-PAGE loading buffer (**Table 8**). Samples were subsequently heated up for 5 min at 95 °C and stored at 4 °C until needed.

Table 8. Composition of SDS Loading Buffer (2X)

Component	Final Concentration	Quantity for 50 mL
Tris-HCl (pH 6.8)	100 mM	788 mg
SDS (sol. 20%)	4%	10 mL
Glycerol	20%	10 mL
Bromophenol blue	1 mg/mL	50 mg
Make up to 50 mL with deionised water		

Just before use, 200 mM of DTT from a previously prepared 1 mM DTT stock solution stored at -20 °C was added.

5.3.11 SDS-PAGE Running buffer (5X)

SDS-PAGE Running Buffer was made up as a 5X stock solution in deionised water as indicated in **Table 9**. When needed, stock solution was diluted down to 1X buffer using deionised water.

Table 9. Composition of SDS-PAGE Running Buffer (5X)

Component	Final concentration	Quantity
Tris base	125 mM	15.1 g
Glycine	1.25 M	94 g
20% SDS	0.5%	25 mL
Make up to 1 L with deionised water		

5.3.12 Staining and Destaining Solutions for SDS-PAGE Gel

SDS-PAGE was stained using destaining solution (see **Table 10**) supplemented with Coomassie Blue G250 (75 mg/L). Once stained with Coomassie Staining Solution, SDS-PAGE gel was destained in order to be able to detect the protein bands. Gel was washed 3 x 60 min in 100 mL of destaining solution. Destaining solution was changed before each wash.

Table 10. Composition of destaining solution for SDS-PAGE Gel

Component	**Final concentration**
Acetic Acid	10% (v/v)
Ethanol	40% (v/v)
Deionised water	50% (v/v)

5.3.13 Western Immunoblotting Buffers

Buffers for western immunoblotting were made up fresh each time on the day of experiment and stored at -80 °C for a few hours until needed. Depending on the membrane used to transfer the proteins, the composition of the buffer was different. See **Table 11** for nitrocellulose membrane and **Table 12** for PVDF membrane.

Table 11. Composition of transfer buffer for western immunoblotting on nitrocellulose membrane

Component	**Final Concentration**	**Quantity**
Glycine	40 mM	2.93 g
Tris-Base 1.5 M pH 8.3	48 mM	32 mL
Methanol	20%	200 mL
Make up to 1 L with deionised water		

Table 12. Composition of transfer buffer for western immunoblotting on PVDF membrane

Component	**Final Concentration**	**Quantity**
Glycine	196 mM	14.4 g
Tris-Base 1.5 M pH 8.3	25 mM	16.7 mL
Methanol	10%	100 mL
Make up to 1 L with deionised water		

5.3.14 Pull-Down Assay Lysis Buffer

Lysis buffer for pull-down assay was prepared on the day of experiment (see **Table 13**) and kept at 4 °C until needed.

Table 13. Composition of lysis buffer for pull-down assay.

Component	Final concentration	Quantity for 1 mL of buffer
10 X protease inhibitor	1 X	100 µL
10 X phosphatase inhibitor	1 X	100 µL
Sodium Phosphate dibasic 500 mM pH 8.0	50 mM	100 µL
Sodium Chloride 3 M	300 mM	100 µL
Glycerol	5% (v/v)	50 µL
Triton-X100	1% (v/v)	10 µL
Deionised water		540 µL

5.4 General Biology Procedure

5.4.1 Plasmid Transformation into Chemically Competent Cells

5 µL of plasmid vector was added to 100 µL aliquot of chemically competent cells (see **section 5.3.7**) and left to incubate on ice for 30 minutes. The cells were then heat shocked by incubating them at 42 °C in a water bath for 30 seconds. Following this, the cells were cooled down on ice and 895 µL of SOC broth (see **section 5.3.3**) was added. The mixture was incubated at 37 °C for an hour with shaking. 100 µL of the culture was then spread over an LB agar plate containing the appropriate antibiotics. The plate was incubated overnight at 37 °C.

5.4.2 Plasmid purification

Following plasmid transformation into cells and LB agar plate incubation (see **section 5.4.1**), colonies on the plate were picked and grown overnight at 37 °C with shaking in 10 mL of LB broth supplemented with appropriate antibiotics.

For a small scale purification, the mixture was then centrifuged for 15 minutes at 2,000 g at 4 °C. The supernatant was discarded and pellet was used to purify the plasmid using a Thermo Scientific GeneJET Plasmid Miniprep kit (ThermoFisher Scientific) following manufacturer's protocol.

For a large scale purification, 250 µL of the overnight culture was used for subculture in 250 mL of fresh LB supplemented with the appropriate antibiotics (1/1000). Bacterial culture was grown overnight at 37 °C. The culture was then centrifuged for 45 minutes at 2,000 g at 4 °C. The supernatant was discarded and pellet was used to purify the plasmid using a ThermoFisher Scientific GeneJET Plasmid Maxiprep kit following manufacturer's protocol.

5.4.3 Running SDS-PAGE Gel

Protein samples were made up by mixing protein extract to SDS-PAGE loading buffer (see **section 5.3.10** - **Table 8**) in a 1:1 ratio and samples were boiled at 95 °C for 5 minutes. SDS-PAGE gel, made as described in **section 5.3.9** were placed in a Mini PROTEAN tetra cell tank (BioRad) and immersed in 1X SDS-PAGE running buffer (see **section 5.3.11** - **Table 9**). The protein samples were then loaded into the wells of the gel along with a size marker (EZ-run Prestained Rec Protein Ladder, Fisher Scientific, UK). The gel was run by applying 180 V for 45 to 55 minutes, until the bromophenol blue migration front reached the bottom of the gel.

5.4.4 SDS-PAGE Staining, Destaining and Visualisation

Following the migration, the gel was placed in a box containing 100 mL of staining solution (see **section 5.3.12**). The box was placed on a rocker for 10 minutes and the gel was then transferred in a box containing 100 mL of destaining solution (see **section 5.3.12** - **Table 10**). The gel was washed on a rocker for 3 x 60 minutes. Destaining solution was replaced with fresh one before each washing.

5.5 Mammalian Cell Culture Procedures

5.5.1 Maintenance of Mammalian Cells

Human Cervical Adenocarcinoma cells (HeLa), were purchased from American Type Culture Collection (ATCC). HeLa ATIC knockout cell line (ATIC KO) was a gift from Dr M. Zikanova and Dr. V Baresova (Charles University and General University Hospital, Prague, Czech Republic).

All cell lines, HeLa, MDA-MB-231 (human breast adenocarcinoma cells) and 786-O (human renal cell adenocarcinoma) were cultured in Dulbecco's Modified Eagle's Medium (DMEM, 319066-021, Life Technologies) supplemented with 10% foetal bovine serum (10082-147, Life Technologies). ATIC KO HeLa cells were cultured in DMEM supplemented with 10% FBS, 1% (v/v) Pen/Strep and 0.03 mM adenine. Cells were kept in a humidified atmosphere 5% CO_2 incubator at 37 °C. Experiments in hypoxic conditions were carried out in a Whitley H35 Hypoxystation (Don Whitley Scientific) in which cells were cultured in humidified atmosphere, 1% O_2, 5% CO_2 and 94% nitrogen at 37 °C.

5.5.2 Mammalian cells passaging

The following volumes are used for cell passaging in a 75 cm^2 flask.

Cell passaging was carried out by removing the growth media from the flask, washing the cells with 5 mL of DBPS once and subsequently incubating the cells with 4 mL of 0.05% trypsin-EDTA in cell culture incubator until all cells had detached. The trypsin was then diluted by adding 6 mL of warm growth media and the cell suspension was transferred into a 15 mL conical tube. Cells were centrifuged for 3 minutes at 400 g. Supernatant was discarded and cell pellet was resuspended in 10 mL of growth media. 11 mL of fresh growth media was added to a new flask followed by 1 mL of the cell suspension, leading to a final 12 mL of cells in culture medium. If a higher confluency was required, a larger volume of cell suspension could be added.

5.5.3 Preparation of mammalian cell stock for cryo-preservation

Culture media was removed from the flask and cells were washed once with DPBS. 4 mL of 0.05% trypsin-EDTA were added per 75 cm^2 flask and cells were incubated until fully detached. 6 mL of growth media was then added to the flask in order to dilute the trypsin and the cell suspension was subsequently transferred to a 15 mL conical tube. Cells were centrifuged for 3 minutes at 400 g. Supernatant was discarded and pellet was resuspended in 10 mL of growth media. The number of cells was counted using a Moxi cell counter and cells were then centrifuged as before. The cell pellet was then resuspended in freezing media (50% FBS, 40% DMEM and 10% DMSO) so as to get the appropriate concentration of cells was transferred to cryo-vials (typically 1.10^6 cells/mL). 1 mL of cell suspension was transferred to each cryo-vial. All cryo-vials were then placed into an isopropanol box which was stored at -80 °C to ensure a progressive freeing of the cells. On next day, cells were transferred into liquid nitrogen for long term storage.

5.5.4 Thawing a frozen stock of mammalian cells

The cryo-vial containing the cells was thawed quickly in a 37 °C water bath. The cells were added to 8 mL of warm growth media previously placed into a 15 mL conical tube. 1 mL of growth media was used to rinse the cryo-vial and subsequently added to the cell suspension, which was then centrifuged for 3 minutes at 400 g. Supernatant was discarded and pellet was resuspended in 12 mL of warm growth media, all of which was then transferred into a new 75 cm^2 flask.

5.5.5 Transient transfection of plasmids

One day before transfection, the cells were plated in 35 mm Petri dishes (Corning) at a confluency of 1.5 to 3.0 x 10^5 cells per plate. One day prior to measurements, cells were transiently transfected with one plasmid or two plasmids. Cells were transfected using Lipofectamine 2000 (Invitrogen) in Opti-MEM-I reduced serum media (Invitrogen) following manufacturer's protocol.

All transfections were carried out with 5 µL of Lipofectamine 2000 and 1 µg of each used plasmid DNA per reaction in a final 1.5 mL volume.

After 5h of incubation with the Lipofectamine-DNA, cells were washed with Dulbecco's Phosphate Buffer Saline (DPBS) and media was replaced with growth media. Cells were incubated in normoxia or hypoxia for the required amount of time.

5.5.6 Transient transfection of siRNA

One day before transfection, the cells were plated in 35 mm Petri dishes (Corning) at a confluency of 1.5 x 10^5 cells per plate. One day prior to measurements, cells were transiently transfected with one plasmid or two plasmids. Cells were transfected using Lipofectamine RNAiMax (Invitrogen) in Opti-MEM-I reduced serum media (Invitrogen) following manufacturer's protocol.

All transfections were carried out with 5 µL of Lipofectamine RNAiMax and 5 nM final of siRNA per reaction in a final 2 mL volume.

After 5h of incubation with the Lipofectamine-siRNA complexes, cells were washed with Dulbecco's Phosphate Buffer Saline (DPBS) and media was replaced with growth media.

5.5.7 Transient co-transfection of plasmid and siRNA

One day before transfection, the cells were plated in 35 mm Petri dishes (Corning) at a confluency of 1.5 to 3.0 x 10^5 cells per plate. One day prior to measurements, cells were transiently

transfected with one plasmid or two plasmids. Cells were transfected using Lipofectamine 2000 (Invitrogen) in Opti-MEM-I reduced serum media (Invitrogen) following manufacturer's protocol.

All transfections were carried out with 5 µL of Lipofectamine 2000, 1 µg of each used plasmid DNA and 5 nM of siRNA per reaction in a final 2 mL volume.

After 5 h of incubation with the Lipofectamine-DNA-siRNA complexes, cells were washed with Dulbecco's Phosphate Buffer Saline (DPBS) and media was replaced with growth media.

5.5.8 Treatment with deferoxamine (DFX)

Media containing DFX was prepared on the day of treatment by diluting 100X stock solution of 10 mM DFX in water into growth media.

Growth media was removed from the cells that had been previously plated in tissue culture dishes. Cells were washed with DBPS once and warm media containing DFX at 100 µM was added to the cells. Cells were placed back into incubator for the required amount of time.

5.5.9 Treatment with 2-deoxyglucose (2-DG)

Media containing 2-DG was prepared on the day of treatment by dissolving 2-deoxyglucose powder into growth media to a final 5 mM solution (12.18 mg of powder into 10 mL of media).

Growth media was removed from the cells that had been previously plated in tissue culture dishes. Cells were washed with DBPS once and warm media containing 2-deoxyglucose at 5 mM was added to the cells. Cells were placed back into incubator or hypoxia station for 6 h.

5.5.10 Treatment with 6-aminonicotinamide (6-AN)

Media containing 6-AN was prepared on the day of treatment by dissolving 6-aminonicotinamide powder (6.3 mg) into 2 mL of water. This solution was placed into a heat block at 70 °C and was regularly vortexed until the powder was fully dissolved. The 2 mL solution was subsequently added to 44 mL of growth media, leading to a 46 mL media solution supplemented with 1 mM of 6-AN.

Growth media was removed from the cells that had been previously plated in tissue culture dishes. Cells were washed with DBPS once and warm media containing 6-aminonicotinamide at 1 mM was added to the cells. Cells were placed back into incubator or hypoxia station for 6 h.

5.5.11 Treatment with Compound 14 (Cpd14)

In this work, Cpd14 was provided by Dr Nagarajan Elumalai (Tavassoli Group, University of Southampton, UK).

Media containing Cpd14 was prepared on the day of treatment by preparing a stock solution of Cpd14 at 50 mM into 100% DMSO (3.1 mg of Cpd14 into 133 µL of DMSO). Stock solution of Cpd14 was then diluted 200X into growth media leading to a 250 µM Cpd14, 0.5% DMSO supplemented media.

Growth media was removed from the cells that had been previously plated in tissue culture dishes. Cells were washed with DBPS once and warm media containing Cpd14 at 250 µM was added to the cells. Cells were placed back into incubator or hypoxia station for 24 h.

5.5.12 Treatment with hypoxanthine

Media containing hypoxanthine was prepared on the day of treatment by dissolving hypoxanthine powder into growth media so as to get a final 60 µM hypoxanthine (4.08 mg of hypoxanthine into 50 mL of growth media).

Growth media was removed from the cells that had been previously plated in tissue culture dishes. Cells were washed with DBPS once and warm media containing hypoxanthine at 60 µM was added to the cells. Cells were placed into hypoxia station for 24 h.

5.5.13 Synchronisation of HeLa cells

Following plasmid transfection, the media was removed and the cells were washed once with 1X DPBS. Fresh warm growth media supplemented with 0.5 mM of dibutyryl-cAMP (DB-cAMP) was added to the cells which were subsequently placed in normoxia and hypoxia for a further 16 h of incubation.

5.5.14 Purinosome-positive cell counting

Cells had previously been transfected with a plasmid encoding for FGAMS-GFP, FGAMS-mCherry or ADSL-GFP and were subsequently treated as required. Following appropriate incubation and treatment time, growth media was removed. Cells were rinsed twice with HBSS media and 1 mL of HBSS was then added to the dish for live imaging. Once placed on the microscope platform, the dish would not be touched or moved until the counting of this condition was done to avoid observing the same cell twice. The platform was placed so as to make the cells in the top left

corner of the dish visible in the eyepieces. Two manual counter were used for the counting, each paced in one hand, the left one counting purinosome negative cells and the right one the purinosome-positive cells. Once the first cells were detected, the platform was moved from left to right until the end of the dish. Then, the platform was moved towards the cells below the last one observed until the last observed cells left the observed area. From this point, the platform was moved from right to left until the end of the dish, and so on, until the appropriate number of cells was counted. Each condition or treatment was observed at least in triplicate.

5.5.15 Cell fixing on slides

To carry out confocal fluorescence microscopy, cells were prepared as described above despite the fact that they were cultured on a glass coverslip 22 x 22 mm placed in a 35 mm dish. Cells were treated similarly to the live cells but were fixed on the coverslip. Briefly, cells grown on the coverslips were washed twice with PBS and then fixed for 20 minutes at room temperature using freshly made 4% w/v paraformaldehyde in PBS. Cells were washed twice with PBS and the coverslip was mounted on a glass slide using DAPI-containing mounting medium.

5.5.16 Proximity Ligation assay

All PLA experiments were performed in 8-well chamber slides (C1782, Nunc Lab-Tek, Sigma-Aldrich). 2 x 10^4 HeLa cells were plated per well to a final volume of 300 µL in DMEM supplemented with 10% FBS. Slides were incubated in normoxia or hypoxia for 24 h.

When analysis was carried out in purine-depleted conditions, HeLa cells were maintained in purine depleted media for one week prior experiment and plated at 2.10^4 cells / well in purine depleted media (RPMI + 5% dFBS)

Following incubation, media was removed from wells and cells were washed twice with 200 µL PBS. Washing steps were performed gently and slides were tapped off to remove any excess of buffer. Cells were then fixed with 100 µL of 4% paraformaldehyde in PBS, RT for 10 minutes. Following fixation, cells were washed once with PBS. Cells were then permeabilised using 200 µL of 0.5% Triton-X100 in PBS, RT, 10 minutes. Permeabilising solution was then removed gently, cells were washed with PBS once and one drop of Duolink Blocking Solution was added per well. Slides were incubated RT for 1 h. Blocking solution was tapped off from the slides and cells were incubated overnight at 4 °C with 40 µL final volume of a mixture of one or two primary antibodies diluted as indicated in **Table 14**. A negative control with only one primary antibody and a technical control with no antibody were included on each slide. In order to provide humidity, slides were placed on a wet tissue and covered with a box during incubation at 4 °C.

All following incubation steps at 37 °C were done using a wet tissue under a box to provide humidity as described above. All treatments were conducted using a final 40 µL of solution per well. All washing steps were made in 70 mL of corresponding washing buffer in a box on an orbital shaker. Washing buffers were used fresh each time. All treatments and washing were tapped off the slides between each step.

On next day, primary antibodies solutions were tapped off the slides and chambers were removed. Slides were washed in 1X Wash Buffer A for 2 x 5 minutes. PLA probes (Anti-Mouse MINUS and Anti-Rabbit PLUS) were diluted 1:5 in Antibody Diluent. PLA probe solution was added to each sample and slides were incubated at 37 °C for 1 h. The slides were washed 2 x 5 minutes in fresh 1X Wash Buffer A. Ligation solution was made by diluting ligation stock 1:5 and ligase 1:40 (1 µL final per sample) in the same solution of sterile dH_2O. Ligation solution was added to sampled and incubated for 30 minutes at 37 °C. Slides were washed for 2 x 2 minutes with 1X Wash Buffer A.

Amplification-Polymerase solution was prepared by diluting amplification stock 1:5 and polymerase 1:80 (0.5 µL final per sample) in sterile dH_2O. Amplification-Polymerase was added to each sample and incubated at 37 °C for 100 minutes. Slides were washed 2 x 10 minutes in 1X Wash Buffer B and 1 minute in 0.01X Wash Buffer B consecutively. The slides were then left to dry at RT and once dried, were mounted with Duolink In Situ Mounting Medium with DAPI ensuring no air bubbles got caught under the coverslip. Nail polish was used to seal the edges of the coverslips and slides were observed on Leica SP8 Inverted scanning confocal microscope. DAPI was imaged using a 405 nm UV laser and PMT detection and Duolink red dye was imaged using a 561 nm solid-state laser line and HyD detection 580-670 nm.

Table 14. Dilutions of primary antibodies for PLA and immunofluorescence

Target protein	Antibody dilution
ADSL	1:100
FGAMS	1:12.5
G6PD	1:100
GART	1:25
GLUT1	1:50
HIF-1α	1:100
MTHFD1	1:50
PFKL	1:50
PFKP (Mouse)	1:125
PGD	1:100
PPAT	1:100
PRPS1	1:100
TOMM20	1:100

5.5.17 Immunofluorescence

HeLa cells were plated at a confluency of 2.10^4 cells per well in 8-well slides (C1782, Nunc Lab-Tek, Sigma-Aldrich). Cells were let to settle for 16 h and were subsequently placed in normoxia or hypoxia for 24 h. Following this, cells were washed three times with 200 µL of cold PBS and subsequently fixed using 150 µL of 4% paraformaldehyde in water. Cells were let to incubate for 10 minutes at room temperature or in the Hypoxystation. After fixing, cells were washed three times with 200 µL of cold PBS and permeabilised with 150 µL of 0.5% TX-100 in PBS added to each well. Cells were incubated in permeabilisation solution for 10 minutes at room temperature (or in Hypoxystation). Following permeabilisation, cells were rinsed once with 200 µL of PBS and 150 µL of Blocking buffer (see **Table 15**) was added to each well. Cells were incubated in blocking solution for 1 h at room temperature. After blocking, 50 µL of primary antibody solution at appropriate dilution (see **Table 14**) was added to each well and cells were incubated at 4 °C for 16 h in a

humidified chamber. Following this, chambers were removed from the slide and cells were washed 3 x 5 minutes in PBS on rocker. 50 µl of secondary antibody solution in 0.2% BSA/PBST was added per well with the antibodies diluted appropriately (Anti-Mouse Alexa 488-conjugated diluted 1:1000 and Anti-Rabbit Alexa 568-conjugated diluted 1:2000). Secondary antibody solution was incubated for 1 h at room temperature in the dark. Cells on the slide were then washed 3 x 5 minutes on rocker in PBS. Coverslip was mounted on slides with DAPI-containing mounting medium. Edges of the coverslip were sealed with nail polish and slides were stored at -20 °C.

Table 15. Composition of Immunofluorescence Blocking Buffer

Component	**Quantity**
BSA	1% w/v
Glycine	22.52 mg / mL
In PBST (PBS + 0.1% Tween-20)	

5.5.18 Mitochondria staining using MitoTracker

Following appropriate treatment and incubation, the media was removed from the dish containing the HeLa cells grown on coverslips. Cells were washed with PBS once and fresh warm media containing MitoTracker Deep Red (M22426, ThermoFisher Scientific) at 1 µM was added to the cells. Cells were incubated at 37 °C with MitoTracker for 30 minutes. Following incubation, media was discarded, cells were washed three times with PBS and were subsequently fixed for 10 minutes at room temperature (or in hypoxia station for hypoxic cells) using a solution of 4% PFA in PBS. After incubation, fixing solution was removed, cells were washed three times with PBS and coverslips were left to dry in the dark prior mounting onto glass slides (see **section 5.5.15**).

Mitotracker was imaged as described in **section 5.5.21**, using excitation laser at 633 nm and HyD detection from 645 to 700 nm.

5.5.19 Live Cell Imaging

Prior to imaging, cells were washed twice with Hank's Balanced Salt Solution (HBSS) (ThermoFisher Scientific).

All live samples were imaged at room temperature (approximately 25 °C) in HBSS using a 40× objective using a Axio Vert. A1 Inverted microscope (Carl Zeiss Microscopy) and a HXP-120V light

source (Carl Zeiss Microscopy). A Fs46 set (exc. 500/20 nm ; em. 535/30 nm), a Fs31 filter set (exc. 565/30 nm ; em. 620/60 nm) and a Fs02 filter set (exc. 365 nm; em. 420 nm) were used to accomplish the detection of GFP, mCherry and DAPI respectively. Image acquisition was carried out using ZEN software (Zeiss).

5.5.20 Live cell recording – time lapse acquisition

HeLa cells were plated in a glass-bottom tissue culture dish (P35G-1.5-14-C, MatTak Corporation), and were transfected with FGAMS-mCherry 16 h prior experiment. On the day of experiment, cell media was changed for phenol red-free DMEM supplemented with 10% FBS. The dish was observed on a Deltavision Elite live imaging system equipped with a 37 °C incubator. HeLa cells were observed using a mCherry filter set. A gas bottle containing a hypoxic gas mixture (1% oxygen, 5% CO_2, 94% nitrogen, BOC) was equipped with a gas regulator (BOC), a gas flowmeter set up at 20 mL/min and gas tubing in order to inject a hypoxic environment directly into the cell dish as displayed in **Figure 27**. Recording was carried out for 4 h and a picture of the cell interest was taken every 15 minutes.

5.5.21 Confocal Fluorescent Microscopy

Fixed cells were imaged with a Nikon plan apochromat 63× oil-immersion objective on a Leica SP8 Inverted scanning confocal microscope. GFP was imaged using the 488 nm argon laser line and PMT detection 518-550 nm (green). mCherry was imaged using a 561 nm solid-state laser line and PMT detection 570-700 nm. Each acquisition was averaged at least four times to get rid of background signals. Z-stacking was performed with 15 steps through the cell volume. DAPI was imaged using a 405 nm UV laser and PMT detection.

5.5.22 Super-Resolution Radial Fluctuations (SRRF)

SRRF imaging of mitochondria and purinosomes was performed using a Nikon plan apochromat 63× oil-immersion objective on a Leica SP8 Inverted scanning confocal microscope. HeLa cells grown on glass coverslips were transfected with plasmid encoding FGAMS-GFP and subsequently incubated in hypoxia as previously described (see **section 5.5.5**). Mitochondria was stained as described in **section 5.5.18** and cells were subsequently fixed and coverslip mounted on glass slides. GFP was imaged using the 488 nm argon laser line and PMT detection 518-550 nm (green). MitoTracker Deep red was imaged using the 633 nm argon laser line and HyD detection 645-700 nm. 100 frames were acquired over time in the shortest possible time (less than 2 minutes per

channel) and the resulting pictures were then processed using NanoJ SRRF plugin on ImageJ (FIJI) software.

5.5.23 Extraction and purification of RNA from mammalian cells

The cells used for RNA extraction and RT-qPCR analyses were transfected as described in **section 5.5.5** with some modifications. 4.0 x 10^5 cells were plated in 60 mm dishes. Cells were transfected with Negative Control siRNA and HIF-1α siRNA using Lipofectamine RNAiMAX (Invitrogen) in Opti-MEM-I, following manufacturer's protocol. After 5h of incubation with the Lipofectamine - siRNA complexes, cells were washed with PBS and media was replaced with growth media. Cells were incubated in normoxia or hypoxia for 24 h.

Total mRNA was extracted from cells using Reliaprep RNA miniprep kit (Promega, UK). Briefly, cells were harvested using Trypsin-EDTA 0.05% subsequently diluted with growth media. Cells were collected and the solution was centrifuged at 400 g for 4 minutes. Supernatants were discarded and pellets were washed twice with PBS. Pellets were then lysed in 100 µL of BL + TG buffer each. Lysates were treated following manufacturer's protocol. RNA was quantified using Nanodrop ND-1000 spectrophotometer. RNA was used fresh for reverse transcription or stored at -80 °C until needed.

5.5.24 Reverse transcription of RNA into cDNA

100 ng to 1 µg of RNA was used as template to synthesize the complementary cDNA using GoScript Reverse Transcription kit (Promega, UK) and thermo cycler PCR machine (CFX-Connect real-time system, BioRad).

Table 16. **Protocol for reverse transcription of RNA into cDNA**

Step	**Temperature**	**Time**
Annealing	25 °C	5 min
Extension	42 °C	60 min
Reverse Transcriptase activation by Heating	70 °C	15 min

Following reverse transcription, cDNA was adjusted to a concentration of 100 ng/µL in nuclease free water (Promega, UK). cDNA was then either stored at -20 °C or directly used as template for qPCR.

5.5.25 Quantitative Polymerase Chain Reaction (RT-qPCR)

qPCR was performed using TaqMan Universal Master Mix (ThermoFisher Scientific) and TaqMan gene expression probes (see **section 5.2.5**). 100 ng of cDNA was used as template in each well. In order to ensure the specificity of each gene expression probe, qPCR reactions with no cDNA template referred as No Template Control (NTC) were carried out for each probe. Technical triplicates were made for each sample (including reference genes and NTC samples) following the volumes indicated in **Table 17**.

Table 17. **Composition of a qPCR reaction**

Component	**Volume per well (µL)**
Nuclease free water	8
2X TaqMan master mix	10
20X TaqMan gene expression Assay	1
cDNA at 100 ng/µL	1

Expression values for each gene were expressed as ΔΔCt. To avoid any bias in the results, the expression of each studied gene was normalised to the average of two reference genes, 18S and β-actin. All expression values were normalised to normoxic gene expression.

5.5.26 Protein extraction from mammalian cells

HeLa cells were lysed by scraping them with radioimmunoprecipitation assay (RIPA) (9806, Cell signalling Technologies) buffer (50 mM Tris pH 7.4, 150 µM NaCl, 1 mM EDTA, 1% (v/v) Triton X-100) supplemented with 1X cOmplete™ protease inhibitor cocktail (Roche). Cell lysates were sonicated 10 x 30/30 sec in an ice water bath and then centrifuged at 10,000 g for 20 minutes at 4 °C. Supernatants were transferred to a microcentrifuge tube and the protein concentrations were measured using a Bradford assay or BCA test (see section **5.5.27**). Samples were mixed 1:1 with SDS loading dye and boiled at 95 °C for 5 minutes. Samples were placed at 4 °C until required.

5.5.27 Protein quantification

Protein concentrations in supernatants were quantified by Bradford assay or using BCA kit (ref, Thermofisher) following manufacturer's instructions.

5.5.28 Western blot analysis

Samples were loaded onto an SDS-PAGE gel (5 to 50 μg per lane depending on studied protein) in order to separate the proteins that were subsequently transferred to PVDF membrane (IPVH00010, Merck Millipore,) or nitrocellulose membrane (10600002, GE Healthcare). To transfer the proteins to nitrocellulose membrane, the membrane, sponges and filter papers were soaked in ice-cold transfer buffer (**Table 11**) for 5 minutes and the apparatus was subsequently mounted with the SDS-PAGE gel. For blotting on PVDF membrane, the sponges and filter papers were soaked in ice-cold transfer buffer (**Table 12**) along with the SDS-PAGE gel and were left to equilibrate for 15 minutes. The PVDF membrane was placed in methanol for 10-20 seconds and subsequently rinsed in deionised water for 2 minutes. The membrane was then placed in ice-cold transfer buffer for 5 minutes and the apparatus was subsequently mounted.

The transfer was carried out at 250 mA for 120 minutes. Membranes were subsequently blocked by incubating them in PBS 0.1% Tween-20 supplemented with 5% powdered milk with gentle agitation on rocker for one hour. The membranes were then incubated with primary antibodies overnight at 4 °C. Antibodies were diluted at appropriate dilutions in 5% milk in PBS 0.1% Tween-20. Prior to incubating with secondary antibodies, membranes were washed three times using PBS 0.1% Tween-20 (washing buffer). Secondary HRP-conjugated anti-rabbit and anti-mouse antibodies were diluted in 5% milk in PBS 0.1% Tween-20 at 1:20 000 and 1:100 000 dilutions, respectively. To ensure a proper loading of the gel, β-actin was used as internal control; HRP-conjugated anti-β-actin antibody was diluted (1: 50 000) in 5% milk in PBS 0.1% Tween-20. Membranes were incubated with HRP-conjugated antibodies for an hour at room temperature. Band visualisation was carried out using Amersham ECL reagent (GE Healthcare, RPN2235) for the proteins of interest or Clarity Western ECL substrate (BioRad, 170-5060) for β-actin. Imaging was then processed using a ChemiDoc Imaging system linked to Image Lab 4.0 software (BioRad).

Optimal conditions including primary antibody dilution and membrane for each protein studied are summarised in **Table 18**.

Table 18. Optimal conditions for western immunoblotting for each target protein.

Target protein	Membrane	Primary Antibody dilution
ADSL	Nitrocellulose	1:500
APRT	Nitrocellulose	1:250
ATIC	Nitrocellulose	1:500
FGAMS	Nitrocellulose	1:1000
GART	Nitrocellulose	1:500
HIF-1α	Nitrocellulose	1:500
HPRT	Nitrocellulose	1:1000
Hsp70-1	Nitrocellulose	1:250
Hsp70-2	Nitrocellulose	1:500
Hsp90	Nitrocellulose	1:1000
PAICS	Nitrocellulose	1:1000
PPAT	Nitrocellulose	1:500
StrepTagII	PVDF	1:1000

5.5.29 Pull-Down Assay

HeLa cells were plated at a confluency of 4 x 10^5 cells per 35 mm dish or 2 x 10^6 cells per 100 mm dish in growth media. On next day, media was removed, cells were washed once with DPBS and subsequently transfected as follow: 24 µg of pCI-neo-StrepTagII constructs were transfected into cells plated in 100 mm dishes using Lipofectamine 2000 in a 1:2.5 ratio, as previously described in **section 5.5.5.** When using cells in 35 mm dishes, 4 µg of plasmid DNA were transfected. Transfection was left to incubate for 5 hours after which the media was exchanged for growth media. Mammalian expression of the StrepTagII fused proteins was let to proceed for 24 h in normoxia. Cells were subsequently placed in normoxia or hypoxia for an additional 24 h, allowing a total expression time of 48h. On the day of the assay, the culture media was removed and cells

were washed with 10 mL of DPBS once. Hypoxic samples were kept in the hypoxia for the entire lysis process. Lysis buffer (see **Table 13**) was added to the dishes which were placed on ice for 30 minutes (200 µL of lysis buffer per 35 mm dish and 1.75 mL of lysis buffer per 100 mm dish). Cell lysates were collected into 1.5 mL or 2 mL microcentrifuge tubes and let on ice for a further 15 minutes to ensure that lysing was complete. Lysates were then centrifuged at 10,000 g for 20 minutes at 4 °C. Supernatant were transferred into fresh microcentrifuge tubes and pellets were discarded.

While lysates were being centrifuged, the magnetic beads were equilibrated following manufacturer's protocol (MagStrep "type 3" XT beads, Iba). 20 µL of beads suspension which corresponds to 1 µL of pure magnetic beads are used for 200 µL of lysate. As such, for each 200 µL lysate, 20 µL of beads suspension was placed into a magnetic separator (Iba) and supernatant was discarded. 200 µL of 1X buffer W (Iba) was added to the beads and the tube was subsequently placed into the magnetic separator. Supernatant was discarded and beads were ready to use.

200 µL of lysate was added to 1 µL of previously washed magnetic beads and the suspension was left to incubate on ice for 30 minutes with a quick vortexing step every 10 minutes. Following incubation, tube was placed into magnetic separator and supernatant was discarded. 100 µL of 1X buffer W was added to the beads in order to wash them. Tube was placed in magnetic separator and supernatant was discarded. This washing process was repeated two more times.

Finally, proteins were eluted from the beads in denaturing conditions by addition of 25 µL of SDS-loading dye (see **Table 8**) per µL of beads. Sample was heated at 95 °C for 5 minutes to ensure full elution and denaturation of proteins. Tube was placed in magnetic separator, SDS-loading dye-containing protein was transferred to a new microcentrifuge tube and kept at 4 °C until required for further electrophoresis.

5.5.30 Proteomics analysis

In order to analyse the proteins caught as prey in the pull down experiment, the pull down samples were prepared as presented in **section 5.5.29** until the last washing step (prior elution and denaturation). Following this last washing step, the washing buffer was removed and the beads were resuspended in 30 µL of a solution of 50 mM ammonium bicarbonate in water. Samples were subsequently submitted to the Centre for Proteomic Research (University of Southampton) for mass spectrometry analysis.

5.5.31 Sample preparation for metabolomics analysis in HeLa cells

Sample preparation protocol was based on previously reported experiment with some modifications.[169] 5 x 10^5 HeLa cells were plated in 100 mm dishes and incubated in normoxia for 24 h. On the next day, cells were washed with PBS and 10 mL of warm growth media was added to each plate. Cells were further incubated for 24 h in normoxia or hypoxia. Following incubation, metabolites were extracted from cells and media as described in the following **section 5.5.35**.

5.5.32 Sample preparation for metabolomics analysis in cells cultured with isotope: $^{13}C_6$-Glucose

Growth media for isotope incorporation was prepared as follow on day of experiment: glucose-free and glutamine-free DMEM (A14430, Life Technologies, UK) was supplemented with 25 mM $^{13}C_6$-Glucose (CLM-1396-1, CK isotopes), 1 mM glutamine (GlutaMAX, 35050061, Life Technologies UK) and 10% FBS.

8 x 10^5 HeLa cells maintained in DMEM + 10 % FBS were plated in 100 mm dishes and incubated in normoxia for 24 h. On the next day, media was removed, cells were washed once with PBS and fresh warm media containing 25 mM $^{13}C_6$-Glucose was added to the dishes. Cells were subsequently placed in normoxia or hypoxia for 2 h and 24 h. Following incubation media from these dishes was discarded, cells were washed twice with PBS and 3 mL of warm trypsin-EDTA was added to the dishes to detach the cells. Once cells were detached, 7 mL of growth media was added to each dish, cell suspensions were collected into 15 mL conical tubes. Cell suspensions were then centrifuged at 160 g for 4 minutes and pellets were washed three times with PBS. Supernatants were discarded and cell pellets were resuspended in 200 µL of ice-cold 100% methanol. Samples were stored at -80 °C until shipment in dry ice to Pennsylvania State University (USA).

5.5.33 Sample preparation for metabolomics analysis in cells cultured with isotope: ^{15}N-serine

Growth media for isotope incorporation was prepared as follow on day of experiment: serine-free MEM (M4655, Corning) supplemented with 60 µM ^{15}N-L-Serine (NLM-2036, CK isotopes) and 10% FBS.

8 x 10^5 HeLa cells maintained in DMEM + 10% FBS were plated in 100 mm dishes and incubated in normoxia for 24 h On the next day, media was removed, cells were washed once with PBS and fresh warm media containing 60 µM ^{15}N-L-Serine was added to the dishes. Cells were

subsequently placed in normoxia or hypoxia for 2 h and 24 h. Following incubation media from these dishes was discarded, cells were washed twice with PBS and 3 mL of warm trypsin-EDTA was added to the dishes to detach the cells. Once cells were detached, 7 mL of growth media was added to each dish, cell suspensions were collected into 15 mL conical tubes. Cell suspensions were then centrifuged at 160 g for 4 minutes and pellets were washed three times with PBS. Supernatants were discarded and cell pellets were resuspended in 200 µL of ice-cold 100% methanol. Samples were stored at -80 °C until shipment in dry ice to Pennsylvania State University (USA).

5.5.34 Sample preparation for metabolomics analysis in cells cultured with isotope: ^{15}N-Glutamine

Growth media for isotope incorporation was prepared as follow on day of experiment: glutamine-free DMEM (11960-044, Life Technologies, UK) was supplemented with 1 mM ^{15}N-amide labelled L-Glutamine (NLM-557, CK isotopes) and 10 % FBS (in purine-rich) or 10% dialysed FBS (purine-depleted).

8 x 10^5 HeLa cells maintained in DMEM + 10% FBS were plated in 100 mm dishes and incubated in normoxia for 24 h. On the next day, media was removed, cells were washed once with PBS and fresh warm media was added to the dishes. Cells were subsequently placed in normoxia or hypoxia for 12 h. Following incubation, 5 mL of media from one dish of each condition (purine rich normoxia, purine rich hypoxia and purine-depleted hypoxia) was transferred to a 15 mL centrifuge tube and kept aside for later treatment. The remaining media from these dishes was discarded, cells were washed twice with PBS and 3 mL of warm trypsin-EDTA was added to the dishes to detach the cells. Meantime the media of the remaining dishes was removed, the cells were washed with PBS once and ^{15}N-glutamine supplemented media was added to the cells. Cells were then let to incubate for the appropriate amount of time. Following incubation, the media was removed, the cells washed with PBS and trypsinised as before and treated as follow :

Once cells were detached, 7 mL of growth media was added to each dish and the cell concentration was measured in the cell suspension using a Moxi Z Mini Cell Counter (Orflo). Cell suspensions were then centrifuged at 160 g for 4 minutes and pellets were washed three times with PBS. Supernatants were discarded and cell pellets were resuspended in 200 µL of ice-cold 100 % methanol. Samples were stored at -80 °C until shipment in dry ice to Pennsylvania State University (USA).

5.5.35 Metabolite extraction

Metabolites extraction protocol was based on previously reported experiment with some modifications.[169] Following appropriate treatment and incubation, metabolites from cells were extracted. When required for analysis, media from each dish was transferred to individual conical tubes to which 1% perchloric acid 1 M (v/v) was added. Tubes were subsequently placed at -80 °C until required. Cells were washed with PBS and detached from the plates using trypsin-EDTA. At this point, the number of cells was measured to allow further normalisation. Cell suspensions were centrifuged at 160 g for 4 minutes and pellets were washed three times with PBS. Supernatants were discarded and pellets were resuspended in 500 µL of 80% methanol in water. Pellets were vortexed, snap frozen and thawed on ice for 10 minutes. This freeze-thaw cycle was repeated two more times. Final suspensions were centrifuged for 15 minutes at 3,000 g, supernatants were collected and pellets were kept for protein quantification. This extraction process was repeated for each sample using 200 µL of 80% methanol in water. Combined supernatants from the two extractions were centrifuged for 30 minutes at 7,000 g and supernatants were transferred to glass vials. Methanol was removed in vacuo and aqueous samples were frozen at -80 °C and subsequently freeze-dried for 72 h. Media samples were thawed on ice and centrifuged for 20 minutes at 9,000 g. Supernatants were then neutralised with 2% (v/v) of 3.5 M of K_2CO_3 and incubated on ice for an hour. Centrifugation step was repeated and supernatants were filter through a PTFE 0.22 µm syringe filter. Samples were transferred to glass vials, frozen at -80 °C and freeze-dried for 72 h.

5.5.36 Metabolomics analysis

For samples produced in **sections 5.5.32, 5.5.33 and 5.5.34**, metabolites were extracted following procedure in **section 5.5.35** by Dr Anthony M. Pedley at Pennsylvania State University (USA). Injections of all samples and subsequent spectra analysis was carried out by Dr Anthony M. Pedley (Pennsylvania State University, USA) using the following procedure.

Samples were reconstituted in either 30 µL of 3% (v/v) methanol in water with 1 µM chlorpropamide and 0.1% (v/v) formic acid and analysed by LC-MS using a modified version of an ion pairing reversed phase negative ion electrospray ionisation method.4 Samples were separated on a Phenomenex Synergi Hydro-RP C18 column (100 × 2.1 mm, 2.5 µm particle size) using a water-methanol gradient. The LC-MS platform consisted of a Dionex Ultimate 3000 quaternary HPLC pump, a Dionex 3000 column compartment, a Dionex 3000 autosampler, and an Exactive Plus Orbitrap Mass Spectrometer controlled by Xcalibur 2.2 software. The HPLC column was maintained at 30 °C and a flow rate of 200 µL/min. Solvent A was 3% (v/v) aqueous methanol with

10 mM tributylamine and 15 mM acetic acid; solvent B was methanol. The gradient was 0 min at 0% solvent B; 5 min at 20% solvent B; 7.5 min at 20% solvent B; 13 min at 55% solvent B; 15.5 min at 95% solvent B; 18.5 min at 95% solvent B; 19.0 min at 0% solvent B; 25 min at 0% solvent B. The Exactive Plus was operated in negative ion mode at maximum resolution (140,000) and scanned from 70 to 1000 m/z.

Peak areas for all metabolites were calculated using Xcalibur 2.2 software.[236,237] All spectra were aligned to one another and metabolites identified using an in-house metabolite reference library. Peak areas were corrected for injection differences using chlorpropamide (internal standard) and normalised to the number of cells or represented as percent of total isotopologue species.

5.5.37 Cell growth measurement

HeLa cells were plated into 24-well plate at 5 x 10^4 cells per well. Cells were let to recover overnight. On next day, cell number at time 0 was quantified. Briefly, media was removed, cells were washed once with DPBS. 200 µL of Trypsin was added to each well. Cells were placed back into incubator until fully detached. 300 µL of warm growth media was added to each well. The cell concentration of each cell suspension was measured using Moxi Z Mini Cell Counter (Orflo) following manufacturer's instructions. The remaining cells were placed in normoxia and hypoxia for 24 h. Following incubation, the same trypsinisation and counting process was repeated. The cell concentration at 24 h was normalised to the cell concentration measured at 0 h.

5.5.38 Cytotoxicity Assay

Hela cells were plated in 96-well plates at a confluency of 5,000 cells per well. Cells were let to recover overnight and on next day, media was removed and cells were washed once with 1X DPBS. Media containing Cpd14 at 50 µM, 100 µM and 250 µM was prepared by diluting a stock solution of Cpd14 (100 % DMSO) so as to get the appropriate compound concentration and 1 % final DMSO concentration in growth media. In parallel, a non-treated condition as well as a DMSO control condition were prepared. Media was added to the cells (100 µL per well) and cells were placed in normoxia or hypoxia for 24 h. Following incubation, cytotoxicity was assessed using Cytotox 96 Non-Radioactive Cytotoxicity Assay (G1780, Promega), including a maximum LDH release control. 50 µL of cell media from each condition was transferred into a new 96-well plate. 50 µL of the CytoTox96 Reagent was added to each well, the plate was covered in foil and let to incubate for 30 minutes at room temperature. Then, 50 µL of Stop Solution was added to each well. Absorbance was read at 490 nm on Clariostar plate reader.

5.6 Data analysis

All statistical analysis were carried out on GraphPad Prism software using unpaired student-t test. Statistical significance was defined as * p-value < 0.05, ** p-value < 0.01, *** p-value < 0.005, **** p-value < 0.0001.

Z-stack and 3D volume reconstructions as well as Pearson's coefficient calculations were carried out using ImageJ software.

Chapter 6 Bibliography

1. McKeown, S. R., Defining normoxia, physoxia and hypoxia in tumours-implications for treatment response. *Br. J. Radiol.* **2014,** *87* (1035), 20130676.

2. Carreau, A.; El Hafny-Rahbi, B.; Matejuk, A.; Grillon, C.; Kieda, C., Why is the partial oxygen pressure of human tissues a crucial parameter? Small molecules and hypoxia. *J. Cell. Mol. Med.* **2011,** *15* (6), 1239-1253.

3. Simon, M. C.; Keith, B., The role of oxygen availability in embryonic development and stem cell function. *Nat. Rev. Mol. Cell. Biol.* **2008,** *9* (4), 285-296.

4. Favret, F.; Richalet, J. P., Exercise and hypoxia: The role of the autonomic nervous system. *Respir. Physiol. Neurobiol.* **2007,** *158* (2-3), 280-286.

5. Michiels, C., Physiological and pathological responses to hypoxia. *Am. J. Pathol.* **2004,** *164* (6), 1875-1882.

6. Brown, J. M.; Giaccia, A. J., The unique physiology of solid tumors: Opportunities (and problems) for cancer therapy. *Cancer Res.* **1998,** *58* (7), 1408-1416.

7. Vaupel, P.; Kallinowski, F.; Okunieff, P., Blood-Flow, Oxygen and Nutrient Supply, and Metabolic Microenvironment of Human-Tumors - a Review. *Cancer Res.* **1989,** *49* (23), 6449-6465.

8. Carmeliet, P.; Jain, R. K., Angiogenesis in cancer and other diseases. *Nature* **2000,** *407* (6801), 249-257.

9. Brown, J. M., Tumor hypoxia in cancer therapy. *Methods Enzymol.* **2007,** *435*, 297-321.

10. Favaro, E.; Lord, S.; Harris, A. L.; Buffa, F. M., Gene expression and hypoxia in breast cancer. *Genome Med.* **2011,** *3*.

11. Vaupel, P., Tumor microenvironmental physiology and its implications for radiation oncology. *Semin. Radiat. Oncol.* **2004,** *14* (3), 198-206.

12. Vaupel, P.; Thews, O.; Hoeckel, M., Treatment resistance of solid tumors - Role of hypoxia and anemia. *Med. Oncol.* **2001,** *18* (4), 243-259.

13. Muz, B.; de la Puente, P.; Azab, F.; Azab, A. K., The role of hypoxia in cancer progression, angiogenesis, metastasis, and resistance to therapy. *Hypoxia* **2015,** *3*, 83-92.

14. Semenza, G. L., HIF-1 and human disease: one highly involved factor. *Genes Dev.* **2000,** *14* (16), 1983-1991.

15. Harris, A. L., Hypoxia - A key regulatory factor in tumour growth. *Nat. Rev. Cancer* **2002,** *2* (1), 38-47.

16. Vaupel, P., The role of hypoxia-induced factors in tumor progression. *Oncologist* **2004,** *9 Suppl 5*, 10-17.

17. Kewley, R. J.; Whitelaw, M. L.; Chapman-Smith, A., The mammalian basic helix-loop-helix/PAS family of transcriptional regulators. *Int. J. Biochem. Cell. Biol.* **2004,** *36* (2), 189-204.

18. Huang, Z. J.; Edery, I.; Rosbash, M., Pas Is a Dimerization Domain Common to Drosophila Period and Several Transcription Factors. *Nature* **1993,** *364* (6434), 259-262.

19. Yang, J. S.; Zhang, L.; Erbel, P. J. A.; Gardner, K. H.; Ding, K.; Garcia, J. A.; Bruick, R. K., Functions of the Per/ARNT/Sim domains of the hypoxia-inducible factor. *J. Biol. Chem.* **2005,** *280* (43), 36047-36054.

20. Jiang, B. H.; Rue, E.; Wang, G. L.; Roe, R.; Semenza, G. L., Dimerization, DNA binding, and transactivation properties of hypoxia-inducible factor 1. *J. Biol. Chem.* **1996,** *271* (30), 17771-17778.

21. Wu, D. L.; Potluri, N.; Lu, J. P.; Kim, Y. C.; Rastinejad, F., Structural integration in hypoxia-inducible factors. *Nature* **2015,** *524* (7565), 303-308.

22. Lisy, K.; Peet, D. J., Turn me on: regulating HIF transcriptional activity. *Cell Death Differ.* **2008,** *15* (4), 642-649.

23. Bracken, C. P.; Whitelaw, M. L.; Peet, D. J., The hypoxia-inducible factors: key transcriptional regulators of hypoxic responses. *Cell. Mol. Life Sci.* **2003,** *60* (7), 1376-1393.

24. Jiang, B. H.; Zheng, J. Z.; Leung, S. W.; Roe, R.; Semenza, G. L., Transactivation and inhibitory domains of hypoxia-inducible factor 1 alpha. Modulation of transcriptional activity by oxygen tension. *J. Biol. Chem.* **1997,** *272* (31), 19253-19260.

25. Carrero, P.; Okamoto, K.; Coumailleau, P.; O'Brien, S.; Tanaka, H.; Poellinger, L., Redox-regulated recruitment of the transcriptional coactivators CREB-binding protein and SRC-1 to hypoxia-inducible factor 1 alpha. *Mol. Cell. Biol.* **2000,** *20* (1), 402-415.

26. Arany, Z.; Huang, L. E.; Eckner, R.; Bhattacharya, S.; Jiang, C.; Goldberg, M. A.; Bunn, H. F.; Livingston, D. M., An essential role for p300/CBP in the cellular response to hypoxia. *Proc. Natl. Acad. Sci. U.S.A.* **1996,** *93* (23), 12969-12973.

27. Freedman, S. J.; Sun, Z. Y. J.; Poy, F.; Kung, A. L.; Livingston, D. M.; Wagner, G.; Eck, M. J., Structural basis for recruitment of CBP/p300 by hypoxia-inducible factor-1 alpha. *Proc. Natl. Acad. Sci. U.S.A.* **2002,** *99* (8), 5367-5372.

28. Ruas, J. L.; Berchner-Pfannschmidt, U.; Malik, S.; Gradin, K.; Fandrey, J.; Roeder, R. G.; Pereira, T.; Poellinger, L., Complex Regulation of the Transactivation Function of Hypoxia-inducible Factor-1 alpha by Direct Interaction with Two Distinct Domains of the CREB-binding Protein/p300. *J. Biol. Chem.* **2010,** *285* (4), 2601-2609.

29. Bannister, A. J.; Kouzarides, T., The CBP co-activator is a histone acetyltransferase. *Nature* **1996,** *384* (6610), 641-643.

30. Huang, L. E.; Arany, Z.; Livingston, D. M.; Bunn, H. F., Activation of hypoxia-inducible transcription factor depends primarily upon redox-sensitive stabilization of its alpha subunit. *J. Biol. Chem.* **1996,** *271* (50), 32253-32259.

31. Bruick, R. K.; McKnight, S. L., A conserved family of prolyl-4-hydroxylases that modify HIF. *Science* **2001,** *294* (5545), 1337-1340.

32. McNeill, L. A.; Hewitson, K. S.; Gleadle, J. M.; Horsfall, L. E.; Oldham, N. J.; Maxwell, P. H.; Pugh, C. W.; Ratcliffe, P. J.; Schofield, C. J., The use of dioxygen by HIF prolyl hydroxylase (PHD1). *Bioorg. Med. Chem. Lett.* **2002,** *12* (12), 1547-1550.

33. Appelhoff, R. J.; Tian, Y. M.; Raval, R. R.; Turley, H.; Harris, A. L.; Pugh, C. W.; Ratcliffe, P. J.; Gleadle, J. M., Differential function of the prolyl hydroxylases PHD1, PHD2, and PHD3 in the regulation of hypoxia-inducible factor. *J. Biol. Chem.* **2004,** *279* (37), 38458-38465.

34. Jaakkola, P.; Mole, D. R.; Tian, Y. M.; Wilson, M. I.; Gielbert, J.; Gaskell, S. J.; von Kriegsheim, A.; Hebestreit, H. F.; Mukherji, M.; Schofield, C. J.; Maxwell, P. H.; Pugh, C. W.; Ratcliffe, P. J., Targeting of HIF-alpha to the von Hippel-Lindau ubiquitylation complex by O-2-regulated prolyl hydroxylation. *Science* **2001,** *292* (5516), 468-472.

35. Ivan, M.; Kondo, K.; Yang, H. F.; Kim, W.; Valiando, J.; Ohh, M.; Salic, A.; Asara, J. M.; Lane, W. S.; Kaelin, W. G., HIF alpha targeted for VHL-mediated destruction by proline hydroxylation: Implications for O-2 sensing. *Science* **2001,** *292* (5516), 464-468.

36. Maxwell, P. H.; Wiesener, M. S.; Chang, G. W.; Clifford, S. C.; Vaux, E. C.; Cockman, M. E.; Wykoff, C. C.; Pugh, C. W.; Maher, E. R.; Ratcliffe, P. J., The tumour suppressor protein VHL targets hypoxia-inducible factors for oxygen-dependent proteolysis. *Nature* **1999,** *399* (6733), 271-275.

37. Lisztwan, J.; Imbert, G.; Wirbelauer, C.; Gstaiger, M.; Krek, W., The von Hippel-Lindau tumor suppressor protein is a component of an E3 ubiquitin-protein ligase activity. *Genes Dev.* **1999,** *13* (14), 1822-1833.

38. Lando, D.; Peet, D. J.; Gorman, J. J.; Whelan, D. A.; Whitelaw, M. L.; Bruick, R. K., FIH-1 is an asparaginyl hydroxylase enzyme that regulates the transcriptional activity of hypoxia-inducible factor. *Gene. Dev.* **2002,** *16* (12), 1466-1471.

39. Lando, D.; Peet, D. J.; Whelan, D. A.; Gorman, J. J.; Whitelaw, M. L., Asparagine hydroxylation of the HIF transactivation domain: A hypoxic switch. *Science* **2002,** *295* (5556), 858-861.

40. Koivunen, P.; Hirsila, M.; Gunzler, V.; Kivirikko, K. I.; Myllyharju, J., Catalytic properties of the asparaginyl hydroxylase (FIH) in the oxygen sensing pathway are distinct from those of its prolyl 4-hydroxylases. *J. Biol. Chem.* **2004,** *279* (11), 9899-9904.

41. Hu, C. J.; Sataur, A.; Wang, L. Y.; Chen, H. Q.; Simon, M. C., The N-terminal Transactivation domain confers target gene specificity of hypoxia-inducible factors HIF-1 alpha and HIF-2 alpha. *Mol. Biol. Cell.* **2007,** *18* (11), 4528-4542.

42. Fukuda, R.; Hirota, K.; Fan, F.; Do Jung, Y.; Ellis, L. M.; Semenza, G. L., Insulin-like growth factor 1 induces hypoxia-inducible factor 1-mediated vascular endothelial growth factor expression, which is dependent on MAP kinase and phosphatidylinositol 3-kinase signaling in colon cancer cells. *J. Biol. Chem.* **2002,** *277* (41), 38205-38211.

43. Richard, D. E.; Berra, E.; Gothie, E.; Roux, D.; Pouyssegur, J., p42/p44 mitogen-activated protein kinases phosphorylate hypoxia-inducible factor 1 alpha (HIF-1 alpha) and enhance the transcriptional activity of HIF-1. *J. Biol. Chem.* **1999,** *274* (46), 32631-32637.

44. Bilton, R. L.; Booker, G. W., The subtle side to hypoxia inducible factor (HIF alpha) regulation. *Eur. J. Biochem.* **2003,** *270* (5), 791-798.

45. Liu, Y. V.; Baek, J. H.; Zhang, H.; Diez, R.; Cole, R. N.; Semenza, G. L., RACK1 competes with HSP90 for binding to HIF-1 alpha and is required for O-2-independent and HSP90 inhibitor-induced degradation of HIF-1 alpha. *Mol. Cell* **2007,** *25* (2), 207-217.

46. Luo, W.; Zhong, J.; Chang, R.; Hu, H.; Pandey, A.; Semenza, G. L., Hsp70 and CHIP selectively mediate ubiquitination and degradation of hypoxia-inducible factor (HIF)-1alpha but Not HIF-2alpha. *J Biol. Chem.* **2010,** *285* (6), 3651-3663.

47. Koh, M. Y.; Darnay, B. G.; Powis, G., Hypoxia-Associated Factor, a Novel E3-Ubiquitin Ligase, Binds and Ubiquitinates Hypoxia-Inducible Factor 1 alpha, Leading to Its Oxygen-Independent Degradation. *Mol. Cell. Biol.* **2008,** *28* (23), 7081-7095.

48. Semenza, G. L.; Wang, G. L., A nuclear factor induced by hypoxia via de novo protein synthesis binds to the human erythropoietin gene enhancer at a site required for transcriptional activation. *Mol. Cell. Biol.* **1992,** *12* (12), 5447-5454.

49. Ema, M.; Taya, S.; Yokotani, N.; Sogawa, K.; Matsuda, Y.; FujiiKuriyama, Y., A novel bHLH-PAS factor with close sequence similarity to hypoxia-inducible factor 1 alpha regulates the VEGF expression and is potentially involved in lung and vascular development. *Proc. Natl. Acad. Sci. U.S.A.* **1997,** *94* (9), 4273-4278.

50. Gu, Y. Z.; Moran, S. M.; Hogenesch, J. B.; Wartman, L.; Bradfield, C. A., Molecular characterization and chromosomal localization of a third alpha-class hypoxia inducible factor subunit, HIF3 alpha. *Gene Expression* **1998,** *7* (3), 205-213.

51. Hara, S.; Hamada, J.; Kobayashi, C.; Kondo, Y.; Imura, N., Expression and characterization of hypoxia-inducible factor (HIF)-3 alpha in human kidney: Suppression of HIF-mediated gene expression by HIF-3 alpha. *Biochem. Biophys. Res. Commun.* **2001,** *287* (4), 808-813.

52. Pasanen, A.; Heikkila, M.; Rautavuoma, K.; Hirsila, M.; Kivirikko, K. I.; Myllyharju, J., Hypoxia-inducible factor (HIF)-3alpha is subject to extensive alternative splicing in human tissues and cancer cells and is regulated by HIF-1 but not HIF-2. *Int. J. Biochem. Cell. Biol.* **2010,** *42* (7), 1189-1200.

53. Heikkila, M.; Pasanen, A.; Kivirikko, K. I.; Myllyharju, J., Roles of the human hypoxia-inducible factor (HIF)-3 alpha variants in the hypoxia response. *Cell. Mol. Life Sci.* **2011,** *68* (23), 3885-3901.

54. Masson, N.; Willam, C.; Maxwell, P. H.; Pugh, C. W.; Ratcliffe, P. J., Independent function of two destruction domains in hypoxia-inducible factor-alpha chains activated by prolyl hydroxylation. *EMBO Journal* **2001,** *20* (18), 5197-5206.

55. Keith, B.; Johnson, R. S.; Simon, M. C., HIF1 alpha and HIF2 alpha: sibling rivalry in hypoxic tumour growth and progression. *Nat. Rev. Cancer* **2012,** *12* (1), 9-22.

56. Birner, P.; Schindl, M.; Obermair, A.; Plank, C.; Breitenecker, G.; Oberhuber, G., Overexpression of hypoxia-inducible factor 1 alpha is a marker for an unfavorable prognosis in early-stage invasive cervical cancer. *Cancer Res.* **2000,** *60* (17), 4693-4696.

57. Kim, S. J.; Rabbani, Z. N.; Dewhirst, M. W.; Vujaskovic, Z.; Vollmer, R. T.; Schreiber, E. G.; Oosterwijk, E.; Kelley, M. J., Expression of HIF-1 alpha, CA IX, VEGF, and MMP-9 in surgically resected non-small cell lung cancer. *Lung Cancer* **2005,** *49* (3), 325-335.

58. Yamamoto, Y.; Ibusuki, M.; Okumura, Y.; Kawasoe, T.; Kai, K.; Iyama, K.; Iwase, H., Hypoxia-inducible factor 1 alpha is closely linked to an aggressive phenotype in breast cancer. *Breast Cancer Res. Treat.* **2008,** *110* (3), 465-475.

59. Lidgren, A.; Hedberg, Y.; Grankvist, K.; Rasmuson, T.; Vasko, J.; Ljungberg, B., The expression of hypoxia-inducible factor 1 alpha is a favorable independent prognostic factor in renal cell carcinoma. *Clin. Cancer Res.* **2005,** *11* (3), 1129-1135.

60. Noguera, R.; Fredlund, E.; Piqueras, M.; Pietras, A.; Beckman, S.; Navarro, S.; Pahlman, S., HIF-1 alpha and HIF-2 alpha Are Differentially Regulated In vivo in Neuroblastoma: High HIF-1 alpha Correlates Negatively to Advanced Clinical Stage and Tumor Vascularization. *Clin. Cancer Res.* **2009,** *15* (23), 7130-7136.

61. Helczynska, K.; Larsson, A. M.; Mengelbier, L. H.; Bridges, E.; Fredlund, E.; Borgquist, S.; Landberg, G.; Pahlman, S.; Jirstrom, K., Hypoxia-Inducible Factor-2 alpha Correlates to Distant Recurrence and Poor Outcome in Invasive Breast Cancer. *Cancer Res.* **2008,** *68* (22), 9212-9220.

62. Forsythe, J. A.; Jiang, B. H.; Iyer, N. V.; Agani, F.; Leung, S. W.; Koos, R. D.; Semenza, G. L., Activation of vascular endothelial growth factor gene transcription by hypoxia-inducible factor 1. *Mol. Cell. Biol.* **1996,** *16* (9), 4604-4613.

63. Hu, C. J.; Wang, L. Y.; Chodosh, L. A.; Keith, B.; Simon, M. C., Differential roles of hypoxia-inducible factor 1 alpha (HIF-1 alpha) and HIF-2 alpha in hypoxic gene regulation. *Mol. Cell. Biol.* **2003,** *23* (24), 9361-9374.

64. Gerber, H. P.; Condorelli, F.; Park, J.; Ferrara, N., Differential transcriptional regulation of the two vascular endothelial growth factor receptor genes - Flt-1, but not Flk-1/KDR, is up-regulated by hypoxia. *J. Biol. Chem.* **1997,** *272* (38), 23659-23667.

65. Simiantonaki, N.; Jayasinghe, C.; Michel-Schmidt, R.; Peters, K.; Hermanns, M. I.; Kirkpatrick, C. J., Hypoxia-induced epithelial VEGF-C/VEGFR-3 upregulation in carcinoma cell lines. *Int. J. Oncol.* **2008,** *32* (3), 585-592.

66. Haigh, J. J., Role of VEGF in organogenesis. *Organogenesis* **2008,** *4* (4), 247-256.

67. Pichiule, P.; Chavez, J. C.; LaManna, J. C., Hypoxic regulation of angiopoietin-2 expression in endothelial cells. *J. Biol. Chem.* **2004,** *279* (13), 12171-12180.

68. Yoshida, D.; Kim, K.; Noha, M.; Teramoto, A., Hypoxia inducible factor 1-alpha regulates of platelet derived growth factor-B in human glioblastoma cells. *J. Neuro-Oncol.* **2006,** *76* (1), 13-21.

69. Rankin, E. B.; Biju, M. P.; Liu, Q. D.; Unger, T. L.; Rha, J.; Johnson, R. S.; Simon, M. C.; Keith, B.; Haase, V. H., Hypoxia-inducible factor-2 (HIF-2) regulates hepatic erythropoietin in vivo. *J. Clin. Invest.* **2007,** *117* (4), 1068-1077.

70. Kapitsinou, P. P.; Liu, Q. D.; Unger, T. L.; Rha, J.; Davidoff, O.; Keith, B.; Epstein, J. A.; Moores, S. L.; Erickson-Miller, C. L.; Haase, V. H., Hepatic HIF-2 regulates erythropoietic responses to hypoxia in renal anemia. *Blood* **2010,** *116* (16), 3039-3048.

71. Jung, F.; Palmer, L. A.; Zhou, N.; Johns, R. A., Hypoxic regulation of inducible nitric oxide synthase via hypoxia inducible factor-1 in cardiac myocytes. *Circ. Res.* **2000,** *86* (3), 319-325.

72. Krishnamachary, B.; Berg-Dixon, S.; Kelly, B.; Agani, F.; Feldser, D.; Ferreira, G.; Iyer, N.; LaRusch, J.; Pak, B.; Taghavi, P.; Semenza, G. L., Regulation of colon carcinoma cell invasion by hypoxia-inducible factor 1. *Cancer Res.* **2003,** *63* (5), 1138-1143.

73. Feldser, D.; Agani, F.; Iyer, N. V.; Pak, B.; Ferreira, G.; Semenza, G. L., Reciprocal positive regulation of hypoxia-inducible factor 1alpha and insulin-like growth factor 2. *Cancer Res.* **1999,** *59* (16), 3915-3918.

74. Chen, J.; Imanaka, N.; Chen, J.; Griffin, J. D., Hypoxia potentiates Notch signaling in breast cancer leading to decreased E-cadherin expression and increased cell migration and invasion. *Br. J. Cancer* **2010,** *102* (2), 351-360.

75. Esteban, M. A.; Tran, M. G. B.; Harten, S. K.; Hill, P.; Castellanos, M. C.; Chandra, A.; Raval, R.; O'Brien, T. S.; Maxwell, P. H., Regulation of E-cadherin expression by VHL and hypoxia-inducible factor. *Cancer Res.* **2006,** *66* (7), 3567-3575.

76. Fujiwara, S.; Nakagawa, K.; Harada, H.; Nagato, S.; Furukawa, K.; Teraoka, M.; Seno, T.; Oka, K.; Iwata, S.; Ohnishi, T., Silencing hypoxia-inducible factor-1 alpha inhibits cell migration and invasion under hypoxic environment in malignant gliomas. *Int. J. Oncol.* **2007,** *30* (4), 793-802.

77. Xie, T.; Yuan, X. L.; Yu, S. Y.; Yang, B.; Dong, L. L., [Interference of HIF-1alpha by RNA reduces the expression of matrix metalloproteinase-2 in human cervical carcinoma HeLa cells]. *Ai Zheng* **2008,** *27* (6), 600-605.

78. Jezierska, A.; Motyl, T., Matrix Metalloproteinase-2 involvement in breast cancer progression: A mini-review. *Med. Sci. Monit.* **2009,** *15* (2), Ra32-Ra40.

79. Eales, K. L.; Hollinshead, K. E. R.; Tennant, D. A., Hypoxia and metabolic adaptation of cancer cells. *Oncogenesis* **2016,** *5*.

80. Baumann, M. U.; Zamudio, S.; Illsley, N. P., Hypoxic upregulation of glucose transporters in BeWo choriocarcinoma cells is mediated by hypoxia-inducible factor-1. *Am. J. Physiol.: Cell Physiol.* **2007,** *293* (1), C477-C485.

81. Chen, C. H.; Pore, N.; Behrooz, A.; Ismail-Beigi, F.; Maity, A., Regulation of glut1 mRNA by hypoxia-inducible factor-1 - Interaction between H-ras and hypoxia. *J. Biol. Chem.* **2001,** *276* (12), 9519-9525.

82. Hayashi, M.; Sakata, M.; Takeda, T.; Yamamoto, T.; Okamoto, Y.; Sawada, K.; Kimura, A.; Minekawa, R.; Tahara, M.; Tasaka, K.; Murata, Y., Induction of glucose transporter 1 expression through hypoxia-inducible factor 1 alpha under hypoxic conditions in trophoblast-derived cells. *J. Endocrinol.* **2004,** *183* (1), 145-154.

83. Iyer, N. V.; Kotch, L. E.; Agani, F.; Leung, S. W.; Laughner, E.; Wenger, R. H.; Gassmann, M.; Gearhart, J. D.; Lawler, A. M.; Yu, A. Y.; Semenza, G. L., Cellular and developmental control of O2 homeostasis by hypoxia-inducible factor 1 alpha. *Genes Dev.* **1998,** *12* (2), 149-162.

84. Liu, Y.; Li, Y. M.; Tian, R. F.; Liu, W. P.; Fei, Z.; Long, Q. F.; Wang, X. A.; Zhang, X., The expression and significance of HIF-1 alpha and GLUT-3 in glioma. *Brain Res.* **2009,** *1304*, 149-154.

85. Greijer, A. E.; van der Groep, P.; Kemming, D.; Shvarts, A.; Semenza, G. L.; Meijer, G. A.; van de Wiel, M. A.; Belien, J. A. M.; van Diest, P. J.; van der Wall, E., Up-regulation of gene expression by hypoxia is mediated predominantly by hypoxia-inducible factor 1 (HIF-1). *J. Pathol.* **2005,** *206* (3), 291-304.

86. Riddle, S. R.; Ahmad, A.; Ahmad, S.; Deeb, S. S.; Malkki, M.; Schneider, B. K.; Allen, C. B.; White, C. W., Hypoxia induces hexokinase II gene expression in human lung cell line A549. *Am. J. Physiol.: Lung Cell Mol. Physiol.* **2000,** *278* (2), 407-416.

87. Kim, J. W.; Tchernyshyov, I.; Semenza, G. L.; Dang, C. V., HIF-1-mediated expression of pyruvate dehydrogenase kinase: A metabolic switch required for cellular adaptation to hypoxia. *Cell Metab.* **2006,** *3* (3), 177-185.

88. Ullah, M. S.; Davies, A. J.; Halestrap, A. P., The plasma membrane lactate transporter MCT4, but not MCT1, is up-regulated by hypoxia through a HIF-1alpha-dependent mechanism. *J. Biol. Chem.* **2006,** *281* (14), 9030-9037.

89. Halestrap, A. P.; Price, N. T., The proton-linked monocarboxylate transporter (MCT) family: structure, function and regulation. *Biochem. J.* **1999,** *343*, 281-299.

90. Wykoff, C. C.; Beasley, N. J.; Watson, P. H.; Turner, K. J.; Pastorek, J.; Sibtain, A.; Wilson, G. D.; Turley, H.; Talks, K. L.; Maxwell, P. H.; Pugh, C. W.; Ratcliffe, P. J.; Harris, A. L., Hypoxia-inducible expression of tumor-associated carbonic anhydrases. *Cancer Res.* **2000,** *60* (24), 7075-7083.

91. Gillies, R. J.; Martinezzaguilan, R.; Martinez, G. M.; Serrano, R.; Perona, R., Tumorigenic-3t3 Cells Maintain an Alkaline Intracellular Ph under Physiological Conditions. *Proc. Natl. Acad. Sci. U.S.A.* **1990,** *87* (19), 7414-7418.

92. Swietach, P.; Vaughan-Jones, R. D.; Harris, A. L.; Hulikova, A., The chemistry, physiology and pathology of pH in cancer. *Philos. Trans. R. Soc., B* **2014,** *369* (1638).

93. Kress, S.; Stein, A.; Maurer, P.; Weber, B.; Reichert, J.; Buchmann, A.; Huppert, P.; Schwarz, M., Expression of hypoxia-inducible genes in tumor cells. *J. Cancer Res. Clin. Oncol.* **1998,** *124* (6), 315-320.

94. Luo, F.; Liu, X.; Yan, N.; Li, S.; Cao, G.; Cheng, Q.; Xia, Q.; Wang, H., Hypoxia-inducible transcription factor-1alpha promotes hypoxia-induced A549 apoptosis via a mechanism that involves the glycolysis pathway. *BMC Cancer* **2006,** *6*, 26.

95. Diedrich, J. D.; Rajagurubandara, E.; Herroon, M. K.; Mahapatra, G.; Huttemann, M.; Podgorski, I., Bone marrow adipocytes promote the Warburg phenotype in metastatic prostate tumors via HIF-1alpha activation. *Oncotarget* **2016,** *7* (40), 64854-64877.

96. Hamaguchi, T.; Iizuka, N.; Tsunedomi, R.; Hamamoto, Y.; Miyamoto, T.; Iida, M.; Tokuhisa, Y.; Sakamoto, K.; Takashima, M.; Tamesa, T.; Oka, M., Glycolysis module activated by hypoxia-inducible factor 1 alpha is related to the aggressive phenotype of hepatocellular carcinoma. *Int. J. Oncol.* **2008,** *33* (4), 725-731.

97. Gao, L.; Mejias, R.; Echevarria, M.; Lopez-Barneo, J., Induction of the glucose-6-phosphate dehydrogenase gene expression by chronic hypoxia in PC12 cells. *Febs Lett.* **2004,** *569* (1-3), 256-260.

98. Samanta, D.; Park, Y.; Andrabi, S. A.; Shelton, L. M.; Gilkes, D. M.; Semenza, G. L., PHGDH Expression Is Required for Mitochondrial Redox Homeostasis, Breast Cancer Stem Cell Maintenance, and Lung Metastasis. *Cancer Res.* **2016,** *76* (15), 4430-4442.

99. Chettimada, S.; Gupte, R.; Rawat, D.; Gebb, S. A.; McMurtry, I. F.; Gupte, S. A., Hypoxia-induced glucose-6-phosphate dehydrogenase overexpression and -activation in pulmonary artery smooth muscle cells: implication in pulmonary hypertension. *Am. J. Physiol.: Lung. Cell Mol. Physiol.* **2015,** *308* (3), L287-L300.

100. Guo, S. H.; Miyake, M.; Liu, K. J.; Shi, H. L., Specific inhibition of hypoxia inducible factor 1 exaggerates cell injury induced by in vitro ischemia through deteriorating cellular redox environment. *J. Neurochem.* **2009,** *108* (5), 1309-1321.

101. Zhao, F.; Mancuso, A.; Bui, T. V.; Tong, X.; Gruber, J. J.; Swider, C. R.; Sanchez, P. V.; Lum, J. J.; Sayed, N.; Melo, J. V.; Perl, A. E.; Carroll, M.; Tuttle, S. W.; Thompson, C. B., Imatinib resistance associated with BCR-ABL upregulation is dependent on HIF-1 alpha-induced metabolic reprograming. *Oncogene* **2010,** *29* (20), 2962-2972.

102. Kucharzewska, P.; Christianson, H. C.; Belting, M., Global Profiling of Metabolic Adaptation to Hypoxic Stress in Human Glioblastoma Cells. *Plos One* **2015,** *10* (1).

103. Patra, K. C.; Hay, N., The pentose phosphate pathway and cancer. *Trends Biochem. Sci.* **2014,** *39* (8), 347-354.

104. Warburg, O., On the origin of cancer cells. *Science* **1956,** *123* (3191), 309-314.

105. Heiden, M. G. V.; Cantley, L. C.; Thompson, C. B., Understanding the Warburg Effect: The Metabolic Requirements of Cell Proliferation. *Science* **2009,** *324* (5930), 1029-1033.

106. Sukhatme, V. P.; Chan, B., Glycolytic cancer cells lacking 6-phosphogluconate dehydrogenase metabolize glucose to induce senescence. *Febs Lett.* **2012,** *586* (16), 2389-2395.

107. Benito, A.; Polat, I. H.; Noe, V.; Ciudad, C. J.; Marin, S.; Cascante, M., Glucose-6-phosphate dehydrogenase and transketolase modulate breast cancer cell metabolic reprogramming and correlate with poor patient outcome. *Oncotarget* **2017,** *8* (63), 106693-106706.

108. Locasale, J. W., Serine, glycine and one-carbon units: cancer metabolism in full circle. *Nat. Rev. Cancer.* **2013,** *13* (8), 572-583.

109. Fujioka, M., Purification and properties of serine hydroxymethylase from soluble and mitochondrial fractions of rabbit liver. *Biochim. Biophys. Acta* **1969,** *185* (2), 338-349.

110. Garrow, T. A.; Brenner, A. A.; Whitehead, V. M.; Chen, X. N.; Duncan, R. G.; Korenberg, J. R.; Shane, B., Cloning of Human Cdnas Encoding Mitochondrial and Cytosolic Serine Hydroxymethyltransferases and Chromosomal Localization. *J. Biol. Chem.* **1993,** *268* (16), 11910-11916.

111. Ye, J. B.; Fan, J.; Venneti, S.; Wan, Y. W.; Pawel, B. R.; Zhang, J.; Finley, L. W. S.; Lu, C.; Lindsten, T.; Cross, J. R.; Qing, G. L.; Liu, Z. D.; Simon, M. C.; Rabinowitz, J. D.; Thompson, C. B., Serine Catabolism Regulates Mitochondrial Redox Control during Hypoxia. *Cancer Discovery* **2014,** *4* (12), 1406-1417.

112. Possemato, R.; Marks, K. M.; Shaul, Y. D.; Pacold, M. E.; Kim, D.; Birsoy, K.; Sethumadhavan, S.; Woo, H. K.; Jang, H. G.; Jha, A. K.; Chen, W. W.; Barrett, F. G.; Stransky, N.; Tsun, Z. Y.; Cowley, G. S.; Barretina, J.; Kalaany, N. Y.; Hsu, P. P.; Ottina, K.; Chan, A. M.; Yuan, B.; Garraway, L. A.; Root, D. E.; Mino-Kenudson, M.; Brachtel, E. F.; Driggers, E. M.; Sabatini, D. M., Functional genomics reveal that the serine synthesis pathway is essential in breast cancer. *Nature* **2011,** *476* (7360), 346-350.

113. Mattaini, K. R.; Sullivan, M. R.; Vander Heiden, M. G., The importance of serine metabolism in cancer. *J. Cell. Biol.* **2016,** *214* (3), 248-257.

114. Snell, K., Enzymes of Serine Metabolism in Normal, Developing and Neoplastic Rat-Tissues. *Adv. Enzyme Regul.* **1984,** *22*, 325-400.

115. Snell, K.; Weber, G., Enzymic imbalance in serine metabolism in rat hepatomas. *Biochem. J.* **1986,** *233* (2), 617-620.

116. Snell, K.; Natsumeda, Y.; Eble, J. N.; Glover, J. L.; Weber, G., Enzymic Imbalance in Serine Metabolism in Human-Colon Carcinoma and Rat Sarcoma. *Br. J. Cancer* **1988,** *57* (1), 87-90.

117. Kaziro, Y.; Itoh, H.; Kozasa, T.; Nakafuku, M.; Satoh, T., Structure and function of signal-transducing GTP-binding proteins. *Annu. Rev. Biochem.* **1991,** *60*, 349-400.

118. Bhattacharya, M.; Babwah, A. V.; Ferguson, S. S. G., Small GTP-binding protein-coupled receptors. *Biochem Soc T* **2004,** *32*, 1040-1044.

119. Bos, J. L.; Rehmann, H.; Wittinghofer, A., GEFs and GAPs: Critical elements in the control of small G proteins. *Cell* **2007,** *130* (2), 385-385.

120. Khakh, B. S.; Burnstock, G., The Double Life of Atp. *Sci. Am.* **2009,** *301* (6), 84-90.

121. Burnstock, G., Purinergic Nerves. *Pharmacol. Rev.* **1972,** *24* (3), 509-581.

122. Fredholm, B. B.; Abbracchio, M. P.; Burnstock, G.; Daly, J. W.; Harden, T. K.; Jacobson, K. A.; Leff, P.; Williams, M., Nomenclature and Classification of Purinoceptors. *Pharmacol. Rev.* **1994,** *46* (2), 143-156.

123. Baldwin, S. A.; Beal, P. R.; Yao, S. Y. M.; King, A. E.; Cass, C. E.; Young, J. D., The equilibrative nucleoside transporter family, SLC29. *Pfluegers Arch. Eur. J. Physiol.* **2004,** *447* (5), 735-743.

124. Gray, J. H.; Owen, R. P.; Giacomini, K. M., The concentrative nucleoside transporter family, SLC28. *Pfluegers Arch. Eur. J. Physiol.* **2004,** *447* (5), 728-734.

125. Yegutkin, G. G., Nucleotide- and nucleoside-converting ectoenzymes: Important modulators of purinergic signalling cascade. *Biochm. Biophys. Acta, Mol. Cell Res.* **2008,** *1783* (5), 673-694.

126. Di Virgilio, F.; Adinolfi, E., Extracellular purines, purinergic receptors and tumor growth. *Oncogene* **2017,** *36* (3), 293-303.

127. Burnstock, G., Pathophysiology and therapeutic potential of purinergic signaling. *Pharmacol. Rev.* **2006,** *58* (1), 58-86.

128. Ohta, A.; Gorelik, E.; Prasad, S. J.; Ronchese, F.; Lukashev, D.; Wong, M. K. K.; Huang, X. J.; Caldwell, S.; Liu, K. B.; Smith, P.; Chen, J. F.; Jackson, E. K.; Apasov, S.; Abrams, S.; Sitkovsky, M., A2A adenosine receptor protects tumors from antitumor T cells. *Proc. Natl. Acad. Sci. U.S.A.* **2006,** *103* (35), 13132-13137.

129. Pellegatti, P.; Raffaghello, L.; Bianchi, G.; Piccardi, F.; Pistoia, V.; Di Virgilio, F., Increased Level of Extracellular ATP at Tumor Sites: In Vivo Imaging with Plasma Membrane Luciferase. *Plos One* **2008,** *3* (7).

130. Burnstock, G.; Di Virgilio, F., Purinergic signalling and cancer. *Purinergic Signalling* **2013,** *9* (4), 491-540.

131. Young, A.; Mittal, D.; Stagg, J.; Smyth, M. J., Targeting Cancer-Derived Adenosine: New Therapeutic Approaches. *Cancer Discovery* **2014,** *4* (8), 879-888.

132. Synnestvedt, K.; Furuta, G. T.; Comerford, K. M.; Louis, N.; Karhausen, J.; Eltzschig, H. K.; Hansen, K. R.; Thompson, L. F.; Colgan, S. P., Ecto-5 '-nucleotidase (CD73) regulation by hypoxia-inducible factor-1 mediates permeability changes in intestinal epithelia. *J. Clin. Invest.* **2002,** *110* (7), 993-1002.

133. Ohta, A.; Sitkovsky, M., Role of G-protein-coupled adenosine receptors in downregulation of inflammation and protection from tissue damage. *Nature* **2001,** *414* (6866), 916-920.

134. Hasko, G.; Linden, J.; Cronstein, B.; Pacher, P., Adenosine receptors: therapeutic aspects for inflammatory and immune diseases. *Nat. Rev. Drug Discovery* **2008,** *7* (9), 759-770.

135. Xie, R.; Xu, J.; Wen, G.; Jin, H.; Liu, X.; Yang, Y.; Ji, B.; Jiang, Y.; Song, P.; Dong, H.; Tuo, B., The P2Y2 nucleotide receptor mediates the proliferation and migration of human hepatocellular carcinoma cells induced by ATP. *J. Biol. Chem.* **2014,** *289* (27), 19137-19149.

136. Li, W. H.; Qiu, Y.; Zhang, H. Q.; Tian, X. X.; Fang, W. G., P2Y2 Receptor and EGFR Cooperate to Promote Prostate Cancer Cell Invasion via ERK1/2 Pathway. *Plos One* **2015,** *10* (7).

137. Mirza, A.; Basso, A.; Black, S.; Malkowski, M.; Kwee, L.; Pachter, J. A.; Lachowicz, J. E.; Wang, Y.; Liu, S. X., RNA interference targeting of A1 receptor-overexpressing breast carcinoma cells leads to diminished rates of cell proliferation and induction of apoptosis. *Cancer Biol. Ther.* **2005,** *4* (12), 1355-1360.

138. Yang, G.; Zhang, S. H.; Zhang, Y. L.; Zhou, Q. M.; Peng, S.; Zhang, T.; Yang, C. F.; Zhu, Z. Y.; Zhang, F. J., The inhibitory effects of extracellular ATP on the growth of nasopharyngeal carcinoma cells via P2Y2 receptor and osteopontin. *J. Exp. Clin. Cancer Res.* **2014,** *33-53*.

139. Gessi, S.; Merighi, S.; Sacchetto, V.; Simioni, C.; Borea, P. A., Adenosine receptors and cancer. *Biochim. Biophys. Acta, Biomembr.* **2011,** *1808* (5), 1400-1412.

140. Shaban, M.; Smith, R. A.; Stone, T. W., Purine suppression of proliferation of Sertoli-like TM4 cells in culture. *Cell Proliferation* **1995,** *28* (12), 673-682.

141. Henderson, J. F.; Khoo, K. Y., On the Mechanism of Feedback Inhibition of Purine Biosynthesis De Novo in Ehrlich Ascites Tumor Cells in Vitro. *J. Biol. Chem.* **1965,** *240*, 3104-3109.

142. Murray, A. W., The biological significance of purine salvage. *Annu. Rev. Biochem.* **1971,** *40*, 811-826.

143. Yamaoka, T.; Kondo, M.; Honda, S.; Iwahana, H.; Moritani, M.; Ii, S.; Yoshimoto, K.; Itakura, M., Amidophosphoribosyltransferase limits the rate of cell growth-linked de novo purine biosynthesis in the presence of constant capacity of salvage purine biosynthesis. *J. Biol. Chem.* **1997,** *272* (28), 17719-17725.

144. Mayer, D.; Natsumeda, Y.; Ikegami, T.; Faderan, M.; Lui, M.; Emrani, J.; Reardon, M.; Olah, E.; Weber, G., Expression of Key Enzymes of Purine and Pyrimidine Metabolism in a Hepatocyte-Derived Cell-Line at Different Phases of the Growth-Cycle. *J. Cancer Res. Clin. Oncol.* **1990,** *116* (3), 251-258.

145. Natsumeda, Y.; Prajda, N.; Donohue, J. P.; Glover, J. L.; Weber, G., Enzymic capacities of purine de Novo and salvage pathways for nucleotide synthesis in normal and neoplastic tissues. *Cancer Res.* **1984,** *44* (6), 2475-2479.

146. Hartman, S. C.; Buchanan, J. M., Nucleic acids, purines, pyrimidines (nucleotide synthesis). *Annu. Rev. Biochem.* **1959,** *28*, 365-410.

147. Soares, A. S.; Costa, V. M.; Diniz, C.; Fresco, P., Inosine Strongly Enhances Proliferation of Human C32 Melanoma Cells through PLC-PKC-MEK1/2-ERK1/2 and PI3K Pathways. *Basic Clin. Pharmacol. Toxicol.* **2015,** *116* (1), 25-36.

148. Goswami, M. T.; Chen, G. A.; Chakravarthi, B. V. S. K.; Pathi, S. S.; Anand, S. K.; Carskadon, S. L.; Giordano, T. J.; Chinnaiyan, A. M.; Thomas, D. G.; Palanisamy, N.; Beer, D. G.; Varambally, S., Role and regulation of coordinately expressed de novo purine biosynthetic enzymes PPAT and PAICS in lung cancer. *Oncotarget* **2015,** *6* (27), 23445-23461.

149. Elion, G. B., The Purine Path to Chemotherapy. *Science* **1989,** *244* (4900), 41-47.

150. Parker, W. B., Enzymology of Purine and Pyrimidine Antimetabolites Used in the Treatment of Cancer. *Chem. Rev.* **2009,** *109* (7), 2880-2893.

151. McCollister, R. J.; Gilbert, W. R., Jr.; Ashton, D. M.; Wyngaarden, J. B., Pseudofeedback Inhibition of Purine Synthesis by 6-Mercaptopurine Ribonucleotide and Other Purine Analogues. *J. Biol. Chem.* **1964,** *239*, 1560-1563.

152. Visentin, M.; Zhao, R. B.; Goldman, I. D., The Antifolates. *Clin. Hematol.* **2012,** *26* (3), 629-648.

153. Goldin, A.; Venditti, J. M.; Humphreys, S. R.; Dennis, D.; Mantel, N.; Greenhouse, S. W., A quantitative comparison of the antileukemic effectiveness of two folic acid antagonists in mice. *J. Natl. Cancer Inst.* **1955,** *15* (6), 1657-1664.

154. Cayley, P. J.; Dunn, S. M. J.; King, R. W., Kinetics of Substrate, Coenzyme, and Inhibitor Binding to Escherichia-Coli Dihydrofolate-Reductase. *Biochemistry* **1981,** *20* (4), 874-879.

155. Srere, P. A., The Metabolon. *Trends Biochem. Sci.* **1985,** *10* (3), 109-110.

156. Barnes, S. J.; Weitzman, P. D. J., Organization of Citric-Acid Cycle Enzymes into a Multienzyme Cluster. *Febs Lett.* **1986,** *201* (2), 267-270.

157. Velot, C.; Mixon, M. B.; Teige, M.; Srere, P. A., Model of a quinary structure between Krebs TCA cycle enzymes: A model for the metabolon. *Biochemistry* **1997,** *36* (47), 14271-14276.

158. Batke, J.; Asboth, G.; Lakatos, S.; Schmitt, B.; Cohen, R., Substrate-Induced Dissociation of Glycerol-3-Phosphate Dehydrogenase and Its Complex-Formation with Fructose-Bis-Phosphate Aldolase. *Eur. J. Biochem.* **1980,** *107* (2), 389-394.

159. Evans, D. R.; Guy, H. I., Mammalian pyrimidine biosynthesis: Fresh insights into an ancient pathway. *J. Biol. Chem.* **2004,** *279* (32), 33035-33038.

160. Ovadi, J.; Matrai, G.; Bartha, F.; Batke, J., Kinetic Pathways of Formation and Dissociation of the Glycerol-3-Phosphate Dehydrogenase Fructose-1,6-Bisphosphate Aldolase Complex. *Biochem. J.* **1985,** *229* (1), 57-62.

161. Schendel, F. J.; Cheng, Y. S.; Otvos, J. D.; Wehrli, S.; Stubbe, J., Characterization and chemical properties of phosphoribosylamine, an unstable intermediate in the de novo purine biosynthetic pathway. *Biochemistry* **1988,** *27* (7), 2614-2623.

162. Rudolph, J.; Stubbe, J., Investigation of the Mechanism of Phosphoribosylamine Transfer from Glutamine Phosphoribosylpyrophosphate Amidotransferase to Glycinamide Ribonucleotide Synthetase. *Biochemistry* **1995,** *34* (7), 2241-2250.

163. Zhang, Q. C.; Petrey, D.; Deng, L.; Qiang, L.; Sin, Y.; Thu, C. A.; Bisikirska, B.; Lefebvre, C.; Accili, D.; Hunter, T.; Maniatis, T.; Califano, A.; Honig, B., Structure-based prediction of protein-protein interactions on a genome-wide scale (vol 490, pg 556, 2012). *Nature* **2013,** *495* (7439), 127-127.

164. An, S.; Kumar, R.; Sheets, E. D.; Benkovic, S. J., Reversible compartmentalization of de novo purine biosynthetic complexes in living cells. *Science* **2008,** *320* (5872), 103-106.

165. Deng, Y. J.; Gam, J.; French, J. B.; Zhao, H.; An, S.; Benkovic, S. J., Mapping Protein-Protein Proximity in the Purinosome. *J. Biol. Chem.* **2012,** *287* (43), 36201-36207.

166. Kyoung, M.; Russell, S. J.; Kohnhorst, C. L.; Esemoto, N. N.; An, S., Dynamic architecture of the purinosome involved in human de novo purine biosynthesis. *Biochemistry* **2015,** *54* (3), 870-880.

167. Kristensen, A. R.; Gsponer, J.; Foster, L. J., A high-throughput approach for measuring temporal changes in the interactome. *Nat. Methods* **2012,** *9* (9), 907-909.

168. Havugimana, P. C.; Hart, G. T.; Nepusz, T.; Yang, H. X.; Turinsky, A. L.; Li, Z. H.; Wang, P. I.; Boutz, D. R.; Fong, V.; Phanse, S.; Babu, M.; Craig, S. A.; Hu, P. Z.; Wan, C. H.; Vlasblom, J.; Dar, V. U. N.; Bezginov, A.; Clark, G. W.; Wu, G. C.; Wodak, S. J.; Tillier, E. R. M.; Paccanaro, A.; Marcotte, E. M.; Emili, A., A Census of Human Soluble Protein Complexes. *Cell* **2012,** *150* (5), 1068-1081.

169. Zhao, H.; Chiaro, C. R.; Zhang, L. M.; Smith, P. B.; Chan, C. Y.; Pedley, A. M.; Pugh, R. J.; French, J. B.; Patterson, A. D.; Benkovic, S. J., Quantitative Analysis of Purine Nucleotides

Indicates That Purinosomes Increase de Novo Purine Biosynthesis. *J. Biol. Chem.* **2015,** *290* (11), 6705-6713.

170. Baresova, V.; Skopova, V.; Sikora, J.; Patterson, D.; Sovova, J.; Zikanova, M.; Kmoch, S., Mutations of ATIC and ADSL affect purinosome assembly in cultured skin fibroblasts from patients with AICA-ribosiduria and ADSL deficiency. *Hum. Mol. Genet.* **2012,** *21* (7), 1534-1543.

171. Baresova, V.; Krijt, M.; Skopova, V.; Souckova, O.; Kmoch, S.; Zikanova, M., CRISPR-Cas9 induced mutations along de novo purine synthesis in HeLa cells result in accumulation of individual enzyme substrates and affect purinosome formation. *Mol. Genet. Metab.* **2016,** *119* (3), 270-277.

172. Greasley, S. E.; Horton, P.; Ramcharan, J.; Beardsley, G. P.; Benkovic, S. J.; Wilson, I. A., Crystal structure of a bifunctional transformylase and cyclohydrolase enzyme in purine biosynthesis. *Nat. Struct. Biol.* **2001,** *8* (5), 402-406.

173. Lee, P.; Colman, R. F., Expression, purification, and characterization of stable, recombinant human adenylosuccinate lyase. *Protein Expression Purif.* **2007,** *51* (2), 227-234.

174. Lee, T. T.; Worby, C.; Bao, Z. Q.; Dixon, J. E.; Colman, R. F., His68 and His141 are critical contributors to the intersubunit catalytic site of adenylosuccinate lyase of Bacillus subtilis. *Biochemistry* **1999,** *38* (1), 22-32.

175. Li, S. X.; Tong, Y. P.; Xie, X. C.; Wang, Q. H.; Zhou, H. N.; Han, Y.; Zhang, Z. Y.; Gao, W.; Li, S. G.; Zhang, X. C.; Bi, R. C., Octameric structure of the human bifunctional enzyme PAICS in purine biosynthesis. *J. Mol. Biol.* **2007,** *366* (5), 1603-1614.

176. Vergis, J. M.; Bulock, K. G.; Fleming, K. G.; Beardsley, G. P., Human 5-aminoimidazole-4-carboxamide ribonucleotide transformylase/inosine 5 '-monophosphate cyclohydrolase - A bifunctional protein requiring dimerization for transformylase activity but not for cyclohydrolase activity. *J. Biol. Chem.* **2001,** *276* (11), 7727-7733.

177. Welin, M.; Grossmann, J. G.; Flodin, S.; Nyman, T.; Stenmark, P.; Tresaugues, L.; Kotenyova, T.; Johansson, I.; Nordlund, P.; Lehtio, L., Structural studies of tri-functional human GART. *Nucleic Acids Res.* **2010,** *38* (20), 7308-7019.

178. Chan, C. Y.; Zhao, H.; Pugh, R. J.; Pedley, A. M.; French, J.; Jones, S. A.; Zhuang, X. W.; Jinnah, H.; Huang, T. J.; Benkovic, S. J., Purinosome formation as a function of the cell cycle. *Proc. Natl. Acad. Sci. U.S.A.* **2015,** *112* (5), 1368-1373.

179. French, J. B.; Zhao, H.; An, S. O.; Niessen, S.; Deng, Y. J.; Cravatt, B. F.; Benkovic, S. J., Hsp70/Hsp90 chaperone machinery is involved in the assembly of the purinosome. *Proc. Natl. Acad. Sci. U.S.A.* **2013,** *110* (7), 2528-2533.

180. Spector, D. L., SnapShot: Cellular bodies. *Cell* **2006,** *127* (5), 1071.

181. Fu, R.; Sutcliffe, D.; Zhao, H.; Huang, X. Y.; Schretlen, D. J.; Benkovic, S.; Jinnah, H. A., Clinical severity in Lesch Nyhan disease: The role of residual enzyme and compensatory pathways. *Mol. Genet. Metab.* **2015,** *114* (1), 55-61.

182. Fridman, A.; Saha, A.; Chan, A.; Casteel, D. E.; Pilz, R. B.; Boss, G. R., Cell cycle regulation of purine synthesis by phosphoribosyl pyrophosphate and inorganic phosphate. *Biochem. J.* **2013,** *454*, 91-99.

183. Kohnhorst, C. L.; Kyoung, M.; Jeon, M.; Schmitt, D. L.; Kennedy, E. L.; Ramirez, J.; Bracey, S. M.; Luu, B. T.; Russell, S. J.; An, S., Identification of a multienzyme complex for glucose metabolism in living cells. *J. Biol. Chem.* **2017,** *292* (22), 9191-9203.

184. Pedley, A. M.; Karras, G. I.; Zhang, X.; Lindquist, S.; Benkovic, S. J., Role of HSP90 in the Regulation of de Novo Purine Biosynthesis. *Biochemistry* **2018,** *57* (23), 3217-3221.

185. An, S.; Deng, Y. J.; Tomsho, J. W.; Kyoung, M.; Benkovic, S. J., Microtubule-assisted mechanism for functional metabolic macromolecular complex formation. *Proc. Natl. Acad. Sci. U.S.A.* **2010,** *107* (29), 12872-12876.

186. Chan, C. Y.; Pedley, A. M.; Kim, D.; Xia, C. L.; Zhuang, X. W.; Benkovic, S. J., Microtubule-directed transport of purine metabolons drives their cytosolic transit to mitochondria. *Proc. Natl. Acad. Sci. U.S.A.* **2018,** *115* (51), 13009-13014.

187. French, J. B.; Jones, S. A.; Deng, H. Y.; Pedley, A. M.; Kim, D.; Chan, C. Y.; Hu, H. B.; Pugh, R. J.; Zhao, H.; Zhang, Y. X.; Huang, T. J.; Fang, Y.; Zhuang, X. W.; Benkovic, S. J., Spatial colocalization and functional link of purinosomes with mitochondria. *Science* **2016,** *351* (6274), 733-737.

188. Ben-Sahra, I.; Howell, J. J.; Asara, J. M.; Manning, B. D., Stimulation of de Novo Pyrimidine Synthesis by Growth Signaling Through mTOR and S6K1. *Science* **2013,** *339* (6125), 1323-1328.

189. Ramanathan, A.; Schreiber, S. L., Direct control of mitochondrial function by mTOR. *Proc. Natl. Acad. Sci. U.S.A.* **2009,** *106* (52), 22229-22232.

190. Robitaille, A. M.; Christen, S.; Shimobayashi, M.; Cornu, M.; Fava, L. L.; Moes, S.; Prescianotto-Baschong, C.; Sauer, U.; Jenoe, P.; Hall, M. N., Quantitative Phosphoproteomics Reveal mTORC1 Activates de Novo Pyrimidine Synthesis. *Science* **2013,** *339* (6125), 1320-1323.

191. An, S.; Kyoung, M.; Allen, J. J.; Shokat, K. M.; Benkovic, S. J., Dynamic Regulation of a Metabolic Multi-enzyme Complex by Protein Kinase CK2. *J. Biol. Chem.* **2010,** *285* (15), 11093-11099.

192. Verrier, F.; An, S.; Ferrie, A. M.; Sun, H.; Kyoung, M.; Deng, H.; Fang, Y.; Benkovic, S. J., GPCRs regulate the assembly of a multienzyme complex for purine biosynthesis. *Nat. Chem. Biol.* **2011,** *7* (12), 909-915.

193. Tong, X. M.; Zhao, F. P.; Thompson, C. B., The molecular determinants of de novo nucleotide biosynthesis in cancer cells. *Curr. Opin. Genet. Dev.* **2009,** *19* (1), 32-37.

194. Snapp, E., Design and use of fluorescent fusion proteins in cell biology. *Curr. Prot. Cell Biol.* **2005,** *Chapter 21*, Unit 21 4.

195. Portnoy, V.; Huang, V.; Place, R. F.; Li, L. C., Small RNA and transcriptional upregulation. *Wiley Interdiscip. Rev.: RNA* **2011,** *2* (5), 748-760.

196. Siomi, H.; Siomi, M. C., On the road to reading the RNA-interference code. *Nature* **2009,** *457* (7228), 396-404.

197. Masson, N.; Ratcliffe, P. J., HIF prolyl and asparaginyl hydroxylases in the biological response to intracellular O-2 levels. *J. Cell Sci.* **2003,** *116* (15), 3041-3049.

198. Woo, K. J.; Lee, T. J.; Park, J. W.; Kwon, T. K., Desferrioxamine, an iron chelator, enhances HIF-1 alpha accumulation via cyclooxygenase-2 signaling pathway. *Biochem. Biophys. Res. Commun.* **2006,** *343* (1), 8-14.

199. Strober, W., Trypan blue exclusion test of cell viability. *Curr. Protoc. Immunol.* **2001,** *Appendix 3*, Appendix 3B.

200. Asby, D. J.; Cuda, F.; Hoakwie, F.; Miranda, E.; Tavassoli, A., HIF-1 promotes the expression of its alpha-subunit via an epigenetically regulated transactivation loop. *Mol. Biosyst.* **2014,** *10* (10), 2505-2508.

201. Uchida, T.; Rossignol, F.; Matthay, M. A.; Mounier, R.; Couette, S.; Clottes, E.; Clerici, C., Prolonged hypoxia differentially regulates hypoxia-inducible factor (HIF)-1 alpha and HIF-2 alpha expression in lung epithelial cells - Implication of natural antisense HIF-1 alpha. *J. Biol. Chem.* **2004,** *279* (15), 14871-14878.

202. Chilov, D.; Camenisch, G.; Kvietikova, I.; Ziegler, U.; Gassmann, M.; Wenger, R. H., Induction and nuclear translocation of hypoxia-inducible factor-1 (HIF-1): heterodimerization with ARNT is not necessary for nuclear accumulation of HIF-1 alpha. *J. Cell Sci.* **1999,** *112* (8), 1203-1212.

203. Forsythe, J. A.; Jiang, B. H.; Iyer, N. V.; Agani, F.; Leung, S. W.; Koos, R. D.; Semenza, G. L., Activation of vascular endothelial growth factor gene transcription by hypoxia-inducible factor 1. *Mol. Cell. Biol.* **1996,** *16* (9), 4604-4613.

204. Wenger, R. H.; Kvietikova, I.; Rolfs, A.; Gassmann, M.; Marti, H. H., Hypoxia-inducible factor-1 alpha is regulated at the post-mRNA level. *Kidney Int.* **1997,** *51* (2), 560-563.

205. Huang, W. J.; Xia, L. M.; Zhu, F.; Huang, B.; Zhou, C.; Zhu, H. F.; Wang, B.; Chen, B.; Lei, P.; Shen, G. X.; De, A., Transcriptional upregulation of HSP70-2 by HIF-1 in cancer cells in response to hypoxia. *Int. J. Cancer* **2009,** *124* (2), 298-305.

206. Gano, J. J.; Simon, J. A., A Proteomic Investigation of Ligand-dependent HSP90 Complexes Reveals CHORDC1 as a Novel ADP-dependent HSP90-interacting Protein. *Mol. Cell. Proteomics* **2010,** *9* (2), 255-270.

207. Marie, S.; Heron, B.; Bitoun, P.; Timmerman, T.; Van den Berghe, G.; Vincent, M. F., AICA-ribosiduria: A novel, neurologically devastating inborn error of purine biosynthesis caused by mutation of ATIC. *Am. J. Hum. Genet.* **2004,** *74* (6), 1276-1281.

208. Spurr, I. B.; Birts, C. N.; Cuda, F.; Benkovic, S. J.; Blaydes, J. P.; Tavassoli, A., Targeting Tumour Proliferation with a Small-Molecule Inhibitor of AICAR Transformylase Homodimerization. *ChemBioChem* **2012,** *13* (11), 1628-1634.

209. Asby, D. J.; Cuda, F.; Beyaert, M.; Houghton, F. D.; Cagampang, F. R.; Tavassoli, A., AMPK Activation via Modulation of De Novo Purine Biosynthesis with an Inhibitor of ATIC Homodimerization. *Chem. Biol.* **2015,** *22* (7), 838-848.

210. Baresova, V.; Skopova, V.; Souckova, O.; Krijt, M.; Kmoch, S.; Zikanova, M., Study of purinosome assembly in cell-based model systems with de novo purine synthesis and salvage pathway deficiencies. *Plos One* **2018,** *13* (7).

211. King, M. E.; Honeysett, J. M.; Howell, S. B., Regulation of de novo purine synthesis in human bone marrow mononuclear cells by hypoxanthine. *J. Clin. Invest.* **1983,** *72* (3), 965-970.

212. Wick, A. N.; Drury, D. R.; Nakada, H. I.; Wolfe, J. B., Localization of the primary metabolic block produced by 2-deoxyglucose. *J. Biol. Chem.* **1957,** *224* (2), 963-969.

213. Krieglstein, J.; Stock, R., Decreased glycolytic flux rate in the isolated perfused rat brain after pretreatment with 6-aminonicotinamide. *Naunyn Schmiedeberg's Arch. Pharmacol.l* **1975,** *290* (2-3), 323-327.

214. Street, J. C.; Mahmood, U.; Ballon, D.; Alfieri, A. A.; Koutcher, J. A., 13C and 31P NMR investigation of effect of 6-aminonicotinamide on metabolism of RIF-1 tumor cells in vitro. *J. Biol. Chem.* **1996,** *271* (8), 4113-4119.

215. Kohler, E.; Barrach, H.; Neubert, D., Inhibition of NADP dependent oxidoreductases by the 6-aminonicotinamide analogue of NADP. *Febs Lett.* **1970,** *6* (3), 225-228.

216. Ho, H.-Y., Cheng, M.-L., Wang, Y.-H. and Chiu, D.T.-Y. Flow cytometry for assessment of the efficacy of siRNA. Cytometry **2006**, *69A*, 1054-1061

217. Giege, P.; Heazlewood, J. L.; Roessner-Tunali, U.; Millar, A. H.; Fernie, A. R.; Leaver, C. J.; Sweetlove, L. J., Enzymes of glycolysis are functionally associated with the mitochondrion in Arabidopsis cells. *Plant Cell* **2003,** *15* (9), 2140-2151.

218. Mowbray, J.; Moses, V., The tentative identification in Escherichia coli of a multienzyme complex with glycolytic activity. *Eur. J. Biochem.* **1976,** *66* (1), 25-36.

219. Sullivan, D. T.; MacIntyre, R.; Fuda, N.; Fiori, J.; Barrilla, J.; Ramizel, L., Analysis of glycolytic enzyme co-localization in Drosophila flight muscle. *J. Exp. Biol.* **2003,** *206* (Pt 12), 2031-2038.

220. Campanella, M. E.; Chu, H. Y.; Low, P. S., Assembly and regulation of a glycolytic enzyme complex on the human erythrocyte membrane. *Proc. Natl. Acad. Sci. U.S.A.* **2005,** *102* (7), 2402-2407.

221. Kohnhorst, C. L.; Kyoung, M.; Jeon, M.; Schmitt, D. L.; Kennedy, E. L.; Ramirez, J.; Bracey, S. M.; Luu, B. T.; Russell, S. J.; An, S., Identification of a multienzyme complex for glucose metabolism in living cells. *J. Biol. Chem.* **2017,** *292* (22), 9191-9203.

222. Zhao, X.; Palacci, H.; Yadav, V.; Spiering, M. M.; Gilson, M. K.; Butler, P. J.; Hess, H.; Benkovic, S. J.; Sen, A., Substrate-driven chemotactic assembly in an enzyme cascade. *Nat. Chem.* **2018,** *10* (3), 311-317.

223. Jin, M. Y.; Fuller, G. G.; Han, T.; Yao, Y.; Alessi, A. F.; Freeberg, M. A.; Roach, N. P.; Moresco, J. J.; Karnovsky, A.; Baba, M.; Yates, J. R.; Gitler, A. D.; Inoki, K.; Klionsky, D. J.; Kim, J. K., Glycolytic Enzymes Coalesce in G Bodies under Hypoxic Stress. *Cell Rep.* **2017,** *20* (4), 895-908.

224. Leiherer, A.; Geiger, K.; Muendlein, A.; Drexel, H., Hypoxia induces a HIF-1 alpha dependent signaling cascade to make a complex metabolic switch in SGBS-adipocytes. *Mol. Cell. Endocrinol.* **2014,** *383* (1-2), 21-31.

225. Gustafsson, N.; Culley, S.; Ashdown, G.; Owen, D. M.; Pereira, P. M.; Henriques, R., Fast live-cell conventional fluorophore nanoscopy with ImageJ through super-resolution radial fluctuations. *Nat. Commun.* **2016,** *7*, 12471.

226. Moffatt, B. A.; Ashihara, H., Purine and pyrimidine nucleotide synthesis and metabolism. *Arabidopsis Book* **2002,** *1*, e0018.

227. Karle, J. M.; Anderson, L. W.; Cysyk, R. L., Effect of Plasma-Concentrations of Uridine on Pyrimidine Biosynthesis in Cultured L1210 Cells. *J. Biol. Chem.* **1984,** *259* (1), 67-72.

228. Ducker, G. S.; Chen, L.; Morscher, R. J.; Ghergurovich, J. M.; Esposito, M.; Teng, X.; Kang, Y. B.; Rabinowitz, J. D., Reversal of Cytosolic One-Carbon Flux Compensates for Loss of the Mitochondrial Folate Pathway. *Cell Metab.* **2016,** *23* (6), 1140-1153.

229. Robey, I. F.; Lien, A. D.; Welsh, S. J.; Baggett, B. K.; Gillies, R. J., Hypoxia-inducible factor-1 alpha and the glycolytic phenotype in tumors. *Neoplasia* **2005,** *7* (4), 324-330.

230. Narisawa-Saito, M.; Inagawa, Y.; Yoshimatsu, Y.; Haga, K.; Tanaka, K.; Egawa, N.; Ohno, S.; Ichikawa, H.; Yugawa, T.; Fujita, M.; Kiyono, T., A critical role of MYC for transformation of human cells by HPV16 E6E7 and oncogenic HRAS. *Carcinogenesis* **2012,** *33* (4), 910-917.

231. O'Brien, R.; Tran, S. L.; Maritz, M. F.; Liu, B.; Kong, C. F.; Purgato, S.; Yang, C.; Murray, J.; Russell, A. J.; Flemming, C. L.; von Jonquieres, G.; Pickett, H. A.; London, W. B.; Haber, M.; Gunaratne, P. H.; Norris, M. D.; Perini, G.; Fletcher, J. I.; MacKenzie, K. L., MYC-Driven Neuroblastomas Are Addicted to a Telomerase-Independent Function of Dyskerin. *Cancer Res.* **2016,** *76* (12), 3604-3617.

232. Peter, M.; Rosty, C.; Couturier, J.; Radvanyi, F.; Teshima, H.; Sastre-Garau, X., MYC activation associated with the integration of HPV DNA at the MYC locus in genital tumors. *Oncogene* **2006,** *25* (44), 5985-5993.

233. Liu, C. L.; Knudsen, G. M.; Pedley, A. M.; He, J. X.; Johnson, J. L.; Yaron, T. M.; Cantley, L. C.; Benkovic, S. J., Mapping Post-Translational Modifications of de Novo Purine Biosynthetic Enzymes: Implications for Pathway Regulation. *J. Proteome Res.* **2019,** *18* (5), 2078-2087.

234. Corn, P. G.; Ricci, M. S.; Scata, K. A.; Arsham, A. M.; Simon, M. C.; Dicker, D. T.; El-Deiry, W. S., Mxi1 is induced by hypoxia in a HIF-1-dependent manner and protects cells from c-Myc-induced apoptosis. *Cancer Biol. Ther.* **2005,** *4* (11), 1285-1294.

235. Sun, L.; Song, L.; Wan, Q.; Wu, G.; Li, X.; Wang, Y.; Wang, J.; Liu, Z.; Zhong, X.; He, X.; Shen, S.; Pan, X.; Li, A.; Wang, Y.; Gao, P.; Tang, H.; Zhang, H., cMyc-mediated activation of serine biosynthesis pathway is critical for cancer progression under nutrient deprivation conditions. *Cell Res.* **2015,** *25* (4), 429-444.

236. Tsugawa, H.; Cajka, T.; Kind, T.; Ma, Y.; Higgins, B.; Ikeda, K.; Kanazawa, M.; VanderGheynst, J.; Fiehn, O.; Arita, M., MS-DIAL: data-independent MS/MS deconvolution for comprehensive metabolome analysis. *Nat. Methods* **2015,** *12* (6), 523-526.

237. Lai, Z. J.; Tsugawa, H.; Wohlgemuth, G.; Mehta, S.; Mueller, M.; Zheng, Y. X.; Ogiwara, A.; Meissen, J.; Showalter, M.; Takeuchi, K.; Kind, T.; Beal, P.; Arita, M.; Fiehn, O., Identifying metabolites by integrating metabolome databases with mass spectrometry cheminformatics. *Nat. Methods* **2018,** *15* (1), 53-56.